Research & Technology Centre

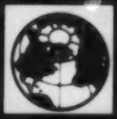

FABRICATION AND FATIGUE EVALUATION OF WELDED JOINTS FOR STRUCTURES IN MARINE ENVIRONMENT - PHASE II

Final Report: M.J. Pates, D.J. Burns
U.H. Mohaupt, J. Forbes
A.S.J. Swamidas, K. Munaswamy
R.M. Hopkins

DSS Contract No. 23SQ.23440-4-9276

DSS Contract Serial No. OSQ84-00431

CANMET Scientific Authority: Dr. O. Vosikovsky

Date: June 1989

MICROMEDIA

340 AP

90-07135/

FABRICATION AND FATIGUE EVALUATION OF WELDED TUBULAR JOINTS FOR STRUCTURES IN MARINE ENVIRONMENTS - PHASE II

by

D.J. BURNS
U.H. MOHAUPT
J. FORBES
University of Waterloo
Waterloo, Ontario
N2L 3G1

A.S.J. SWAMIDAS
K. MUNASWAMY
R.M. HOPKINS
Memorial University
St. John's, Newfoundland
A1B 3X5

M.J. PATES
Project Manager
Materials Technology Centre
Fleet Technology Limited

Contents

Abstract 1 (a)

Résumé 1 (b)

1 Introduction 2

2 Test Specimen and Rigs 5

2.1 Tubular Joint 5

2.2 Test Rig – University of Waterloo 6

2.3 Test Rig – Memorial University 7

2.3.1 Saddle Tank and Seawater Test Preparation 7

2.4 Fatigue Crack Detection and Sizing 9

2.4.1 ACPD Measurements at Memorial 9

2.4.2 DCPD Measurements at Waterloo 11

3 Strain Gauge Measurements 13

3.1 Axial Loading Tests at Memorial 14

3.2 In-plane and Out of Plane Bending Tests at Waterloo 15

4 Results and Discussion of Static Tests 16

4.1 Static Tests – Strain Gauge Data 16

4.1.1 Axial Brace Loading Tests at Memorial 16

4.1.2 Axial, In-plane and out-of-plane bending tests at Waterloo . . . 18

5 Results and Discussion of Fatigue Tests 22

5.1 Failure Modes and Fatigue Life N_3 23

5.2 Crack Initiation and Crack Shape Development 26

5.2.1 Axial Loading Fatigue Tests at Memorial 26

5.2.1.1 Comparison of Beachmarks and A.C. Potential Results 26

5.2.1.2 Crack Initiation Lives (N_1) 27

5.2.1.3 Comparison of Fatigue Lives N_1, N_3 and N_4 28

5.2.1.4 Stiffener Failure 30

5.2.1.5 Crack Shape Development and Stress Distribution 31

5.2.1.6 Crack Growth Rate 33

5.2.2 In-plane and Out of Plane Bending Fatigue Tests at Waterloo . . 33

5.2.2.1 Comparison of Beachmarks and DCPD Data 33

5.2.2.2 Crack Initiation Lives (N_1) 34

5.2.2.3 Crack Shape Development 37

5.2.2.4 Effect of Stiffeners on Crack Shape Development 39

5.2.2.5 Crack Growth Rate 39

5.2.2.6 Stiffener Stresses 40

6 Summary and Conclusions 41

7 Acknowledgements 45

8 **References**

Appendices
- Appendix 1 - Definitions of the Spot Stresses and Stress Concentration Factors
- Appendix 2 - Fabrication of Tubulars for Fatigue Testing in Air and Seawater
- Appendix 3 - Procedure of Measuring Crack Depth by ACPD Technique
- Appendix 4 - Strain Gauge Data Sheets - Memorial and Waterloo
- Appendix 5 - Memorial Data - a vs N and da/dn vs a plots

Abstract

Large scale tubular joints welded in the T configuration have been fatigue tested to determine the effects of stiffening internally with two ring plates welded in the chord tube. All tubular joints were subjected to constant amplitude loading; the mode of loading on the brace tube was axial, in-plane bending or out of plane bending. Two unstiffened and seven stiffened joints were tested in air; two stiffened joints were cathodically protected (-0.85 V Ag/AgCl) and tested in artificial seawater at 5±2°C. Strain gauges were used to determine the stress distributions produced by each mode of loading. Potential drop techniques were used to detect crack initiation at the chord toe of the brace/chord weld and to monitor crack shape development. These tests have shown:

1. that this arrangement of two simple ring stiffeners leads to large reductions in stress concentration factor (SCF) for out of plane bending or axial brace loading.
2. that these reductions in SCF at the hot spots lead to large increases in fatigue load carrying capacity. This improvement in fatigue performance can be quantified using the hot spot stress design procedure presently used for unstiffened joints.
3. that this arrangement of two simple ring stiffeners leads to significant cyclic stresses at the internal diameter of the rings. A fatigue analysis for this location should be part of the fatigue assessment for stiffened tubular joints. Using a machined rather than flame cut inner diameter is recommended.
4. that, in general, crack shape development in stiffened joints is very similar to that observed in tests on unstiffened joints. However the stiffener arrangement used in these tests appears to have limited surface crack length prior to through-thickness cracking of the chord (life N_3) and to have caused the crack to turn as it approached the inside of the chord. Both of these effects are beneficial from a fatigue viewpoint and merit further study.
5. that crack growth rates were significantly higher in the cathodically protected joints than in similar joints tested in air. Also in the present tests on stiffened tubular joints and in previous tests on pipe-plate specimens, the fatigue life (N_3) for tests in air were always higher than that for equivalent tests with optimum cathodic protection in artificial seawater.

Résumé

Des noeuds tubulaires de grande dimension, soudés en T, ont fait l'objet d'essais de fatigue afin d'établir l'effet du raidissement interne obtenu en soudant des tôles annulaires à l'intérieur de la membrure. Tous les noeuds ont été soumis à une charge d'amplitude constante; le mode de chargement imposé à l'entretoise était une traction axiale, une flexion dans le plan, ou une flexion hors–plan. Deux noeuds non-raidis ainsi que sept noeuds raidis ont été soumis à des essais dans l'air; deux noeuds raidis ont été soumis à des essais dans de l'eau de mer synthétique à 5 ± 2°C, avec protection cathodique (−0.85 V Ag/AgCl). Des jauges de contrainte ont été utilisées pour établir la répartition des contraintes causée par chaque mode de chargement. La technique de la mesure de la chute de potentiel à été utilisée pour déceler l'armorçage des fissures au pied de la soudure entretoise/membrure (du côté de la membrure), ainsi que pour vérifier l'évolution du profil de la fissure.

Ces essais ont démontré:

1. que cet arrangement de deux simples raidisseurs annulaires cause une grande diminution du facteur de concentration des contraintes (SCF) pour une flexion hors-plan et une traction axiale de l'entretoise.

2. que ces diminutions du SCF au point chaud entraînent une forte augmentation de la résistance au chargement en fatigue. Cette amélioration de la performance en fatigue peut être évaluée quantitativement en utilisant la contrainte au point chaud comme paramètre de design, tel qu'on le fait actuellement pour les noeuds non-raidis.

3. que cet arrangement de deux simples raidisseurs annulaires cause des contraintes cycliques importantes au diamètre intérieur des anneaux. Une analyse de fatigue à cet endroit devrait faire partie de l'évaluation en fatigue des noeuds tubulaires raidis. On recommande que le diamètre intérieur des anneaux soit usiné plutôt que coupé au chalumeau.

4. qu'en général, l'évolution du profil de la fissure dans les noeuds raidis est très semblable à celle qu'on a observé durant les essais des noeuds non-raidis. Par contre, l'arrangement des raidisseurs utilisé dans ces essais semble avoir limité la longueur en surface de la fissure avant que celle-ci ne traverse complètement la membrure (durée de vie N_3) et semble avoir forcé la fissure à changer de parcours lorsque celle-ci s'approchait de la surface intérieure de la membrure. Ces deux effets sont bénéfiques du point de vue de la fatigue, et devraient faire l'objet d'études supplémentaires.

5. que la vitesse de propagation des fissures était considérablement plus élevée lors des essais avec protection cathodique que lors des essais de joints semblables dans l'air. De plus, lors des essais actuels de noeuds tubulaires ainsi que lors d'essais précédents sur des assemblages 'tube sur tôle', la durée de vie en fatigue (N_3) pour les essais dans l'air était toujours supérieure à celle obtenue durant les essais avec protection cathodique optimale.

1 Introduction

The prediction of the fatigue performance of tubular welded joints, used in the construction of offshore structures, has received much attention during the last decade [1-3]. There have been many fatigue tests in air on unstiffened tubular joints having a T configuration, Figure 1(a), or other simple geometry. A major aim of most of these tests has been the validation of the so-called hot spot S-N design procedure [1]. The weld toe location where the maximum stress range and fatigue crack initiation is expected to occur is called the hot spot. The hot spot stress range is obtained by multiplying the nominal stress range in the brace tube, see Figure 1(a), by a stress concentration factor (SCF). A procedure used to define this SCF experimentally is discussed in Appendix 1. Parametric equations giving SCF for various unstiffened joint geometries and modes of loading (axial, in-plane or out of plane bending) have been published [4].

When a designer has calculated the hot spot stress range for a particular joint and mode of loading he estimates the fatigue life using a design S-N curve, derived from the large data base mentioned earlier. For example, Figure 2, shows the basic design, T, curve from the UK Department of Energy (DOE) Guidance Notes [5]. This curve is for joints operating in air and having a chord thickness of 32 mm. Significant penalties must be applied for joints having larger chord thickness and/or operating in seawater without cathodic protection. However the design curve for air is recommended by DOE for joints with cathodic protection in seawater. These DOE recommendations regarding the influence of sections thickness and environment have been the subject of some controversy [3] and studied extensively in the Canadian Offshore Steels Research Program [6]. Also the applicability of this hot spot S-N design approach for complex joints required more study.

This report summarises a study of the fatigue behaviour of a complex joint often used by designers; a joint with internal ring stiffeners. Designers use internal ring stiffeners to reduce the flexibility of the chord member: this reduces the SCF at the hot spot and improves fatigue performance. An improvement in fatigue performance can also be obtained by increasing section thickness but as mentioned earlier there is a penalty associated with increase in section thickness. This contract (test program) on T tubular joints with two internal ring stiffeners was designed to complement and extend a UKOSRPII test program on such joints and to tie in with a Lloyd's Register project

[7] on the stress analysis of stiffened joints. One of the sponsors of this Lloyd's project was CANMET.

A summary of the UKOSRPII test program at the National Engineering Laboratory (NEL) was published in 1988 by Holmes, Brown and Kerr [8]. Six large scale T tubular joints were fatigue tested in air with axial brace loading; three had simple (light) ring stiffeners and three had flanged (heavy) ring stiffeners. These test geometries are shown in Figure 3. During the planning of our test program, discussions were held with the aforementioned authors. Although their test program was still ongoing it was already clear that there were some disadvantages associated with heavy stiffeners and that flame cut ring stiffeners were themselves liable to crack early. Therefore the present study has concentrated on T tubular joints with simple (light) ring stiffening, using rings with a machined inside diameter and welding procedures designed to minimize the risk of ring cracking.

The results of fatigue tests on eleven tubular joints are presented in this report. A report on the fabrication and inspection of the tubular joints is available, a summary is presented in Appendix 2. Two of these joints were unstiffened; the remainder had two simple ring stiffeners. This test program, Table 1, was designed to investigate the effect of mode of loading on fatigue crack initiation and propagation in ring stiffened joints and at the same time provide some information on the behaviour of cathodically protected tubular joints operating in seawater. In other parts of the Canadian program, T plate-plate and pipe-plate specimens, see Figure 1 (b) and (c), had already indicated that cathodic protection was not as beneficial as assumed in the DOE guidelines and it was deemed wise to confirm this in this test program on tubular joints.

The test frames for these tubular joint tests were designed by U.H. Mohaupt as part of a previous contract. Detailed descriptions of these test frames are given in a contract report [9]; only brief descriptions are given herein.

One unstiffened and four stiffened joints were tested at Memorial University, Table 1(a). All of these joints were fatigued with constant amplitude, axial brace loading. The unstiffened joint and two stiffened joints were tested in air at 3 to 4 Hertz to provide a direct comparison with the UKOSRPII test program on similar joints in air. The other two stiffened joints were cathodically protected and tested in seawater at 0.2 Hertz. Detailed reports on each of these tests are available; a summary of results is presented herein.

Table 1: (a) Memorial University Fatigue Testing Schedule; (b) Waterloo Schedule of Tests.

Table 1(a)

Specimen	Environment	Nominal Hot Spot Stress Range
TA1 (unstiffened)	air	250 MPa
TA2 (stiffened)	air	250 MPa
TA3 (stiffened)	air	160 MPa
TA4 (stiffened)	cathodic protection 0.85 Ag/AgCl	250 MPa
TA5 (stiffened)	cathodic protection 0.85 Ag/AgCl	160 MPa
TA6 (stiffened)	spare	

Table 1(b)

Specimen	Mode of Loading	Environment	Nominal Hot Spot Stress Range
TB1 (unstiffened)	IPB	Air	250 MPa
TB2 (stiffened)	IPB	Air	250 MPa
TB3 (stiffened)	IPB	Air	160 MPa*
TB4 (stiffened)	OPB	Air	250 MPa
TB5 (stiffened)	OPB	Air	160 MPa
TB6 (stiffened)	IPB	Air	160 MPa (repeat)

* accidentally overloaded

One unstiffened and five stiffened joints were tested at the University of Waterloo, Table 1(b). All of these joints were tested in air with constant amplitude loading at a frequency of approximately 3 Hertz. The unstiffened joint and three of the stiffened joints were subjected to in-plane bending; one of these stiffened joint tests ended prematurely. The other two stiffened joints were subjected to out of plane bending. Detailed reports of each of these tests are available; a summary of results is presented herein.

The results of fatigue tests on tubular joints are usually presented as plots of hot spot stress (S) against cycles to produce a through wall crack (N_3); prior to the development of a through wall crack there is usually no significant loss of joint stiffness. Fatigue cracks initiate at the weld toe early in this fatigue life (N_3) so there is interest [10] in developing linear elastic fracture mechanics (LEFM) techniques to predict fatigue life (N_3) or the residual life (N_R) of joints found to contain cracks during in-service inspection.

The success of an LEFM approach depends very much on the method used to model crack shape development and the definition of initial crack size(s). In all of the fatigue tests in the Canadian Offshore Steels Research Program, potential drop (PD) techniques have been used to detect crack initiation and monitor crack shape development. The ACPD technique used previously by Vosikovsky at CANMET [11] was used in these tubular joint tests at Memorial University. The DCPD technique used previously by Yee, Lambert, [12] Mohaupt and Burns at Waterloo was adapted by J. Forbes for these tubular joint tests at Waterloo. Since these ACPD and DCPD techniques have been described in detail previously only brief descriptions are given in this report. This PD data is used herein to define crack initiation lives, N_1, and to assess the influence, if any, of ring stiffening and mode of loading on crack propagation life ($N_p = N_3 - N_1$). The data on crack shape development is analyzed to indicate the features that should be included in any LEFM model for predicting N_p or N_R (residual life).

2 Test Specimen and Rigs

2.1 Tubular Joint

Two tubular joints were fabricated without ring stiffeners and ten tubular joints were fabricated with two ring stiffeners as shown in Figure 4. All tubular joints had a chord diameter of 914 mm and a brace diameter of 457 mm. The nominal wall thickness of the brace and chord was 19 mm. The steel plate used to fabricate the chord tube was CSA grade 40.21 M.350 WT and the brace tubes were cut from A106GrB ($S_y = 350MPa$) seamless tube. The ring stiffeners were machined from the 19 mm plate.

Welding procedures are given in Appendix 2. The stiffener positions shown in Figure 4 were also the positions used for the UKOSRPII stiffened joints, which were fabricated from 16 mm plate, see Figure 3. As mentioned earlier, Lloyd's Register have studied the influence of stiffener spacing on stress concentration factor. Research by Lloyd's Register with acrylic models in 1982 [7] has been used to prepare Figure 5. This figure compares estimates of SCF for unstiffened and stiffened joints. The abscissa is the pitch (p) of the stiffeners divided by the diameter, d, of the brace tube. The SCF's are presented for three modes of loading: – axial (longitudinal) brace loading, in-plane brace bending (IPB) and out of plane brace bending (OPB). For axial and OPB brace loading the stiffeners have a major effect on SCF. For IPB the effect is much less significant; for IPB the maximum reduction in SCF appears at p/d of 1.0 but this analysis does not account for other hot spots created if the stiffeners are directly under the brace tube. For this test program and the tests at NEL, the stiffener spacing was p/d of 0.6.

2.2 Test Rig – University of Waterloo

Figures 6 and 7 show the test rig built for the tests at the University of Waterloo. Figure 6 shows the configuration used for IPB tests. The loads are applied through a crosshead by two MTS servo-controlled hydraulic actuators. This side by side arrangement gives in-plane bending when the actuators act in opposition or axial (longitudinal) brace loading when the actuators act together. At Waterloo, axial loading was only used in static tests to provide SCF values for comparison with data obtained at Memorial.

Figure 7 shows the configuration used for out of plane brace bending. For these tests the ends of the chord tube were keyed to prevent rotation. Figure 8 shows the special end clamps used to connect the chord ends to the test rig. These end clamps, with their associated bearings, and the linkages connecting the actuators to the crosshead and base frame facilitate alignment of the specimen. The end clamps avoid restraint problems inherent in conventional bolted joints, which have been used by others in tubular joint tests. Also the chord length of our test specimen, Figure 4, is longer than that used in the UKOSRPII (NEL) tests, Figure 3. This facilitated alignment and minimized end restraint effects [4].

The linkages below the actuators have their pivot points at almost the same level as the brace-chord weld. This pivot location and the clevis joints between the crosshead and actuators also minimizes any tendency to overconstrain the specimen before and during the development of fatigue cracks.

2.3 Test Rig – Memorial University

Figures 9 and 10 show the rig built for the tests at Memorial University. This rig, shown in plan view in Figure 9, had to be designed so that the polar axes of the brace and chord members lay in the horizontal plane; the laboratory ceiling was too low to have the tubular joint and existing MTS actuator in the vertical plane. The load cell supplied with this actuator has a maximum rated capacity of 2727 MN. This servo-controlled actuator has a double-ended swivel joint; another swivel joint was fabricated to fit between the actuator and brace of the tubular joint. These swivel joints and special end clamps, identical to those used on the Waterloo rig, ensured that the test specimen was not over-restrained.

2.3.1 Saddle Tank and Seawater Test Preparation

To provide for the circulation of synthetic seawater, a saddle tank was fabricated from Lexan material and mounted at the intersection of the brace and chord as shown in Figure 10. Lexan was selected because of its clarity, machinability and resistance to chemicals, cold, impact and breakage. Since only the vicinity of the weld toe needed to be exposed to synthetic seawater, the Lexan enclosure was designed just large enough to accommodate the ACPD probes and the cathodic protection hardware. The saddle tank was secured in place using nylon straps and bolted flanges. A water-tight seal was applied between it and the tubular by using a combination of live-rubber and silicone seal.

A series of protective coatings were applied to all the strain gauges immersed in seawater. Two coats of Devoe 235 marine epoxy paint were also applied to all steel surfaces that were to be exposed to the seawater, excluding the area immediately adjacent to and including the weld beads. The objective here was to minimize the total current required for cathodic protection and, in doing so, provide strict control over the current density in the region of interest. The area of uncoated steel measured approximately 720 cm^2 for tubular TA4 and approximately 1005 cm^2 for tubular TA5.

A circulation system, consisting of seawater holding tank, saddle tank, a circulation pump and assorted tubing and connectors, provided the necessary supply of synthetic seawater to the specimen. A large (1000L) Xactics tank contained the bulk of the seawater and insulated it from the warmer surroundings. Holes were drilled in the tank to accommodate a stainless steel cooling coil and circulation hoses. A variable-speed, magnetically-coupled gear pump was used to transfer the seawater from the holding tank to the saddle tank. The circulation rate was established by adjusting the pump speed. The seawater returned to the holding tank under the action of gravity. The water flow rate was bout one litre per minute.

The cooling system comprised a portable refrigeration unit and 316 stainless steel cooling coil. A filtered air-compressor saturated the seawater in the holding tank with oxygen while providing sufficient agitation to enhance the cooling rate and prevent ice build-up on the cooling coil. An external thermostat was used to control the refrigerant as demanded. The tests were conducted at 5±2°C.

The required quantities of synthetic seawater (including heavy metal additions) were made according to ASTM standard D1141-75 (1980), using distilled water and reagent grade chemicals. Atomic adsorption was used to determine the major ion (Ca and Mg) concentrations of the seawater and its salinity was measured using a refractometer. The results of these tests are summarized in Table 2. In order to prevent contamination of the seawater, only inert (non-corrosive) maerials were used in the fabrication of seawater enclosures and circulation pumps.

Measurement of dissolved oxygen content and temperature was accomplished with a Galvanic Cell Oxygen Analyzer (GCOA). This instrument was capable of continuous measurement of dissolved oxygen content with an accuracy of ±0.1 mg/L. A dissolved oxygen probe was positioned in the tank in close proximity to the outlet hose. The GCOA was also used to measure temperature with an accuracy of ±0.2°C. Temperature measurements were obtained using a thermistor whose leads were connected to the rear of the GCOA. A full range analog pH meter was used to monitor seawater pH during each test. Environmental parameters are also given in Table 2.

Cathodic protection was achieved using a specially-built potentiostat, a ring-shaped platinum wire electrode and a copper/copper sulfate reference electrode. The platinum wire anode was carefully positioned and shaped to ensure a uniform distribution of cathodic current close to the weld toe. The potentiostat was equipped with front panel jacks that were connected directly to

Table 2: Environmental Parameters & Chemical Analysis of Synthetic Seawater

Concentration (mg/ml)	Ca = 40.0 Mg = 133.6
Salinity %	37
Ph	Begin = 8.2 Stable at 8.4
Dissolved Oxygen	Close to Saturation at 10 mg/litre at 5°C
Temperature Tolerance	±2.5°C

a DVM for periodic measurement of reference potential and supplied current. An electrochemical potential of -900mV vs Cu/$CuSO_4$ (equivalent to -850mV vs Ag/AgCl in seawater) was employed in both tests.

2.4 Fatigue Crack Detection and Sizing

Potential drop (PD) techniques were used to detect the initiation of fatigue cracks and to monitor crack shape development thereafter. Since nine of the eleven specimens used were tested in air and eight were finally cut open to inspect the crack surfaces, it was possible to "beachmark" periodically to provide another measure of crack shape development. The first beachmark was made by ink staining to indicate the number and shape of initial cracks; this was done sometime after the first PD indication of crack initiation. The other beachmarks were made periodically by reducing the load range and doubling the loading frequency, thereby producing a small crack extension (beachmark) that was always visible during postmortem examination of the failure surface.

2.4.1 ACPD Measurements at Memorial

A Unit Inspection Crack Microgauge was used for ACPD measurements. Figure 11 is a block diagram showing pairs of active and reference parts at the weld toe and the data acquisition system. The probes were spot welded. Each active pair spanning the weld toe had a radial span of 10 mm and each associated reference pair had the same radial spacing.

All of the tubulars tested at Memorial were subjected to axial brace loading. Therefore crack initiation was likely to occur at both of the saddle points, see S_1 on Figure 9. Figures 12 and 13 show for unstiffened and stiffened joints respectively the arrangement of PD probes used at each saddle site to detect initiation and propagation of the fatigue crack. Twenty to twenty-five active probe pairs, with a circumferential spacing of 6 mm, were spot welded each side of each saddle point. A further five to ten active probe pairs were spot welded with a longer, 10 mm circumferential spacing, as shown in Figures 12 and 13. In other words there were 50 to 60 active probe pairs at each saddle site.

A high frequency AC field (5000 Hz) was applied across the weld toe by means of five to six pairs of shielded lead wires which were placed far away from the weld toe (300 to 400 mm away) to provide a uniform AC field across the weld surface. In the absence of a crack, there is an initial potential drop across each probe pair: V_c across the active pair and V_r across the reference pair which satisfies the equation,

$$\frac{\Delta_r}{V_r} = \frac{\Delta_c}{V_c} \tag{1}$$

where Δ_r is the radial reference probe separation and Δ_c is the radial active probe separation.

After a crack develops at the weld toe, V_c will have changed to V_c' while V_r will have remained nearly the same at V_r'. This increase in V_c is due to the AC field having to conform to the surface of the steel because of its high frequency. Since the crack effectively increases the surface distance between the active probe pair, the resistance along that path is greater and consequently the voltage drop is greater. If the crack has a straight front, this increase in effective surface distance is related to the voltage drop by the following equation.

$$\frac{\Delta_r}{V_r'} = \frac{(2a + \Delta_c)}{V_c'} \tag{2}$$

where a is equal to half the increase in distance or crack depth. Combining equations (1) and (2) and solving for crack depth a gives:

$$a = (\frac{\Delta_c}{2})(\frac{V_c'}{V_r'} - \frac{V_c}{V_r}) \tag{3}$$

which is the equation used in the data acquisition software to obtain an approximate crack depth for on-line monitoring.

To use the ACPD results for predicting actual crack depths, apparent crack depths are corrected using a calibration function that compensates for the irregular crack development. This calibration function was obtained from the data base accumulated during earlier tests on T-plate joints. From the accumulated data base, plots of measured crack depth (from beachmarks and ink stains) vs. the indicated ACPD crack depth were generated, see Figure 14 for overview of data. Using linear regression analysis, a calibration curve was developed. This was a composite curve having different curves for initiation, coalescence and propagation. With this technique, cracks as small as 0.2 mm could be detected and deeper crack depths ascertained to within ±0.5 mm.

Details of the test setup, and the precautions to be taken to avoid electromagnetic loops during the data measurement and for line contacts during data analysis are given in Appendix 3.

Initial readings of alternating current potential difference (ACPD) of all the active and reference probes were taken and the ratios of active probe readings to reference probe readings stored in the disk; these ratios were utilized later to calculate the crack depth at various locations around the weld toe.

ACPD readings were taken at frequent intervals of load cycles. When the indicated crack depth from the computer printout was around 0.5 to 1 mm, ink was introduced into the indicated crack region, which later on would indicate crack initiation points, crack depths and shape around the weld toe region.

At different stages of crack propagation through the thickness of the chord wall, beachmarks were introduced using the following procedure. The ACPD readings were used to calculate an approximate crack growth rate $(\Delta_a/\Delta N)_c$ for that crack depth, a. This crack growth rate was used with the Paris equation to obtain a particular value of $C(\Delta K)^m$ where ΔK is the range of crack tip stress intensity factor and C and m are material parameters.

Using the required beachmarking depth Δ_a of 0.1 mm, and reducing the stress intensity factor at mean load to $\Delta K/2$, the approximate number of load cycles for beachmarking was obtained as

$$\Delta N = (0.1)(2^m/(\Delta_a/\Delta N)_c$$

since $C(\Delta K)^m = (\Delta_a/\Delta N)_c$. Keeping the mean load constant, the load range was reduced to half the actual test load range. Then the tubular joint was subjected to the computed loading cycles, at a frequency of 6 to 8 Hz, to obtain beachmarks. The ACPD readings were taken before and after beachmarking to determine the approximate growth in crack depth. If found to be insufficient the number of load cycles was further increased to obtain the desired crack depth extension.

2.4.2 DCPD Measurements at Waterloo

A schematic of the pulsed DCPD system used for this and earlier crack measurement studies on T-plates and pipe-plates [12,13] is shown schematically in Figure 15. The current is supplied by a DC power supply of 50 amp capacity; the polarity is switched approximately twice every second to counteract thermocouple effects and to eliminate the effect of amplified zero offset errors.

Current bars were fixed to the specimens as shown in Figure 15. The current bars were 6.25 $mm \times 50$ mm copper straps secured to the brace and the chord with large cinch clamps. The copper bar attached to the brace covered 900 mm of brace circumference. For the in-plane bending specimens, the copper strap attached to the chord covered 1200 mm of chord circumference and for the out-of-plane loading case, the copper bar was 1500 mm long. The chord material was ground smooth to provide for a good electrical contact between the copper bars and the steel. Prior to affixing the copper bars, the ground surfaces were coated with a high conductivity electrical grease to prevent surface corrosion and improve electrical conductivity.

Each specimen was fitted with 98 or 99 active probe pairs. Each active probe pair consisted of two probes straddling the weld toe with a span of 6.35 mm. Probe pairs were distributed along the weld toe with a separation (or pitch) of 6.4 mm for ± 400 mm about the crown or saddle centerline. The probes were 0.9 mm welding wire spot welded to the first weld bead and the chord material. The probes were distributed about the crown for the in-plane bending tests and the saddle for the out-of-plane tests, see Figures 16 - 18.

As shown schematically in Figure 19, reference probes were welded to the chord material 25.4 mm radially from the active probe on the chord material. It was not necessary to have a reference probe at every active probe location. About 26 reference probes were used on each specimen; they were used with every fourth active pair if strain gauges were not required at those locations.

The data acquisition system is shown schematically in Figure 15. The PRO380 computer sent a "probe pair" select signal to the amplifier which in turn selected the appropriate channel in the multiplexer switching box and timed the pulse signal from the power supply. The amplifier had a "track and hold circuitry" which sampled the voltage only during the last quarter of each half cycle before the polarity was switched. Sampling in the last 1/4 of each half cycle was done to allow sufficient settling time for the transients to die out. By the time the voltage sampling started the current field had reached steady state conditions. The procedure was repeated for the next half cycle until a stable high/low voltage was established. The maximum plus/minus voltages were amplified, measured and then subtracted to obtain the voltage signal which was relayed back to the computer where it was stored on the computer hard disk.

Specimen cycling was periodically stopped and the mean load applied when taking the potential drop readings. The computer selected all 126 crack and reference probe pairs in sequence, read and stored the information.

The cycle frequency at which DCPD readings were taken depended on the crack depth and how fast the cracks grew. On all specimens, initial readings were taken at 5000 to 7500 cycle intervals to document crack initiation. For the 250 MPa specimens this schedule was maintained for the whole test. However for the 160 MPa tests, beyond initiation the frequency of readings was reduced to 10000 to 20000 cycle intervals.

Figure 19 insets show schematically how the active probe voltage, V_c, and reference probe voltage, V_r, vary as a crack of depth, a, progresses through a chord wall of thickness, T. After N cycles, this crack depth is a_n and the voltages are V_{cn} and V_{rn}. If normalized voltage, V_{cn}/V_{rn}, is plotted against crack depth one obtains the curve shown in Figure 20. When there is no crack, the normalized voltage is often about 0.25 but can vary between 0.2 and 0.4. This variation is a function of weld reinforcement angle and the radial spacing of the probes.

To convert measured voltage changes to crack depth one needs a set of calibration curves equivalent to Figure 20. The calibrations curves were obtained using two dimensional aluminum foil analogues [12] having the geometry shown in Figure 19. Calibration curves were obtained for weld reinforcement angles from 20 to 60 degrees in increments of 10 degrees and for normalized crack depths, a/T, in increments of 0.05. The effect of variations from the desired (6.4 mm) probe spacing were also investigated using foil analogues. Since a replica of the actual weld profile in each tubular joint was made before fatigue testing, it was possible to define an appropriate calibration curve for each probe pair. The efficacy of this two dimensional calibration procedure will be demonstrated later by comparing DCPD predictions of crack depth with beachmark measurements.

3 Strain Gauge Measurements

In this study, estimates of hot spot stress and stress concentration factor were obtained from strain gauge measurements. Strain and stress definitions mentioned herein are explained in Appendix 1.

The strain gauge pattern used on each tubular was much more extensive than that required to define hot spot stress and stress concentration factor. These additional gauges were used to check symmetry of loading and to estimate stress variation around the chord/brace weld. For LEFM calculations it is necessary to estimate the stress variations through the chord wall. This was achieved by using strain gauges on the outside and inside surface of the chord tube.

As mentioned in the introduction, some of the NEL stiffened tubulars developed fatigue cracks in the stiffeners or stiffener welds. To assess the stiffener stressing in our tests, strain gauges were put on the stiffeners.

The strain gauges used on the Waterloo University T-Joint specimen were; Specimen TB1 - Micro measurements, temperature compensation (steel), rectangular rosettes, No. EA-06-250 RA-120. Specimens TB2- TB6, inclusive, were fitted with Showa Manufacturing Co. Ltd., temperature compensational (steel) delta rosettes No. N34-FA-2-120-11. The single filament axial gauges used on all specimens were Micro measurements temperature compensation (steel), No. EA-06-259BF-120.

At Memorial University the triangular 60° rosettes and uniaxial foil strain gauges used in the tests were manufactured by the "SHOWA" Measuring instruments Co. of Japan. The triangular rosette gauge type was N-34-FA-2-12-11 and the uniaxial gauge type was N11-FA-2-12-11 with a gauge length of 2.0 mm, resistance of 120 Ω and a gauge factor of $2.10 \pm 1\%$.

3.1 Axial Loading Tests at Memorial

A schematic diagram of the test rig, with the tubular in position is shown in Fig. 10. The tubular joint was mounted in the test rig horizontally. The end A of the chord was chosen arbitrarily on the left side as one looks in towards the chord from the brace end. The other end was denoted as B. Due to the symmetry of the specimen geometry and loading, crack initiation was expected to occur either at the top or bottom (hidden) saddle point. The bottom saddle point was chosen as 0° and the angular locations marked around the chord/brace intersection in an anti-clockwise sense (ie, the end A is at 270° the top saddle point is at 180° and the end B is at 90°). One quarter (270° to 360°) of the chord outside surface was instrumented extensively with three rows of triangular rosette strain gauges at 0°, 10°, 20°, 30°, 45°, 60°, 75° and 90°, respectively. The remaining three quarters of the chord surface were instrumented sparingly in order to check the symmetry of loading on the test specimen. Also, at both the crown and saddle points, two rows of triangular rosette strain gauges were mounted on the outside surface of the brace to obtain the stress concentration factors. Away from the welded zone, on the outside surface of the brace, uniaxial gauges were mounted to check the axiality of the loading as well as any variation in axial stresses due to variation in brace thickness along the circumference and the length. The inside chord surface was also instrumented with triangular rosette strain gauges at the same locations as on the outside surface. These locations were found using an ultrasonic flaw-detector with a transmitter on the ID and a receiver on the OD. One half of the stiffening ring below the brace was also strain gauged to monitor the strains in the ring. The schematic diagrams of locations and orientation of various gauges and the distances from the weld toe are shown in Figs. 21 to 24. A total of 88 to 135 strain gauge rosettes and 8 to 16 uniaxial gauges were used to obtain the stress distribution around the brace-chord intersection and in the stiffener ring.

3.2 In-plane and Out of Plane Bending Tests at Waterloo

Figures 16 and 17 show the strain gauge layout used for the in-plane bending tests on the unstiffened joint and the stiffened joints. Since the hot spot is at the crown, the angular measurements are made from the crown. These tubulars were subjected to repeated ($R = 0.05$) rather than reversed bending ($R = -1$) so only one of the crown areas was extensively strain gauged.

Figure 18 shows the strain gauge layout used for the out of plane bending tests. For this case the hot spot is at the saddle; since these tubulars were subjected to repeated bending ($R = 0.05$) only one of the saddle areas was extensively strain gauged.

As mentioned earlier, the test rig used at Waterloo could be used to apply axial brace loading if the actuators acted together. In this program, this function was only used during static tests to determine stress concentration factors for comparison with those obtained at Memorial. The loads used in these axial tests at Waterloo had to be kept low, particularly for stiffened joints, because the load cells available were only suitable to measure the much smaller forces applied with the bending configurations. Nevertheless useful data was obtained for all three modes of loading with the unstiffened joint and for two modes of loading (axial and IPB or axial and OPB) for each of the stiffened joints, TB2 to TB6. Additional strain gauges were added to some tubulars to obtain this axial loading data. A photograph of the external strain gauges and the PD probes on one of these tubulars is included as Figure 25. This photograph also serves to show a typical weld profile. Figure 26 shows the pattern of single gauges put on the stiffener rings.

4 Results and Discussion of Static Tests

4.1 Static Tests – Strain Gauge Data

4.1.1 Axial Brace Loading Tests at Memorial

Initial strain gauge readings were taken at zero load. Each specimen was loaded in increments up to 75% of the maximum load calculated to be necessary for the subsequent fatigue test. At each load increment the strain gauge readings were taken. The load was reduced back to zero. With zero load on the specimen, the strain readings were taken again to check for any residual strains. A small amount of residual strain was observed at this stage. From the observed readings, the maximum fatigue load to be applied to the tubular specimen was recalculated. The specimen was loaded up to 90% of this maximum load 3 or 4 times. In the last step, the load was again increased in increments to the maximum load, taking readings at every load step. After bringing the load down to zero, the residual strains were observed to be almost negligible.

Data sheets for each specimen, TA1 to TA5, are presented in tables in Appendix 4. These sheets contain a very small sample of the strain data gathered in these static tests plus a summary of estimates of hot spot strains and stresses, strain and stress concentration factors and the ratio of bending to membrane stress at the hot spot.

These data sheets have in turn been used to prepare a summary sheet, Table 3, for all of these axial brace loading tests. As expected there were some differences between the strains measured at the two saddle points, S1 and S2. These differences show as differences in the hot spot (saddle) stress level between the two sides of the chord of 5.9% for the unstiffened joint, TA1, and 8.2% (TA2), 10.2% (TA3), 5.2% (TA4) and 10.1% (TA5) for the stiffened joints; these differences are attributed to local variation in the weld geometry, non-uniform thickness of chord and brace due to fabrication and welding procedures. As shown in Appendix 4, there was a considerable variation of axial strain in the brace, due to local thickness variation; this must have contributed to the variation of the hot spot stresses at the saddle points. The ratio of the SCF/SNCF remained almost constant for the two saddle points, being 1.1 to 1.2 for the unstiffened

Table [illegible] Memorial University Static Test Results.

Specimen No. and environment	Maximum load (kN) and load ratio	Actual and nominal hot spot stress ranges (MPa)		Nominal brace stress range (MPa)	Stress concentration factor		Actual hot spot strain range ($\mu\epsilon$)		Nominal brace strain range ($\mu\epsilon$)	Strain concentration factor		Ratio of SCF/SNCF		Bending stress range at hot spot (MPa)		Ratio of bending stress to total stress at hot spot		Membrane stress range at hot spot (MPa)		Ratio of membrane stress to total stress at hot spot	
		side 1	side 2		side 1	side 2	side 1	side 2		side 1	side 2	side 1	side 2	side 1	side 2	side 1	side 2	side 1	side 2	side 1	side 2
TA1 (Air)	315 (0.16)	248 (250)	236 (250)	10	24.8	23	1020	966	47.3	21.6	20.4	1.2	1.1	2.0	214	0.84	0.91	41.1	22	0.16	0.10
TA2 (Air)	1065 (0.05)	253 (250)	233 (250)	39	6.4	5.9	969	897	184	5.3	4.9	1.2	1.2	182	163	0.72	0.70	71	70	0.28	0.30
TA3 (Air)	630 (0.05)	161 (160)	144 (160)	23	7.0	6.3	533	561	107	5.9	5.3	1.2	1.2	137	126	0.85	0.87	24	19	0.15	0.13
TA4 (Seawater with cath prot)	1125 (0.05)	242 (250)	255 (250)	41	6.0	6.3	952	985	141	5.0	5.2	1.2	1.2	194	196	0.80	0.77	49	59	0.20	0.23
TA5 (Seawater with cath prot)	660 (0.05)	144 (160)	160 (160)	24	6.0	6.7	567	625	112	5.0	5.6	1.2	1.2	113	120	0.79	0.75	30	40	0.21	0.25

joint and 1.2 for the stiffened joints.

These static tests on the unstiffened joint gave a stress concentration factor of 23.3 to 24.8. Adding two ring stiffeners reduced this stress concentration factor to 5.9 to 7.0. The corresponding values obtained by Lloyd's Register with acrylic models of the UKORSP II joint, see Figure 5, were 25 and 7.5. In static tests prior to fatigue testing the UKOSRPII specimens, NEL obtained stress concentration factors of 23.4 and 7 for unstiffened and stiffened joints. Overall the agreement between the three sets of data is very good and suggests that adding the two ring stiffeners in this position should increase the fatigue, axial load carrying capacity by a factor of about 24/7. Of course, this prediction depends on the assumption that hot spot stress range is as a good indicator of fatigue performance for stiffened joints as it is for unstiffened joints.

The maximum weld toe stresses in the chord along the weld toe were obtained by linearly extrapolating from the strain measurements of the first two rows of the gauges. These radial stresses at the weld toe and at gauge locations were normalized with respect to the corresponding maximum radial (hot spot) stress of each joint. These normalized radial stresses are shown in Figs. 27 to 31, over ±90° from the saddle point location. As can be seen, the stress distribution in the unstiffened joint (Fig. 27) is quite distinct from that in the stiffened ones (Figs. 28 to 31). In the unstiffened joint, the weld-toe stresses drop gradually from a maximum at the saddle point to a minimum at the crown points. In the stiffened joints, these stresses are almost constant over ±15° range from the saddle point and then drop to a minimum around ±30°. The presence of the stiffeners leads to a more uniform radial stress distribution, excluding the area directly over the stiffeners.

4.1.2 Axial, In-plane and out-of-plane bending tests at Waterloo

Strain gauge readings were taken on the unstiffened joint, TB1, for each mode of loading. During these static tests, the loads were limited so that the near weld strains never exceeded 50% of the values calculated for the subsequent in-plane bending fatigue test. Also the strain gauge readings obtained in these "static" in-plane bending tests were used to recalculate the load to be applied in the fatigue test. This fatigue load was applied for three cycles; during each cycle the load was increased incrementally and strain gauge readings were taken.

A similar procedure was followed for the stiffened joints, TB2 to TB6, except that only two "static" modes of loading were used for each joint. Strain gauge readings were taken during static cycles of axial load and during static cycles of in-plane or out-of-plane bending. During these static cycles, the loads were limited so that the near weld strains never exceeded 50% of the values calculated for the subsequent in-plane or out of plane bending fatigue test.

Data sheets for each specimen, TB1 to TB6, are presented in Appendix 4. Since these tubulars were subjected to repeated bending, a distinction is made between the hot spot where fatigue cracks will develop (positive stress and stress concentration factors) and the so-called "compressive" hot spot (negative stress and stress concentration factors). A comparison of these positive and negative SCF's is an indication of fabrication quality and loading symmetry.

Table 4 compares stress concentration factors for stiffened and unstiffened joints for the three modes of loading. As expected, see Figure 5, the stiffeners lead to a relatively small reduction in SCF for in-plane bending and substantial reductions in SCF for out of plane bending and for axial loading.

The reduction in SCF for out of plane bending, 17 reduced to 4.7, agrees well with the Lloyds prediction (Figure 5) of 17.5 reduced to 5.3. The reduction for in-plane bending, 4.3 reduced to 3.2 - 3.6, is also in reasonable agreement with the Lloyds prediction, 4.5 to 3.5. The reduction for axial loading, 24.1 to 6.2 - 6.9, is in good agreement with values obtained in the tests at Memorial, see previous section.

As mentioned earlier, NEL also carried out static tests on UKOSRPII specimens (Figure 3). Their results for three loading modes are compared in Table 5 with the data obtained at Waterloo. The agreement is good considering the difference in wall thickness, 16 mm compared to 19 mm, and scatter that one always expects when testing welded joints of this complexity.

Polar plots of normalized radial stress, equivalent to those shown in Figures 27 - 31, have been used to prepared Figure 32. This figure is an overview of the static tests at Waterloo. It is based on radial stresses obtained by linear extrapolation to the weld toe (See Appendix 1); therefore at the hot spots, the normalized radial stress is 1.0.

The Waterloo data for axial loading, Figure 32 (c), shows the same trend as the Memorial data, Figures 27 to 31. Introducing the stiffeners leads to a much more uniform radial stress distribution. However most of the change in distribution shape occurs outside the stiffeners. If the stiffeners limit surface crack length, the data on

Table 4: Waterloo Static Strain Gauge Test Results.

Specimen No. Mode of Loading Unstiffened or Ring Stiffened All Specimens Tested In Air		Max. Load $K N^{-m}$ Load Ratio (R) For All Specimens $M_{min}/M_{max} = 0.05$	Actual and (Nominal) Hot Spot Stress Range (MPa)		Actual Brace Stress and Strain Range		Actual Stress Concentration Factor SCF		Actual Strain Concentration Factor SNCF		Ratio of SCF/SNCF		Bending Stress Range At Hot Spot		Membrane Stress Range At Hot Spot		Ratio of Bending Stress to Total Stress $\sigma_B/(\sigma_B+\sigma_m)$		Ratio of Membrane Stress to Total Stress $\sigma_m/(\sigma_B+\sigma_B)$		Strength of Biaxial Stresses σ_θ/σ_R Gauges 13.2 mm from weld toe	
			Crack Side	Other Side	σ MPa	ϵ $\times 10^6$	Crack Side	Other Side	Crack Side	Other Side	Crack Side	Other Side	Crack Side	Other Side	Crack Side	Other Side	Crack Side	Other Side	Crack Side	Other Side	Crack Side	Other Side
TB1 Unstiffened	IPB	171 (Fatigue Test)	248 (250)	247 (250)	58.3	283	4.3	4.2	3.5	3.5	1.2	1.2	181	185	67	62.5	0.73	0.75	0.27	0.25	0.73	0.74
	OPB	Static Test Only	-	-	-	-	17.2	17.0	14.1	14.2	1.2	1.2	-	-	-	-	0.92	0.91	0.08	0.09	0.53	0.50
	Axial	Static Test Only	-	-	-	-	24.0	22.0	20.2	18.5	1.2	1.2	-	-	-	-	0.88	0.88	0.12	0.12	0.53	0.52
TB2 Stiffened	IPB	236 (Fatigue test)	246 (250)	231 (250)	81	392	3.0	2.9	2.4	2.3	1.3	1.3	180	172	65.8	59	0.73	0.75	0.27	0.25	0.75	0.76
	Axial	Static Test Only	-	-	-	-	6.1	6.1	4.9	5.0	1.3	1.2	-	-	-	-	0.77	0.76	0.23	0.24	0.7	0.65
TB3 Stiffened	IPB	149 (Fatigue test)	160 (160)	165 (160)	51.5	249	3.1	3.1	2.51	2.6	1.2	1.2	121	-	38.7	-	0.76	-	0.24	-	0.74	0.77
	Axial	Static Test Only	-	-	-	-	-	-	-	-	-	-	-	-	-	-	-	-	-	-	-	-
TB4 Stiffened	OPB	164 (Fatigue Test)	246 (250)	246 (250)	52	252	4.7	4.7	4.1	4.1	1.15	1.17	193	191	52.3	54.7	0.78	0.78	0.22	0.22	0.44	0.45
	Axial	Static Test Only	-	-	-	-	6.4	6.1	5.3	5.1	1.2	1.2	-	-	-	-	0.79	0.76	0.21	0.24	0.65	0.64
TB5 Stiffened	OPB	110 (Fatigue Test)	157 (160)	161 (160)	36	173	4.4	4.5	3.8	3.9	1.2	1.2	118	121	39	39	0.75	0.75	0.25	0.25	0.45	0.46
	Axial	Static Test Only	-	-	-	-	5.6	6.3	4.5	5.1	1.2	1.2	-	-	-	-	0.76	0.75	0.24	0.25	0.68	0.67
TB6 Stiffened	IPB	147 (Fatigue Test)	163 (160)	161 (160)	44.7	216	3.7	3.6	2.9	2.9	1.3	1.2	124	119	39	42	0.76	0.74	0.24	0.26	0.71	0.72
	Axial	Static Test Only	-	-	-	-	-	5.4	-	4.4	-	1.3	-	-	-	-	-	-	-	-	-	0.71

Mode of Loading	Unstiffened T-Joint		Stiffened T-Joint	
	Waterloo	NEL	Waterloo	NEL
In-Plane Bending CROWN	4.2	5.7	3.1	4.3
Out-of-Plane Bending SADDLE	17·1	22	4.7	5.2
Axial SADDLE	23.8	23.4	6·4	7.

Table 5. Comparison of SCFs at Waterloo and National Engineering Laboratories for T-Joints.

Figure 32(c) suggests that crack shape development for axial loading may be similar for the stiffened and unstiffened joints.

For out of plane bending, the stiffeners reduce the weld length over which the normalized radial stress is near unity; this occurs within the stiffeners so the surface growth in stiffened joints may be slower than in unstiffened joints.

For in-plane bending the stiffeners reduce the weld length over which the normalized radial stress is near unity. However the unstiffened and stiffened joints have a large weld length over which the normalized stress is near unity so both types of joints are likely to quickly develop fatigue cracks having a very low aspect ratio.

5 Results and Discussion of Fatigue Tests

In this report, the NEL (UKORSP) definitions [8] of the various stages of fatigue failure of tubular joints have been followed. These are

N_1 First discernable surface cracking as noted by any method available. This stage is considered to have passed if the initial surface crack length is found to exceed 20 mm. In the tests at Waterloo and Memorial, potential drop techniques have been used to define crack initiation (N_1). In the tests at Memorial an assessment was made of the so-called "10% drop in hot spot strain" method for defining N_1; this assessment (see 5.2.1.2) shows that this method is much less sensitive than the P-D method.

N_2 Intermediate surface cracking is detected by visual examination without the use of crack enhancement fluids or optical aids. This is not used herein. Instead potential drop data is used to define a life N_{co} at which the various cracks that have been initiated along the weld toe, coalesce to form one or two dominant cracks of irregular shape.

N_3 First through-plate thickness cracking. This was determined by periodic monitoring of the PD pairs and by visual, inspections of the inside of the tubular joint.

N_4 End of Test. For unstiffened joints this is usually dictated by loss of specimen stiffness which leads to unacceptable actuator stroke or side loads. For the stiffened joints tested in this program, the end of test followed soon after failure of the stiffeners.

It should be noted that the DOE guidelines [5] use a different nomenclature. The DOE definition of N_2 corresponds to N_3 used herein. The DOE design curves, Figure 2, are derived from fatigue life data for through-thickness cracking ie, equivalent to the N_3 data reported herein.

For these tests at Waterloo and Memorial, the hot spot stresses were always calculated from strain gauge measurements. Some of the specimens tested with axial loading developed fatigue cracks at both saddles. When plotting these results on S-N diagrams, the hot spot stress (S) used is for the side, which first developed a through thickness crack.

5.1 Failure Modes and Fatigue Life N_3

When unstiffened tubular T joints are subjected to cyclic loading, the fatigue cracks usually initiate at or near the hot spots at the weld toe on the chord tube. These very small cracks grow and soon coalesce to form a surface crack of low aspect ratio (crack depth/crack surface length) that then propagates through the chord wall. In all of the tests discussed herein this was the mode of failure. No cracks were detected in the ring stiffeners prior to N_3. As mentioned in the introduction, these ring stiffeners had machined inside and outside diameters and the welding procedure were designed to minimize the risk of weld ring cracking. In similar tests at NEL [8] two of three stiffened joints (G1) developed fatigue cracks at the flame cut inner diameter of the rings; these grew rapidly to give complete failure of the stiffeners at about 83% of N_3.

The fatigue lives (N_3) obtained in the tests at Memorial and Waterloo are compared on Figures 33 - 36 with the data obtained in these NEL stiffened joint (G1) tests, with data obtained previously in pipe-to-plate tests at Waterloo [14] and with fatigue curves derived using the DOE tubular data base and the DOE correction for thickness effect [5]. Figures 33 and 34 compare data for tests in air. Figures 35 and 36 compare data for tests conducted in seawater with free corrosion, or so-called optimum cathodic protection (-0.85 V Ag/AgCl) or cathodic overprotection (-1.1 V Ag/AgCl).

In the DOE guidelines, the basic (air design) S-N curve for tubular joints is defined as the mean 32 mm data curve less two standard deviations (2SD) based on the 16 mm data base [5]. The mean 32 mm data curve and the basic air design S-N curve are shown on Figure 33 for comparison with the aforementioned data sets. All of the tubular joint data obtained in the present program and the pipe-plate data lie within $\pm 2SD$ of the mean 32 mm data curve. One of the three NEL stiffened tubular (G1) joints had a life that lies more than +2SD beyond the mean 32 mm data curve.

The DOE curves shown on Figure 33 are derived from a data base which includes (mixes) data from tests with different modes of loading. It will be noticed that the fatigue lives (N_3) obtained in the present tests on tubulars with in-plane bending are noticably shorter than those obtained with out-of-plane bending or axial loading. It will be argued later that these life differences can be related to the effect that mode of loading has on crack shape development.

In the DOE guidelines, the correction for thickness effect is expressed as a factor on fatigue strength or a factor on life where

$$\text{Factor on Life} = (\frac{32}{t})^{3/4}$$

The minimum thickness to be considered in this equation is 22 mm. The effects of this correction factor are also are shown on Figure 33. In the present tests on stiffened tubular joints the wall thickness was 19 mm. In similar tests at NEL the wall thickness was 16 mm and in our tests on pipe-plate specimens, the plate was 25 mm thick. Figure 33 compares the NEL, Memorial and Waterloo experimental data with the mean and basic S-N curves corrected for a thickness of 22 mm; the maximum allowable in the DOE guidelines. All of the experimental (air) data lie above the 22 mm air design curve.

There is little evidence to support the DOE guideline that limits the thickness correction to $t \geq 22$ mm. In another part of the Canadian Offshore Steels Research Program [15], the thickness effect has been demonstrated in tests with plate thickness from 16 to 103 mm. Therefore the DOE thickness equation has been used to convert all of the data from Figure 33 to a common thickness of 19 mm and to derive a 19 mm air design line, which is a 19 mm mean minus 2SD as before. This approach, Figure 34, reduces the scatter but one of the NEL results still lies beyond + 2SD.

The DOE guidelines include a recommendation that the air design curves, Figure 2, also be used for cathodically protected joints of medium strength steel in seawater. A caution is given that over protection may be detrimental to fatigue life and a penalty factor of two on life is recommended for unprotected joints in seawater. Also there is no knee at 10^7 cycles in the design S-N curve for unprotected joints.

At Memorial, two stiffened joints with optimum cathodic protection were tested in synthetic seawater. At Waterloo, pipe-plate specimens were tested in seawater either without protection or with optimum cathodic protection or with cathodic overprotection. Figure 35 compares all of this environmental data (N_3) to DOE mean air curves and DOE air design curves for 32 or 22 mm. Here the stiffened tubular (19 mm) data should be compared to the DOE limit (22 mm) curve and the pipe-plate (25 mm) data to a DOE 25 mm curve (found by interpolation).

It will be noticed in Figure 35 that all of this environmental data lies below the mean air curves for 22-32 mm. In the pipe-plate studies the unprotected and overprotected specimens had lives that were factors of 2 to 3 less than specimens tested in air (see Figure 33 for air data). In the pipe-plate tests and in the present tests on stiffened tubular joints, N_3 for the tests in air were always higher than N_3 for tests with optimum cathodic protection. Nevertheless, the two stiffened tubular joints and two pipe-plate specimens tested with optimum cathodic protection had fatigue lives that lie above the appropriate air design line. This provides some support for the DOE guideline for joints with optimum protection but the present tests and much more extensive testing of plate-plate specimens [16] clearly indicates that optimum protection does not always restore in-air fatigue performance. Also the pipe-plate tests with over protection, Figure 35, serve to emphasize the caution included in the DOE guidelines about overprotection; here cathodic overprotection was worse than free corrosion from a fatigue viewpoint.

Figure 36 compares these sets of environmental data to mean and design curves for unprotected joints. These 22 mm curves have been derived from the DOE mean air and basic (design) curves by applying the thickness correction factor and a penalty factor of two on life for lack of protection. All of the experimental data lies above this design curve but almost all data still lies below the DOE mean curve for unprotected joints.

The potentials used in the plate-plate, pipe-plate and tubular joint fatigue tests of the Canadian Offshore Steel Research Program were the same as those used in most of the ECSC/UKORSP test programs. It is interesting to compare these test potentials with values obtained on platforms protected with sacrificial anodes. In a recent paper on the use of initial current density in cathodic protection design, Evans [17] mentions that most platforms in the North Sea are polarized to between -0.90 and -1.0V (Ag-AgCl). He lists the results of surveys after one year of Kotter (southern North Sea) drilling and production platforms. For the drilling platform the potential varied between -0.92 and -0.99 V and for the production platform the potentials varied between -0.92 and -0.99 V. While these potentials may be optimum from a corrosion protection and cost viewpoint [17], they may not be optimum from a fatigue viewpoint and probably do not restore the in-air fatigue performance. Hence the present debate on the need to review the DOE guidelines on fatigue of protected joints.

5.2 Crack Initiation and Crack Shape Development

The modes of loading and potential drop techniques used to monitor cracks were different in the Memorial and Waterloo tests. Therefore these results will be presented separately in sections 5.2.1 and 5.2.2, with comparisons where necessary in section 5.2.2 and an overview in section 6.

5.2.1 Axial Loading Fatigue Tests at Memorial

5.2.1.1 Comparison of Beachmarks and A.C. Potential Results

Inkstaining and beachmarking were used to determine the crack front shape development and to verify the ACPD crack depth predictions. Three to five beachmarks were introduced at different crack depths in the tubular joints tested in air. After the completion of each test, the cracked sections were broken open and the crack depth at each AC probe location measured using a travelling microscope. Since these tubular joints were subjected to axial loading, there were two saddle areas (Sides 1 and 2) where initiation might occur. For all joints except the joints TA1 and TA2, where the cracks penetrated the chord wall thickness on both sides, wall penetration occurred only on one side, viz., on side 2.

For joints tested in air (TA1 to TA3), the crack depths were computed from ACPD data, normalized with respect to the thickness of the chord, and compared with the beachmark measurements, See Figures 37 - 40. Also in these figures, ±5% variation about the beachmark readings are plotted for easy comparison. It can be seen from these figures that the ACPD technique predicts the crack depth with an acceptable accuracy. The largest errors occur near the ends of cracks where the ACPD technique overestimates the crack depth, due to the sharp transition in the nature of voltages sensed by the crack microgauge.

The earlier part of crack growth, is shown in Fig. 41 for the unstiffened joint, TA1. From this figure, the initiation and coalescence of the multiple-nucleated cracks to a dominant single crack can be seen. Figures 42 and 43 show the expanded view of crack initiation and coalescence for the stiffened joint TA2, tested at the nominal hot spot stress range of 250 MPa in air.

Figures 44 and 45 show the earlier portion of crack growth in the chord for side 1 and side 2 of the stiffened joint TA3, tested at a nominal hot spot stress range of 160 MPa in air. The cracks initiated on side 2 approximately 150 k cycles ahead of side 1. Crack growth was much slower on side 1 and the crack never grew through the thickness of the chord wall.

Figures 46 to 51 show similar curves for the joints tested in seawater, at a nominal hot spot stress range of 250 MPa (TA4) and 160 MPa (TA5), respectively. Even though there was not much difference between the initiation lives for the sides 1 and 2, the crack growth rate on side 1 was very low; again there was the crack growth through the wall on side 2.

5.2.1.2 Crack Initiation Lives (N_1)

Figures 37 to 51 show only a small sample of ACPD measurements. By reviewing the ACPD data for each probe it was possible to identify the weld toe locations (probes) where crack initiation was first detected. Figures 52 - 56 show for each side (saddle area) of each tubular, the data obtained from these "initiation site" probes. The data are presented as apparent crack depth, a, versus cycles. To obtain an initiation life, N_1, a second order linear regression analysis was used to obtain the best-fit curves shown on Figures 52 - 56. The initiation life, N_1, was defined as the number of cycles to produce an apparent crack depth, a, of 0.5 mm. These PD estimates of N_1 are summarized in Table 6.

The actual depth of a small surface crack when it is first detected by an ACPD probe obviously depends on its relative location to the probes. It has been estimated [11] that a 0.1 mm deep crack might be detected if a probe pair happened to be located at the middle of the surface length of the crack. If the nearest probe pair happened to be not over the crack or not over the crack centre, the sensitivity is lower. An examination of ink stains and PD data obtained in plate-plate fatigue tests [13] indicates that this probe layout and equipment was likely to detect surface cracks with a depth of 0.5 mm; Figures 52 - 56 show that cracks were detected before they reached the 0.5 mm apparent depth for defining N_1.

In some of the ECSC programs, strain gauges near the hot spot were used to detect

Table 6: Crack Initiation Lives Obtained from ACPD and 10% Strain Drop Readings

Specimen	Crack initiation life from potential drop readings (kilo cycles)		Crack initiation life from 10% strain drop (kilo cycles)	
	Side 1	Side 2	Side 1	Side 2
TA1	N/A	103.0	180.0	125.0
TA2	142.3	115.0	260.0	212.0
TA3	440.0	300.0	635.0	450.0
TA4	39.0	35.5	N/A	N/A
TA5	285.0	252.0	420.0	330.0

crack initiation. Figures 57 to 60 show the strain history for saddle point strain gauges, that were 13.2 mm away from the weld toe. At the cracked side, the strain drops rather early. This occurs because the strain gauge comes into the "strain-shadow" of the crack, which develops between the strain gauge and the weld. This decrease even reversed the strain from tension to compression. However if crack initiation does not occur directly in front of the strain gauges at the saddle points, the crack does not affect the saddle strain gauge at all.

As the hot spot crack grows, the load has to be transmitted by the cracked ligament; this may sometimes increase the strain away from the hot spot. As soon as the crack grows deeper the surface strain decreases. This reduction occurs in a gradual manner till breakthrough occurs. The crack initiation cycles (N_1) determined from 10% drop in the strain at the hot spot location gives more scatter in the data for initiation lives and overestimates the crack initiation life compared to ACPD estimates, see Table 6 and Figure 61.

5.2.1.3 Comparison of Fatigue Lives N_1, N_3 and N_4

The smaller of the PD estimates of initiation life, N_1, from Table 6 are compared in Table 7 with the number of cycles, N_3, to produce a through-thickness crack and the number of cycles, N_4, at which the fatigue test was terminated.

Frequent monitoring of the ACPD probes and inspection of the inside of the tubular joint proved to be a very effective technique for detecting through thickness cracking (N_3). For the in-air tests, the development of a plastic ligament (line) prior to breakthrough served to focus the inspection. For the seawater tests, leakage was soon obvious.

Table 7: Fatigue Lives

Specimen	ACPD Initiation life N_1	Breakthrough life N_3	End of test N_4	$\frac{N_1}{N_3}$	$\frac{N_4}{N_3}$
TA1	103,000	665,000	890,000	0.16	1.34
TA2	115,000	411,600	630,650	0.28	1.53
TA3	300,000	1,348,900	1,766,800	0.22	1.31
TA4	35,500	142,300	161,000	0.25	1.13
TA5	252,000	540,000	652,000	0.47	1.21

The number of cycles, N_4, at which the test was stopped was very dependent on the crack development in that particular specimen. This affected actuator control, leakage of seawater and sometimes led to significant mechanical noise. For the stiffened joints, crack propagation through the stiffeners soon led to control and/or noise problems and a decision to terminate the test.

The actuator displacement was monitored, during the progress of the tests on stiffened joints. This displacement was normalized with respect to the displacement obtained when no crack was present and the plots are shown in Figs. 62 to 65. The figures show that there was no appreciable increase in the displacement of the actuator until the end of the tests on stiffened joints.

Table 7 lists the ratio of ACPD initiation life, N_1, to N_3. Except for specimen TA5, the ratio N_1/N_3 falls within the range reported for other tests on tubular (unstiffened) joints [18]. In their tests on three joints with simple ring stiffeners (G_1 type), NEL report N_1/N_3 ratio of 0.35, 0.56, and 0.05 where N_1 was determined using miniature strain gauges and an eddy current NDT technique; "When crack growth had been established, ACPD equipment was introduced as required to quantify crack depth" [8].

The N_1/N_3 ratio in Table 7 and Figures 52 - 56 show that small cracks developed early in the fatigue life of these tubular joints and provide some support for the argument [10] that it may be useful to develop an alternative life prediction method using linear elastic fracture mechanics (LEFM) methodology. To develop such a method and/or to develop an LEFM method for predicting the residual life (N_R) of joints found to contain cracks during in-service inspection, requires an understanding of crack shape development and the influence, if any, of stiffeners on crack shape development. This aspect is addressed in the next two sections.

5.2.1.4 Stiffener Failure

In all of these axial loading tests, through-thickness cracking of the chord occurred sometime before the fatigue cracks propagated into and through the stiffeners. Since the end of test (N_4) followed soon after stiffener failure, the ratio N_4/N_3 in Table 7 indicates that there was always some margin, 13 to 53%, between through-thickness cracking and stiffener failure.

In two of the three tests on similar joints (type G1) at NEL [8], cracks initiated at the flame cut inner diameter of the ring stiffeners and grew rapidly to produce complete failure of the stiffeners at about 83% of N_3. As Holmes et al [8] say in their paper this "casts doubt on the applicability of the hot spot stress approach to (design) ring stiffened tubular joints". To understand their problem one requires information on the stressing of such stiffeners. In the present tests, strain gauges were put on the stiffeners and monitored periodically. Normalized stress distributions for the inside surface (ID) of a stiffener are shown in Figures 66 to 69; these circumferential stresses are normalized with respect to the hot spot (radial) stress at the dominant saddle position (S1 or S2). Only slight changes occurred in these stiffener stresses as the fatigue cracks grew through the chord wall. However the range of these stiffener stresses at the 90° (270) positions was about 0.8 of specified minimum yield for the tubular joints tested at the higher hot spot stress range (nominally 250 MPa). If the inside surface of the stiffeners in these tubulars tested at 250 MPa had been flame cut rather than machined it is possible that they would have failed by fatigue from this flame cut surface as did the stiffeners in the two NEL joints tested at even higher hot spot stress ranges (307 and 377 MPa). This type of failure did not occur in the NEL joint tested at a hot spot stress range of 206 MPa.

This analysis of fatigue stresses in the stiffener rings indicates that it would be wise to specify that the inside surface of the rings be machined. Flame cut rings may not fail before N_3 if the service loading on the joint produces hot spot stresses significantly lower than those used in the higher stress tests in the NEL program. However as Holmes et al [8] point out "failure of ring stiffeners in service would be difficult to detect and probably impossible to repair" so machining the rings appears to be a good investment.

5.2.1.5 Crack Shape Development and Stress Distribution

The beachmarks and/or ACPD estimates of crack shape, (see Figures 37 to 51) have been combined with the stress distributions, Figures 27 to 31 obtained from strain gauge measurements, to produce Figures 70 to 75. Since there were strain gauges on the inside and outside of the chord, it was possible to split the normalized radial stress at the weld toe into membrane and bending components. Figures 70 - 75 shows the so-called total (normalized radial) stress distribution with a value of 1.0 at the hot spot at the saddle. At all locations around the weld toe, the bending component dominates (80% of total) so this bending distribution is also plotted on Figures 70 - 75. The difference between the total and bending stress distribution is shaded since this gives a visual indication of the membrane stress component.

The polar plot used to show these estimates of weld toe stress has also been used to replot crack shape development. The first crack profile on Figure 70 is based on inkstain measurements; the other profiles are based on beachmarks since this unstiffened joint was tested in air. As expected [10] small surface cracks developed in the saddle area and coalesced to form a surface crack of low aspect ratio. In all cases, Figures 70 to 75, the coalescence into an irregular surface crack of low aspect ratio occurred at depth of about 3 to 4 mm.

By examining the ACPD records it was possible to estimate when this coalescence phase ended. Table 8 lists these estimates of coalescence life (N_{co}) for comparison with initiation life (N_1) and through thickness cracking (breakthrough) life (N_3). Table 9(a) shows the coalescence phase of crack propagation, $N_{co} - N_1$, and the ratio of this phase to $N_3 - N_1$, which is the propagation life, N_p.

The coalescence phase, $N_c - N_1$, is a significant fraction of N_p; it has already been shown [19,20] that inadequate recognition of this in LEFM models can lead to poor estimates of fatigue life, N_p, and confusion when interpreting fatigue data on thickness effects.

After coalescence, ie, after an irregular surface crack of low aspect ratio had developed, in the unstiffened joint there was growth through the wall and along the surface; In the stiffened joints the surface crack growth prior to N_3 was limited by the stiffeners, Figures 71 to 75. In the higher (250 MPa) stress tests the cracks initiated over a much wider portion of the weld toe, viz., ±30° degrees. It was observed that as the crack grew through the thickness, the stress distribution in between the stiffeners

Table 8: Memorial University Fatigue Data Initiation, Coalescence and Breakthrough.

Specimen	Load type	Hot Spot Stress range (MPa)				Environment	N_1 Initiation life (k cycle)		Ratio of Initiation to breakthrough life		N_{CO} Coalescence life (k cycle)		Ratio of Coalescent to breakthrough life		N_3 Breakthrough life (k cycle)	
		side 1		side 2												
		Nominal	Actual	Nominal	Actual		side 1	side 2	side 1	side 2	side 1	side 2	side 1	side 2	side 1	side 2
TA1	Axial	250	250	250	236	Air	N/A*	103	N/A*	0.16	N/A*	140	N/A*	0.21	N/A*	665
TA2	Axial	250	253	250	233	Air	142	115	0.346	0.26	240	240	0.58	0.54	411.6	441
TA3	Axial	160	160	160	144	Air	440	300	–	0.22	1040	580	–	0.43	N/A**	1348
TA4	Axial	250	242	250	255	Seawater	39	35	–	0.25	122.2	71	–	0.50	N/A**	142
TA5	Axial	160	144	160	160	Seawater	285	252	–	0.47	472.4	319	–	0.60	N/A**	540

- * The ACPD probe readings were defective.
- ** The crack did not breakthrough the wall thickness.

change considerably, whereas the change in the stresses beyond the stiffener locations was minimal.

5.2.1.6 Crack Growth Rate

ACPD measurements of the variation of crack depth with cycles are presented in Figures A5-1 to A5-21 in Appendix 5 for particular probe positions. These are for either the position where crack initiation was first detected or the position (dominant) where eventually the crack depth was maximum. The angular positions of these "initiation" or "dominant" probes are given in the captions of these figures. Also the captions for the "initiation" probe indicates the distance from the saddle point at which initiation was first detected. From the crack growth data for these locations, crack growth rates were calculated using a sliding seven point difference formulation. The crack growth rates as a function of crack depth/thickness ratio, are given in Figures A5-22 to A5-35 in Appendix 5.

For an overall comparison, crack growth and crack growth rate curves for the saddle point are shown in Figures 76 and 77 for all the joints. Examination of these crack growth and crack growth rate curves shows that through almost 70% of the wall thickness ($a = 2.5 - 15.5$mm), cracks grow at an almost constant rate. For shorter cracks, the growth rate after initiation period increases sharply as the multiple cracks coalesce into a single dominant crack. Crack growth slows down before the dominant crack breaks though the wall.

The crack growth rates in the joints tested with optimum cathodic protection in seawater are higher than those measured in joints tested in air at the same hot spot stress level. This reduction in propagation life was expected; it has been argued that optimum cathodic protection tends to restore or enhance the initiation life compared to in-air values but that cathodic protection tends to reduce propagation life, particularly if overprotection is used. This increase in crack growth rate is usually attributed to hydrogen effects at the tip of the fatigue crack [16].

5.2.2 In-plane and Out of Plane Bending Fatigue Tests at Waterloo

5.2.2.1 Comparison of Beachmarks and DCPD Data

Figures 78 to 82 compare crack depths obtained from beachmarks (solid lines) with

DCPD measurements for each probe location. To give a visual indication of the accuracy of the DCPD predictions, a ±5% variation about the beachmarking is shown as chain-dot lines. In almost all cases the agreement between DCPD predictions and beachmarks is excellent. This comparison is not made for TB3; this specimen was overloaded accidentally after initiation had occurred and it was decided to not cut out the crack for post-mortem examination.

5.2.2.2 Crack Initiation Lives (N_1)

Figures 78 to 82 show only a small sample of DCPD measurements. By reviewing the DCPD data for each active probe pair, it was possible to identify the weld toe locations ("initiation" probes) where crack initiation was first detected. Since these tubular joints were subjected to repeated bending, in-plane or out of plane, it was known that fatigue cracks would develop at or near the "tension" hot spot on each joint. Figures 83 to 88 show for each joint the data obtained from the "initiation" probes. The data is presented as apparent crack depth, a, versus cycles. The initiation life, N_1, was defined as the number of cycles to produce an apparent crack depth "a" of 0.5 mm at this initiation probe location. Figures 83 to 88 show very clearly that the "initiation" probes detected a change in potential long before the apparent crack depth of 0.5 mm was reached. It has been estimated that the probe layout and spacing used in this and earlier studies on plate-plate and pipe-plate specimens is likely to detect small surface cracks with a depth of about 0.5 mm [13].

These DCPD estimates of initiation life, N_1, are compared in Table 9(b) with the number of cycles, N_3, to produce a through thickness crack and the number of cycles, N_4, at which the fatigue test was terminated. As in the axial loading tests at Memorial, the PD monitoring and visual inspection of the inside of the chord tube proved to be a very effective way for detecting through thickness cracking, N_3. N_4 followed soon after the cracks had propagated through the stiffeners. Plots of normalized brace deflection vs crack depth are presented in Figures 89 to 93. There was a noticeable increase in brace deflection in the unstiffened joint as the crack broke through the chord wall. There was little or no increase in brace deflection in the stiffened joints as the crack broke through the wall.

In these tests at Waterloo (Table 9(b)) and the axial loading tests at Memorial (Table 9(a)), the same apparent crack depth (0.5 mm) was used to define N_1. In the

Table 9(a): **Benchmark Cycle Points for Waterloo Specimens.**

N_1 = Crack Initiation Defined by DCPD Apparent Crack Depth 0.5 mm
N_2 = Not Applicable
N_3 = Through Thickness Cracking
N_{CO} = Cycles at Which Multiple Small Cracks Coalesced to Form One or Two Single Cracks From Start of Test
N_C = $N_{CO} - N_1$ = Number of Cycles in Coalescence Process
N_P = $N_3 - N_1$ = Total Number of Propagation Cycles
N_S = $N_3 - N_{CO}$ = Propagation of Single Low Aspect Ratio Crack

Specimen Loading Mode $\Delta\sigma_{HS}$ Unstiffened/ Stiffened	Initiation $N_1 \times 1000$ Cycles Apparent Crack Depth $a \approx 0.5$ mm		Cycles at Which Crack Coalesced From Start Of Test $N_{CO} \times 1000$		Cycles in Crack Coalescence Process $N_C = (N_{CO} - N_1) \times 1000$				A_{co} mm (Approximate)	Through Thickness Cracking From start Of Test $N_3 \times 1000$ Cycles	Total Propagation Life $N_P = (N_3 - N_1) \times 1000$ Cycles		Cycles in Single Crack Propagation $N_S = (N_3 - N_{CO}) \times 1000$		
	N_1	N_1/N_3	N_{CO}	N_{CO}/N_3	N_C	N_C/N_3	N_C/N_P	N_C/N_s			N_P	N_P/N_3	N_s	N_s/N_3	N_s/N_P
TB1 IPB 248 Unstiffened Air	99	0.42	146	0.62	47	0.20	0.35	0.53	2.3	235	136	0.58	89	0.38	0.65
TB2 IPB 246 Stiffened Air	54	0.27	108	0.55	54	0.27	0.36	0.57	2.6	202	148	0.73	94	0.47	0.64
TB3* IPB 160 Stiffened Air	82	0.18	** -	-	-	-	-	-	-	*** 470	388	0.83	—	-	-
TB4 IPB 256 Stiffened Air	86	0.26	127	0.4	41	0.13	0.17	0.21	2.6	325	239	0.74	198	0.61	0.83
TB5 OPB 157 Stiffened Air	328	0.16	496	0.24	167	0.08	0.09	0.1	2.7	2111	1783	0.85	1616	0.77	0.91
TB6 IPB 163 Stiffened Air	256	0.37	393	0.57	137	0.2	0.32	0.46	2.6	690	434	0.63	297	0.43	0.68

* Specimen Accidently Overloaded.
** Specimen Not Cut Open. No Inkstain or Beachmark Data.
*** Total Life Based on Extrapolation From Propagation Data From TB6.

Table 9(b): Benchmark Cycle Points for Memorial Specimens.

N_1 = Crack Initiation Defined by DCPD Apparent Crack Depth 0.5 mm
N_2 = Not Applicable
N_3 = Through Thickness Cracking
N_{CO} = Cycles at Which Multiple Small Cracks Coalesced to Form One or Two Single Cracks From Start of Test
N_C = $N_{CO} - N_1$ = Number of Cycles in Coalescence Process
N_P = $N_3 - N_1$ = Total Number of Propagation Cycles
N_S = $N_3 - N_{CO}$ = Propagation of Single Low Aspect Ratio Crack

Specimen Loading Mode $\Delta\sigma_{HS}$ Unstiffened/ Stiffened	Initiation $N_1 \times 1000$ Cycles Apparent Crack Depth $a \approx 0.5$ mm		Cycles at Which Crack Coalesced From Start Of Test $N_{CO} \times 1000$		Cycles in Crack Coalescence Process $N_C = (N_{CO} - N_1) \times 1000$				A_{co} mm (Approximate)	Through Thickness Cracking From start Of Test $N_3 \times 1000$ Cycles	Total Propagation Life $N_P = (N_3 - N_1) \times 1000$ Cycles		Cycles in Single Crack Propagation $N_S = (N_3 - N_{CO}) \times 1000$		
	N_1	N_1/N_3	N_{CO}	N_{CO}/N_3	N_C	N_C/N_3	N_C/N_P	N_C/N_s			N_P	N_P/N_3	N_s	N_s/N_3	N_s/N_P
TA1 Axial 236 Unstiffened Air	103	0.17	140	0.23	37	0.06	0.07	0.8	3-4	603	500	0.83	463	0.77	0.93
TA2 Axial 253 Stiffened Air	115	0.28	240	0.58	125	0.3	0.42	0.73	3-4	412	297	0.72	172	0.42	0.58
TA3 Axial 144 Stiffened Air	300	0.22	580	0.43	280	0.21	0.27	0.36	3-4	1349	1049	0.78	769	0.57	0.73
TA4 Axial 255 Stiffened Seawater	0.36	0.25	71	0.5	35	0.25	0.33	0.5	3-4	142	106	0.75	71	0.5	0.66
TA5 Axial 160 Stiffened Seawater	252	0.47	319	0.6	67	0.12	0.23	0.3	3-4	540	288	0.53	221	0.41	0.77

five in-plane or out of plane bending tests in air, the ratio of N_1/N_3 varied between 0.16 and 0.42. In the three axial tests in air, the ratio of N_1/N_3 varied between 0.17 and 0.28. In the two axial tests with cathodic protection in seawater, the ratio of N_1/N_3 varied between 0.25 and 0.47.

Some of the scatter in these values of N_1/N_3 occurs because PD measurements were made at point locations along the weld. If the nearest probe pair is not over the initiation site or over the centre of the initiated crack, the PD sensitivity is lower. Another cause of scatter must be the variation in weld toe profile along the weld. This characteristic of the welding process has been examined in detail in other parts of the Canadian program [21]. These profile variations, other weld toe defects [22] and (normal) fabrication tolerances explain why small cracks develop at various locations along the weld toe. The detailed plots of potential drop (apparent crack depth) vs cycles shown in Figures 52 to 56 and in Figures 83 to 88 indicate that the first small cracks develop significantly earlier than the N_1 ($a_1 = 0.5$ mm) values reported in Tables 7 and 9(b). In other words crack propagation was the dominant phase in all of the present fatigue tests on unstiffened and stiffened joints. Another indication of the nature and extent of the early part of this crack propagation phase has been obtained from the inkstains made in the tests at Waterloo. This and the later stages of crack development will now be examined.

5.2.2.3 Crack Shape Development

The size and shape of the inkstains are shown in Figures 94 to 113. These microscope measurements (solid lines) are shown with ±10% bounds (chain dot lines). These inkstains were made sometime after many of the PD probes had detected crack growth. Therefore these figures also show DCPD estimates of crack depth as (—·—) lines. Four figures are used to show the early crack development for each tubular; each figure shows one quarter of the crack length. For example Figures 94 to 97 show the early crack development for the unstiffened tubular joint TB1. The inset diagram on the first of each set of four figures, eg., Figure 94, shows how the set of figures map the crack front.

Since the PD measurements are made at discrete points along the weld toe, the PD estimates of crack shape are smoothed versions of the actual profiles. The inkstains show that initiation occurred at various points along the weld toe and that these small cracks grow independently for sometime. The PD measurements tend to hide this multiple initiation and at the same time underestimate maximum crack depth.

As the crack deepens the PD measurements become more accurate; see earlier comparisons of PD measurements and beachmarks in Figures 78 - 82. Overviews of PD estimates of crack shape development are presented in Figures 114 to 124 for tubular TB1 to TB6. In all cases except TB3, which ended prematurely because of overloading, two figures are presented for each tubular. The first of these two figures show crack development to a maximum depth of 5 mm; the other figure shows crack development throughout the chord wall.

These measurements of inkstains, beachmarks and PD estimates of crack shape have been used to prepare plots of crack aspect ratio (maximum crack depth /crack surface length) against crack depth for each tubular. These figures, 125 - 130, also show abscissa scales of normalized crack depth (a/T) and normalized propagation life ($N - N_1/N_3 - N_1$). Most of the data shown for $a < 4$ mm was obtained from inkstains; as mentioned earlier, the DCPD technique tends to smooth the crack shape in the early stages of crack development.

Figures 125 - 130 show that a single crack of low aspect ratio (≈ 0.05) was fully developed in these tubulars by the time the (maximum) crack depth was 4 mm. Figures 125 - 130 also show the estimates of coalescence life, N_{co}, for these tubulars. These estimates are compared in Table 9 (a and b) with similar estimates for the tubulars tested with axial brace loading at Memorial. In all cases coalescence into one or two dominant cracks had occurred when $a < 4$ mm and this coalescence phase accounted for 7 to 42% of the propagation phase. Some of this large variation in the estimates of this coalescence phase occurs because of difficulty in interpreting the data ie, defining dominant cracks. Some of this variation must also occur because of the role that local weld toe geometry and defects play in the crack initiation process [22].

By including or excluding (accelerating) the coalescence phase in LEFM models, it should be possible to obtain upper and lower bounds on N_P. From a design viewpoint the lower bound is of more interest and it might be possible to obtain this with LEFM (propagation) evaluation for a crack of fixed, low (say 0.05) aspect ratio.

This modelling problem is discussed in some detail in a paper by Burns et al [10]. In that paper it was argued that differences between the stress fields for axial and in-plane bending loading of unstiffened joints would lead to differences in crack shape development and life. It was argued that differences in stress field would influence both coalescence behaviour and the subsequent development of the dominant crack present from a/T of 0.2 or thereabout. When ring stiffeners are present, they change the stress field and may also act as barriers on crack length. The effects of mode of loading and stiffeners on crack shape development will now be examined. The crack development in the in-plane and out of plane bending tests at Waterloo will be compared with the axial brace loading tests at Memorial, See section 5.2.1.5.

5.2.2.4 Effect of Stiffeners on Crack Shape Development

As discussed earlier there are very noticeable differences between the out of plane and in-plane bending stress fields. These stress fields are shown on Figures 131 to 135 together with polar plots of crack shape development. As with the data for axial loading, Figures 70 to 75, normalized stress distributions are shown for extrapolated 'total' radial stress and the bending component of this stress. The difference (area) between the total and bending stress distributions is shaded since this gives a visual indication of the membrane component.

First compare the polar plots for an unstiffened joint subject to axial loading, Figure 70, and an unstiffened joint subject to in-plane bending, Figure 131. Here the differences in stress distribution are very obvious and the in-plane bending crack clearly develops over a longer arc of weld as discussed in [10].

Next compare the polar plots for stiffened joints subject to axial loading in air, Figures 71 - 73, and similar joints subjected to in-plane bending in air, Figures 131 and 132. In some of these cases, the stiffeners rather than the shapes of the stress distributions seem to be limiting crack growth along the surface.

Finally compare the plots for stiffened joints subject to out of plane bending, Figures 133 and 134, and similar joints subjected to in-plane bending. Figures 131 and 132. Again the stiffeners rather than the shapes of the stress distributions seem to be limiting crack growth along the surface. However there is a clear indication that cracks of lower aspect ratio develop with in-plane bending.

5.2.2.5 Crack Growth Rate

In some of the axial loading tests at Memorial there was a very noticeable drop in crack growth rate as the crack propagated through the last few millimetres of the wall thickness (see Figure 77). In both of the out of plane bending tests on stiffened joints this slow down was very noticeable.

Figure 136 compares DCPD measurements of the variation of crack depth with cycles for all of the tubulars tested at Waterloo. Both of the stiffened joints subjected to out of plane bending show a marked change in behaviour when the crack was about 16 mm deep. The effect on the joint tested at the lower hot spot stress (157 MPa) was very significant. It led to a very large increase in N_3 which in turn influences the N_1/N_3 and N_c/N_3 values discussed earlier.

The crack depth vs cycles data shown in Figure 136 for the "initiation" probes has been used to prepare crack growth rate vs crack depth curves. Figures 137 to 142. These figures, which should be compared with figures in Appendix 5 for the axial loading tests, show very clearly an order of magnitude drop in crack growth rate when $a \geq 16$mm in the out of plane bending tests. This drop in growth rate was accompanied by a change in crack propagation angle, which has been observed in other tests on tubular joints and was very noticeable in pipe-plate tests when $a/T > 0.8$ [12]. Examination of the failure surfaces of these out of plane bending specimens suggests that crack turning may start near the stiffeners and as the maximum crack depth increases this turning (mode change) tendency spreads toward the hot spot position. It is very clear that the order of magnitude drop in crack growth rate at points near the hot spot position coincides with a significant change in propagation angle.

5.2.2.6 Stiffener Stresses

None of the stiffeners in these tubulars, subjected to in-plane or out of plane bending, failed prior to N_3. However the strain gauge measurements indicate that the stiffener stresses were high for out of plane bending and emphasize the need for machined rather than flame cut surfaces.

The strain gauge data has been used to prepare the normalized stress distributions shown in Figures 143 to 146. In these polar plots, the circumferential stress on the inner diameter (ID) of the stiffener ring is normalized with respect to its value at some angular position (0/360° for in plane bending and 315° for out of plane bending). In some cases these figures also show estimates of circumferential stress on the outside diameter of the chord over the stiffener ring.

Figure 143 is for tubular TB2 subjected to in-plane bending. In this case the ID circumferential stress at the angular position 0/360° was only 0.33 of the hot spot stress at the crown of the brace/chord weld. At the 55° and 305° angular positions, the circumferential stress at the stiffener ID reaches a maximum of about 2 × 0.33 of the hot spot stress.

Figure 145 is for tubular TB4 subjected to out of plane bending; a similar picture was obtained for TB5 (Figure 146). At the angular position 40°, the ID circumferential stress was -0.71 of the hot spot stress at the saddle (tension) of the brace-chord weld. At about 330°, the stiffener stress was almost 1.8 × 0.63 of the hot spot stress. For TB5 the corresponding value was about 1.8 × 0.64. These estimates indicate that there were high cyclic stresses (0 to 284 MPa) at the ID of the **machined ring** when the hot spot stress cycled from about 0 to 250 MPa as it did in TB4. If the ID of the stiffeners in TB4 had been flame cut it is possible that the stiffeners would have failed before N_3.

6 Summary and Conclusions

This test program on T tubular joints with two internal ring stiffeners was designed to compliment and extend a UKOSRPII fatigue test program at NEL [8] on such joints and to tie in with a project of Lloyd's Register [7] on the stress analysis of stiffened joints.

One unstiffened joint (TA1) and four stiffened joints (TA2 to TA5) were fatigued with constant amplitude, axial brace loading. The unstiffened joint TA1 and two stiffened joints (TA2 and TA3) were tested in air at 3-4 Hertz to provide a direct comparison with the UKOSRP/NEL test program on similar (type G1) joints. The other two stiffened joints (TA4 and TA5) were tested with optimum cathodic protection (-0.85 V Ag/AgCl) in artificial seawater at 5 ± 2°C and a frequency of 0.2 Hz.

One unstiffened joint (TB1) and three stiffened joints (TB2, TB3 and TB6) were tested with constant amplitude in-plane bending in air at about 3 Hz. Two stiffened joints (TB4 and TB5) were tested with constant amplitude, out of plane bending in air at about 3 Hz.

All eleven joints were subjected to repeated loading ($R \approx 0$) after extensive studies with strain gauges of the stress distributions around the brace/chord weld. Potential drop techniques were used to detect the initiation of small cracks (apparent depth of 0.5 mm) at or near the hot spots. Beachmarking and potential drop measurements were used to monitor the development of the fatigue crack along the brace/chord weld and through the thickness of the chord tube.

The stress concentration factors at the hot spots of these joints are generally in good agreement with values obtained by Lloyd's Register using acrylic models and with values obtained at NEL with their type G1 joints, prior to fatigue testing. The introduction of two single ring stiffeners as shown in Figure 4, reduces the stress concentration factor from about 24 to 7 for axial loading and from about 17 to 5 for out of plane bending. As expected the reduction in stress concentration factor for in-plane bending was much less; 4 reduced to 3.

The usual criterion for defining the fatigue life of a tubular joint is the number of cycles (N_3) to produce a through thickness crack in the chord. This life definition and the hot spot stress are the parameters used in the UK Department of Energy (DOE) guidelines when deriving an air design (basic) fatigue curve. This design curve includes an allowance for scatter but other factors must be applied to allow for thickness effects and for the detrimental effect of operating in seawater without cathodic protection.

The fatigue data (N_3) obtained in this test program have been compared to DOE design curves, Figures 33, 35 and 36. In all cases the data lies within the ±2 Standard Deviation (SD) scatterbands used in the derivation of the DOE curves. This demonstrates that this hot spot fatigue design procedure is suitable for T tubular joints with two simple ring stiffeners.

The two stiffened tubular joints tested with optimum cathodic protection in seawater had fatigue lives that lie above the appropriate air design curve. This provides some support for the DOE recommendation that the air design line be used for joints with cathodic protection. However an analysis of potential drop data to obtain crack growth rates shows very clearly that crack growth rates were significantly higher in the cathodically protected joints than in the joints tested in air. This observation and other studies in the Canadian Offshore Steel Research Program, using plate/plate and pipe/plate specimens with optimum cathodic protection or overprotection, show that cathodic protection does not always restore in-air fatigue performance and that a more conservative curve should be adopted for the fatigue design of tubular joints with cathodic protection. Therefore a more conservative approach has been taken in the CSA Preliminary Standard S473 Steel Structures Part III - Code for the Design, Construction and Installation of Fixed Offshore Structures, which will shortly be issused for public comment.

During the planning of this test program, discussions were held with Holmes, Brown and Kerr of NEL. Although their test program on stiffened joints was still ongoing it was already clear that their simple ring stiffeners were failing by fatigue from the flame cut, internal diameter before the weld toe crack had propagated through the chord wall. These stiffener failures in two of three tests or type G1 joints led Holmes et al [8] to question the use of the hot spot design approach for such joints.

In the present test program, the ring stiffeners were machined to minimize the risk of ring cracking from the ID prior to N_3. In nine tests on stiffened joints, none of the rings cracked before a through thickness crack had developed in the chord tube. However extensive strain gauging of the ring stiffeners in the present tests showed that axial brace loading or out of plane bending produced stresses at the ID of the stiffener that were very significant. When the hot spot stress at the saddle points was 250 MPa, the ring ID stress was 0.8 of the specified minimum yield (YS) for axial loading and 0.81 of YS for out of plane bending. If these ring stiffeners had been flame cut rather than machined on the ID it is possible that premature failure of the ring stiffeners would have been a problem as it was in the UKORSPII/NEL tests. As Holmes et al [8] point out "failure of ring stiffeners in service would be difficult to detect and probably impossible to repair" so machining the rings appears to be a good investment.

Potential drop measurements and inkstains indicate that fatigue cracks developed at or near the hot spots at an early stage in the fatigue life (N_3) these joints. This has been observed by others and is the basis for the argument that linear elastic fracture mechanic (LEFM) techniques should be developed for predicting N_3 or the residual life (N_R) of joints found to contain cracks during in-service inspection. The success of an LEFM approach depends very much on the modelling of crack shape development. In the present tests on stiffened joints, the crack shape development was in general very similar to that usually observed in tests on unstiffened joints. In particular small cracks develop first at or near the hot spot but other small cracks soon develop along the weld toe. These toe cracks coalesce to form a relatively long crack so that when the crack is a few millimeters deep it has a low aspect ratio (< 0.2). It has been argued that this aspect ratio is a function of the mode of loading ie, the shape of the radial stress distribution along the weld toe. The present tests on unstiffened and stiffened joints provide some support for this argument.

In the present test program one unstiffened joint was tested with axial brace loading (TA1) and one with in-plane bending (TB1). The stress distributions derived from strain gauge measurements, Figures 70 and 131, are very different and the in-plane bending crack clearly develops over a longer arc of weld, ie, it developed a lower aspect ratio than the crack caused by axial brace loading so N_p should be and was lower for in-plane bending.

An analysis of crack shape development in stiffened joints shows that dominant cracks of low aspect ratio had developed when the crack was 2-4 mm deep and that prior to N_3 the stiffeners acted as barriers to the surface length of this dominant crack. There is also evidence, particularly in the out of plane bending tests, that the stiffeners caused the crack to turn as it approached the ID of the chord. In the lower stress, out of plane bending tests, the crack turning was probably responsible for the very large drop in crack growth rate during the last three millimetres of growth, which led to a large increase in N_3. Ignoring crack turning and assuming mode 1 cracking throughout the chord wall will lead to conservative LEFM estimates of fatigue crack propagation life for stiffened joints. Also the results of the present tests indicate that it is reasonable to assume that the stiffeners limit surface crack growth prior to N_3 and that the crack aspect ratio can be assumed to be crack depth/stiffener spacing when the crack is a few millimeters deep.

LEFM models based on these observations of crack shape development are presently being developed by J. Forbes as part of his Ph.D. research. Assessment of these models was not a requirement of this contract. This contract research has:

1. shown that this arrangement of two simple ring stiffeners leads to large reductions in stress concentration factor (SCF) for out of plane bending or axial brace loading.

2. shown that these reductions in SCF at the hot spots lead to large increases in fatigue load carrying capacity. This improvement in fatigue performance can be quantified using the hot spot stress design procedure presently used for unstiffened joints.

3. shown that this arrangement of two simple ring stiffeners leads to significant cyclic stresses at the internal diameter of the rings. A fatigue analysis for this location should be part of the fatigue assessment for stiffened tubular joints. Using a machined rather than flame cut inner diameter is recommended.

4. provided some support for the DOE fatigue guideline that the air design curve is suitable for joints with cathodic protection. However an analysis of crack growth

rates shows that these rates were significantly higher in cathodically protected joints than in similar joints tested in air. Also in the present tests on stiffened tubular joints and in previous tests on pipe-plate specimens, N_3 for tests in air were always higher than N_3 for tests with optimum cathodic protection.

5. shown that, in general, crack shape development in stiffened joints is very similar to that observed in tests on unstiffened joints. However the stiffener arrangement used in these tests appears to have limited surface crack length prior to N_3 and to have caused the crack to turn as it approached the ID of the chord. Both of these effects are beneficial from a fatigue viewpoint and merit further study.

7 Acknowledgements

Other engineers who made significant contributions to this project were G. Hewitt (Waterloo), C.C. Monahan and P.G. Williams (Memorial), and J. Bain (AMCA International). The assistance of laboratory staff at Waterloo and Memorial Universities is gratefully acknowledged; the detail design of both rigs was done by the late A. DeGroot.

8 References

1. Steel in Marine Structures. Proc of International Conference, European Coal and Steel Community (ECSC) – Institut de Recherches de la Siderurgie Francaise (IRSID) Paris, Oct. 1987.

2. Steel in Marine Structures, Proc of the 3rd International ECSC Offshore Conference on Steel in Marine Structures (SIMS 87) Delft – Elsevier 1987.

3. Salama MM et al. Proc of 8th International Conf. on Offshore Mechanics and Arctic Engineering, ASME, 1989.

4. Efthymiou M and Durkin S, Stress Concentrations in T/Y and Gap/Overlap K joints. Proc of Conf on Behaviour of Offshore Structures, pp.429-440, Elsevier Amsterdam, 1985.

5. Department of Energy (UK) Background to new fatigue design guidance for steel welded joints in offshore structures. H.M.S.O. 1984 ISBN 011 441456 0.

6. Thomson R and Tyson W. An Overview of the National Canadian Offshore Steel Research Program. Ibid 2, pp.29-33.

7. Lloyd's Register of Shipping, Stress Concentration Factors For Tubular Complex Joints, Interim Technical Report No.1A, October 1984, Ring – Stiffened T-Joints Project Document, CJPD 6.

8. Holmes R., Brown G.M. and Kerr J., How Ring Stiffeners can affect Tubular Node Fatigue and Failure Mode. Offshore Technology Conference, Houston, May 1988, Paper OTC 5835.

9. Pates, M.J., and Burns D.J., Final Report (Task 2) Detailed Plans, Costs, and Schedules for Tubular T-Joint Fabrication and Corrosion Fatigue Testing. AMCA Report No. 2-184-037/5A November 1984.

10. Burns D.J., Lambert, S.B., and Mohaupt, U.H., Crack Growth Behaviour and Fracture Mechanics Approach, Plenary Paper PS6, pp.137-160, Ibid 2.

11. Vosikovsky, O., Chaar, M., and Bouchard, R., Calibration of A.C. Potential Drop Technique for Sizing Fatigue Cracks in Welded Joints, CANMET – PMRL Report 87-1[TR], January 1987.

12. Lambert, S.B., Fatigue Crack Growth in Welded Joints in Seawater, Ph.D. Thesis, University of Waterloo, 1988.

13. Mohaupt, U.H., Burns, D.J., Kalbfleisch, J.G., Vosikovsky, O., and Bell, R., Fatigue Crack Development, Thickness and Corrosion Effects in Welded Plate to Plate Joints, Ibid 2, pp.269-280.

14. Lambert, S.B., Burns, D.J., Mohaupt, U.H., and Vosikovsky, O., The Influence of Seawater and Cathodic Protection on Fatigue Crack Growth in a Pipe-Plate Model of Tubular Joints, Ibid 3, pp.437-446.

15. Vosikovsky, O., Bell, R., Burns, D.J., and Mohaupt, U.H., Thickness Effect in Fatigue Life of Welded Joints - Review of Canadian Program, Ibid 3, pp.9-19.

16. Vosikovsky, O., Bell, R., Burns, D.J., and Mohaupt, U.H., Effects of Cathodic Protection and Thickness on Corrosion Fatigue Life of Welded Plate T-Joints, Ibid 2, pp.787-798.

17. Evans, S., Use of Initial Current Density in Cathodic Protection Design, Presented at Corrosion/87, NACE 1987, Materials Performance, Feb.1988, pp.9-11.

18. Dover, W.D., and Wilson T.J., Corrosion Fatigue of Tubular Welded T Joints, Proc. of International Conference on Fatigue and Crack Growth in Offshore Structures, Edited by Dover, Glinka and Reynolds. I. Mech. E., London, 1986 - 2, pp.135-153.

19. Bell, R., Vosikovsky, O., Burns, D.J., and Mohaupt, U.H., A Fracture Mechanics Model for Life Prediction of Welded Plate Joints, Ibid 2, pp.901-910.

20. Yee, R., Burns, D.J., Mohaupt, U.H., Bell, R., and Vosikovsky, O., Thickness Effect and Fatigue Crack Development in Welded Joints, Proc. of 7th International Conference on Offshore Mechanics and Arctic Engineering, Houston, 88, ASME, pp.447-457.

21. Bell, R., Vosikovsky, O., and Bain, J.A., The Significance of Weld Toe Undercuts in the Fatigue of Steel Plate T Joints, International Journal of Fatigue, January 1989, pp.3-11.

22. Otegui, J.L., Kerr, H.W., Burns, D.J., and Mohaupt, U.H., Fatigue Crack Initiation from Defects at Weld Toes in Steel, To appear in International Journal of Pressure Vessels and Piping, 1989.

FIGURES

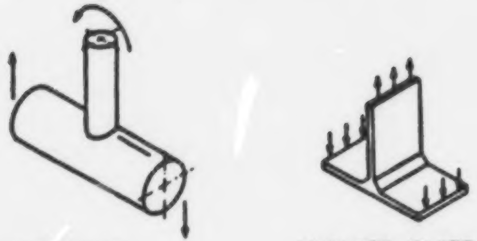

a) TUBULAR

b) PLATE - PLATE

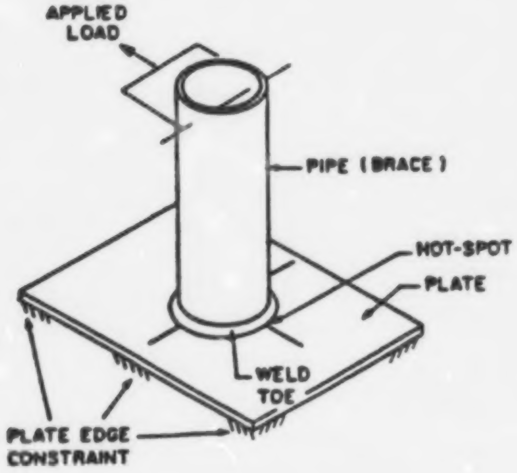
APPLIED LOAD
PIPE (BRACE)
HOT-SPOT
PLATE
WELD TOE
PLATE EDGE CONSTRAINT

c) PIPE PLATE

Figure 1: Full penetration welded joint fatigue specimens (not to scale).

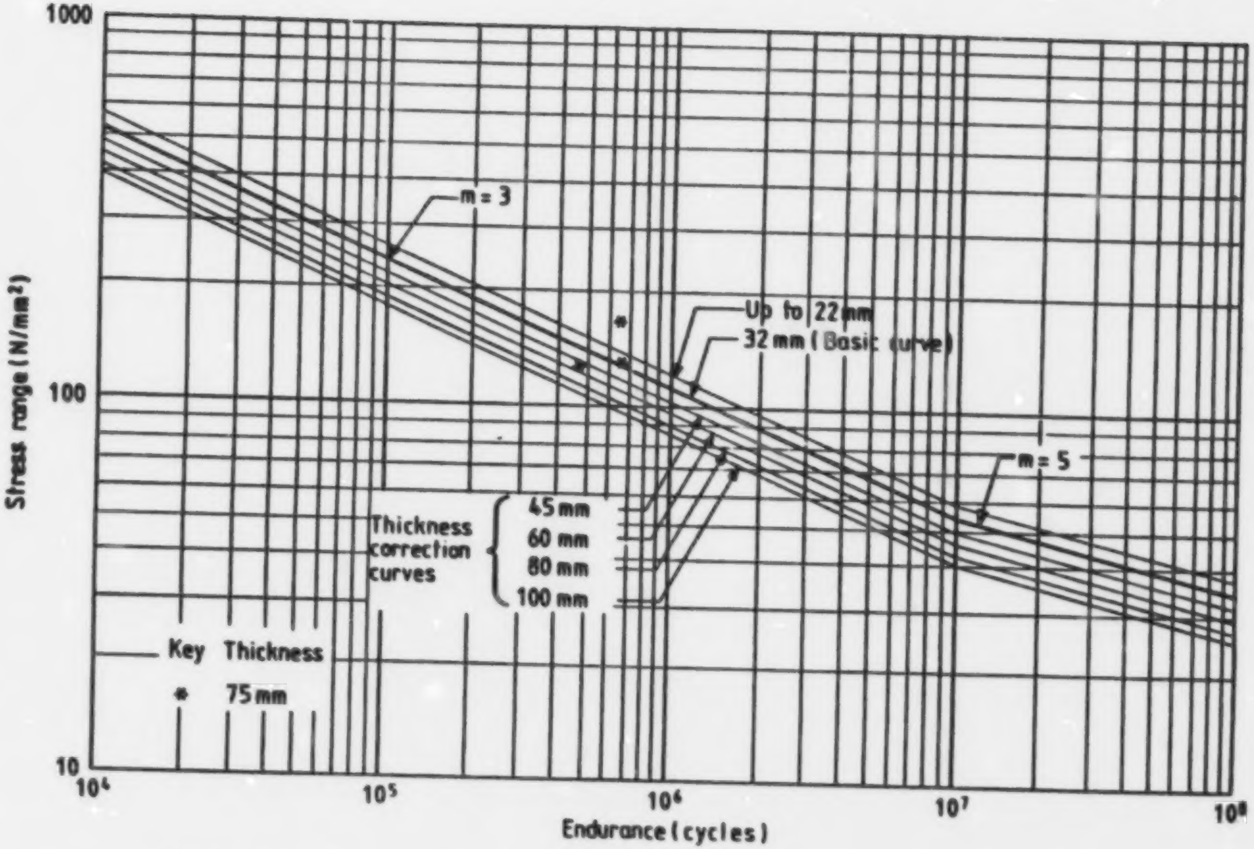

Figure 2: General form of S-N design curves for welded tubular joints in air

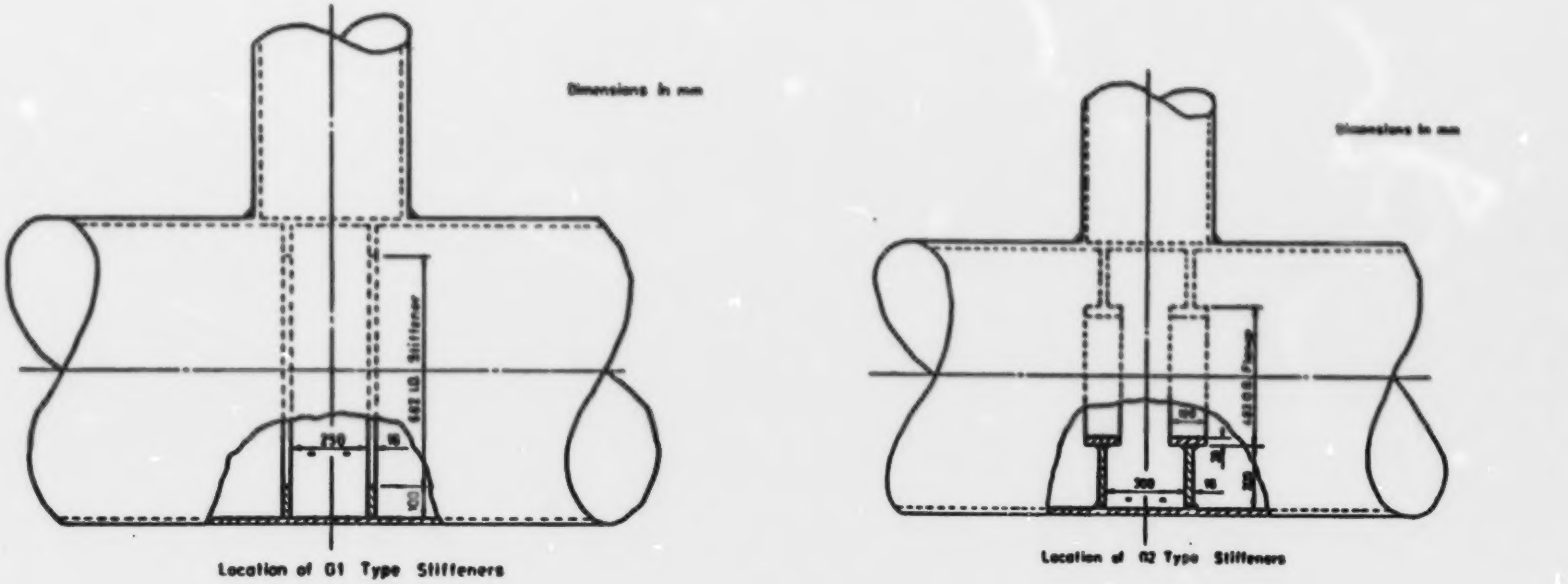

Dimensions in mm
682 I.D. Stiffener
250
16
100
Location of D1 Type Stiffeners
Dimensions in mm
1412 I.D. Flange
150
20
300
16
220
Location of D2 Type Stiffeners

Figure 3: NEL light and heavy ring stiffened specimens Holmes, Brown and Kerr.

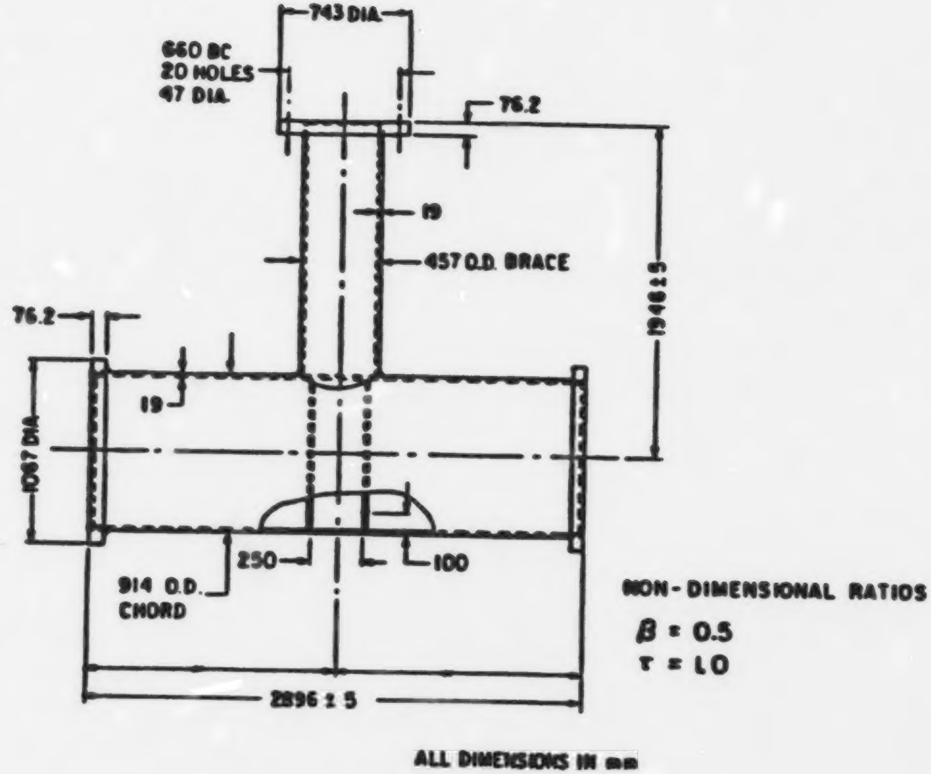
743 DIA
660 BC
20 HOLES
47 DIA
76.2
19
457 O.D. BRACE
1946±5
76.2
19
1067 DIA
250
100
914 O.D.
CHORD
2896 ± 5
NON-DIMENSIONAL RATIOS
β = 0.5
τ = 1.0
ALL DIMENSIONS IN mm

Figure 4: Tubular T-joint - Canadian offshore structures fatigue research program.

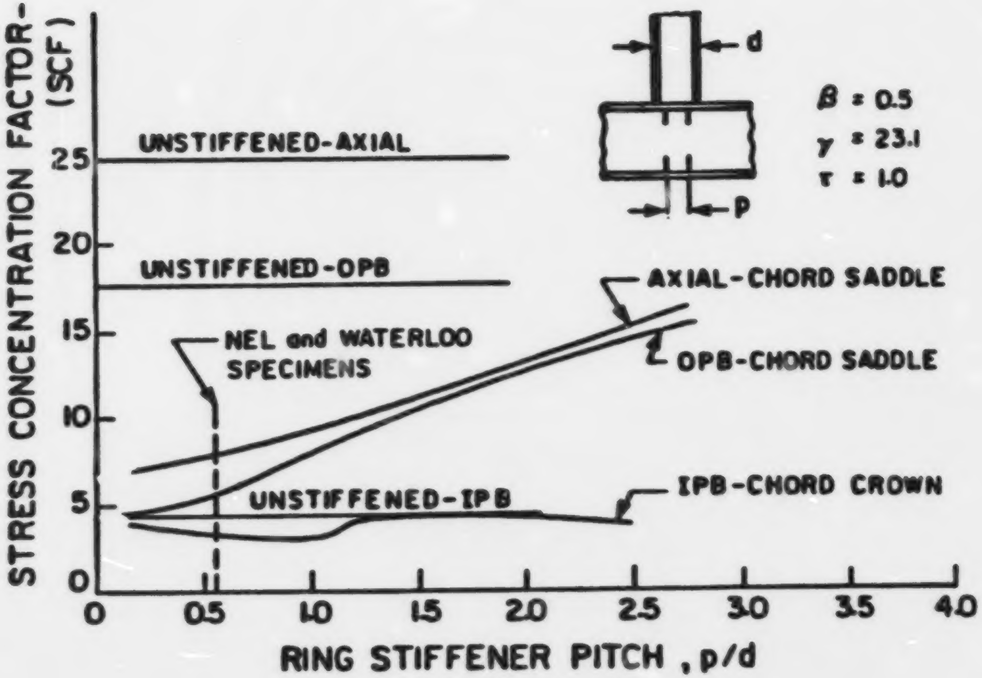

Figure 5: SCF's as a function of ring stiffener pitch (spacing) for stiffened and unstiffened tubular T-joint.

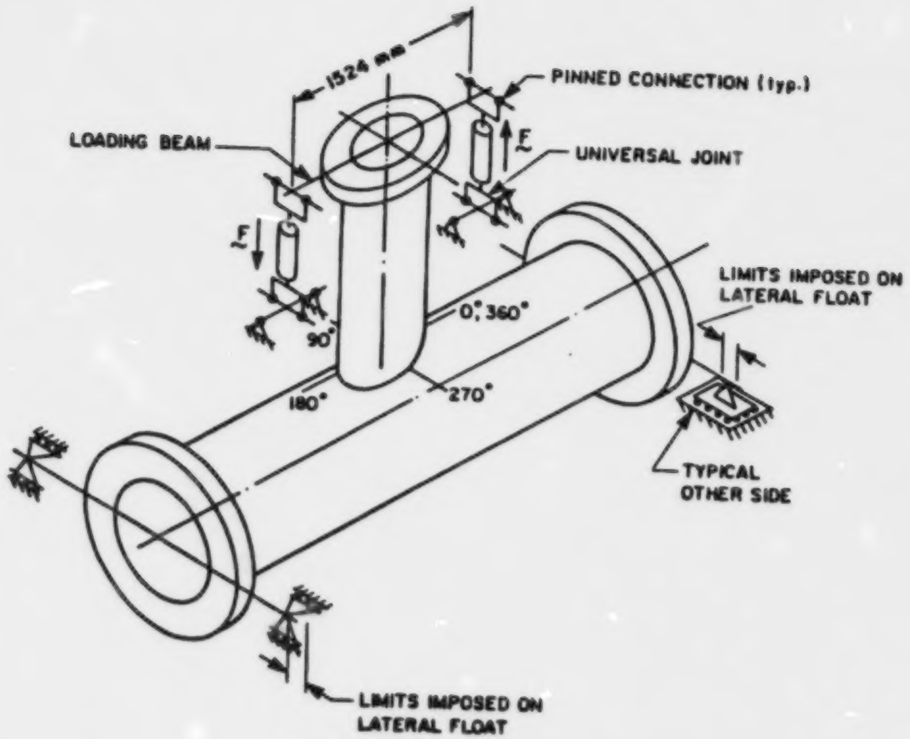
1524 mm
PINNED CONNECTION (typ.)
LOADING BEAM
F
UNIVERSAL JOINT
F
LIMITS IMPOSED ON LATERAL FLOAT
0°, 360°
90°
180°
270°
TYPICAL OTHER SIDE
LIMITS IMPOSED ON LATERAL FLOAT

Figure 6a: Schematic of mechanical elements used to apply in-plane bending load on T-joint specimen. Note the boundary conditions and universal joints facilitate a "floating" application of the land, thus ensuring the application of a "pure moment".

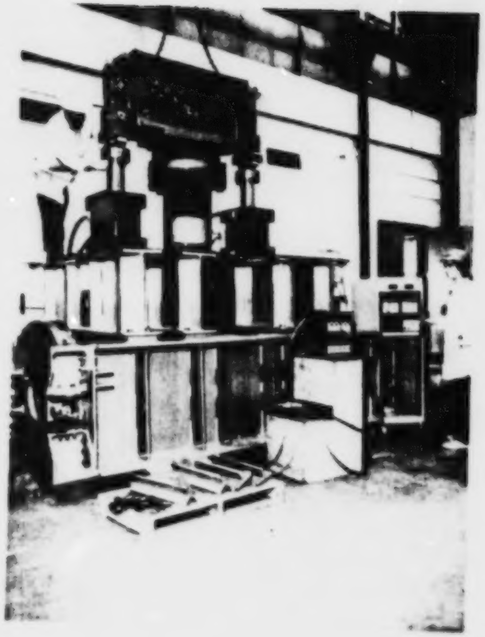

Figure 6b: Specimen mounted in test rig.

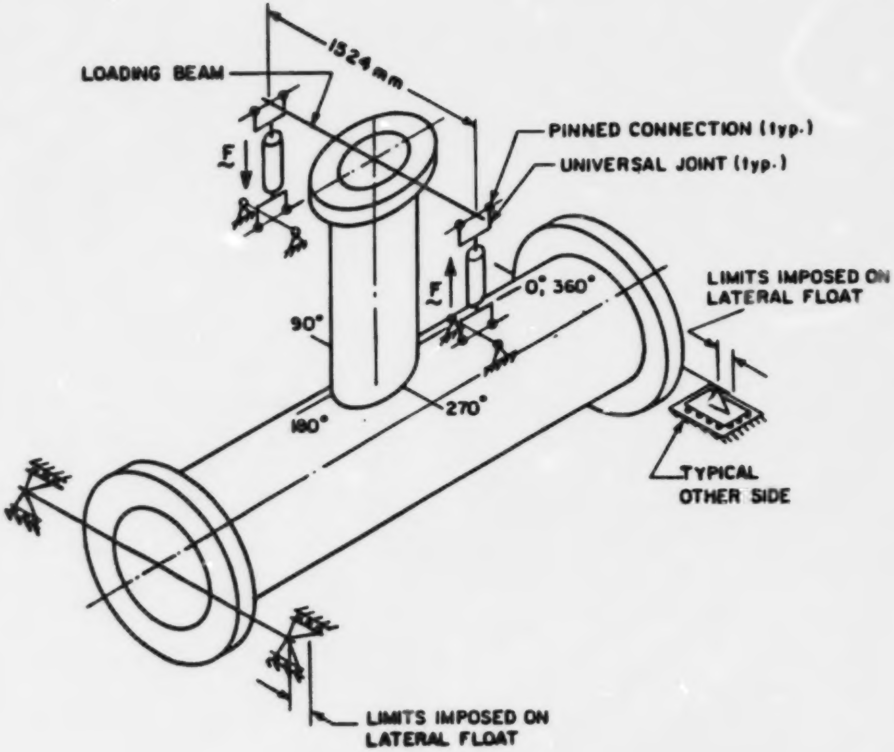
LOADING BEAM
1524 mm
PINNED CONNECTION (typ.)
UNIVERSAL JOINT (typ.)
F
F
0°, 360°
90°
180°
270°
LIMITS IMPOSED ON LATERAL FLOAT
TYPICAL OTHER SIDE
LIMITS IMPOSED ON LATERAL FLOAT

Figure 7a: Schematic of mechanical elements used to apply out-of-plane bending load on T-joint specimen. Note the boundary conditions and universal joints facilitate a "floating" application of the load, thus ensuring the application of a "pure moment".

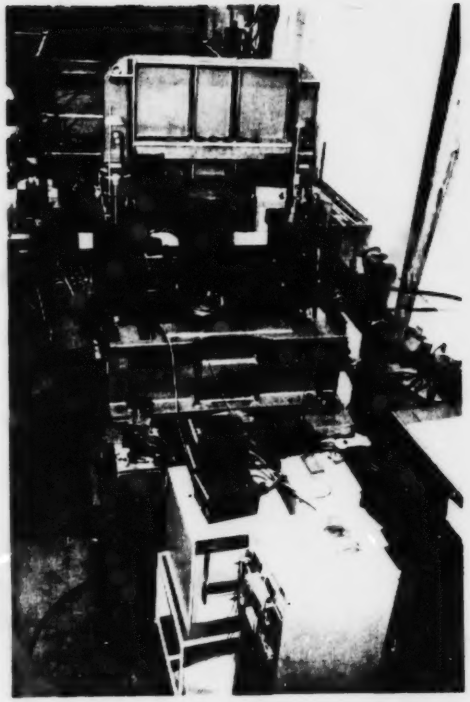

Figure 7b: Specimen mounted in test rig.

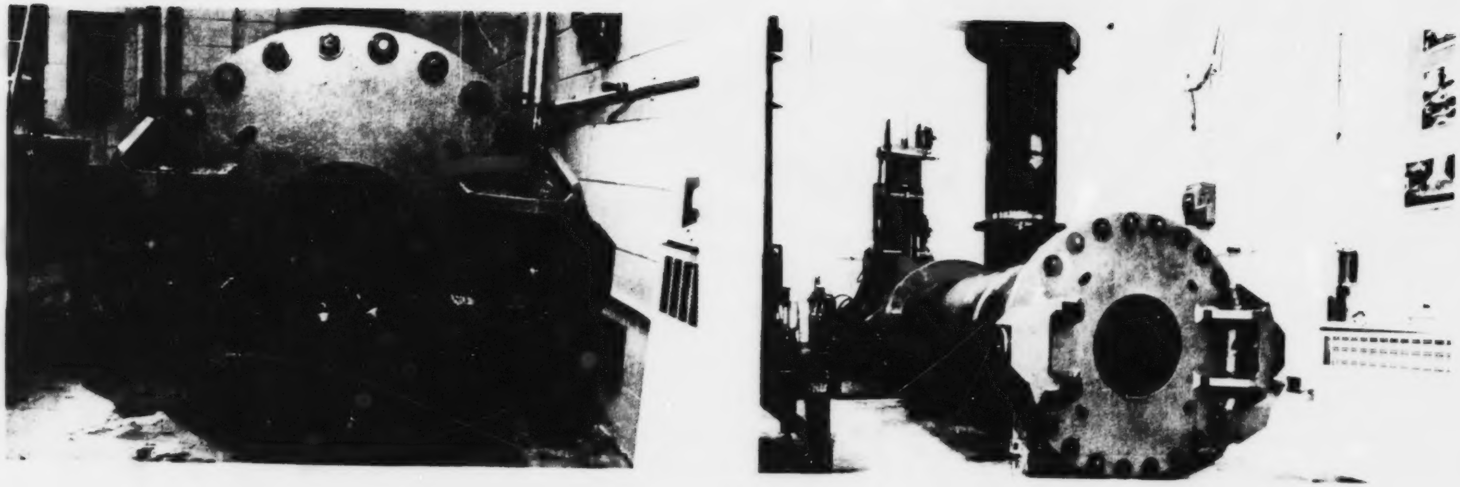

Figure 8: T-joint chord end flange.

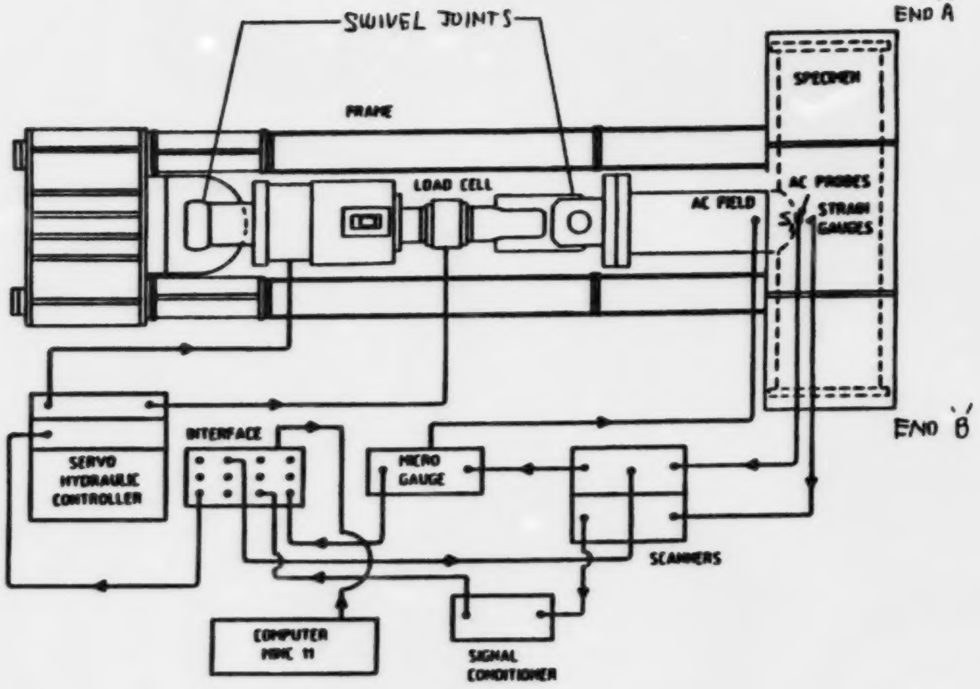
SWIVEL JOINTS
END A
FRAME
SPECIMEN
LOAD CELL
AC FIELD
AC PROBES
STRAIN GAUGES
END B
SERVO HYDRAULIC CONTROLLER
INTERFACE
MICRO GAUGE
SCANNERS
COMPUTER MINC 11
SIGNAL CONDITIONER

Fig. 9 Block diagram for data acquisition system.

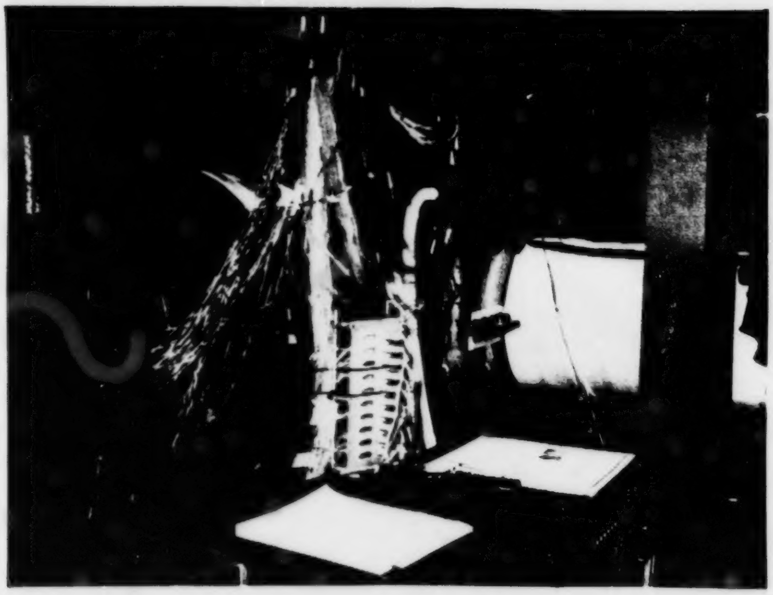

Figure 10: T-Joint specimen showing seawater tank

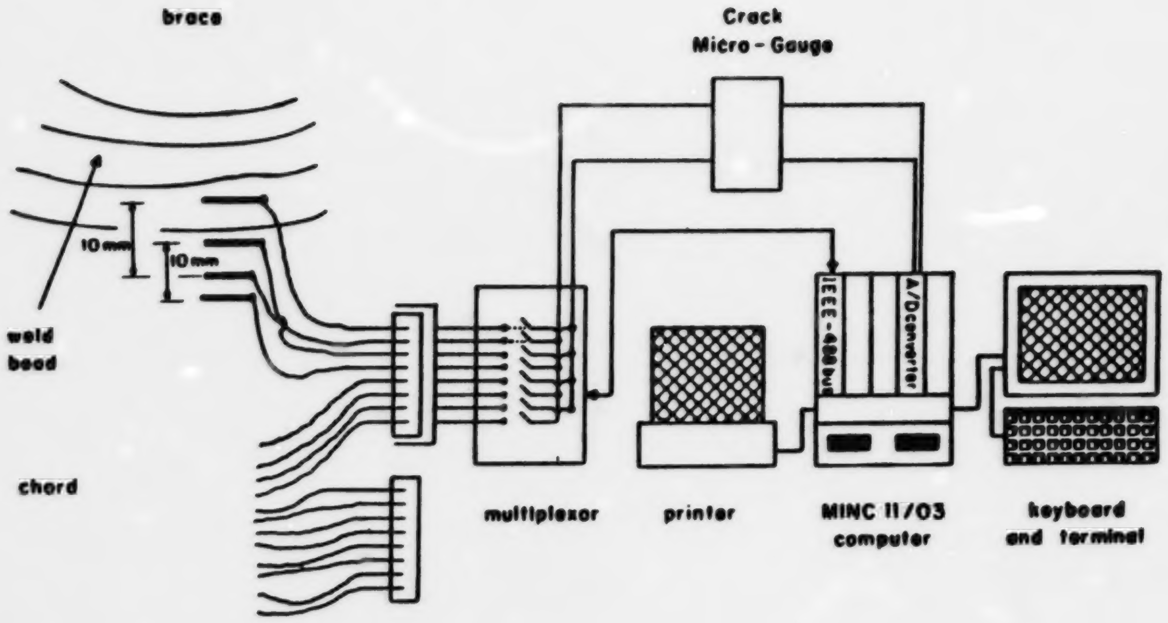
brace
Crack
Micro - Gauge
weld
bead
10 mm
10 mm
IEEE - 488 bus
A/D converter
chord
multiplexor
printer
MINC 11/03
computer
keyboard
and terminal

Fig. 11 Block diagram for A.C.P.D. probe connection

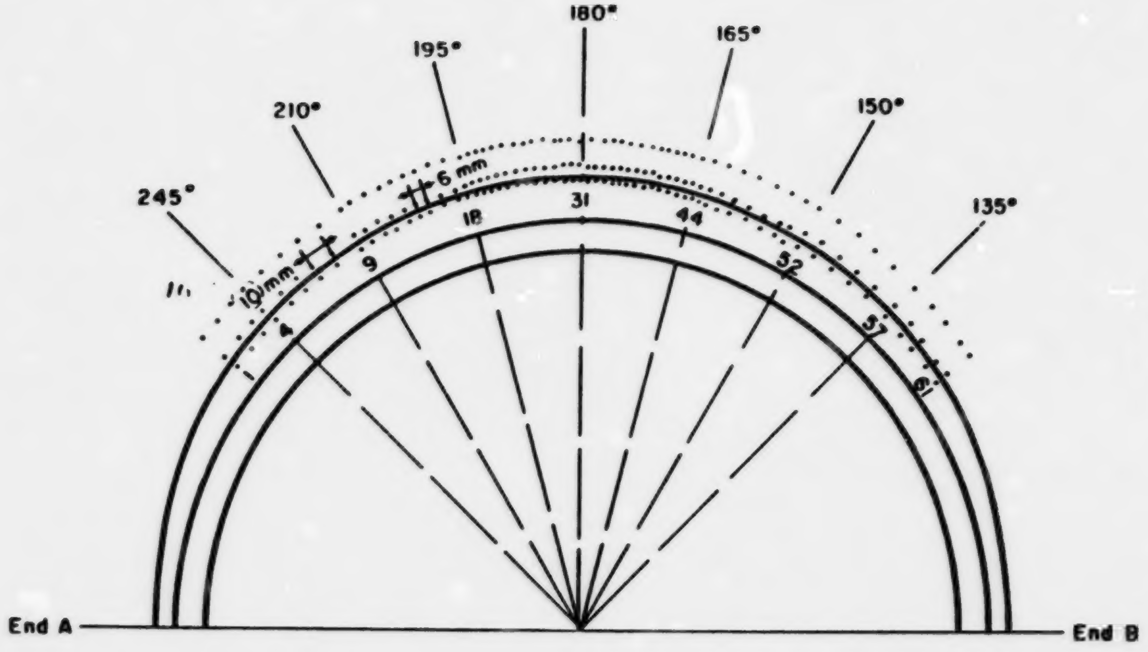
180°
165°
195°
210°
150°
245°
135°
6 mm
10 mm
4
9
18
31
44
52
57
61
End A
End B

Fig. 12 Plan view of chord surface - ACPD Probe locations
- unstiffened joint

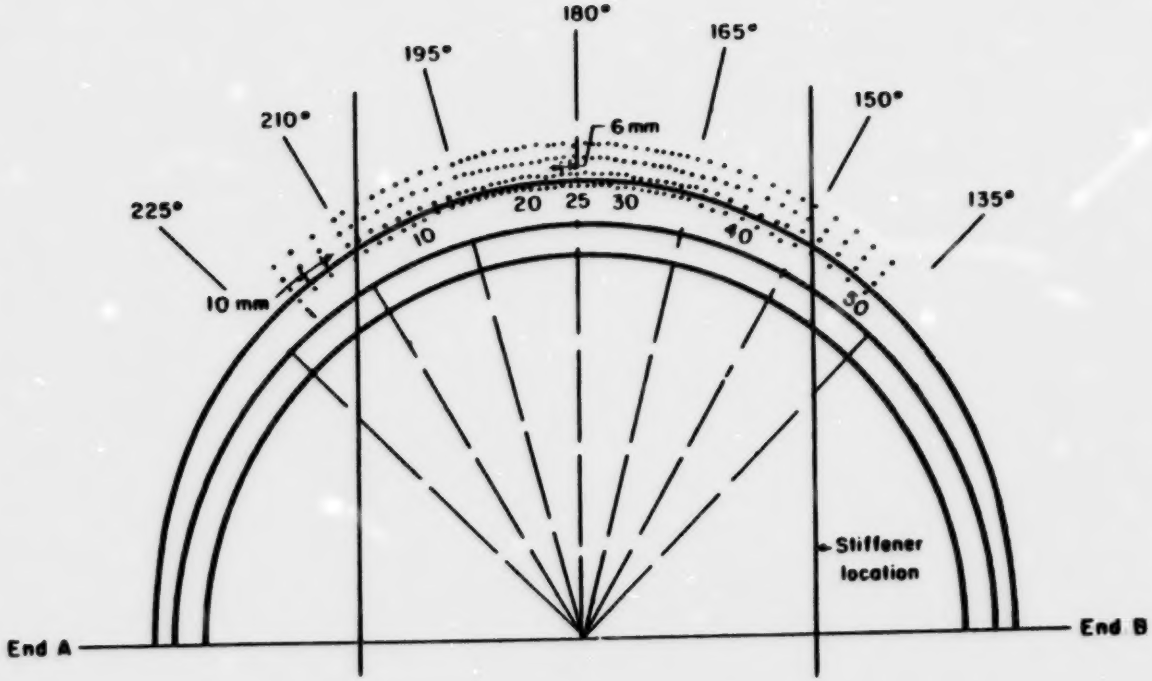
180°
195°
165°
210°
150°
225°
135°
6 mm
10 mm
10
20
25
30
40
50
Stiffener location
End A
End B

Fig. 13 Plan view of chord surface - ACPD Probe locations
- stiffened joint

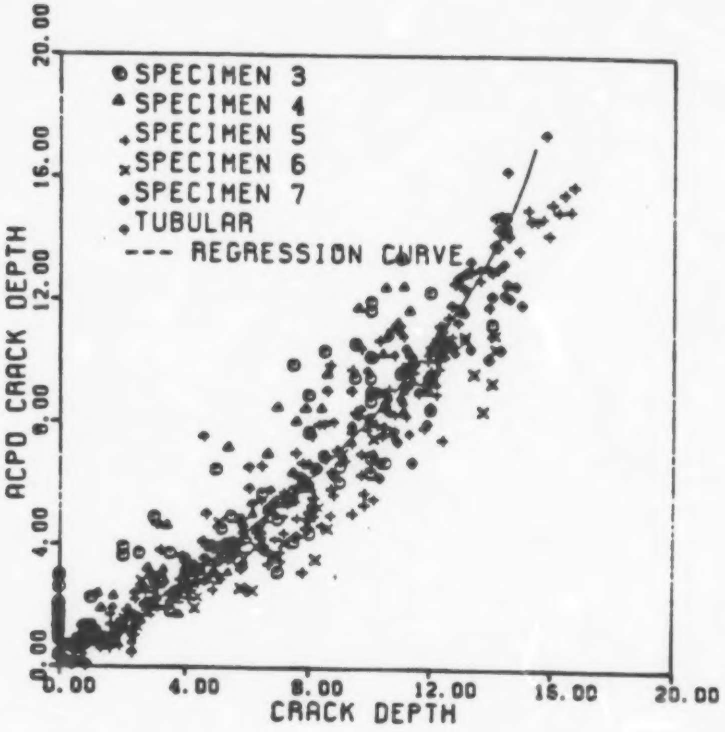

FIG. 14 MEASURED DATA AND REGRESSION CURVE

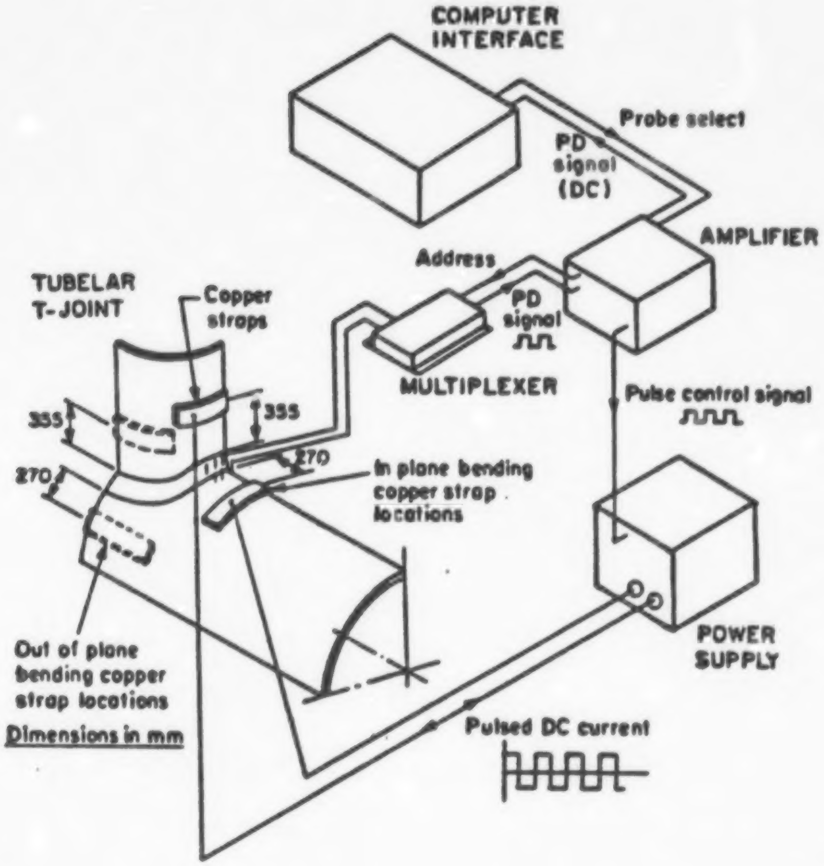
COMPUTER INTERFACE
Probe select
PD signal (DC)
AMPLIFIER
Address
PD signal
MULTIPLEXER
Pulse control signal
TUBELAR T-JOINT
Copper straps
355
355
270
270
In plane bending copper strap locations
Out of plane bending copper strap locations
Dimensions in mm
POWER SUPPLY
Pulsed DC current

Figure 15: Schematic of direct current potential drop (DCPD) crack monitoring system.

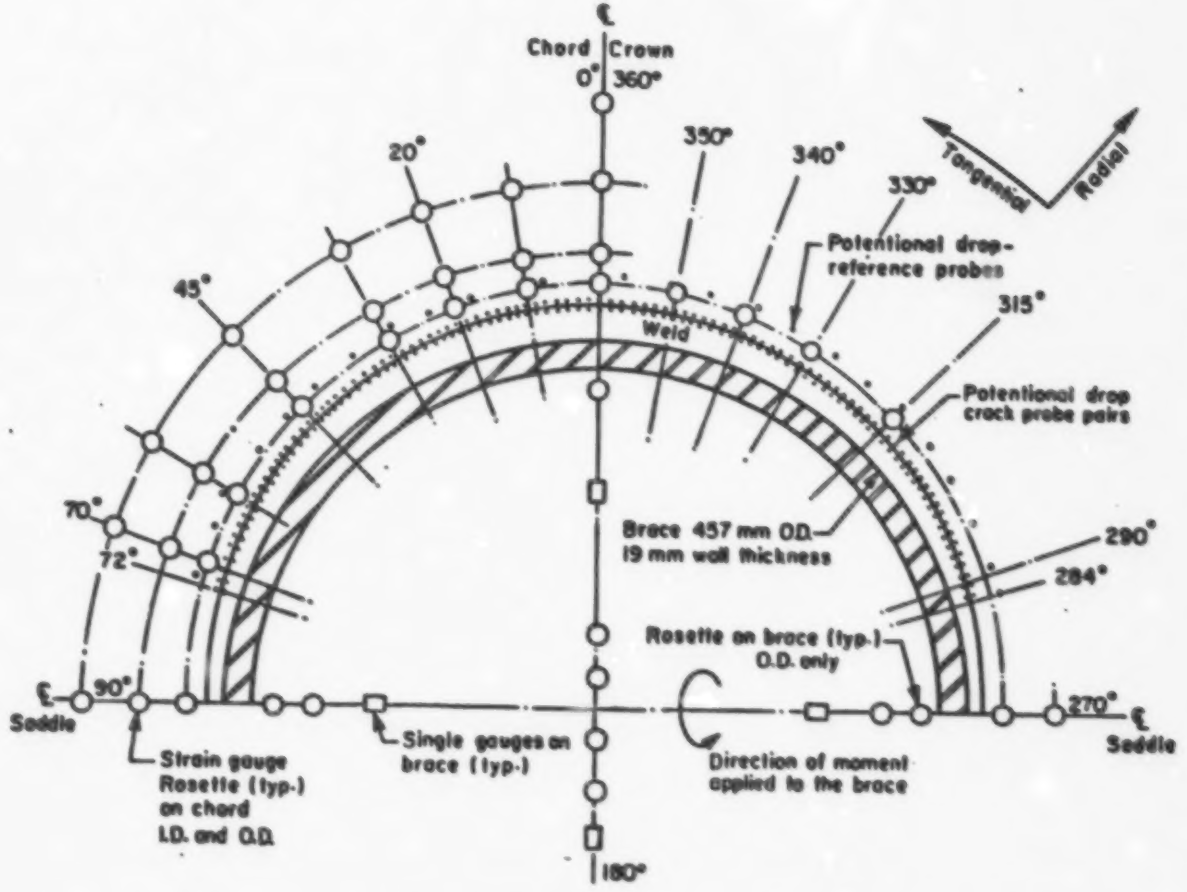
Chord
Crown
0°
360°
20°
45°
70°
72°
90°
Saddle
350°
340°
330°
315°
290°
284°
270°
Saddle
180°
Tangential
Radial
Potentional drop-reference probes
Potentional drop crack probe pairs
Weld
Brace 457 mm O.D. 19 mm wall thickness
Rosette on brace (typ-) O.D. only
Strain gauge Rosette (typ-) on chord I.D. and O.D.
Single gauges on brace (typ-)
Direction of moment applied to the brace

Figure 16: Unstiffened tubular T-joint DCPD probe and strain gauge layout in-plane bending.

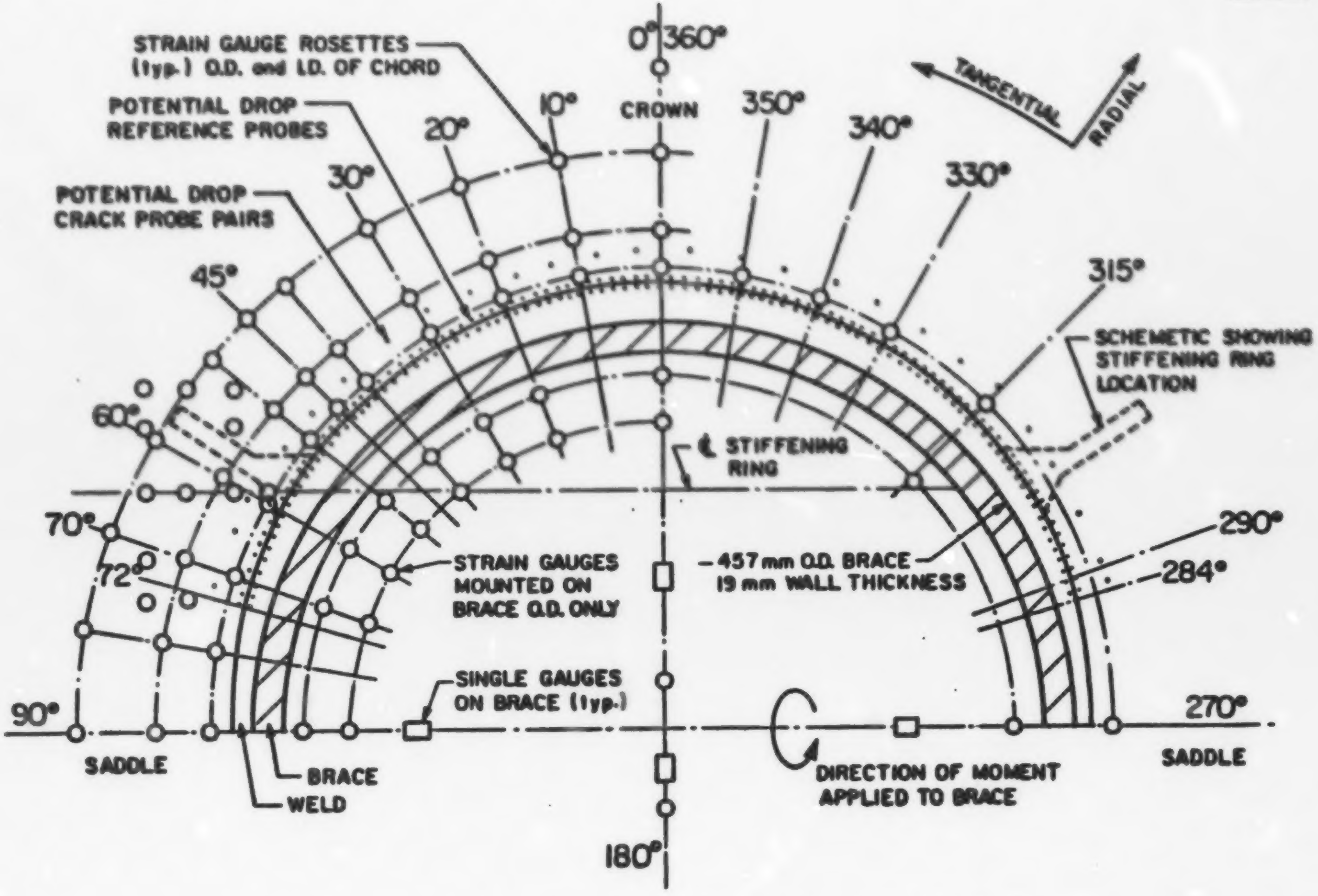
STRAIN GAUGE ROSETTES (typ.) O.D. and I.D. OF CHORD
POTENTIAL DROP REFERENCE PROBES
POTENTIAL DROP CRACK PROBE PAIRS
0° 360°
CROWN
10°
20°
30°
45°
60°
70°
72°
90°
SADDLE
350°
340°
330°
315°
290°
284°
270°
SADDLE
180°
TANGENTIAL
RADIAL
SCHEMATIC SHOWING STIFFENING RING LOCATION
℄ STIFFENING RING
STRAIN GAUGES MOUNTED ON BRACE O.D. ONLY
457 mm O.D. BRACE 19 mm WALL THICKNESS
SINGLE GAUGES ON BRACE (typ.)
BRACE
WELD
DIRECTION OF MOMENT APPLIED TO BRACE

Figure 17: Stiffened tubular T-joint (in-plane bending) DCPD probe and strain gauge layout.

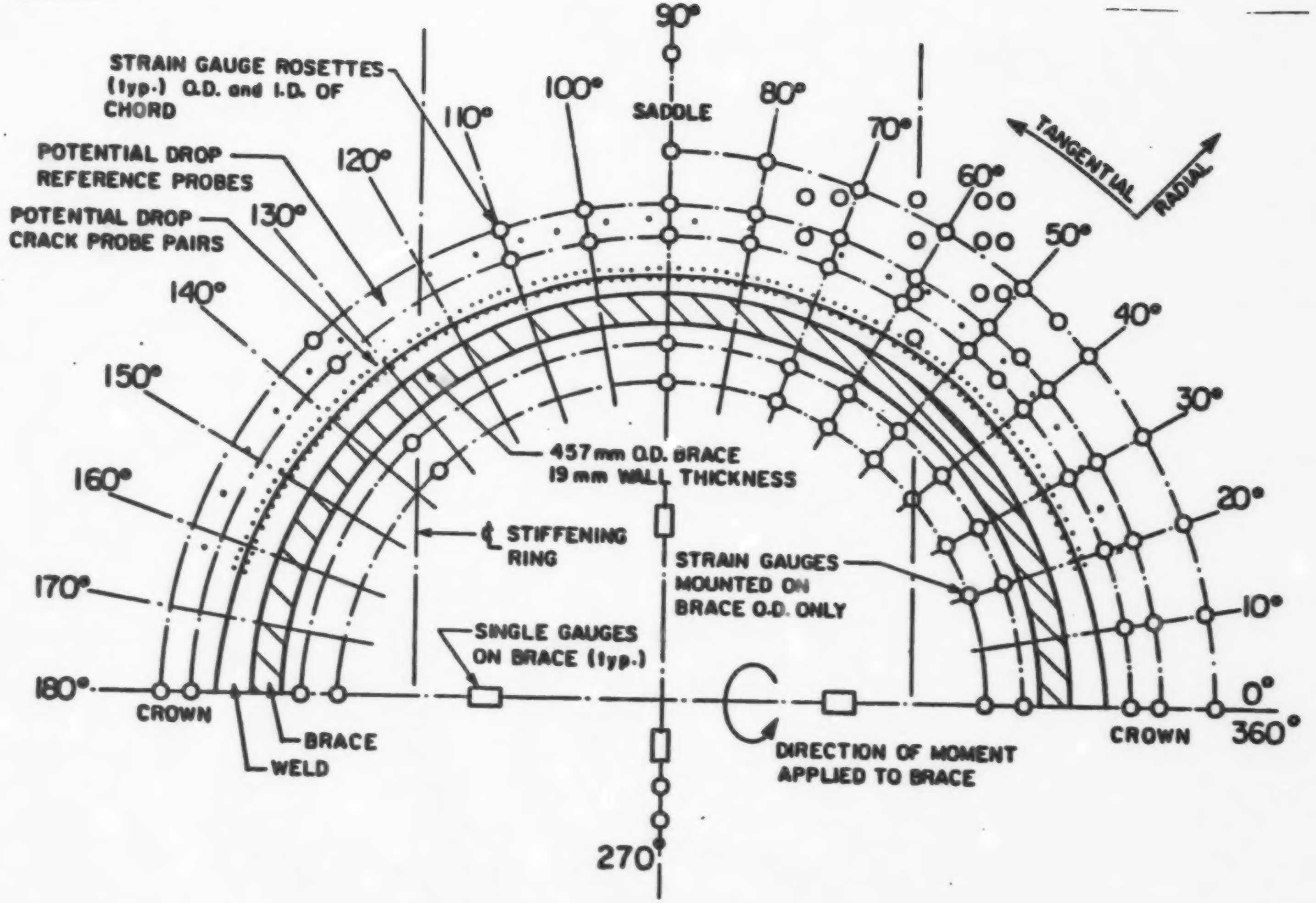

STRAIN GAUGE ROSETTES (typ.) O.D. and I.D. OF CHORD
POTENTIAL DROP REFERENCE PROBES
POTENTIAL DROP CRACK PROBE PAIRS
TANGENTIAL
RADIAL
90°
SADDLE
100°
110°
120°
130°
140°
150°
160°
170°
180°
80°
70°
60°
50°
40°
30°
20°
10°
0°
360°
270
CROWN
CROWN
BRACE
WELD
457 mm O.D. BRACE 19 mm WALL THICKNESS
℄ STIFFENING RING
SINGLE GAUGES ON BRACE (typ.)
STRAIN GAUGES MOUNTED ON BRACE O.D. ONLY
DIRECTION OF MOMENT APPLIED TO BRACE

Figure 18: Stiffened tubular T-joint (out-of-plane bending) DCPD probe and strain gauge layout.

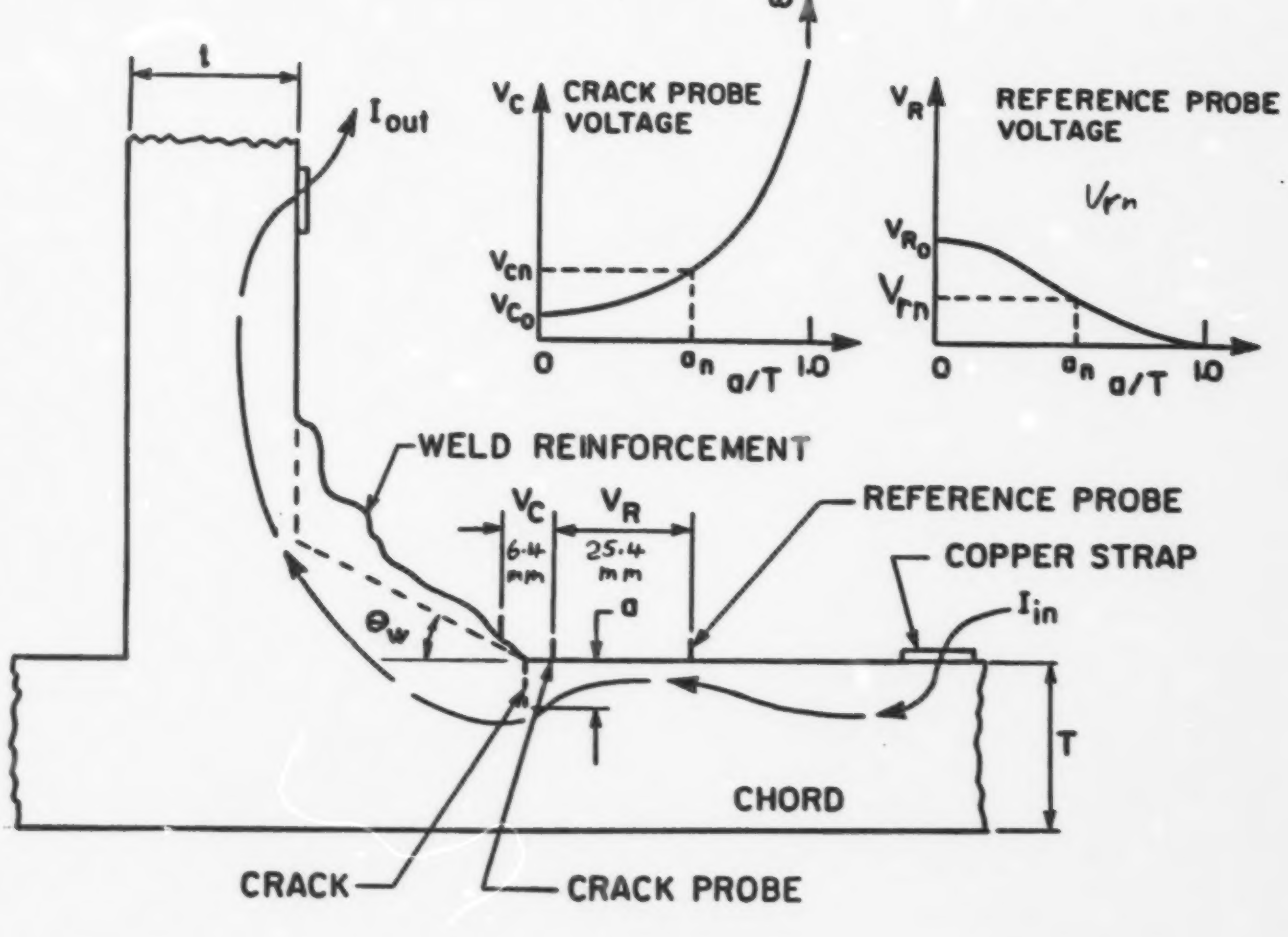
t
I_{out}
V_C
CRACK PROBE VOLTAGE
∞
V_{cn}
V_{C_0}
0
a_n
a/T
1.0
V_R
REFERENCE PROBE VOLTAGE
V_{rn}
V_{R_0}
V_{rn}
0
a_n
a/T
1.0
WELD REINFORCEMENT
V_C
V_R
6.4 mm
25.4 mm
REFERENCE PROBE
COPPER STRAP
I_{in}
a
θ_w
T
CHORD
CRACK
CRACK PROBE

Figure 19 DCPD Probe Locations at Weld Geometry.

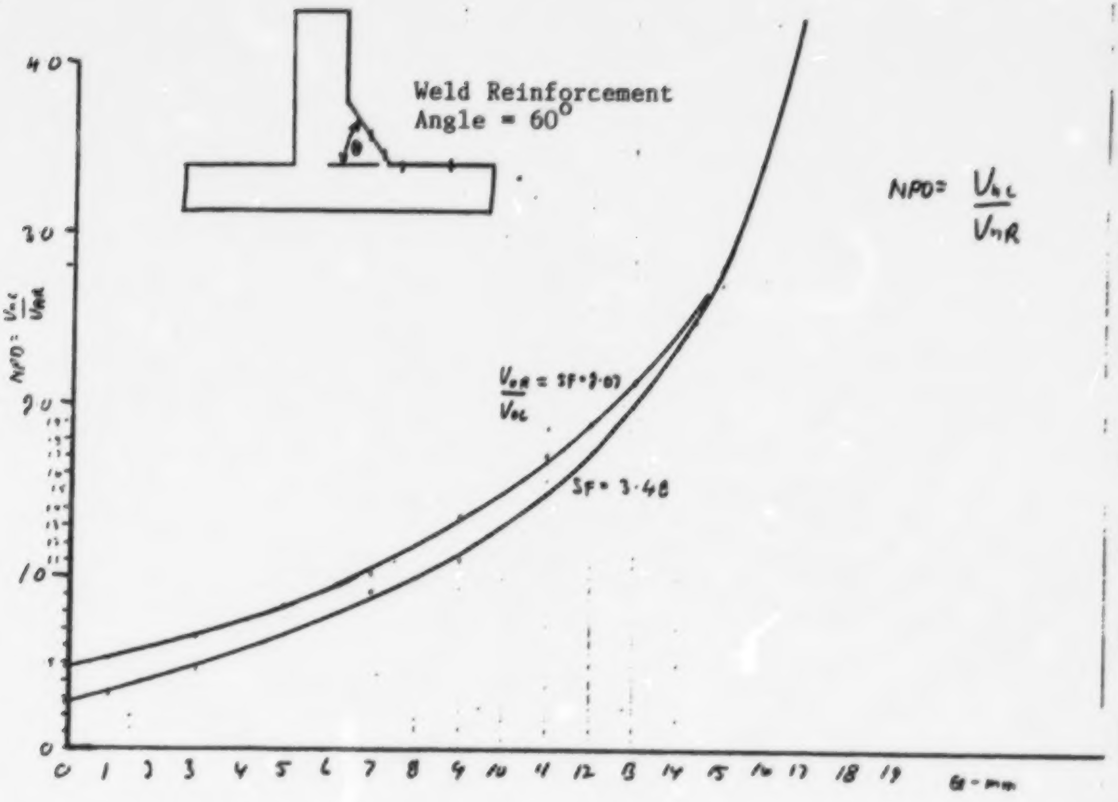

Figure 20: Foil Calibration Curves for DCPD

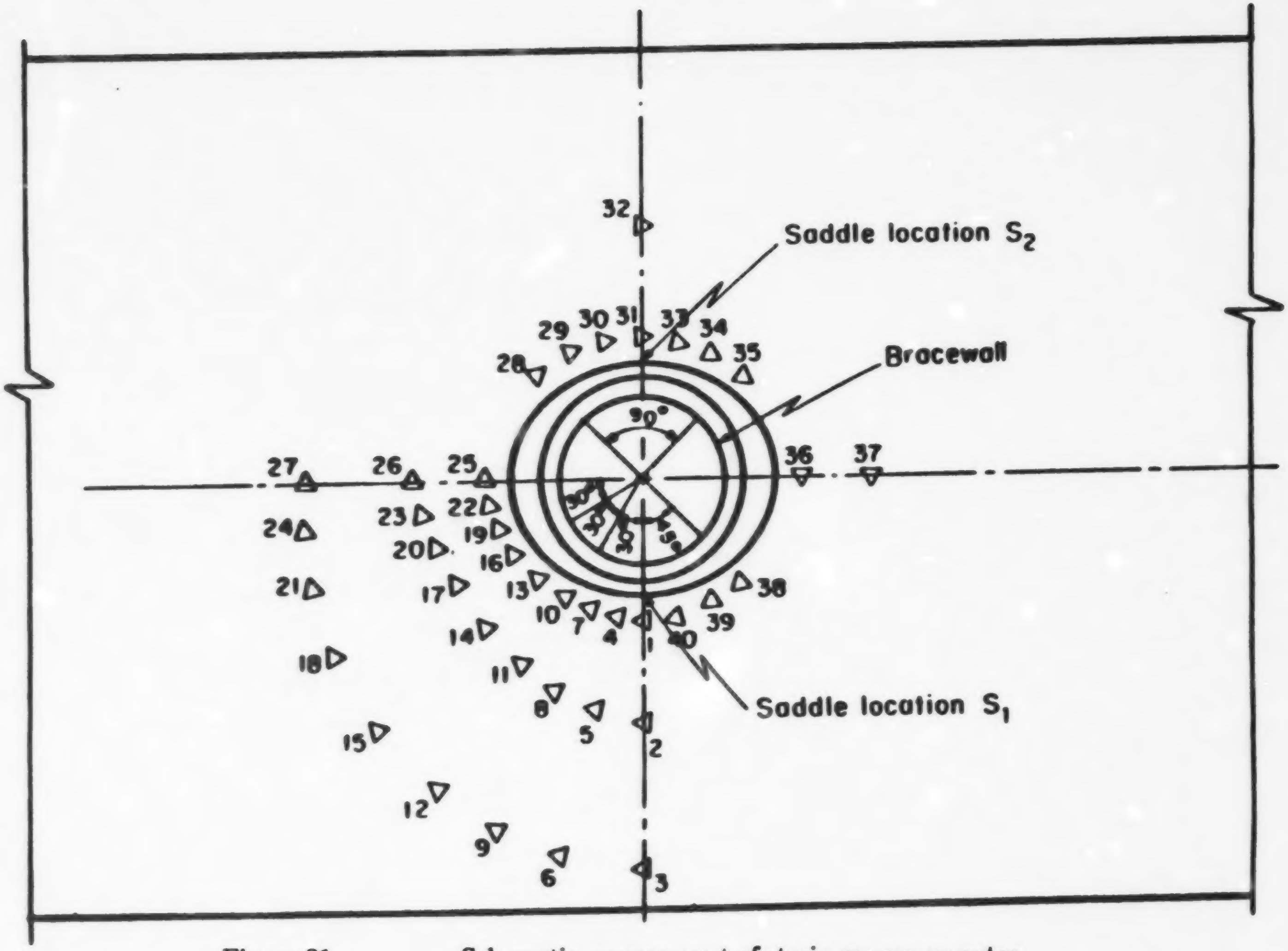
Saddle location S_2
Bracewall
Saddle location S_1
90°
45°
30°
1
2
3
4
5
6
7
8
9
10
11
12
13
14
15
16
17
18
19
20
21
22
23
24
25
26
27
28
29
30
31
32
33
34
35
36
37
38
39
40

Figure 21: Schematic arrangement of strain gauges on outer and inner surface of chord – unstiffened joint.

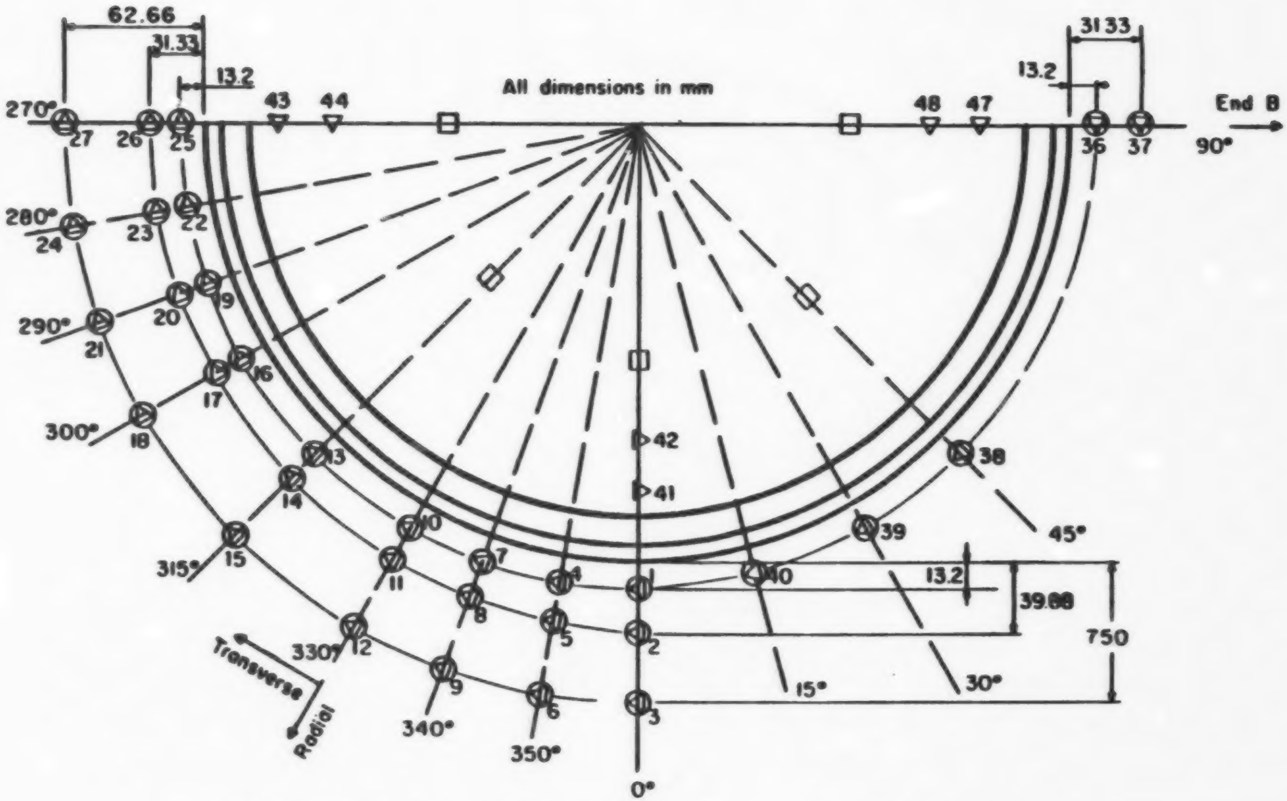
All dimensions in mm
62.66
31.33
13.2
31 33
13.2
13.2
39.88
750
End B
270°
280°
290°
300°
315°
330°
340°
350°
0°
15°
30°
45°
90°
1
2
3
4
5
6
7
8
9
10
11
12
13
14
15
16
17
18
19
20
21
22
23
24
25
26
27
36
37
38
39
40
41
42
43
44
47
48
Transverse
Radial

Fig. 22: Plan view of chord surface, strain gauge locations and orientations --unstiffened joint

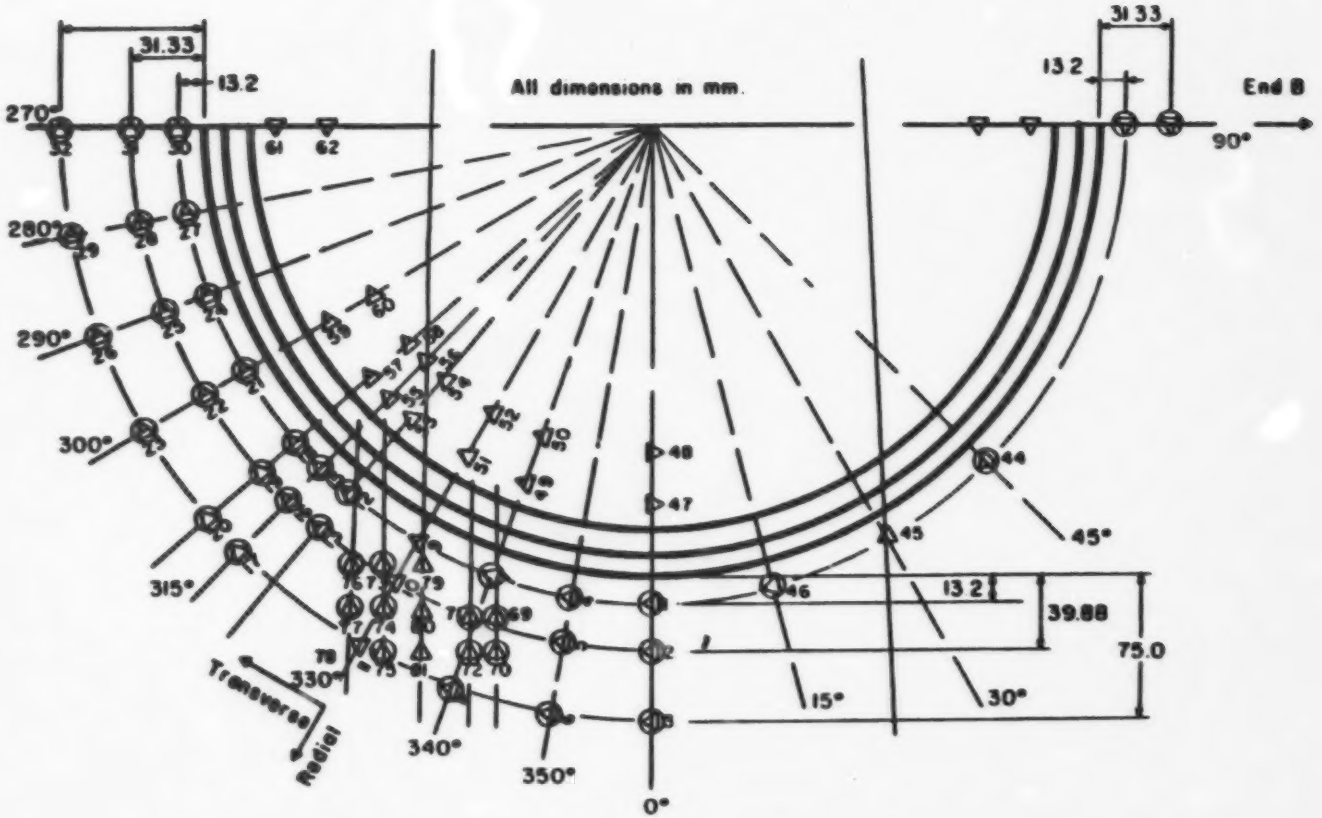
All dimensions in mm.
31.33
13.2
270°
280°
290°
300°
315°
330°
340°
350°
0°
15°
30°
45°
90°
End B
39.88
75.0
Transverse
Radial
32
31
30
29
28
27
26
25
24
61
62
44
45
46
47
48
69
70
72
73
74
75
76
77
78
79
81

Fig. 23 Plan view of chord surface, strain gauge locations and orientations stiffened joint.

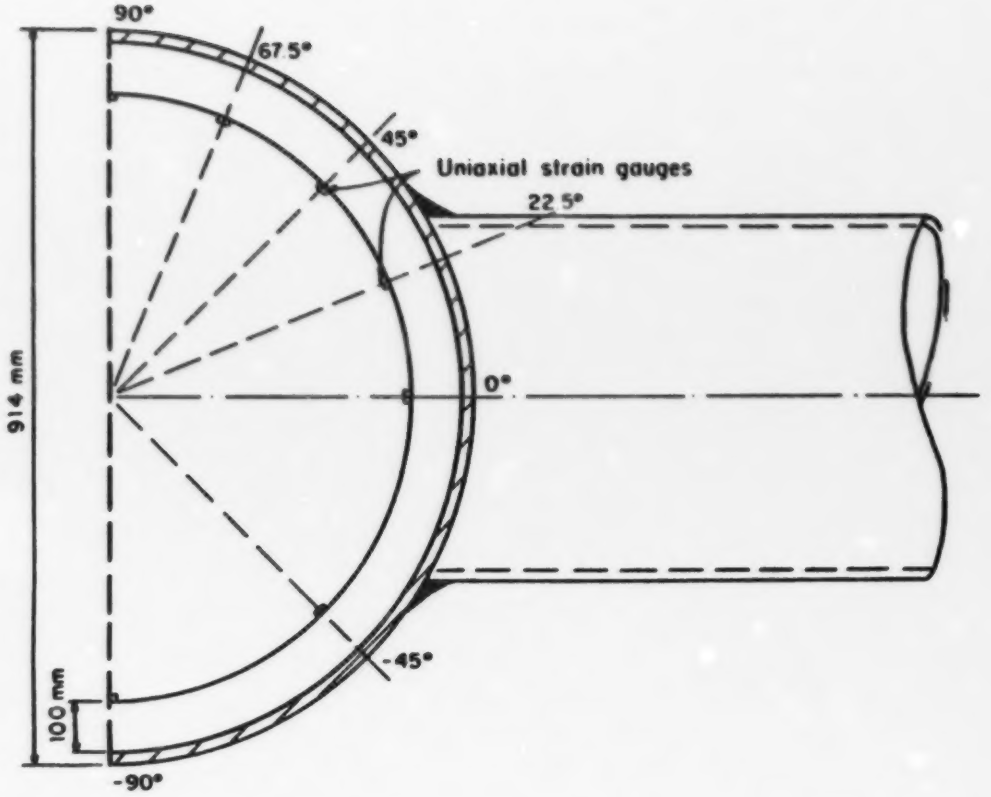
90°
67.5°
45°
Uniaxial strain gauges
22.5°
0°
-45°
-90°
914 mm
100 mm

Fig. 24 Strain gauge locations on the stiffener.

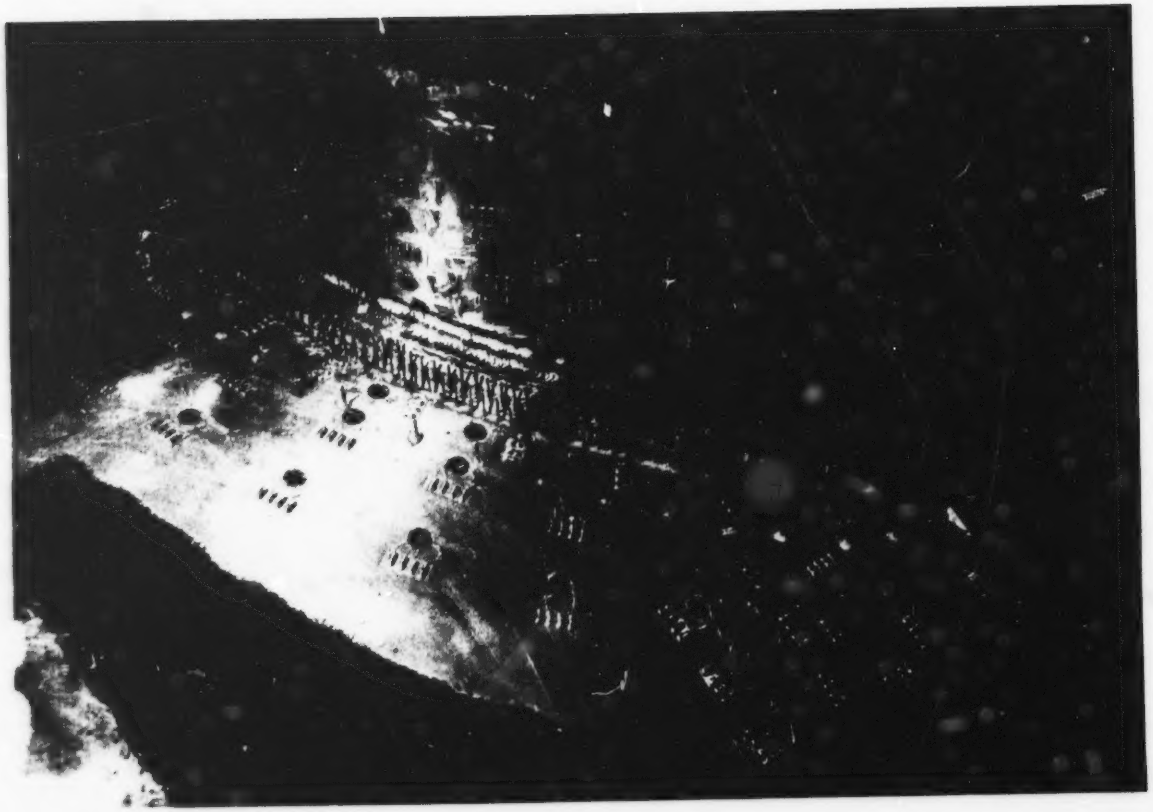

Figure 25: Photograph showing typical installation of strain gauge rosettes and potential drop probes.

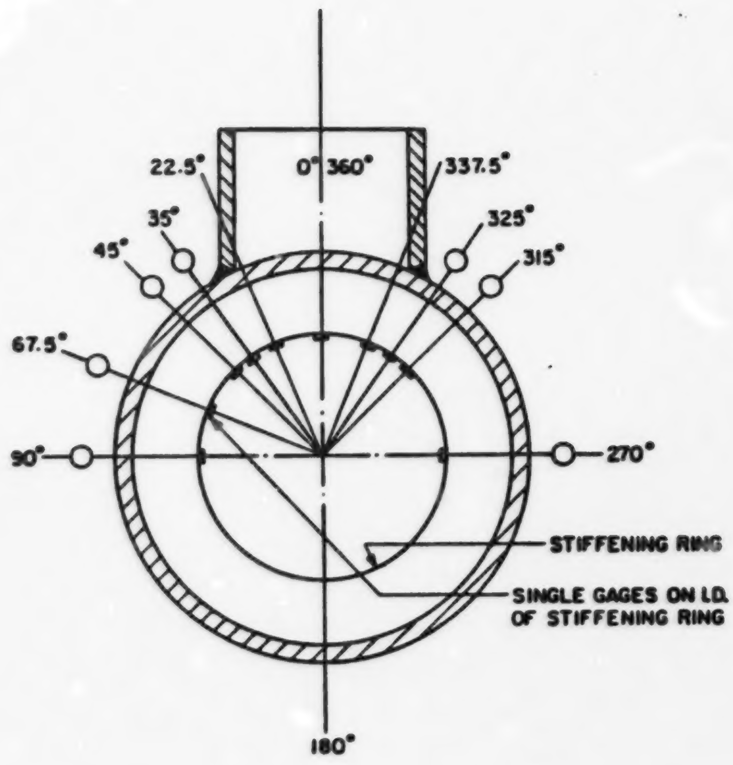
22.5°
0° 360°
337.5°
35°
325°
45°
315°
67.5°
90°
270°
STIFFENING RING
SINGLE GAGES ON I.D. OF STIFFENING RING
180°

Figure 26: Cross section of chord showing strain gauges designed to document the stress distribution in the stiffening ring O.D. and I.D.

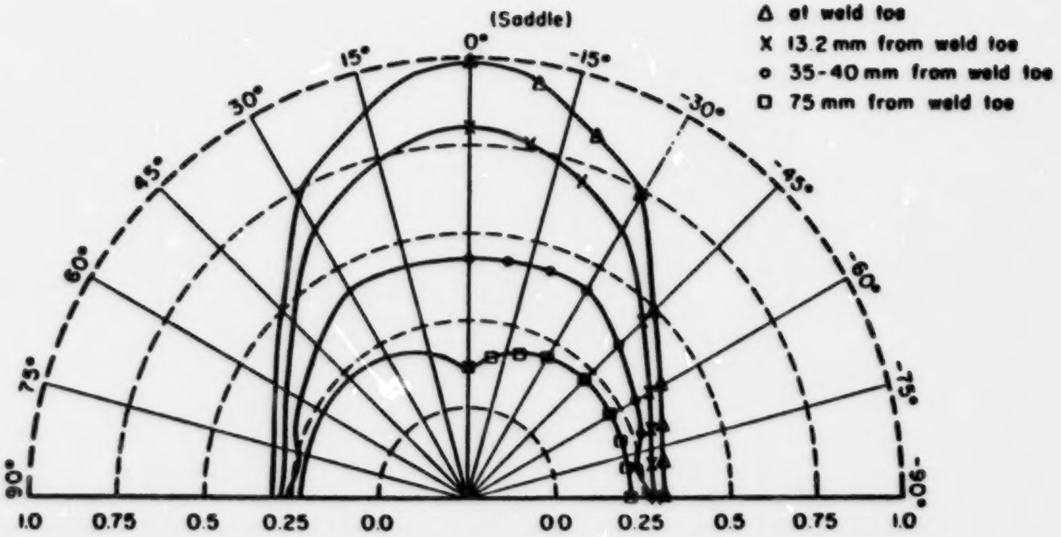

Fig. 27 Polar plot of normalized radial stress around the brace on the outside surface of the chord – unstiffened tubular T–joint TA1 subjected to axial tensile load - 250 MPa

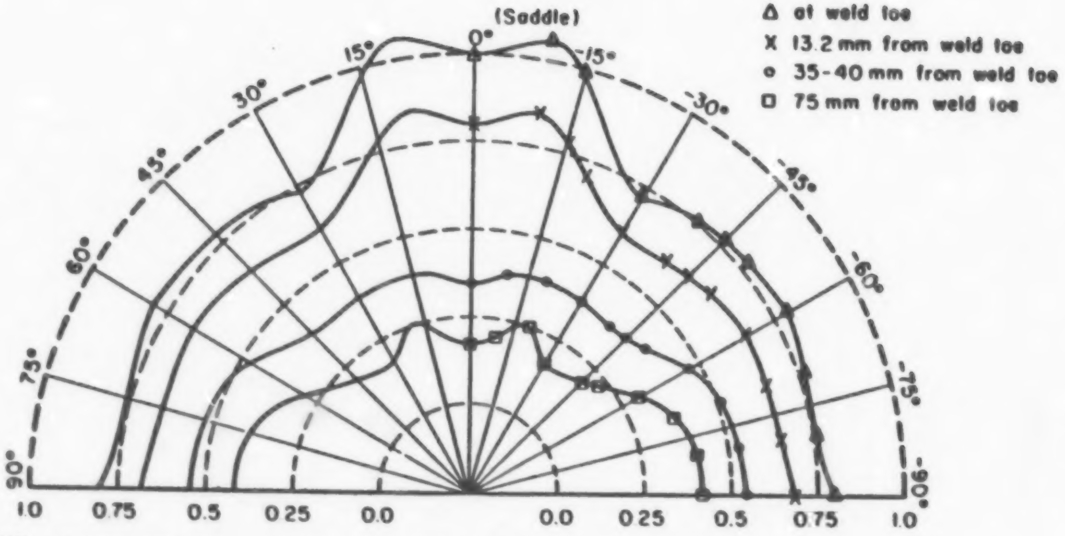

Fig. 28 Polar plot of normalized radial stress around the brace on the outside surface of the chord – stiffened tubular joint TA2 subjected to axial tensile load – 250 MPa

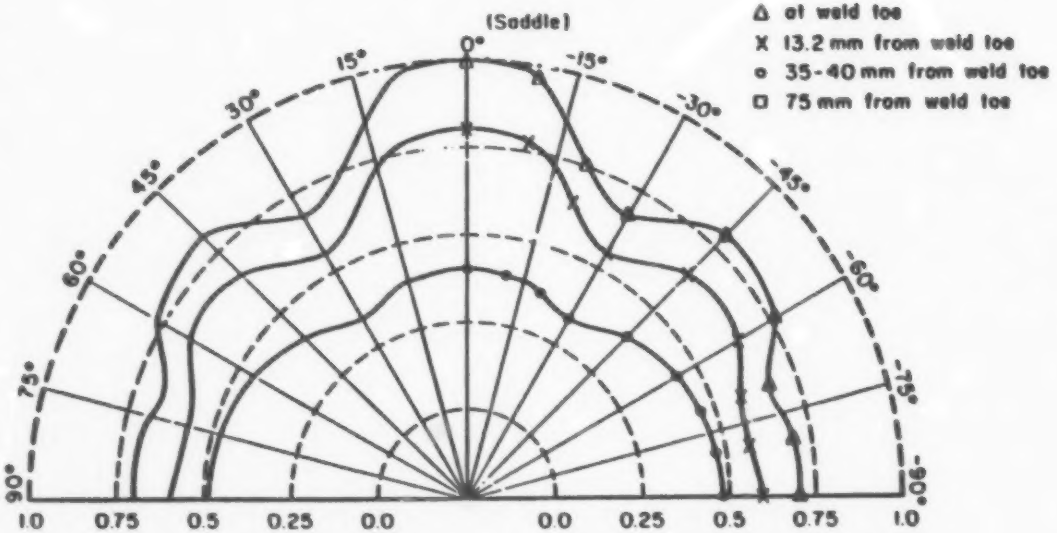

Fig. 29 Polar plot of normalized radial stress around the brace on the outside surface of the chord-stiffened tubular joint TA3 subjected to axial tensile load - 160 MPa

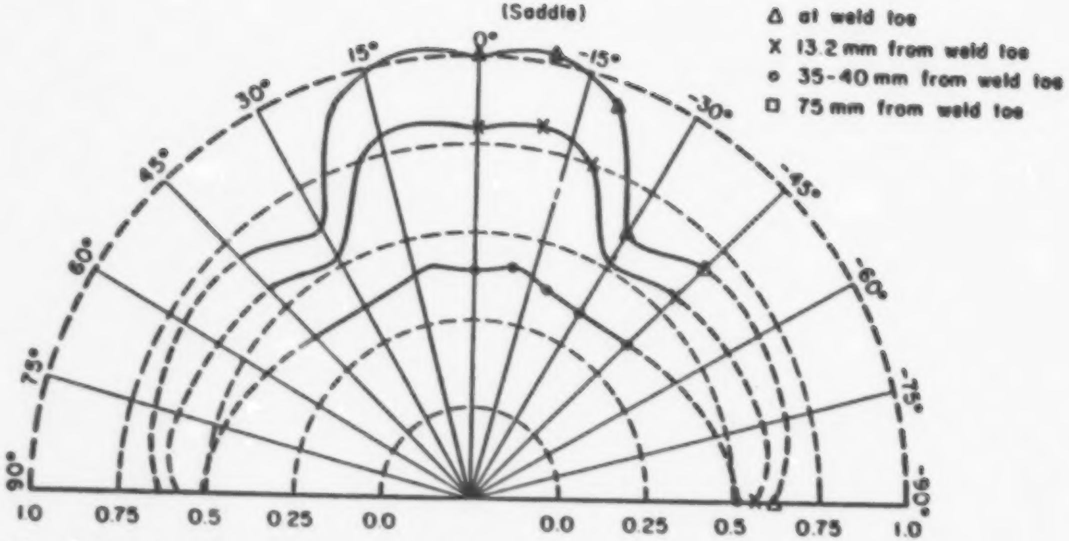

Fig. 30 Polar plot of normalized radial stress around the brace on the outside surface of the chord – stiffened tubular joint TA4 in seawater subjected to axial tensile load and cathodic projection – 250 MPa.

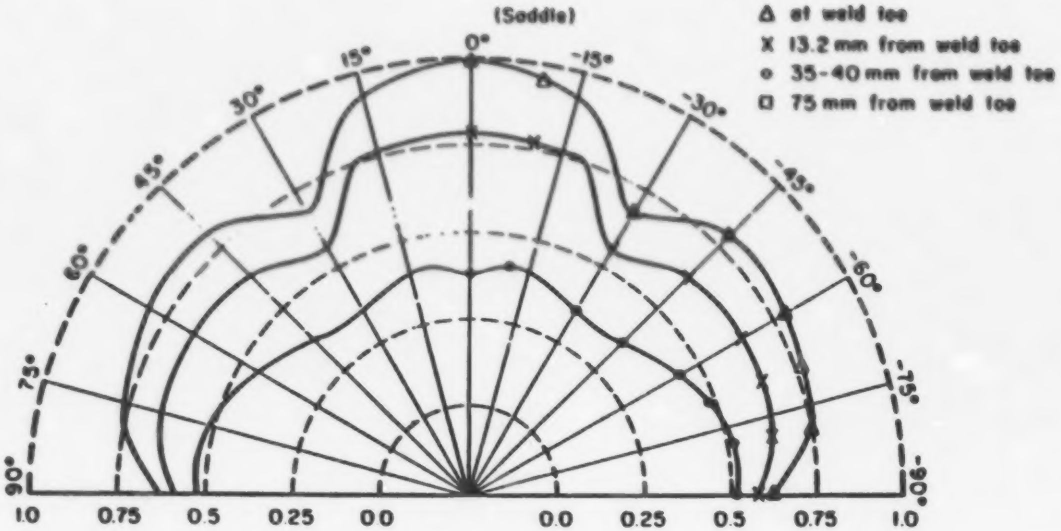

Fig. 31 Polar plot of normalized radial stress around the brace on the outside surface of the chord-stiffened tubular joint TA5 in seawater subjected to axial tensile load and cathodic projection – 160.0 MPa.

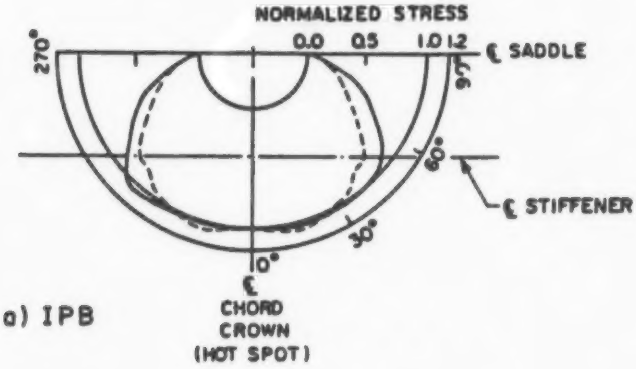

a) IPB

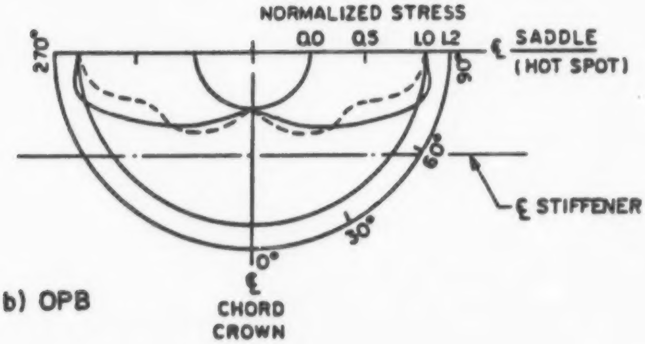

b) OPB

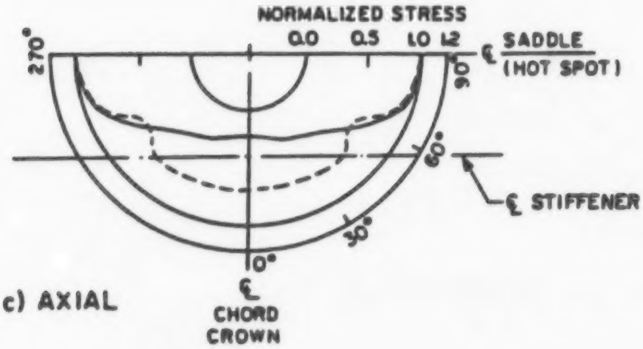

c) AXIAL

Figure 32: Comparisons of Stress Distributions in Chord for Stiffened and Unstiffened T-Joints.

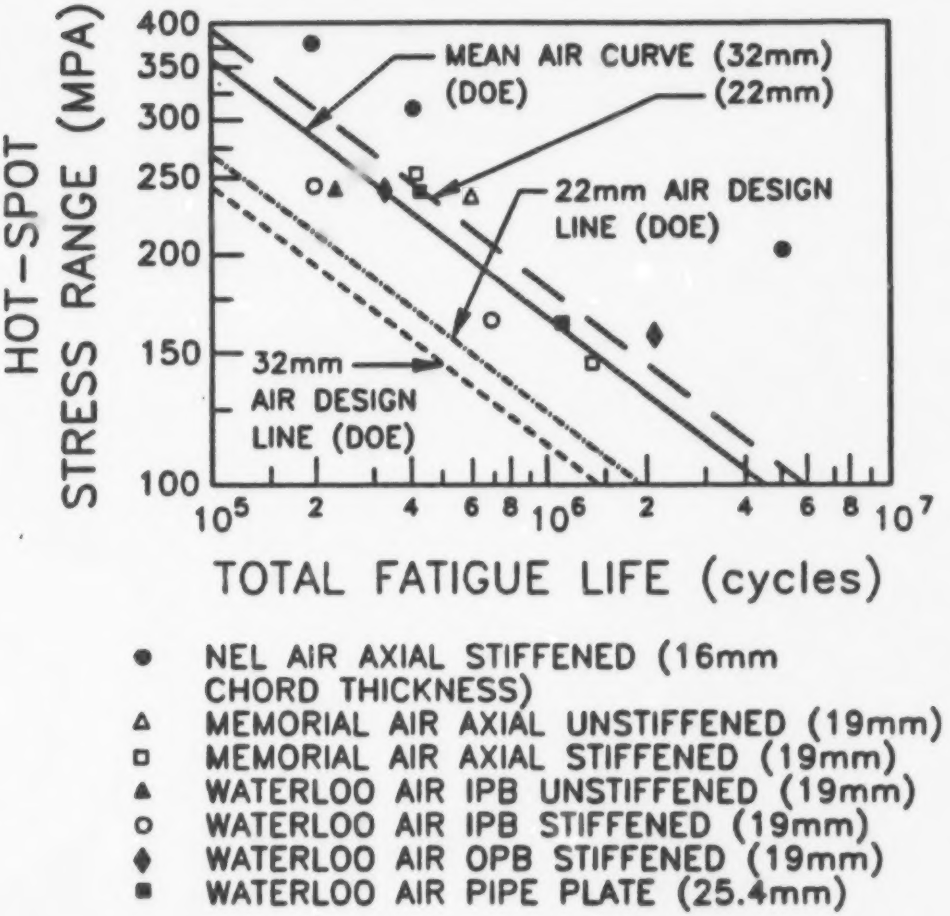

Figure 33 AIR FATIGUE TEST DATA.
SPECIMENS NOTED ABOVE.

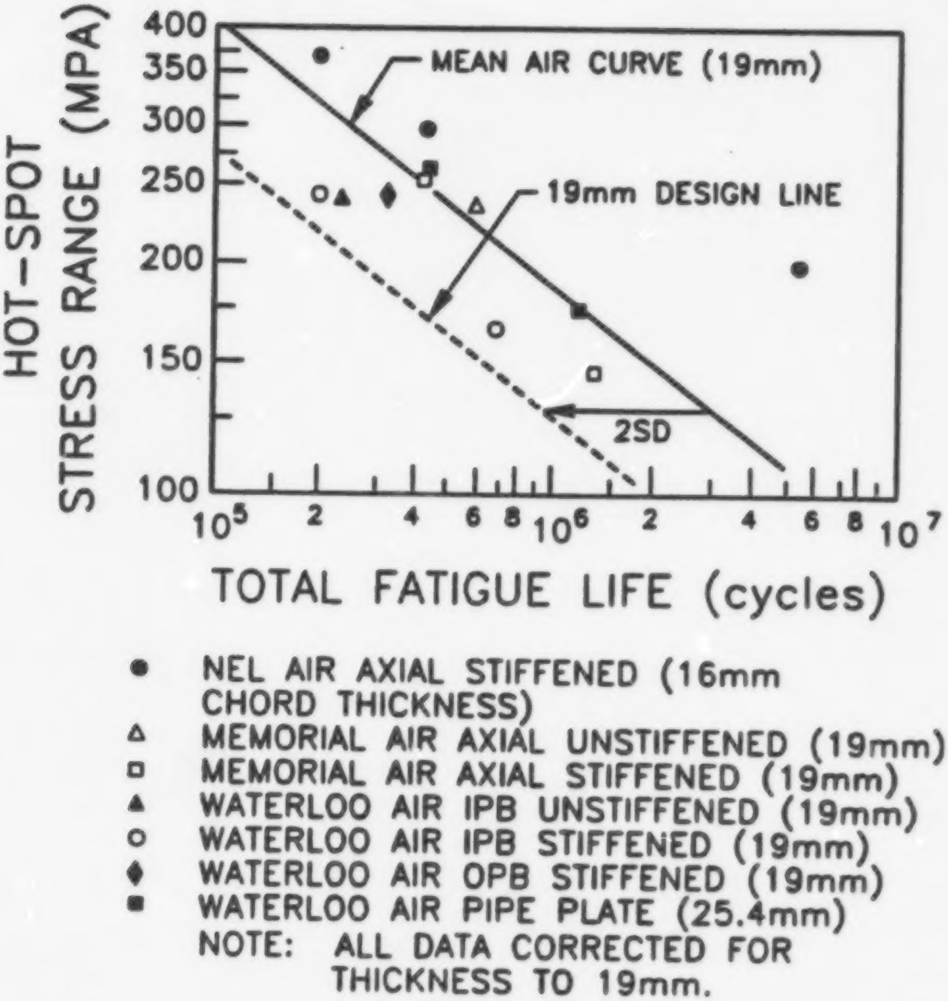

Figure 34 AIR FATIGUE TEST DATA. SPECIMENS NOTED ABOVE.

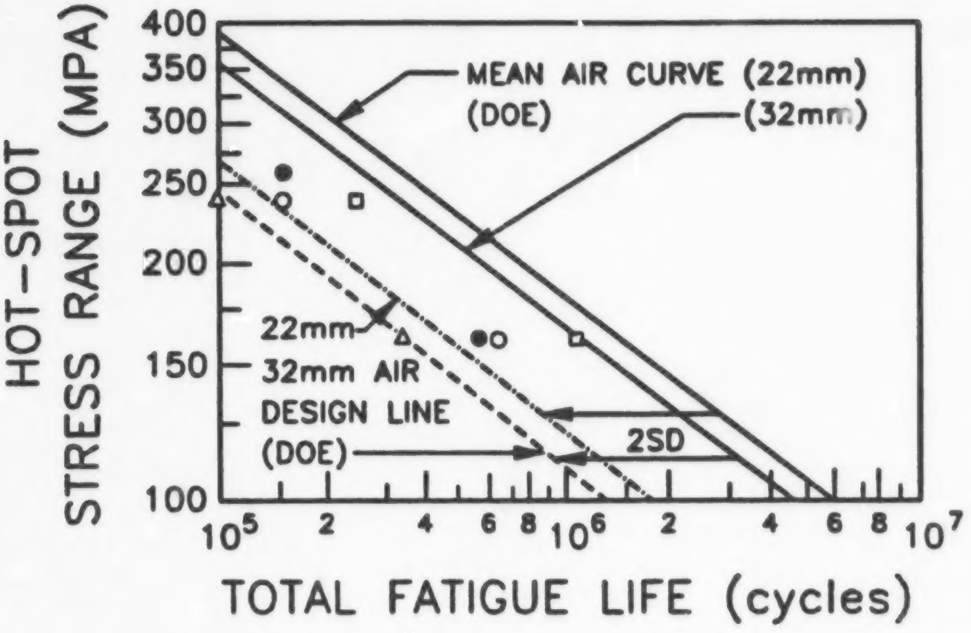

- ● MEMORIAL STIFFENED TUBULAR T-JOINT, AXIAL LOADING, SEAWATER WITH OPTIMUM CATHODIC PROTECTION (19 mm)
- ○ WATERLOO-PIPE PLATE, BENDING, SEAWATER FREE CORROSION (25.4 mm)
- □ WATERLOO-PIPE PLATE, BENDING, SEAWATER OPTIMUM CATHODIC PROTECTION (25.4 mm)
- △ WATERLOO-PIPE PLATE, BENDING, SEAWATER CATHODIC OVER PROTECTION (25.4 mm)

Figure 35 CORROSION FATIGUE DATA. SPECIMENS NOTED ABOVE.

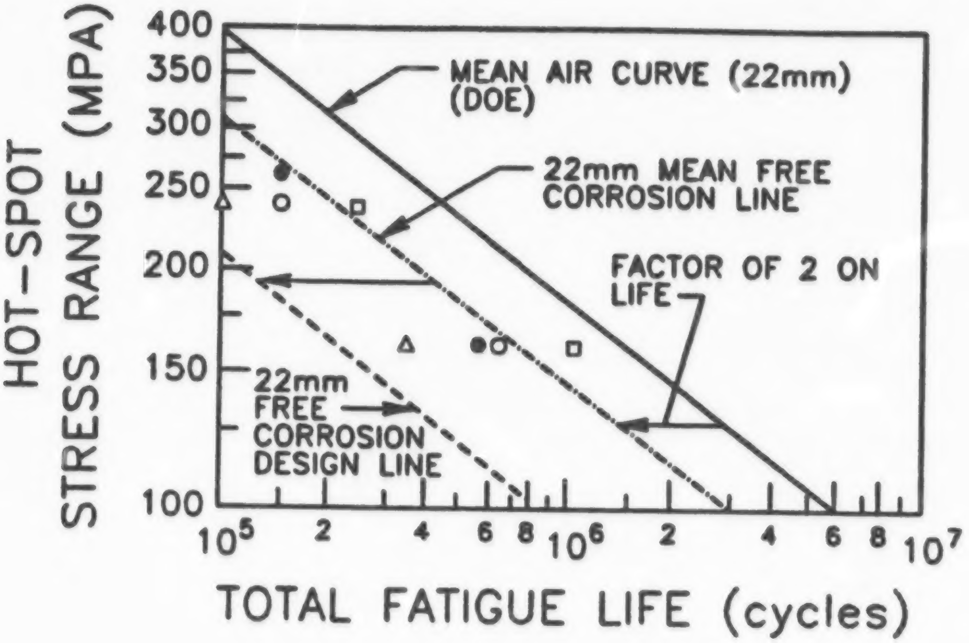

- ● MEMORIAL STIFFENED TUBULAR T-JOINT, AXIAL LOADING, SEAWATER WITH OPTIMUM CATHODIC PROTECTION (19 mm)
- ○ WATERLOO-PIPE PLATE, BENDING, SEAWATER FREE CORROSION (25.4 mm)
- □ WATERLOO-PIPE PLATE, BENDING, SEAWATER OPTIMUM CATHODIC PROTECTION (25.4 mm)
- △ WATERLOO-PIPE PLATE, BENDING, SEAWATER CATHODIC OVER PROTECTION (25.4 mm)

Figure 36 CORROSION FATIGUE DATA. SPECIMENS NOTED ABOVE.

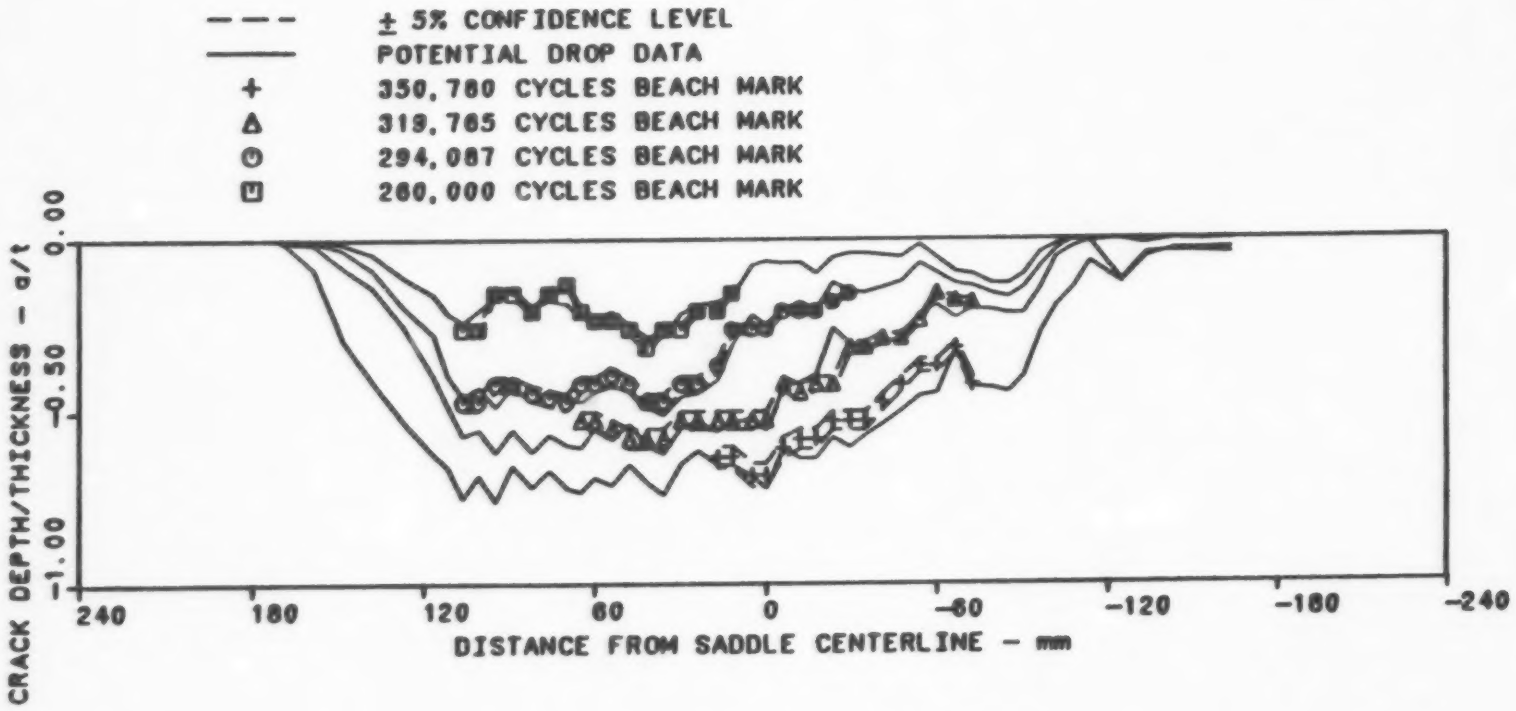

FIG. 37 CRACK DEPTH vs. POSITION
POTENTIAL DROP AND BEACH MARK COMPARISION
STIFFENED TUBULAR JOINT - TA2 SIDE 1
AXIAL LOAD - HOT SPOT STRESS RANGE 250 MPa

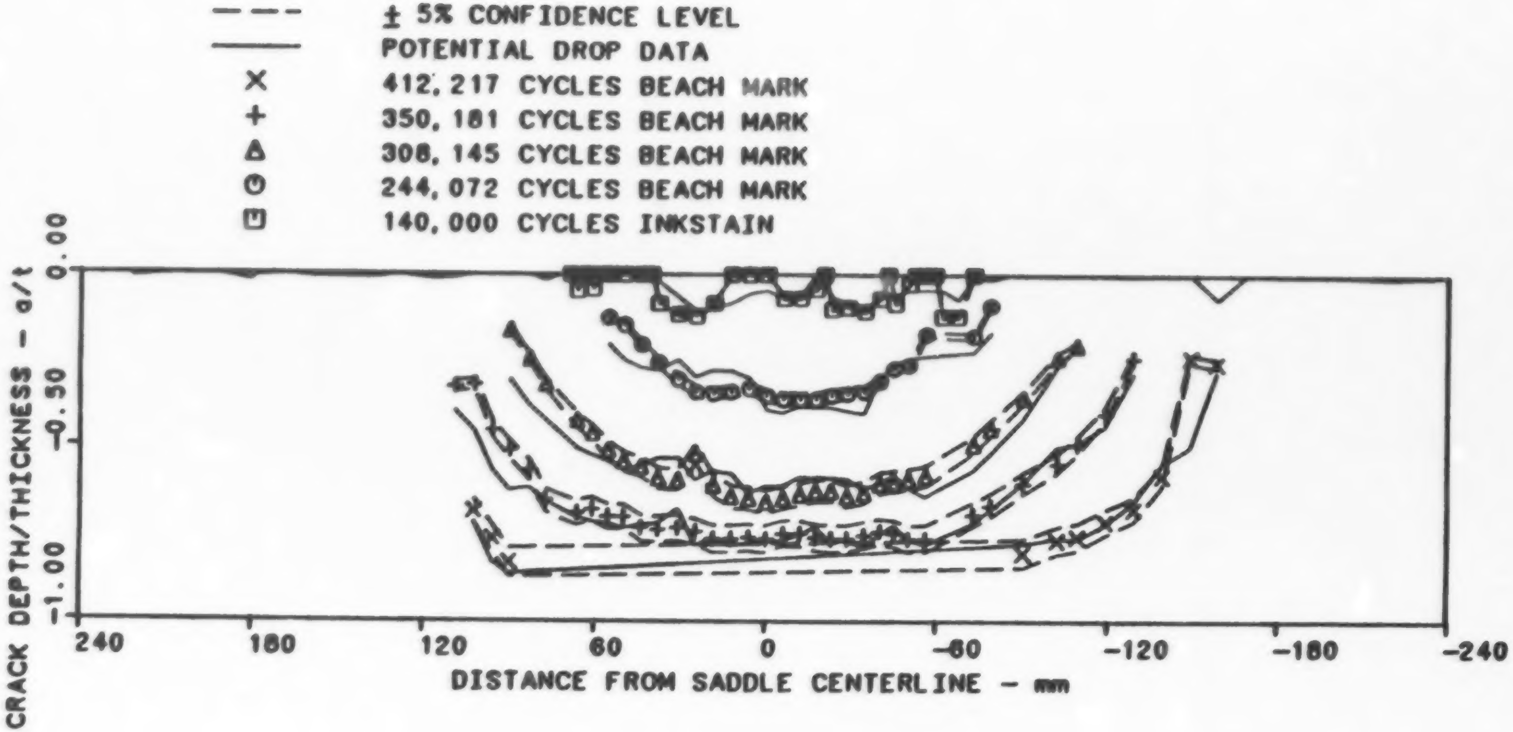

FIG. 38 CRACK DEPTH vs. POSITION
POTENTIAL DROP AND BEACH MARK COMPARISION
UNSTIFFENED TUBULAR JOINT - TA1 SIDE 2
AXIAL LOAD - HOT SPOT STRESS RANGE 250 MPa

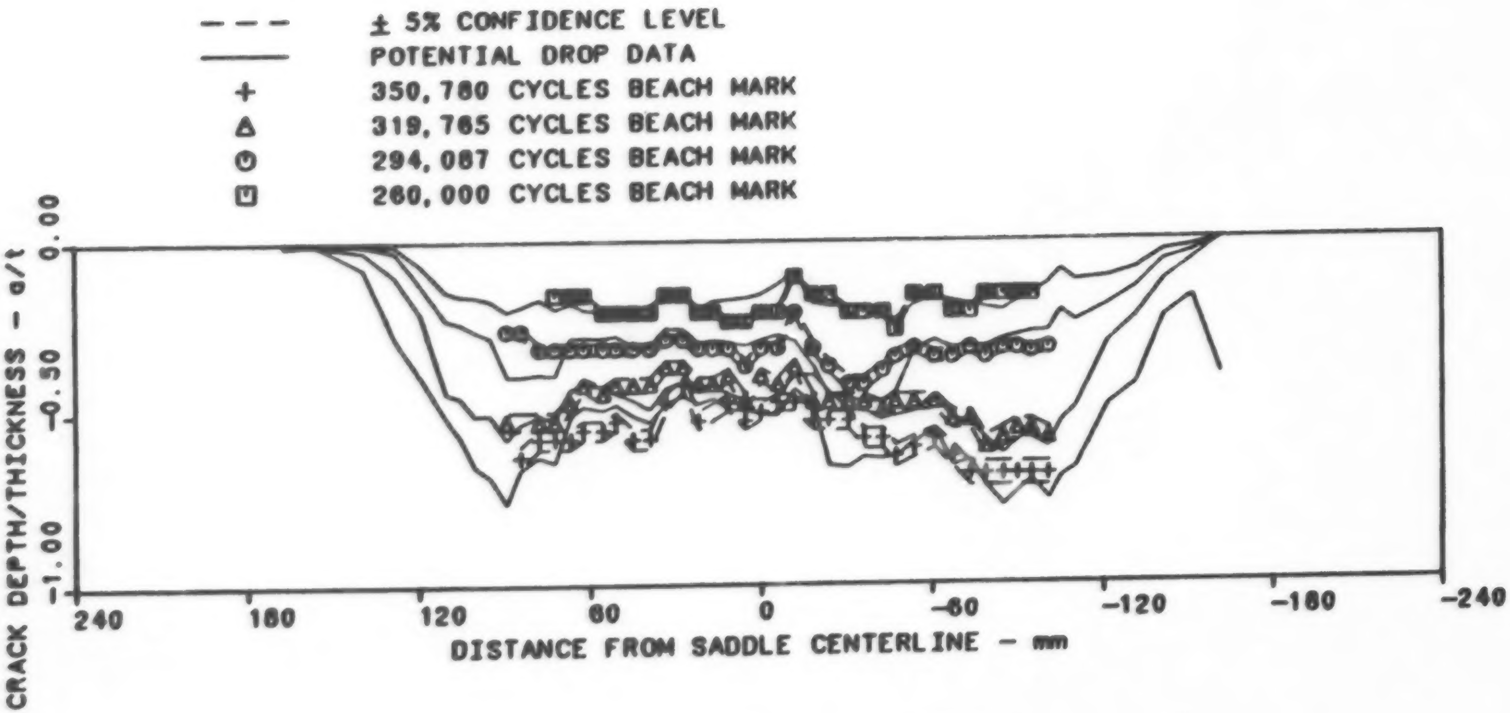

FIG. 39 CRACK DEPTH vs. POSITION
POTENTIAL DROP AND BEACH MARK COMPARISION
STIFFENED TUBULAR JOINT - TA2 SIDE 2
AXIAL LOAD - HOT SPOT STRESS RANGE 250 MPa

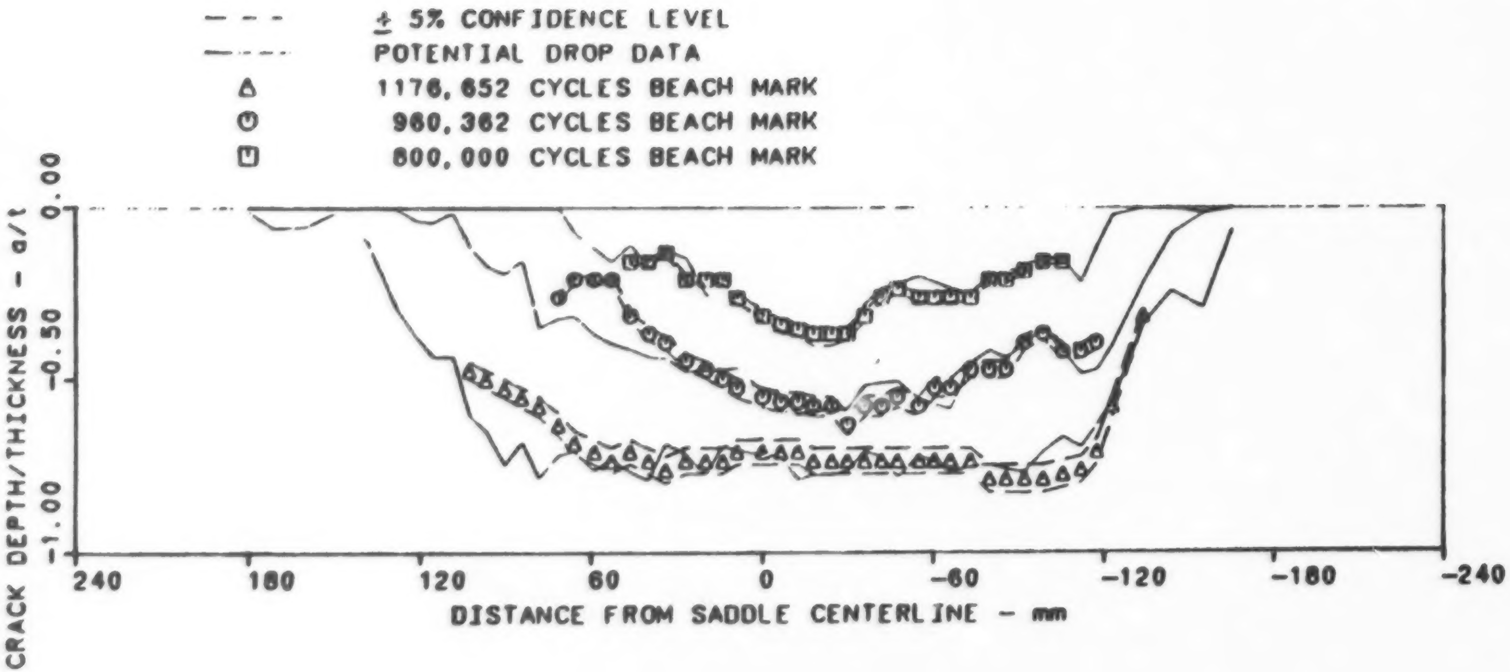

FIG. 40 CRACK DEPTH vs. POSITION
POTENTIAL DROP AND BEACH MARK COMPARISION
STIFFENED TUBULAR JOINT - TA3 SIDE 2
AXIAL LOAD - HOT SPOT STRESS RANGE 160 MPa

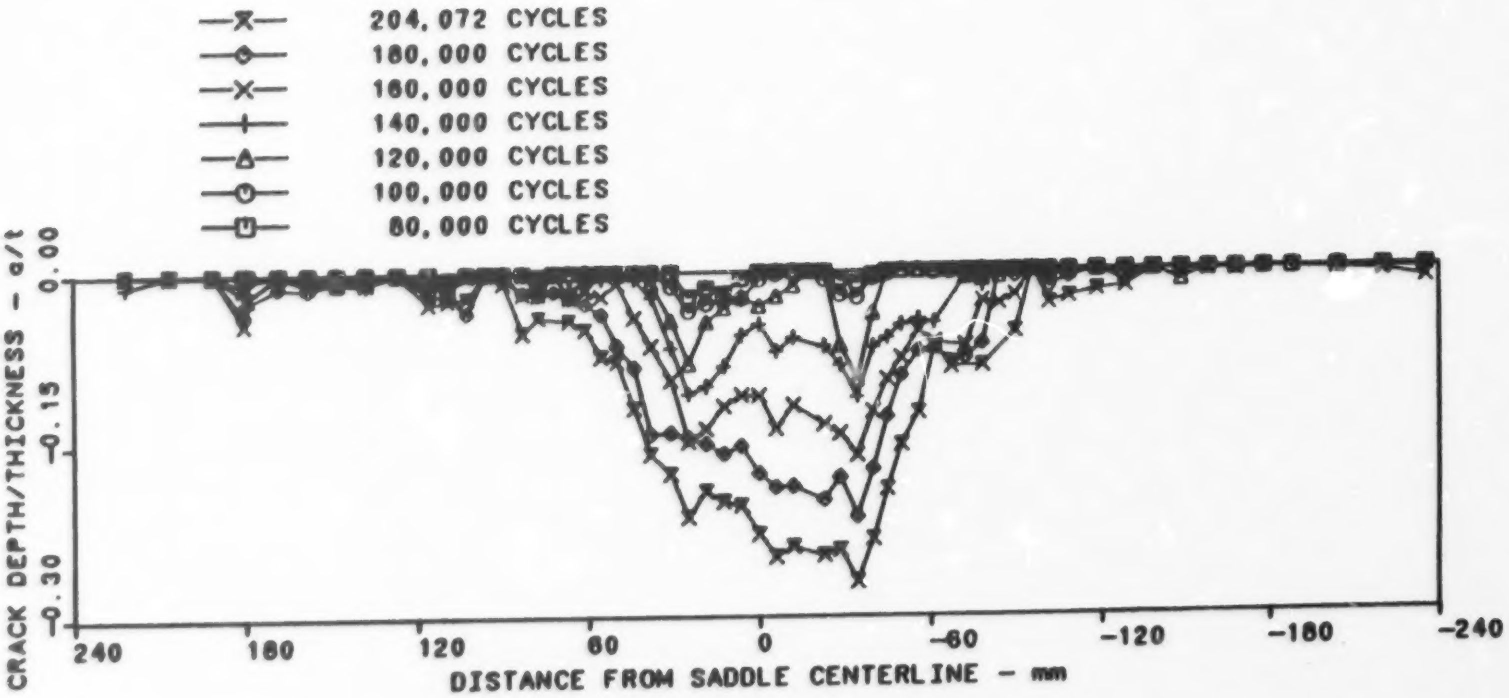

FIG. 41 CRACK DEPTH vs. POSITION
A.C POTENTIAL DROP RESULTS
(MAGNIFIED EARLIER PART OF CRACK GROWTH)
UNSTIFFENED TUBULAR JOINT - TA1 SIDE 2
AXIAL LOAD - HOT SPOT STRESS RANGE 250 MPa

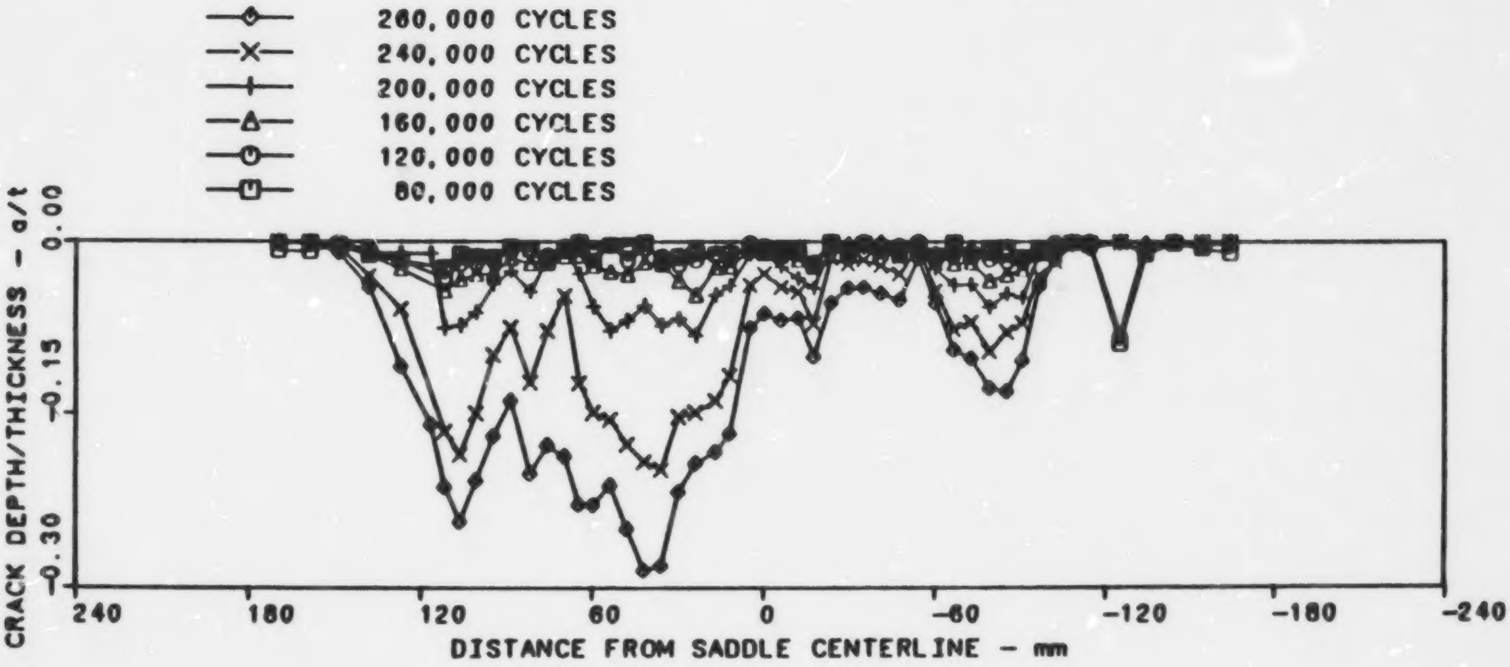

FIG. 42 CRACK DEPTH vs. POSITION
A.C POTENTIAL DROP RESULTS
(MAGNIFIED EARLIER PART OF CRACK GROWTH)
STIFFENED TUBULAR JOINT - TA2 SIDE 1
AXIAL LOAD - HOT SPOT STRESS RANGE 250 MPa

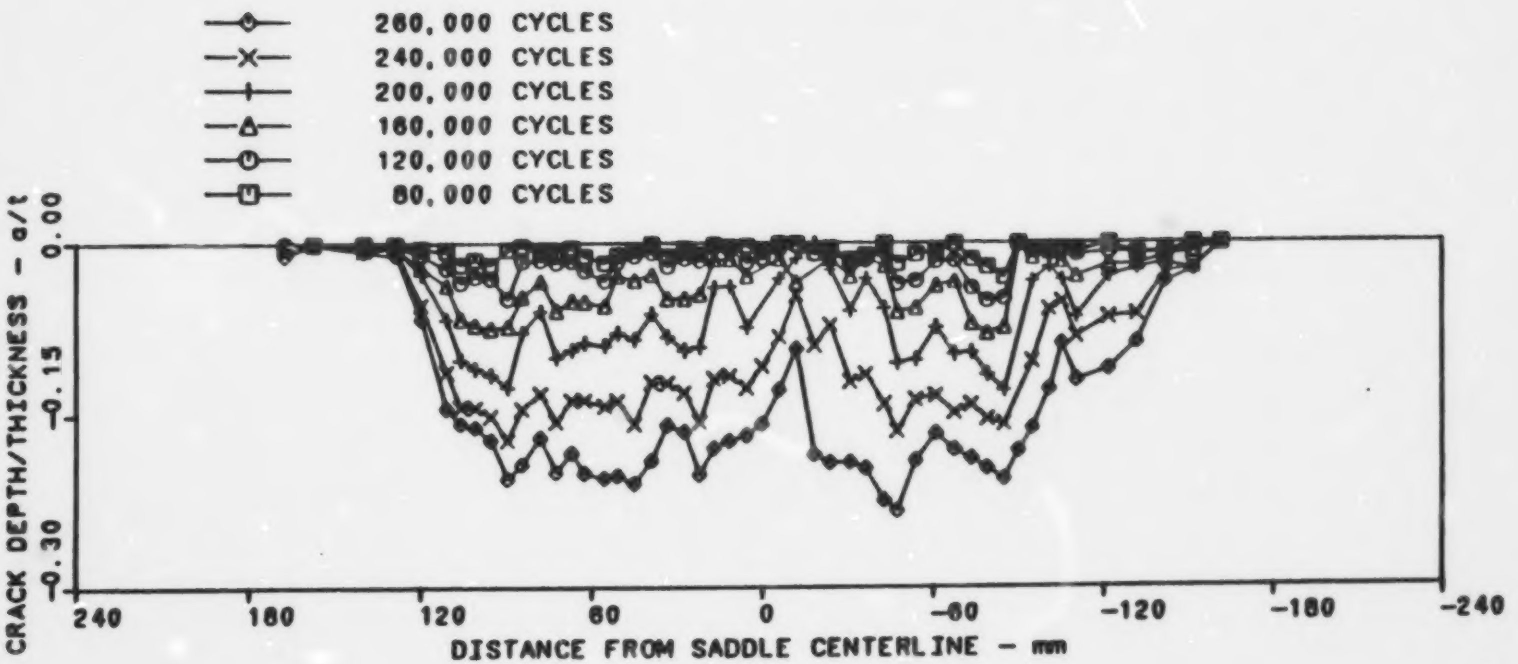

FIG. 43 CRACK DEPTH vs. POSITION
A.C POTENTIAL DROP RESULTS
(MAGNIFIED EARLIER PART OF CRACK GROWTH)
STIFFENED TUBULAR JOINT - TA2 SIDE 2
AXIAL LOAD - HOT SPOT STRESS RANGE 250 MPa

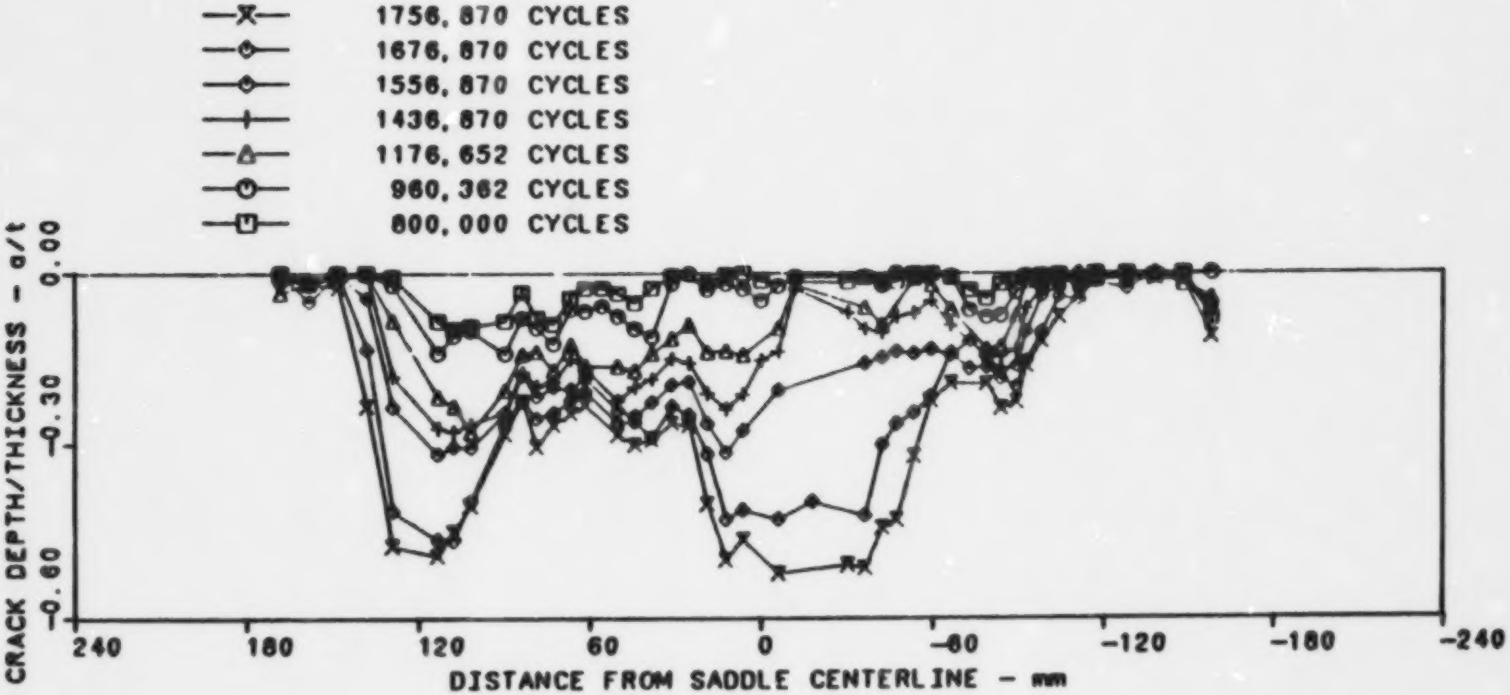

FIG. 44 CRACK DEPTH vs. POSITION
A.C POTENTIAL DROP RESULTS
STIFFENED TUBULAR JOINT - TA3 SIDE 1
AXIAL LOAD - HOT SPOT STRESS RANGE 160 MPa

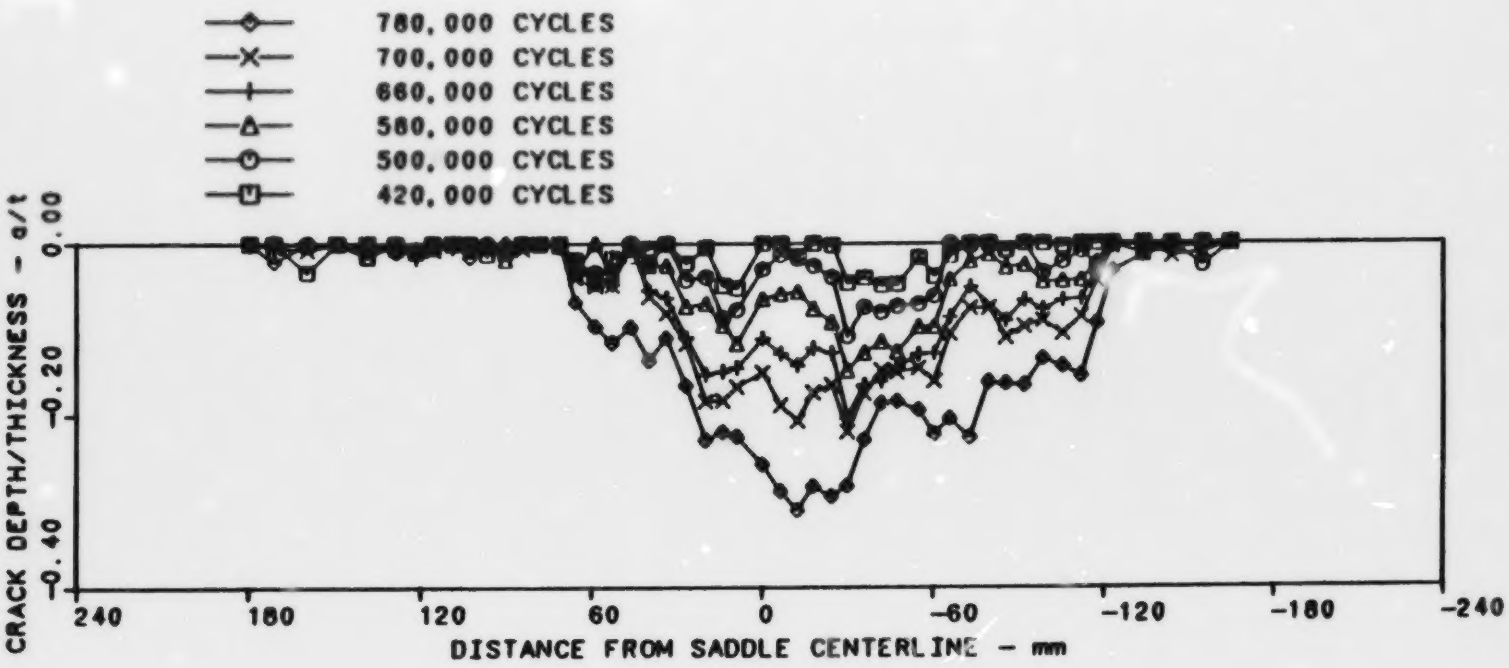

FIG. 45 CRACK DEPTH vs. POSITION
A.C POTENTIAL DROP RESULTS
(MAGNIFIED EARLIER PART OF CRACK GROWTH)
STIFFENED TUBULAR JOINT - TA3 SIDE 2
AXIAL LOAD - HOT SPOT STRESS RANGE 160 MPa

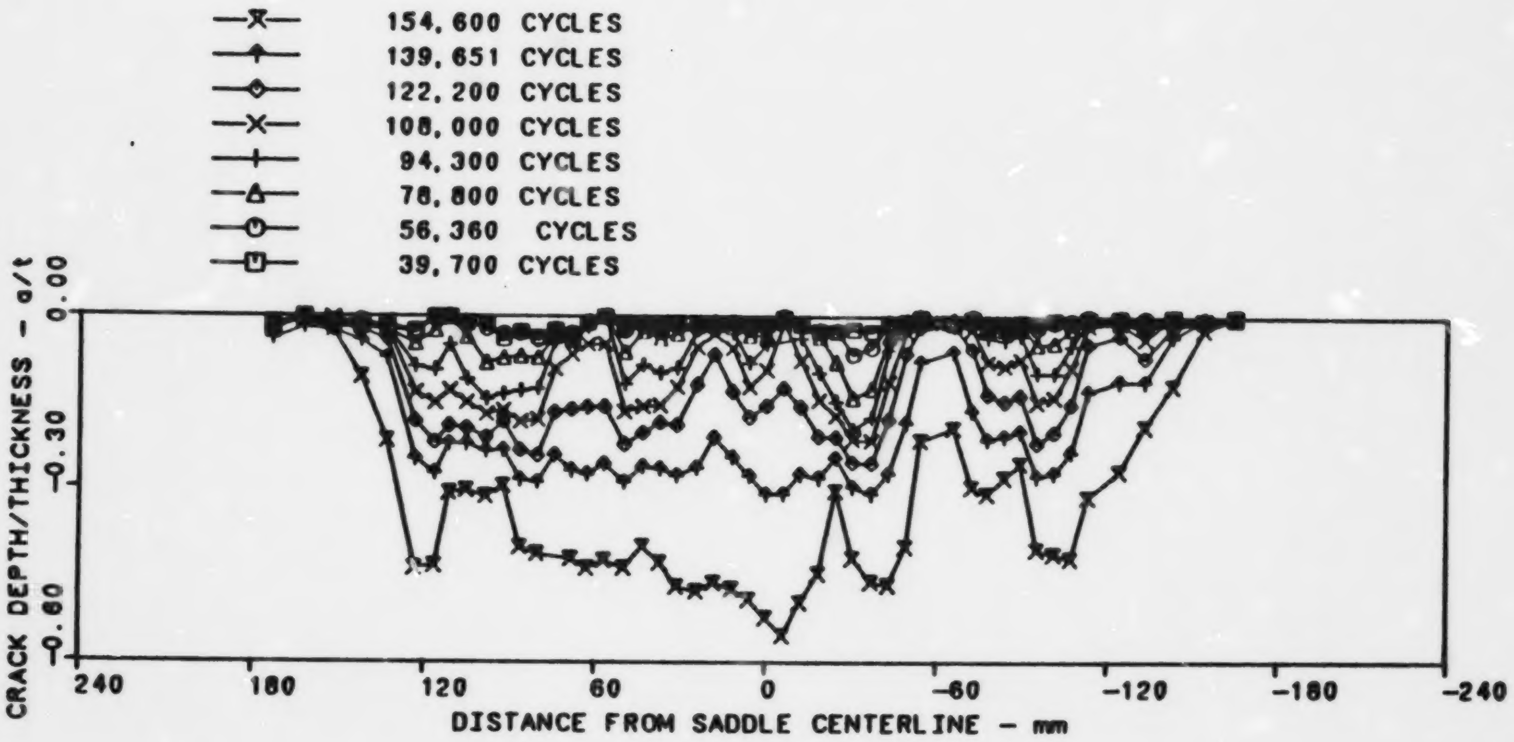

FIG. 46 CRACK DEPTH vs. POSITION
A.C POTENTIAL DROP RESULTS
STIFFENED TUBULAR JOINT - TA4 SIDE 1
AXIAL LOAD - HOT SPOT STRESS RANGE 250 MPa

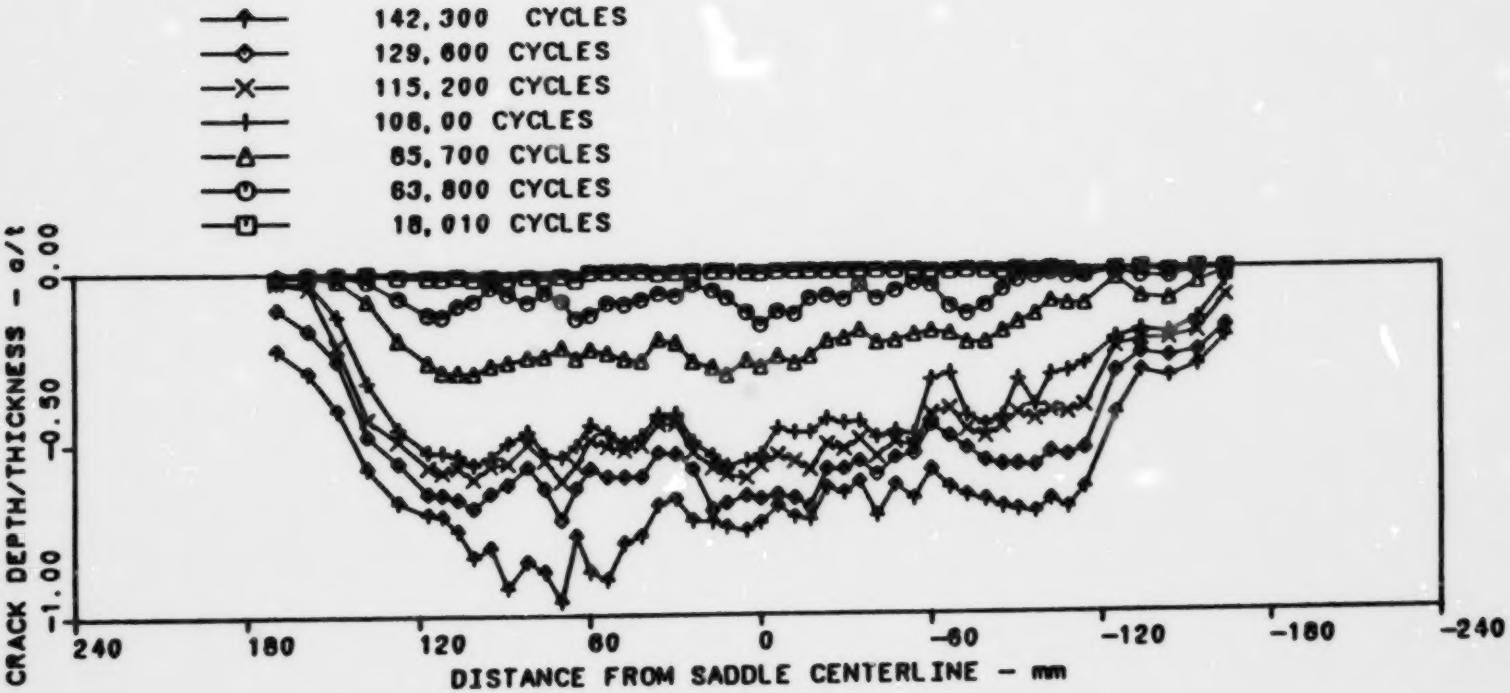

FIG. 47 CRACK DEPTH vs. POSITION
A.C POTENTIAL DROP RESULTS
STIFFENED TUBULAR JOINT - TA4 SIDE 2
AXIAL LOAD - HOT SPOT STRESS RANGE 250 MPa

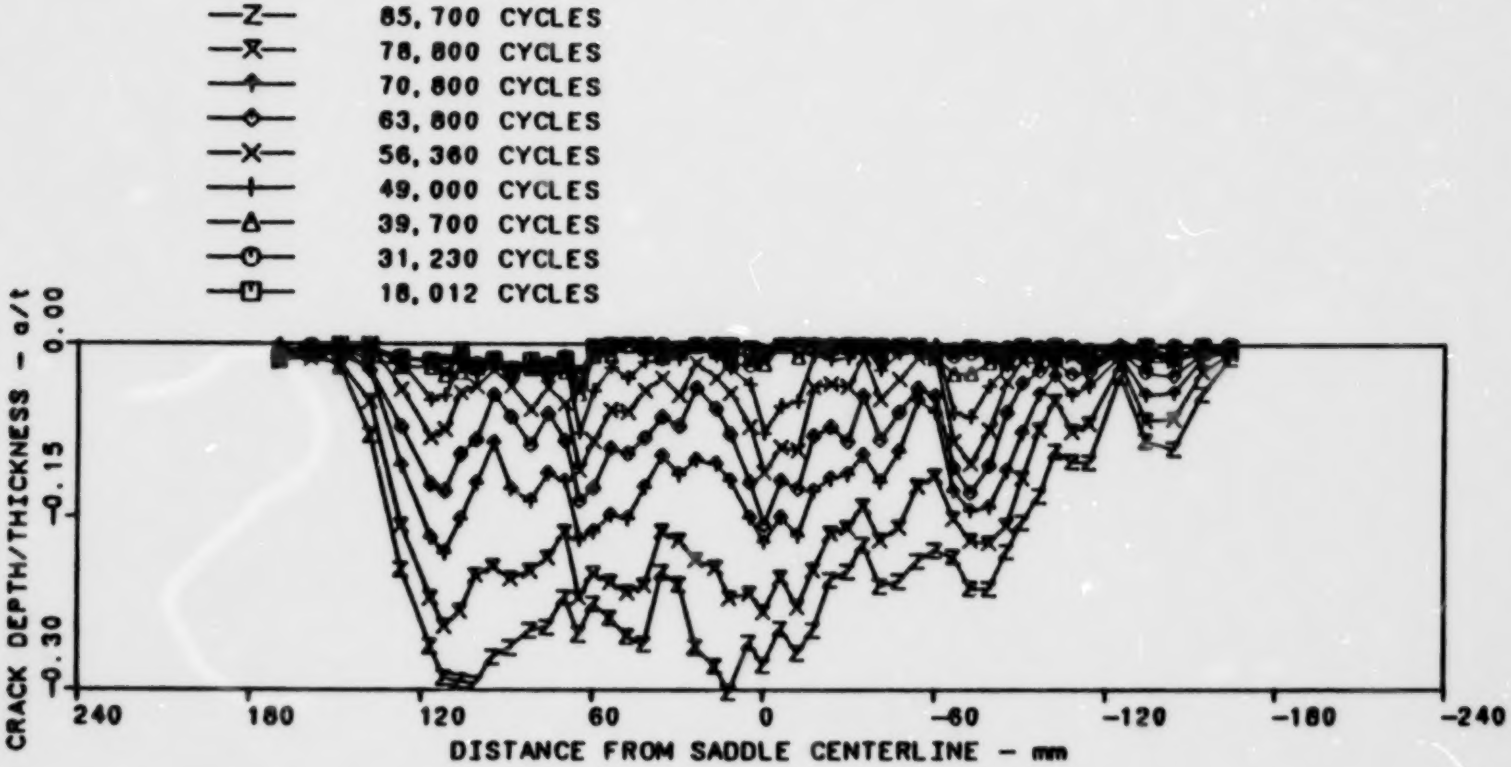

FIG. 48 CRACK DEPTH vs. POSITION
A.C POTENTIAL DROP RESULTS
(MAGNIFIED EARLIER PART OF CRACK GROWTH)
STIFFENED TUBULAR JOINT - TA4 SIDE 2
AXIAL LOAD - HOT SPOT STRESS RANGE 250 MPa

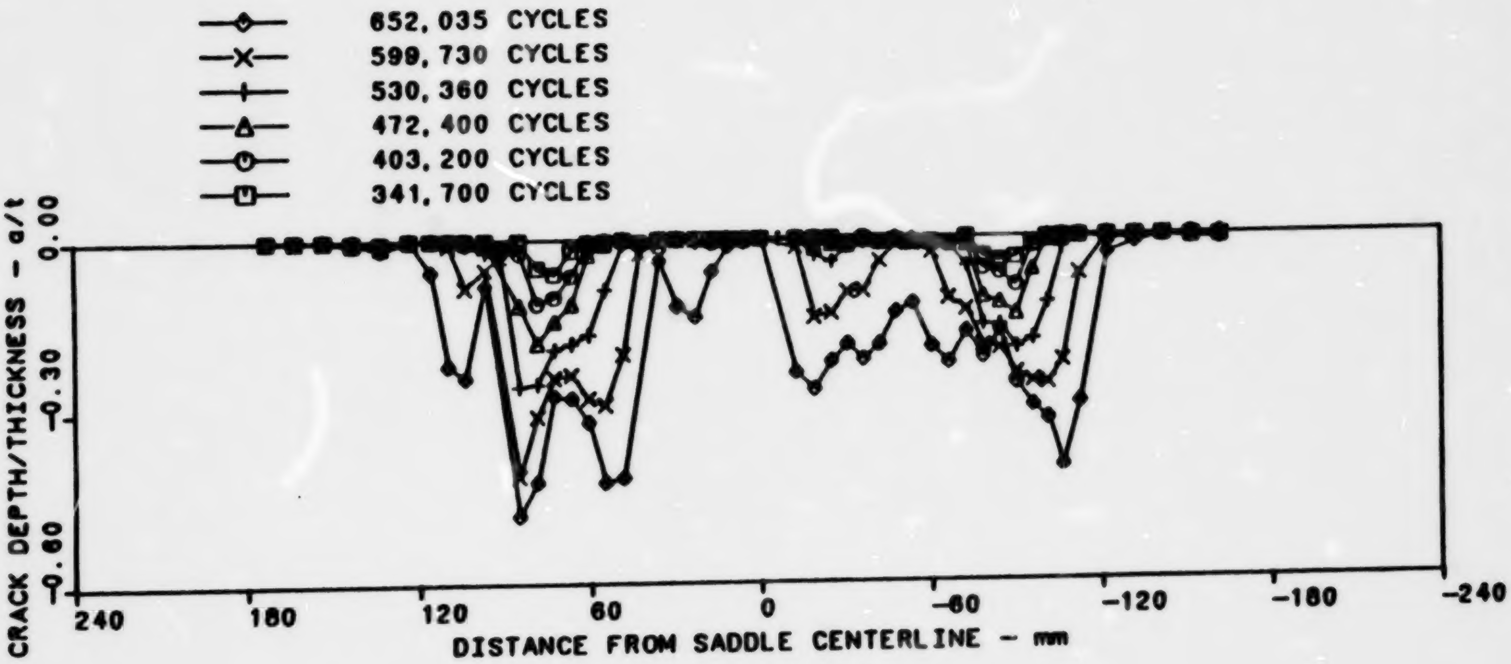

FIG. 49 CRACK DEPTH vs. POSITION
A.C POTENTIAL DROP RESULTS
STIFFENED TUBULAR JOINT – TA5 SIDE 1
AXIAL LOAD – HOT SPOT STRESS RANGE 160 MPa

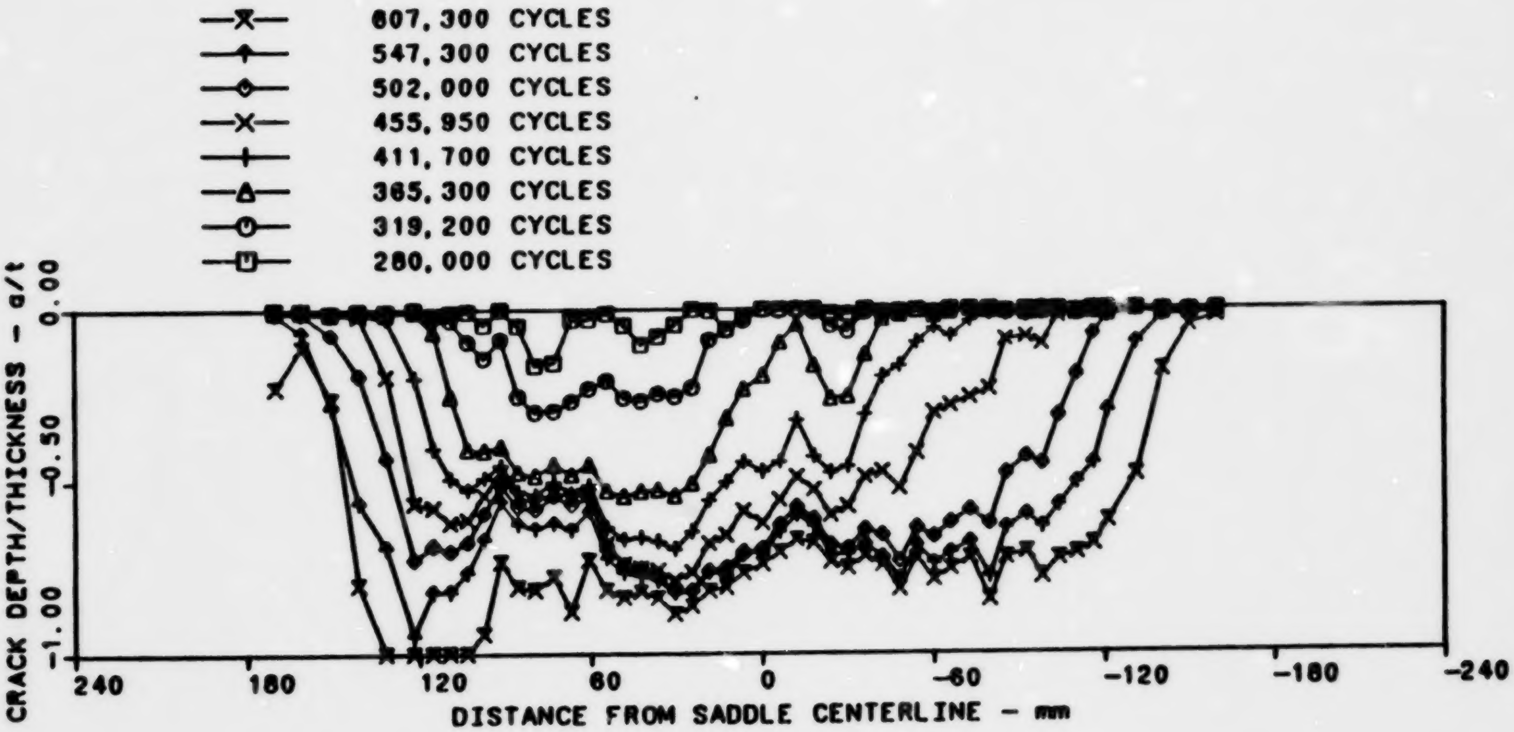

FIG. 50 CRACK DEPTH vs. POSITION
A.C POTENTIAL DROP RESULTS
STIFFENED TUBULAR JOINT - TA5 SIDE 2
AXIAL LOAD - HOT SPOT STRESS RANGE 160 MPa

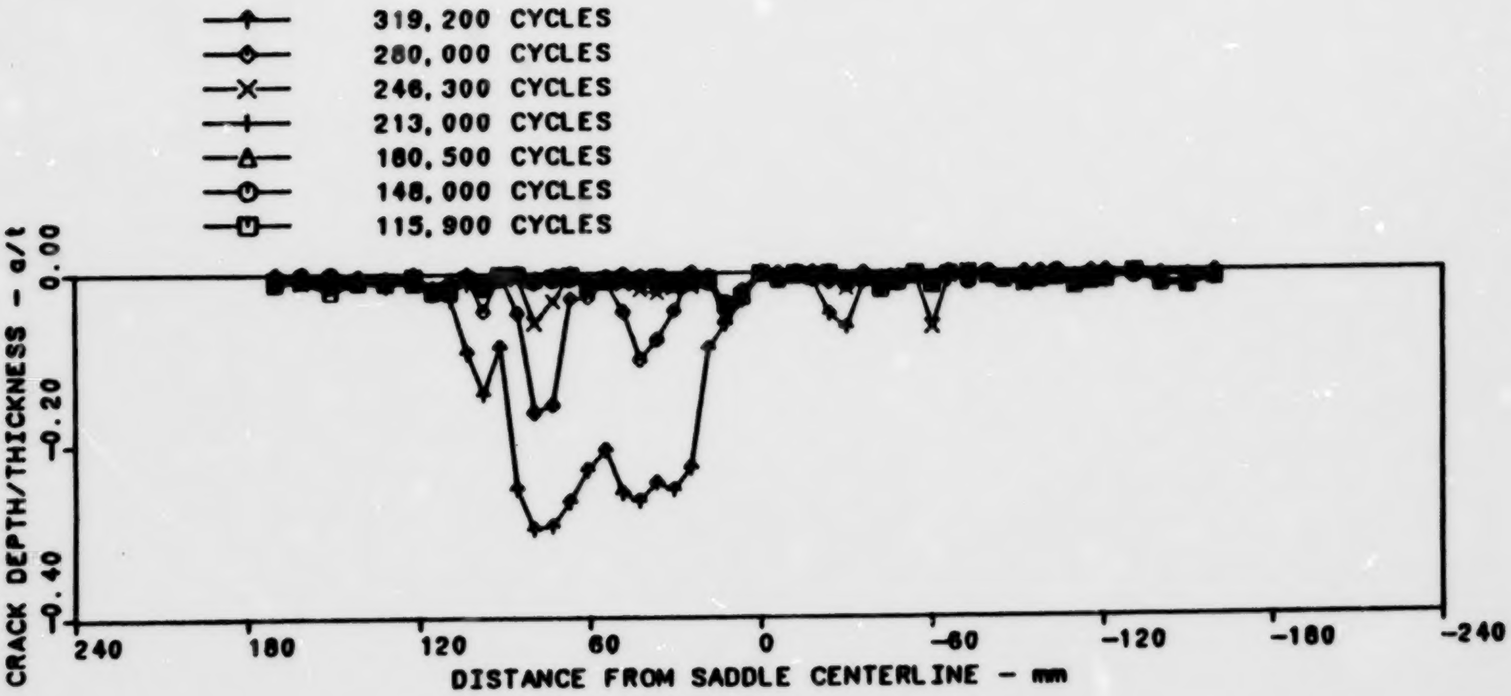

FIG. 51 CRACK DEPTH vs. POSITION
A.C POTENTIAL DROP RESULTS
(MAGNIFIED EARLIER PART OF CRACK GROWTH)
STIFFENED TUBULAR JOINT - TA5 SIDE 2
AXIAL LOAD - HOT SPOT STRESS RANGE 160 MPa

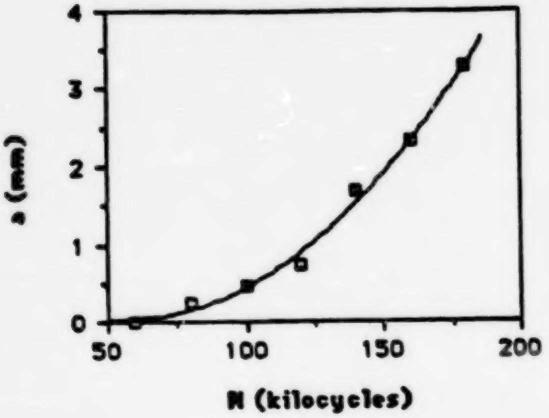

Side 2. - Tranverse distance from saddle point 18 mm
Angular position from saddle point 176°
Initiating life N_1 = 103,000 cycles

Fig. 52 Crack depth vs. cycles for crack initiating location
- Unstiffened joint (TA1)
- Nominal hot spot stress range 250 MPa

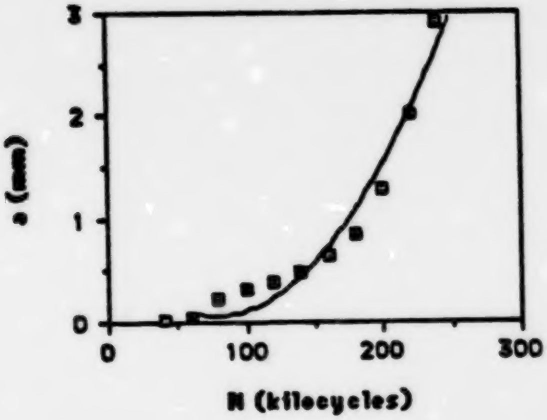

Side 1. - Tranverse distance from saddle point 30 mm
Angular position from saddle point 7°
Initiang life N_1= 142,300 cycles

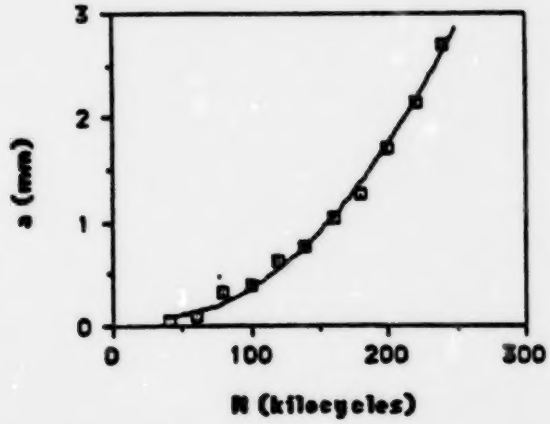

Side 2. -Transverse distance from saddle point 35 mm
Angular position from saddle point 167.5°
Initiating life N_1 = 115,000 cycles

Fig. 53 Crack depth vs. cycles for crack initiating location
- Stiffened joint (TA2)
- Nominal hot spot stress range 250 MPa

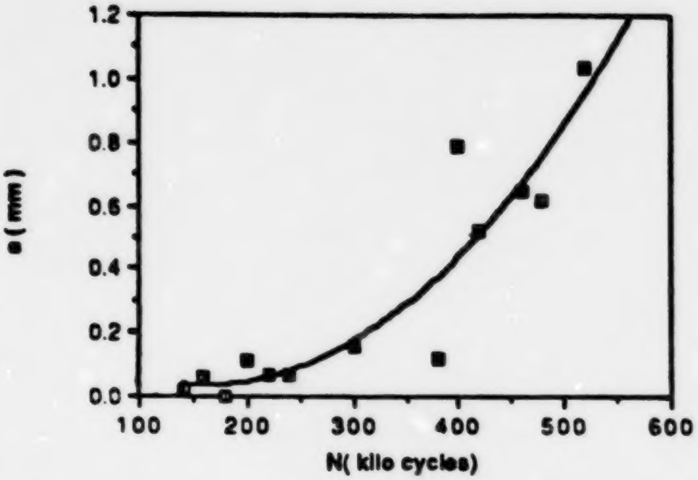

Side 1. - Transverse distance from saddle point 73 mm
Angular position from saddle point 343.5
Initiating life N_1 = 440,000 cycles

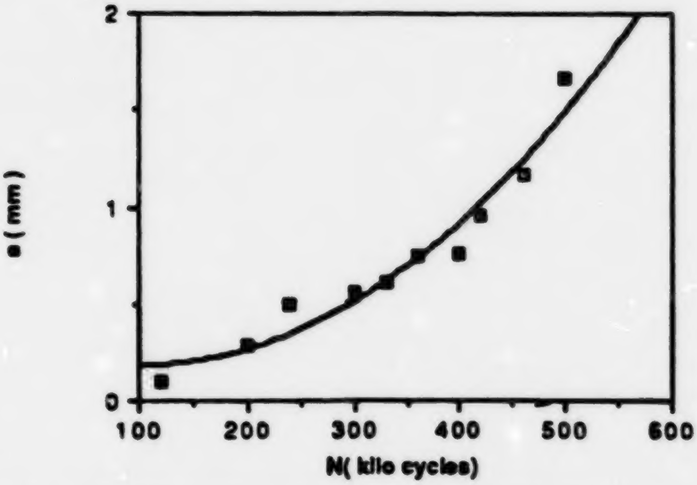

Side 2. - Transverse distance from saddle point 60.5 mm
Angular position from saddle point 166.3°
Initiating life N_1 = 300,000 cycles

Fig. 54 Crack depth vs. cycles for crack initiating location
- Stiffened joint (TA3)
- Nominal hot spot stress range 160 MPa

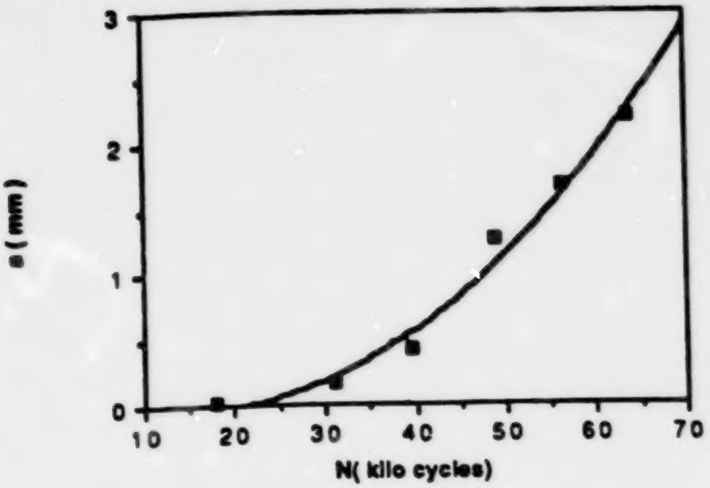

Side 1. - Traverse distance from saddle point -30.5 mm
Angular position from saddle point 7
Initiating life N_1 =39,000 cycles

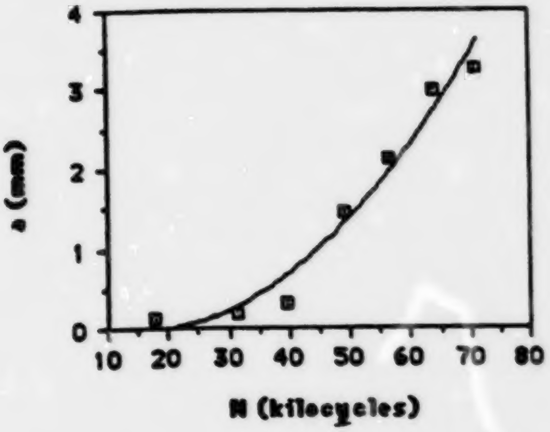

Side 2. - Transverse distance from saddle point 0 mm
Angular position from saddle point 180°
Initiating life N_1 = 35,500 cycles

Fig. 55 Crack depth vs. cycles for crack initiating location
- Stiffened joint (TA4)
- Nominal hotspot stress range 250 MPa

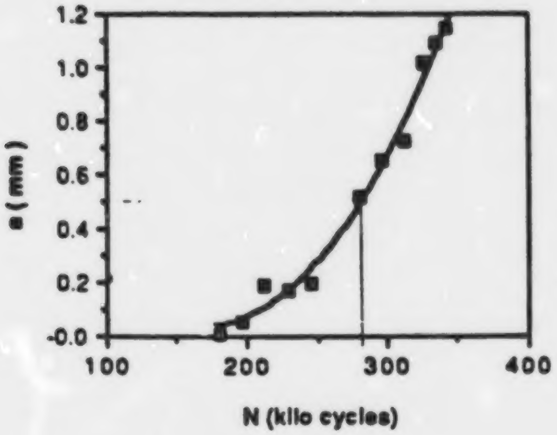

Side 1. - Transverse distance from saddle point 72.7 mm
Angular position from saddle point 343.5°
Initiating life N_1 = 285,000 cycles

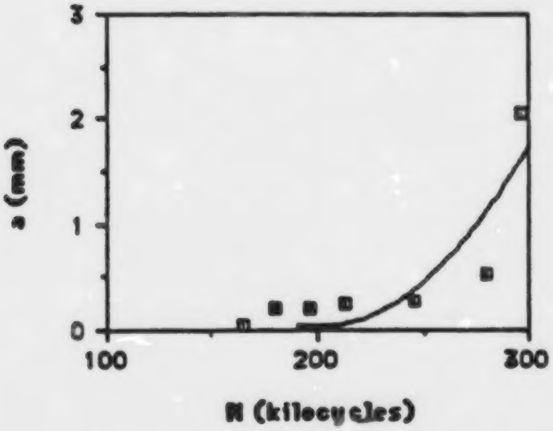

Side 2. - Transverse distance from saddle point 61 mm
Angular position from saddle point 193.9°
Initiating life N_i = 252,000 cycles

Fig. 56 Crack depth vs. cycles for crack initiating location
- Stiffened joint (TA5)
- Nominal hot spot stress range 160 MPa

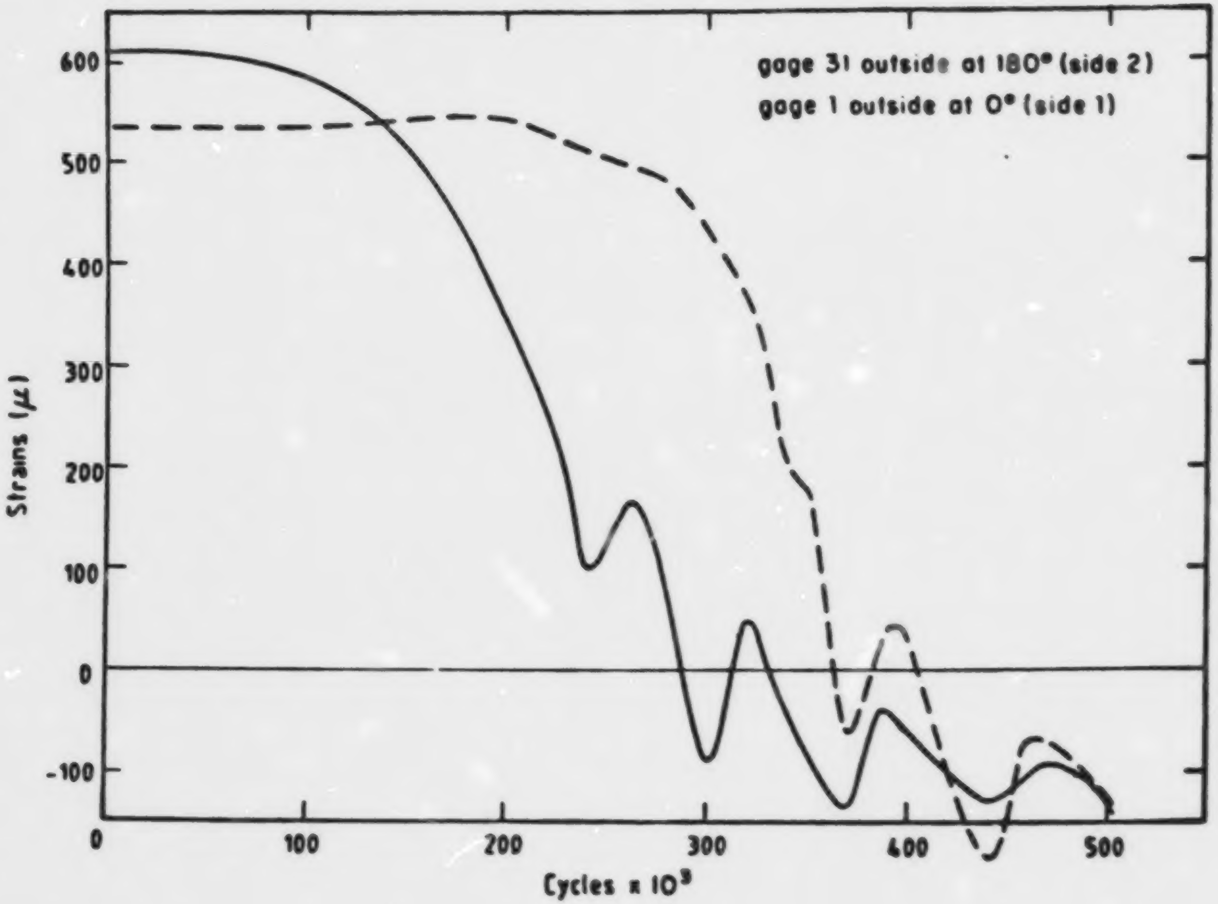

Fig. 57 Radial strain vs cycles at saddle point, T-joint (TA1), axial load - mean load (183 kN)

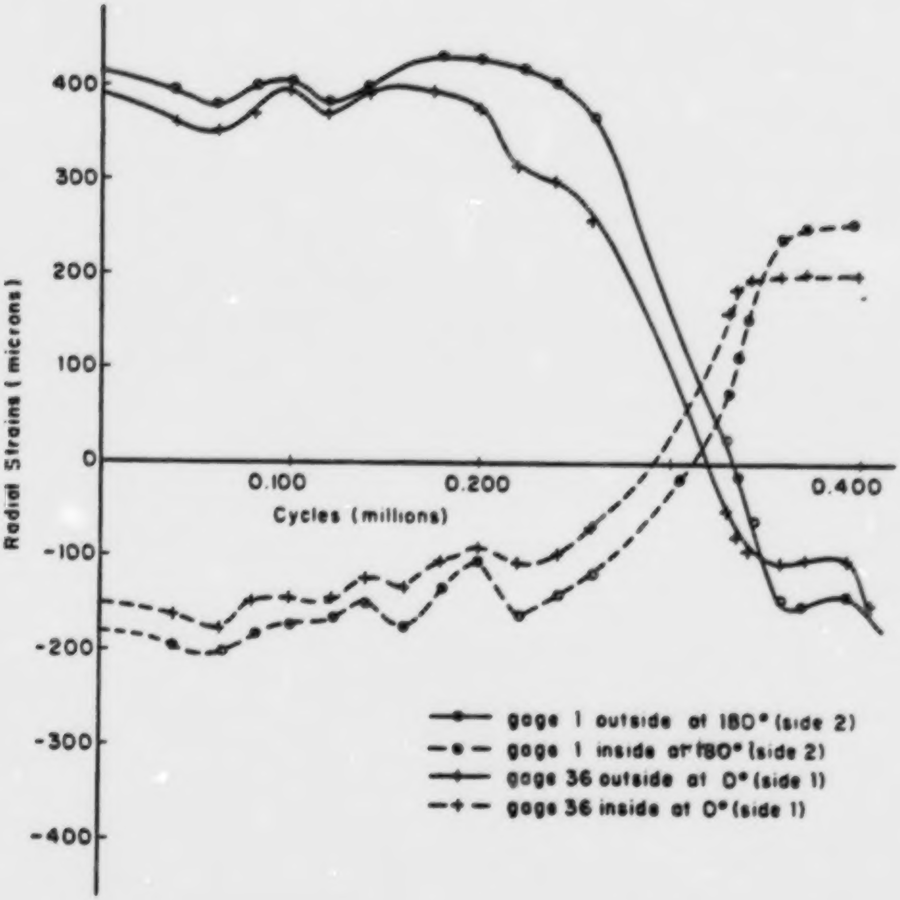

Fig. 58 Radial strain vs. cycles at saddle points of joint (TA2), axial load - mean load (570 kN)

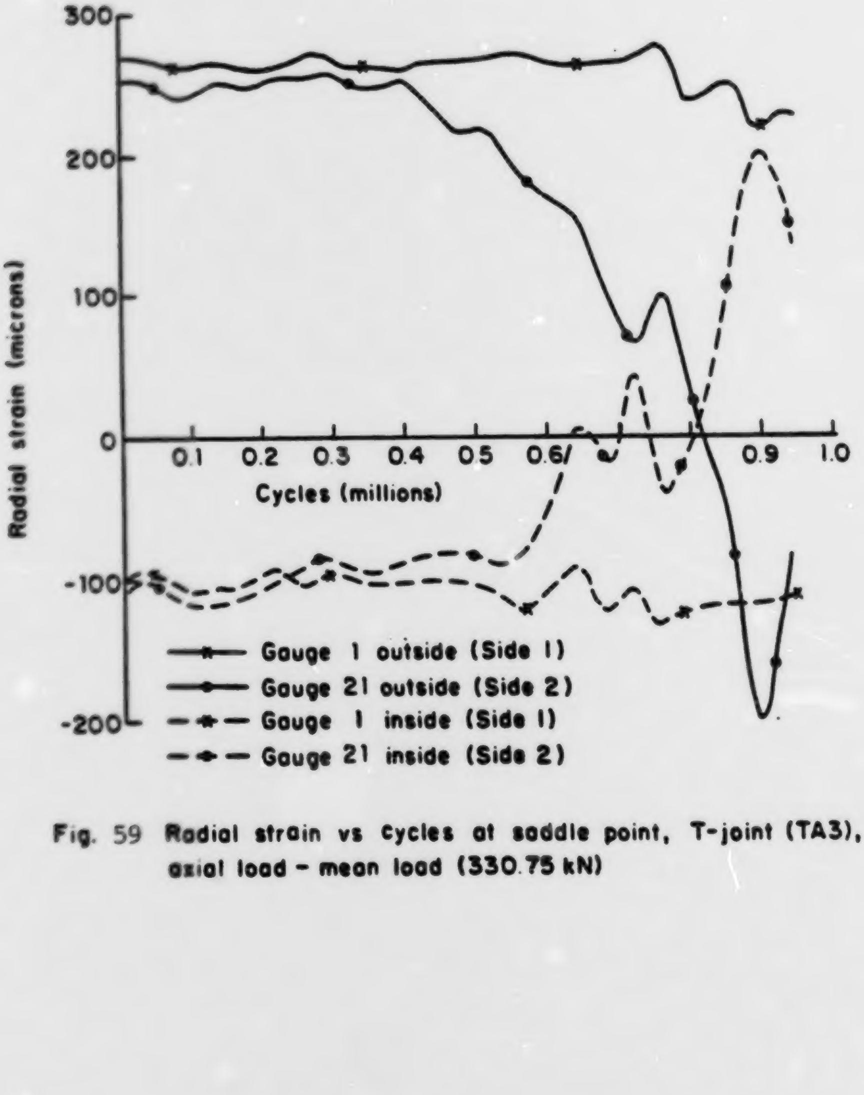

Fig. 59 Radial strain vs cycles at saddle point, T-joint (TA3), axial load - mean load (330.75 kN)

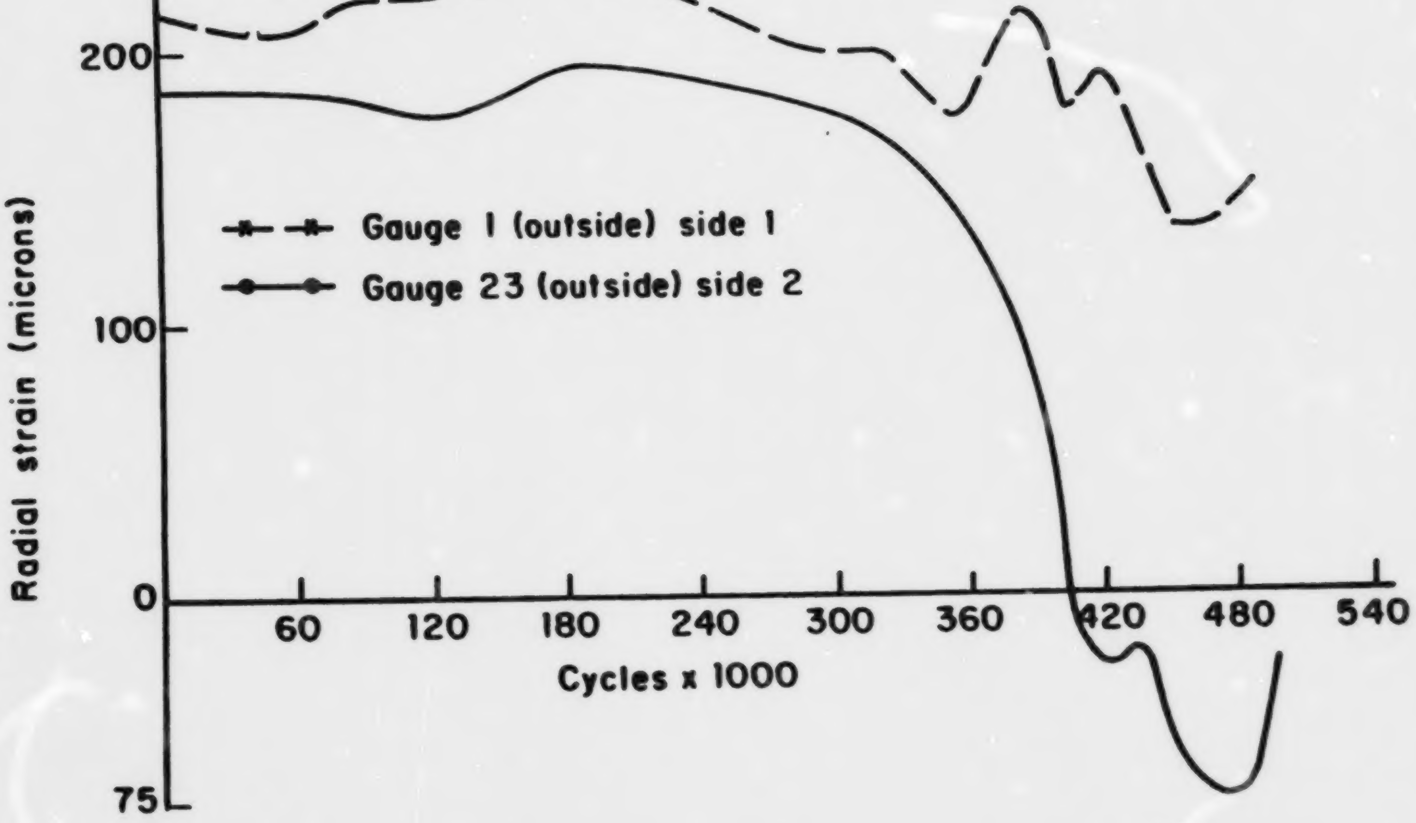

Fig. 60 Radial strain vs cycles at saddle point, T-joint (TA5), axial load - mean load (346.5 kN)

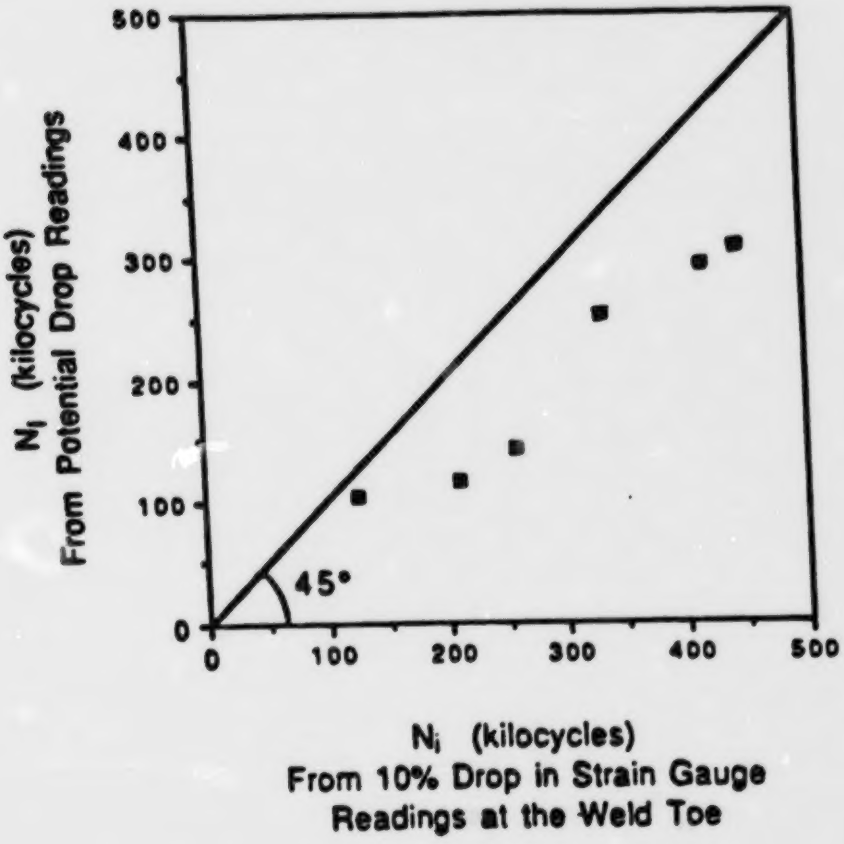

Figure 61 Comparison of Crack Initiation Lives Obtained from ACPD and 10% Strain Drop Readings

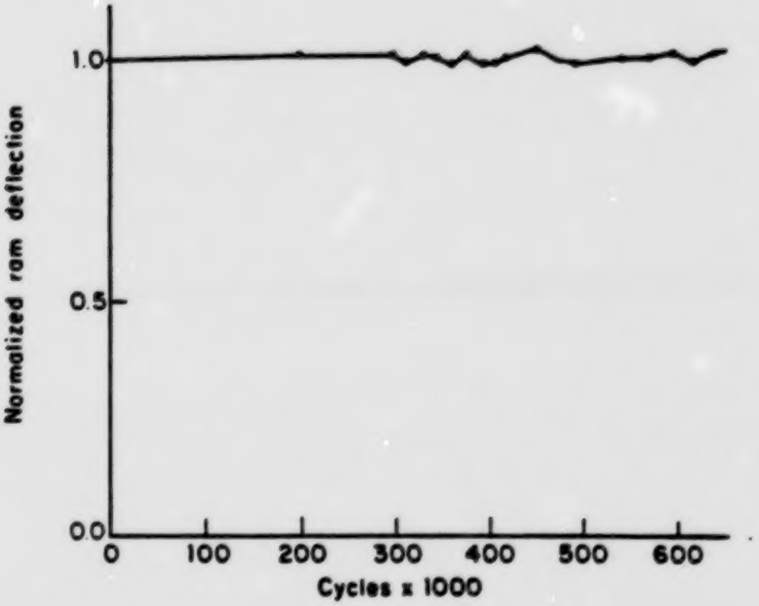

Fig. 62 Normalized actuator displacement variation (TA2)

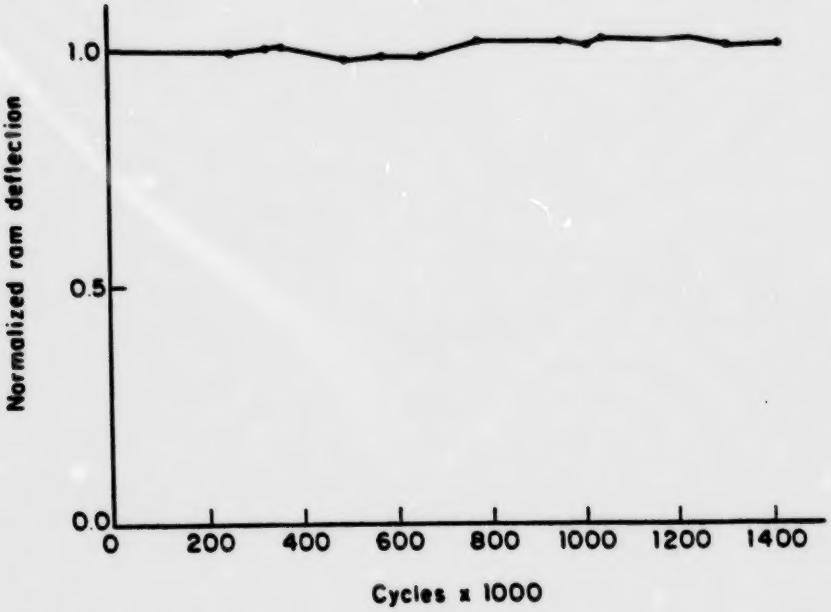

Fig. 63 Normalized actuator displacement variation (TA3)

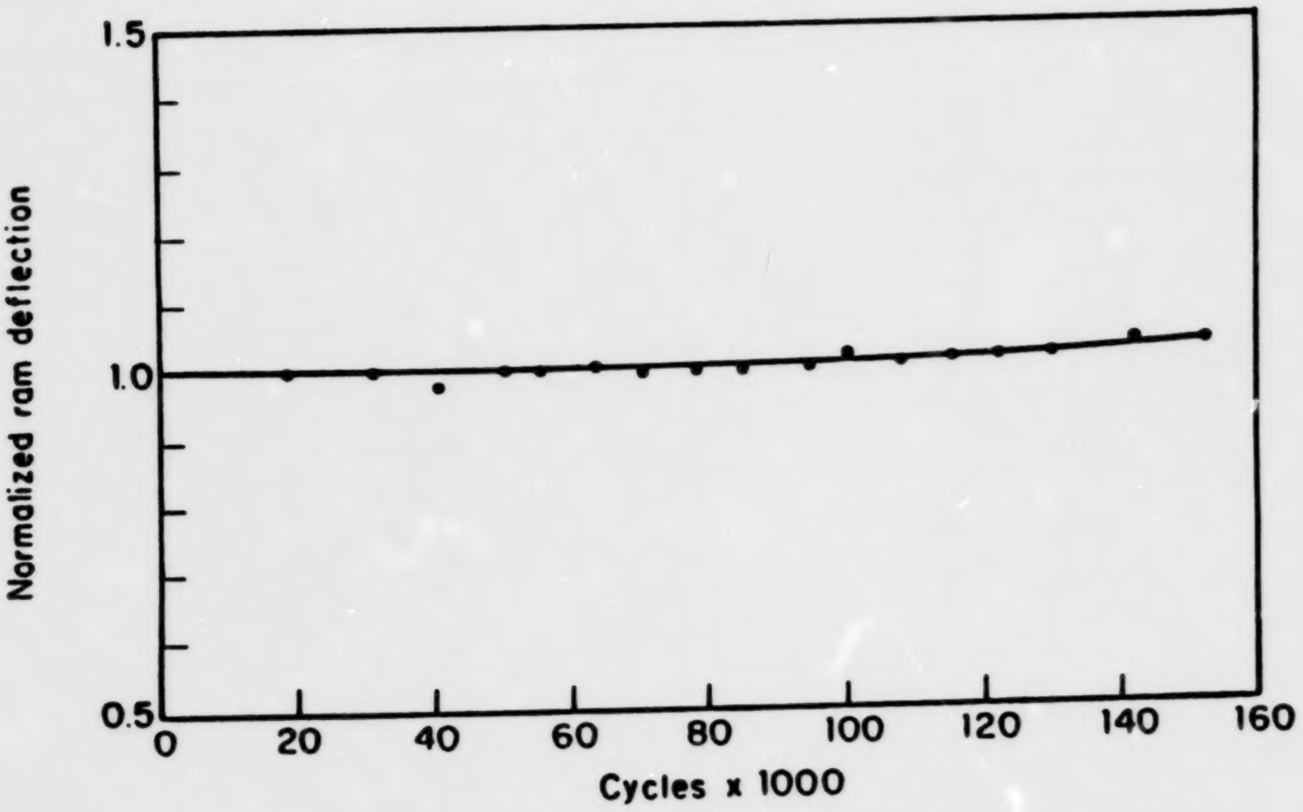

Fig. 64 Normalized actuator displacement variation (TA4)

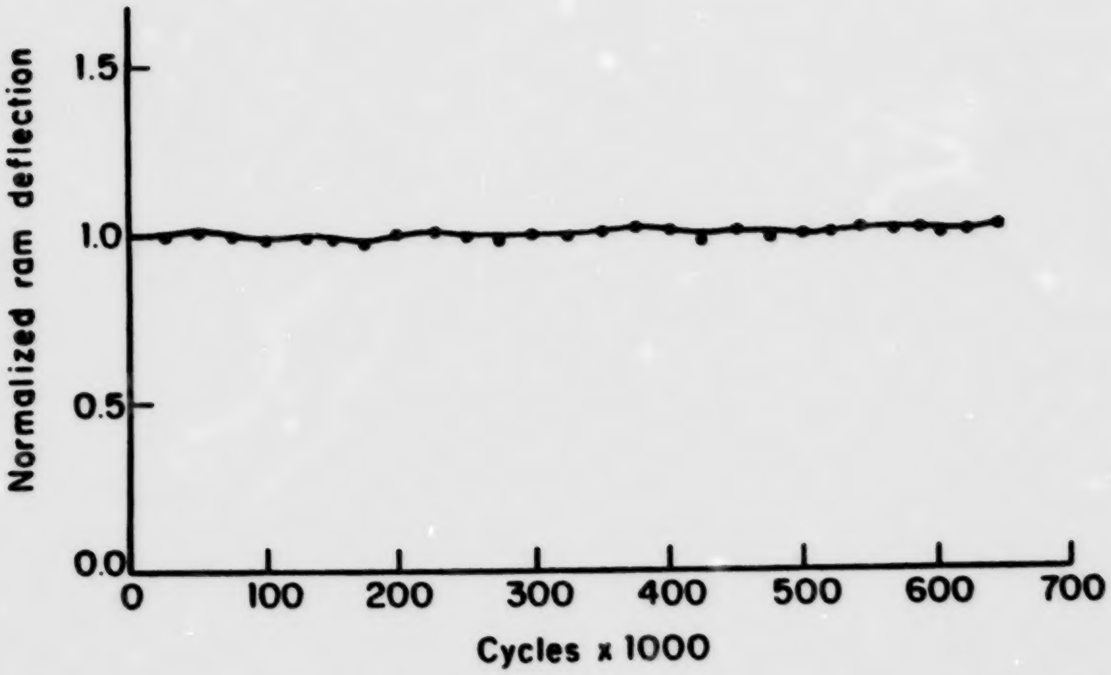

Fig. 65 Normalized actuator displacement variation (TA5)

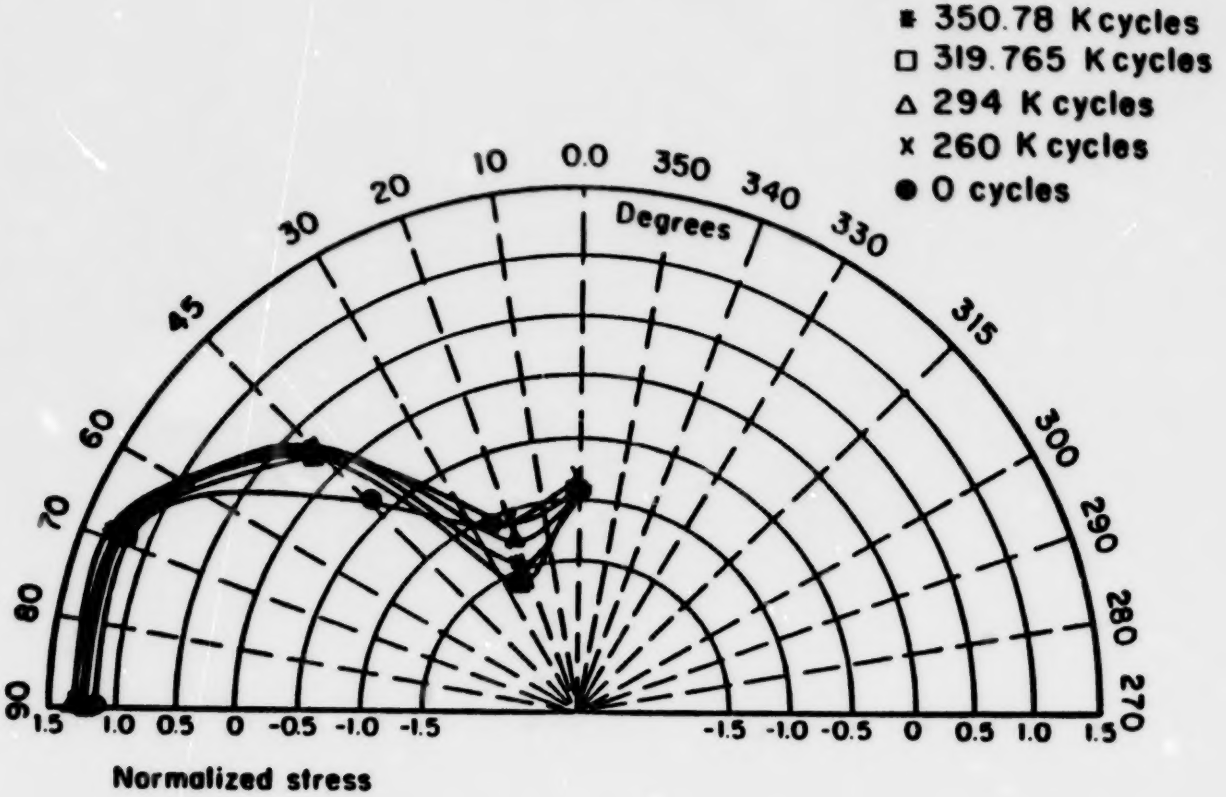

Fig. 66 Normalized stress distribution on inside surface of stiffener, T-joint (TA2) - at mean load (normalizing stress $\sigma_0 = 112$ MPa)

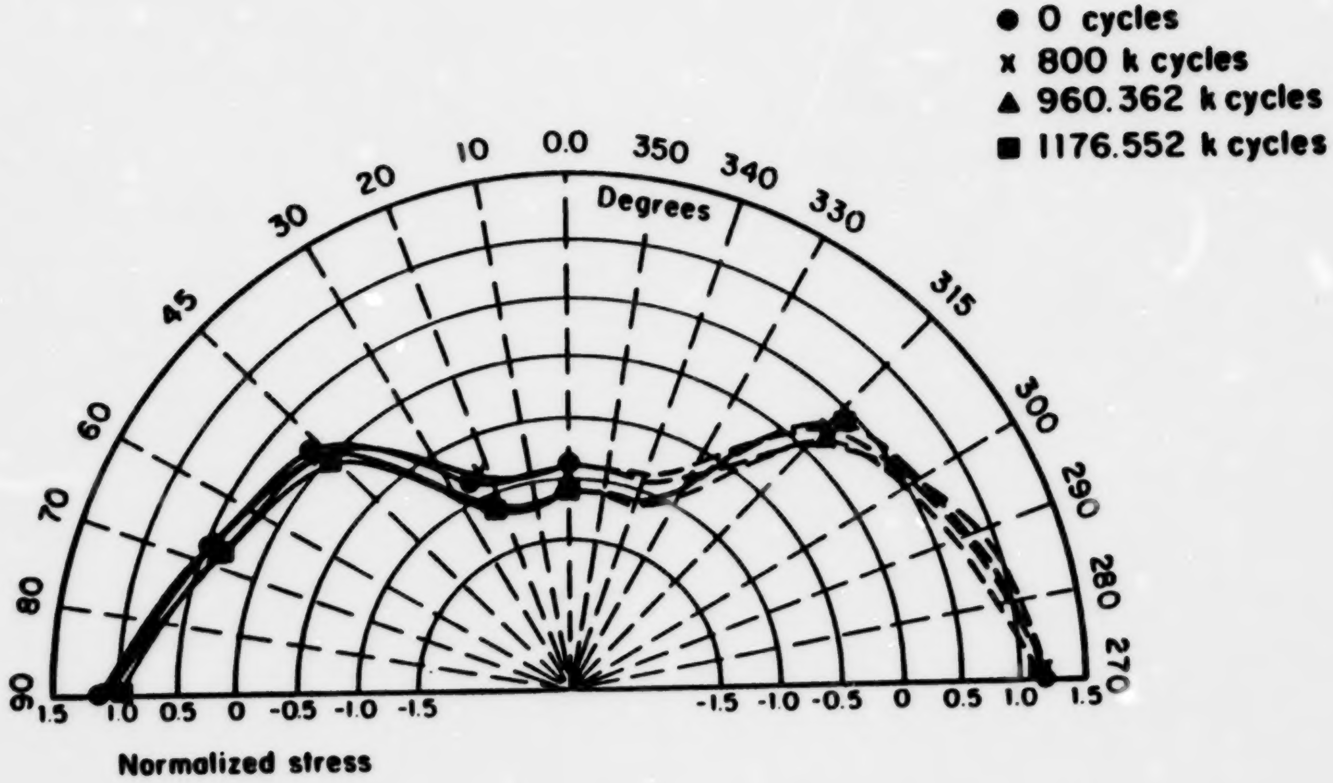

Fig. 67 Normalized stress distribution on inside surface of stiffener, T-joint (TA3) - at mean load (normalizing stress $\sigma_0 = 68.2$ MPa)

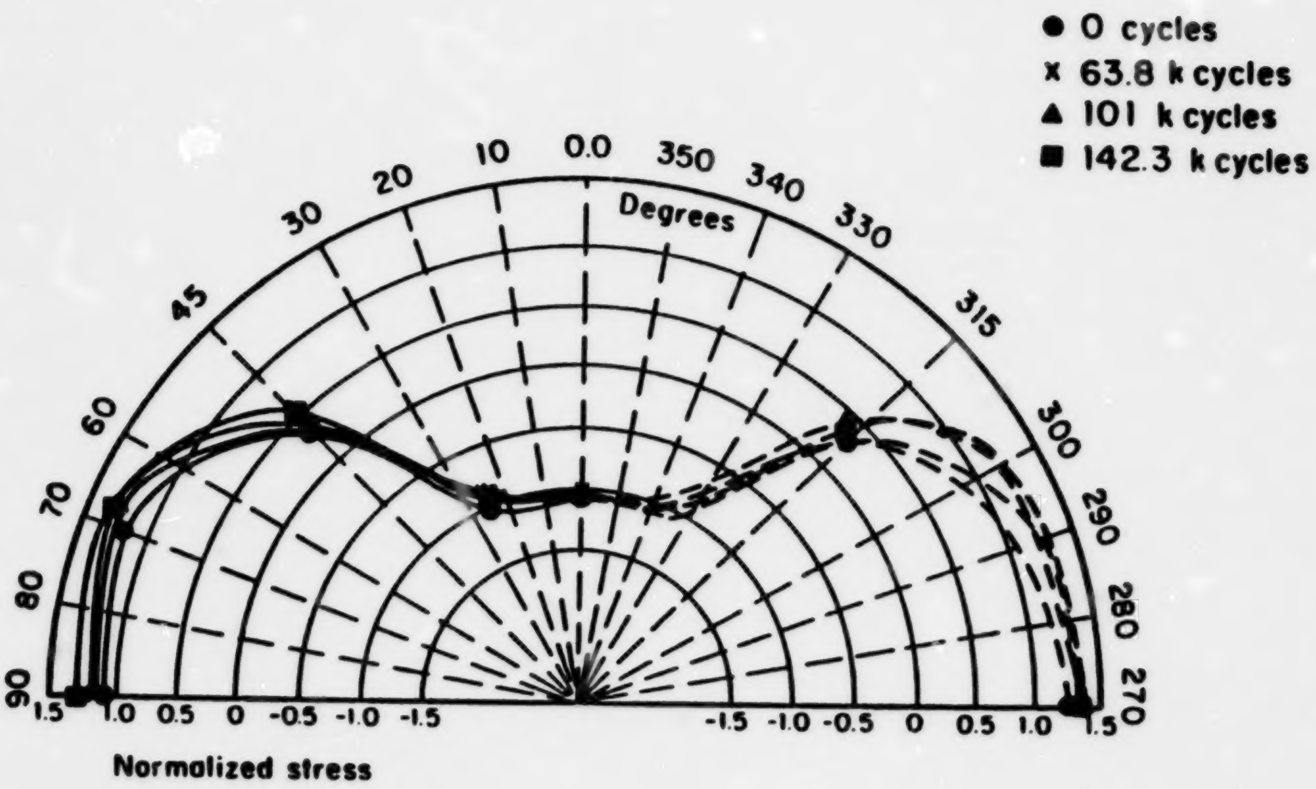

Fig. 68 Normalized stress distribution on inside surface of stiffener, T-joint (TA4) - at mean load (normalizing stress σ_0 = 115.17 MPa)

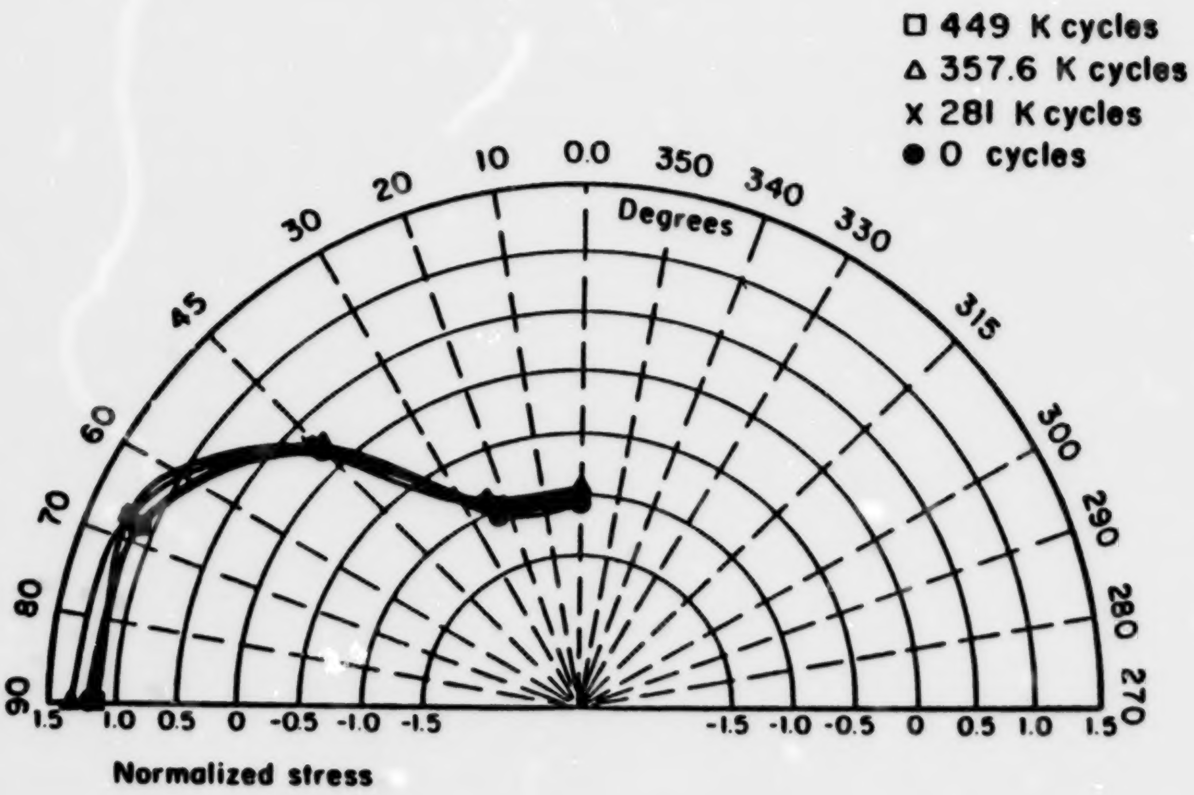

Fig. 69 **Normalized stress distribution on inside surface of stiffener, T-joint (TA5) - at mean load (normalizing stress σ_0 = 68.8 MPa)**

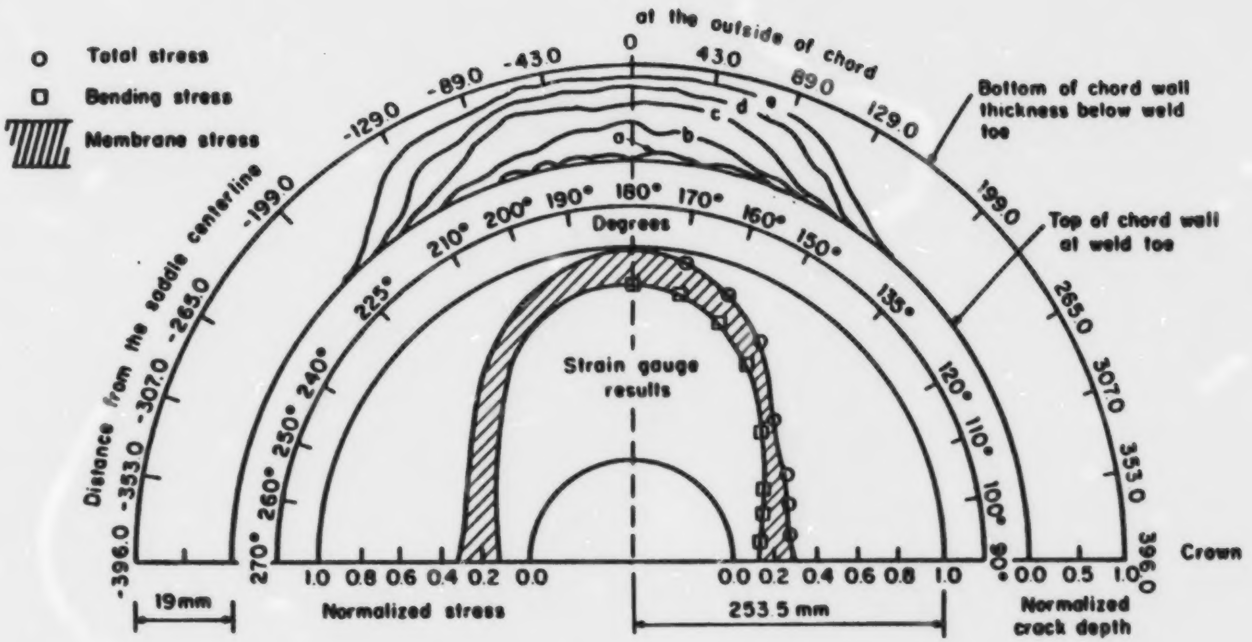

Fig. 70 Crack profile and normalized stress distribution for unstiffened tubular joint TAI (side 2) - 250 MPa at saddle

N_1 = 103,000 cycles (0.5 mm depth)
a = 140,000 cycles (Ink stain)
b = 244,072 cycles (Beach mark)
c = 308,145 cycles (Beach mark)
d = 350,181 cycles (Beach mark)
e = 412,217 cycles (Beach mark)
N_3 = 665,000 cycles (Break through)
N_4 = 890,000 cycles (End of test)

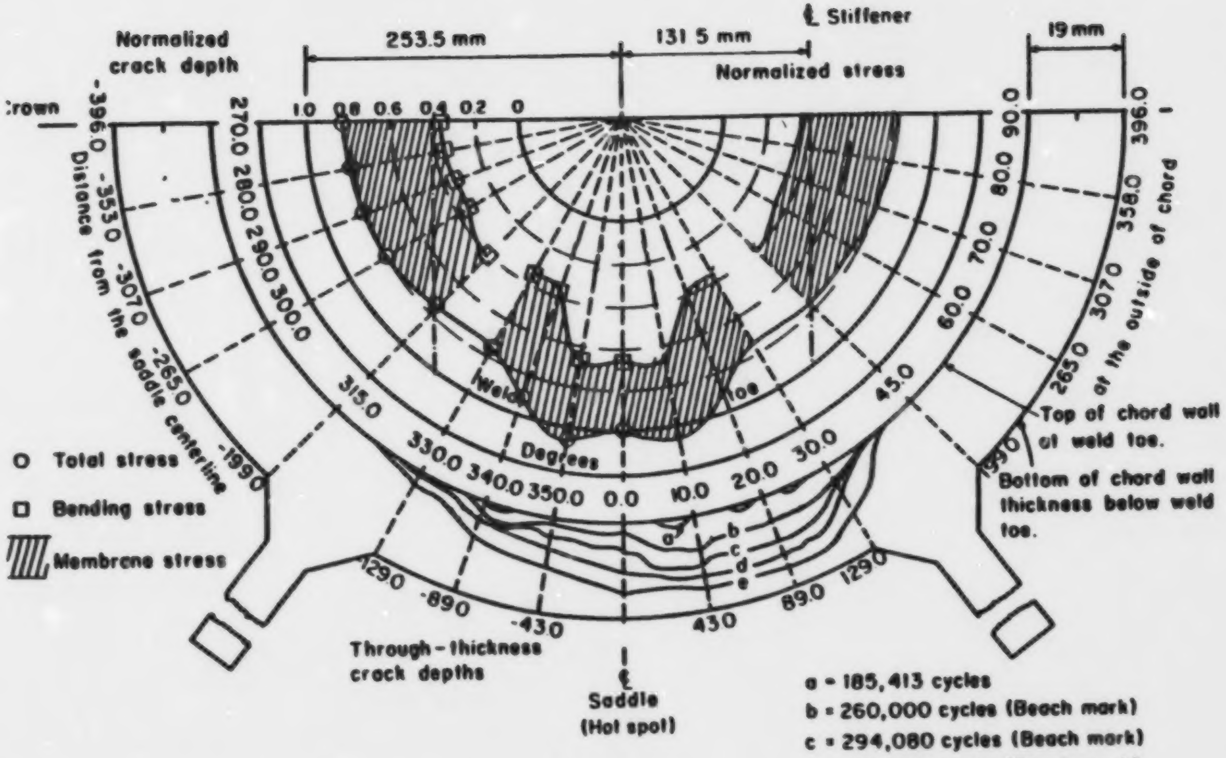

Fig. 7.1 Crack profile and normalized stress distribution for stiffened tubular joint TA2 (side 1) – 250.0 MPa at saddle

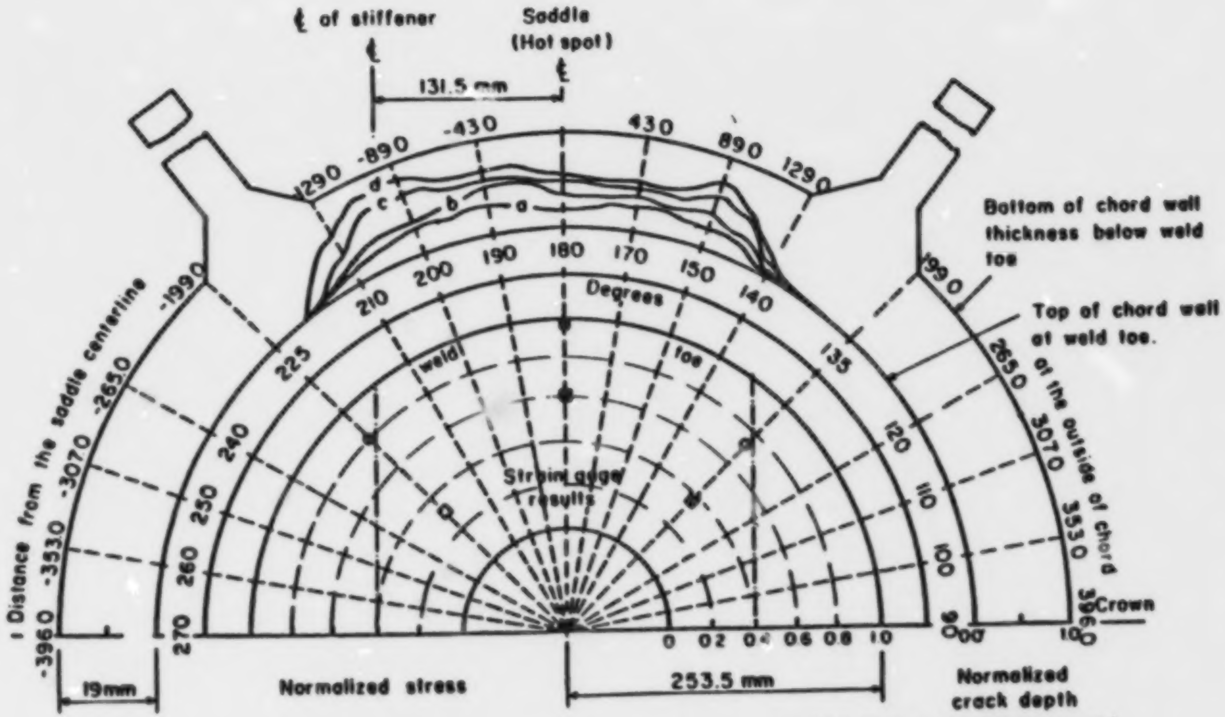
℄ of stiffener
Saddle (Hot spot)
℄
℄
131.5 mm
-1290
-890
-430
430
890
1290
-1990
1990
-2650
-3070
-3530
-3960
2650
3070
3530
3960
d
c
b
a
Bottom of chord wall thickness below weld toe
Top of chord wall at weld toe.
at the outside of chord
Crown
210
200
190
180
170
150
140
135
120
110
100
90
225
240
250
260
270
Degrees
weld
toe
Strain gage results
I Distance from the saddle centerline
0
0.2
0.4
0.6
0.8
1.0
0.0
1.0
19mm
Normalized stress
253.5 mm
Normalized crack depth

Fig. 72 Crack profiles and normalized stress distribution for stiffened tubular joint TA2 (side 2) - 250 MPa at saddle

a = 260,000 cycles (Beach mark)
b = 294,0 0 cycles (Beach mark)
c = 319,765 cycles (Beach mark)
d = 350,780 cycles (Beach mark)
N_1 = 115,000 cycles (0.5 m depth)
N_3 = 441,600 cycles (Break through)
N_4 = 630,650 cycles (End of test)

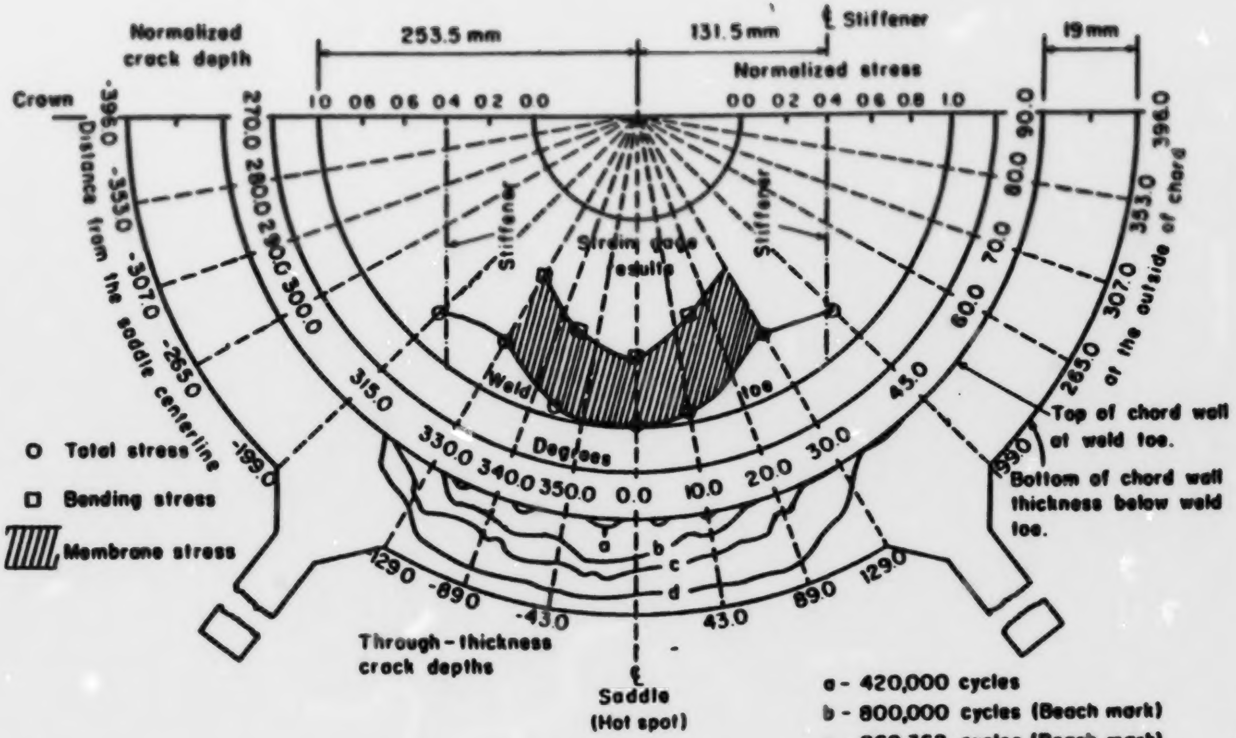

Fig. 73 Crack profile and normalized stress distribution for stiffened tubular joint TA3 (side 2) - 160.0 MPa at saddle

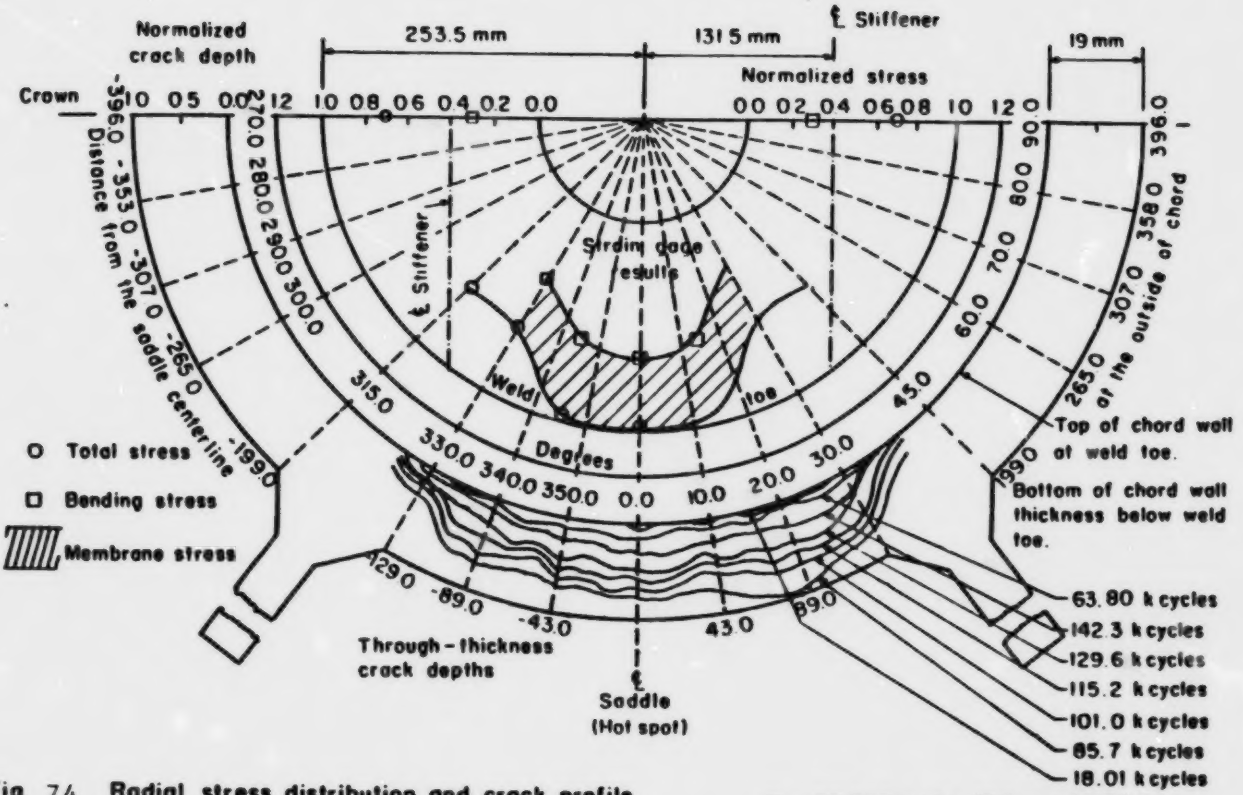
Normalized crack depth
Crown
253.5 mm
131.5 mm
℄ Stiffener
19 mm
Normalized stress
1.0 0.5 0.0
1.2 1.0 0.8 0.6 0.4 0.2 0.0
0.0 0.2 0.4 0.6 0.8 1.0 1.2
0
-396.0 -353.0 -307.0 -265.0 -199.0
Distance from the saddle centerline
270.0 280.0 290.0 300.0 315.0 330.0 340.0 350.0 0.0 10.0 20.0 30.0 45.0 60.0 70.0 80.0 90.0
396.0 358.0 307.0 265.0 199.0
of the outside of chord
Strain gage results
℄ Stiffener
Weld toe
Degrees
Top of chord wall at weld toe.
Bottom of chord wall thickness below weld toe.
○ Total stress
□ Bending stress
▨ Membrane stress
-129.0 -89.0 -43.0 43.0 89.0
Through-thickness crack depths
℄ Saddle (Hot spot)
63.80 k cycles
142.3 k cycles
129.6 k cycles
115.2 k cycles
101.0 k cycles
85.7 k cycles
18.01 k cycles

Fig. 74 Radial stress distribution and crack profile development for the stiffened tubular joint TA4 (side 2) - 250 MPa at saddle (seawater)

N_1 = 35,500 cycles (0.5 mm depth)
N_2 = 142,300 cycles (Break through)
N_4 = 161,000 cycles (End of test)

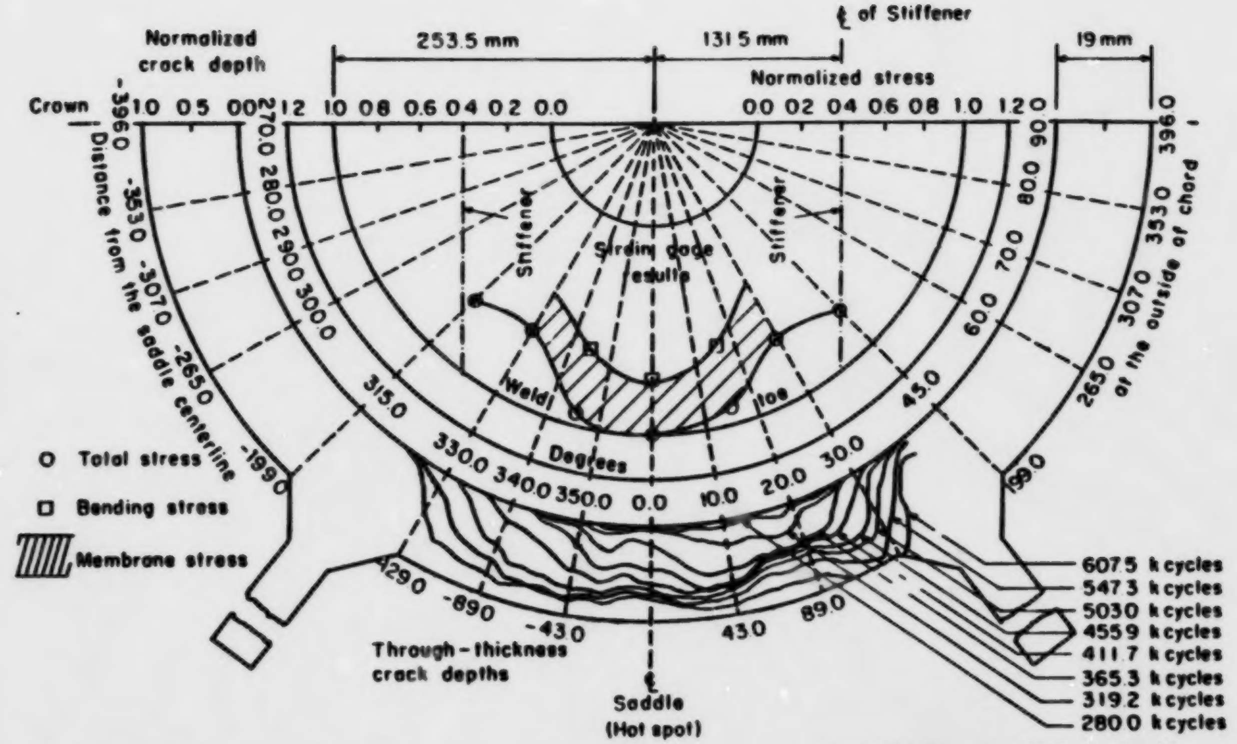

Fig 75 Radial stress distribution and crack profile development for the stiffened tubular joint (TA5 - side 2) - 160.0 MPa (in seawater)

N_1 = 252,000 cycles (0.5 mm depth)
N_3 = 540,000 (Breakthrough)
N_4 = 652,000 (End of test)

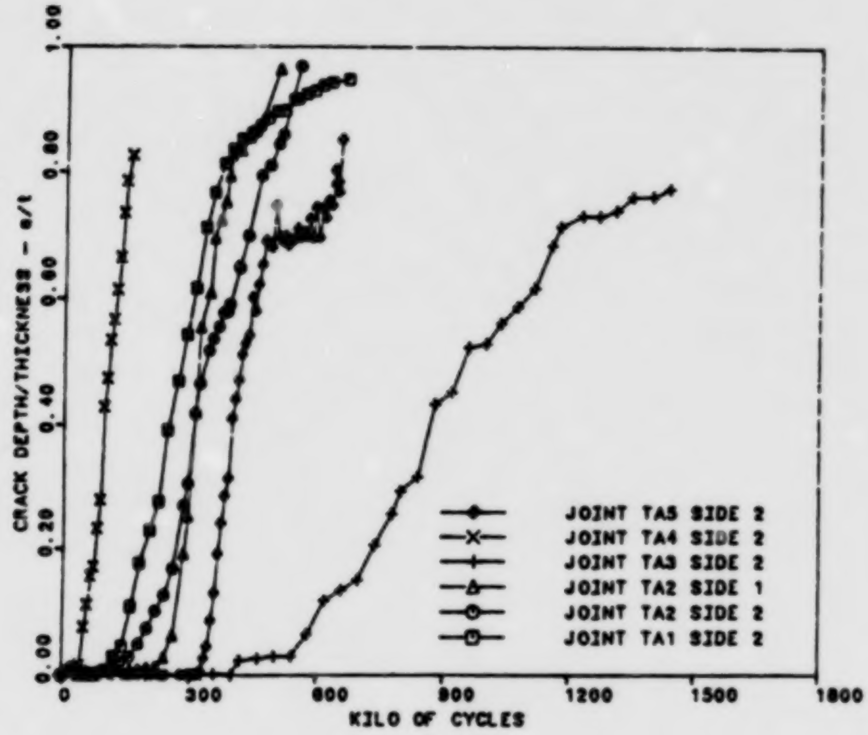

FIG. 76 CRACK GROWTH CURVES FOR ALL JOINTS AT SADDLE POINTS

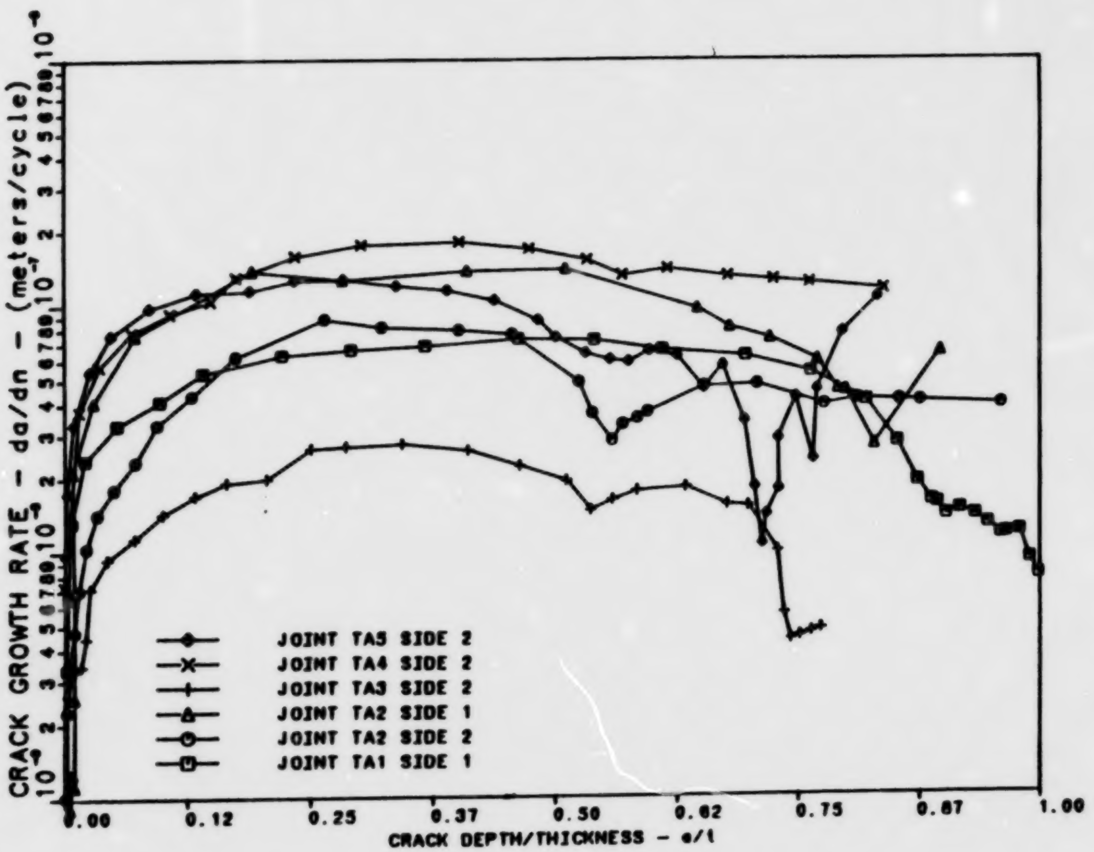

FIG. 7.7 CRACK GROWTH RATE vs. CRACK DEPTH
FOR ALL THE JOINTS AT SADDLE POINTS

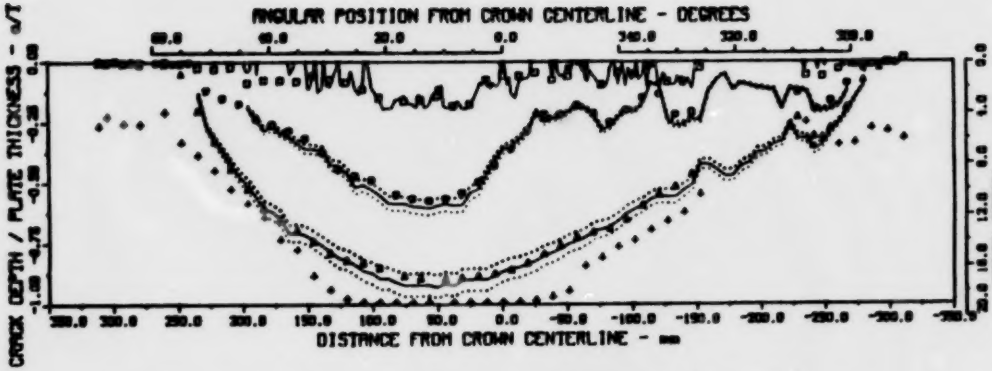

FIGURE 78 CRACK DEPTH VERSUS POSITION (TB1)
COMPARISON OF DCPD RESULTS AND INKSTAIN / BEACHMARX DATA
UNSTIFFENED TUBULAR T-JOINT **** IN-PLANE BENDING
R-RATIO - 0.05 **** HOT-SPOT STRESS RANGE- 248 MPa

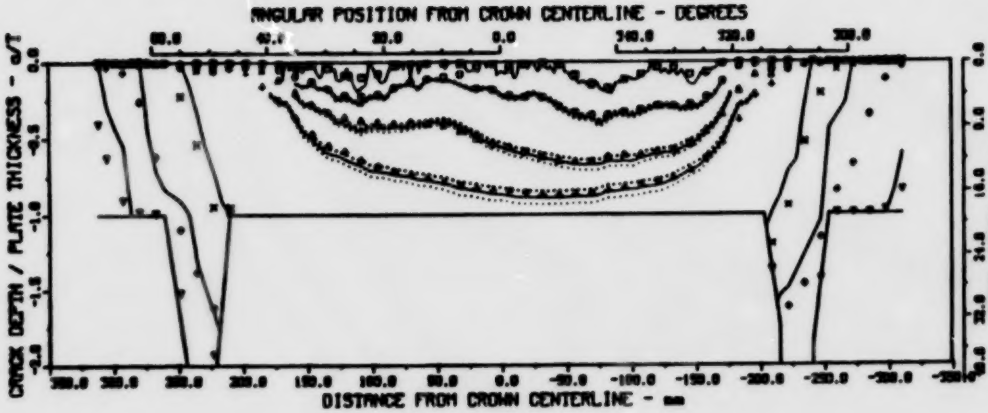

FIGURE 79 CRACK DEPTH VERSUS POSITION (TB2)
COMPARISON OF DCPD RESULTS AND INKSTAIN / BEACHMARK DATA
STIFFENED TUBULAR T-JOINT ---- IN-PLANE BENDING
R-RATIO - 0.05 ---- HOT-SPOT STRESS RANGE- 246 MPa

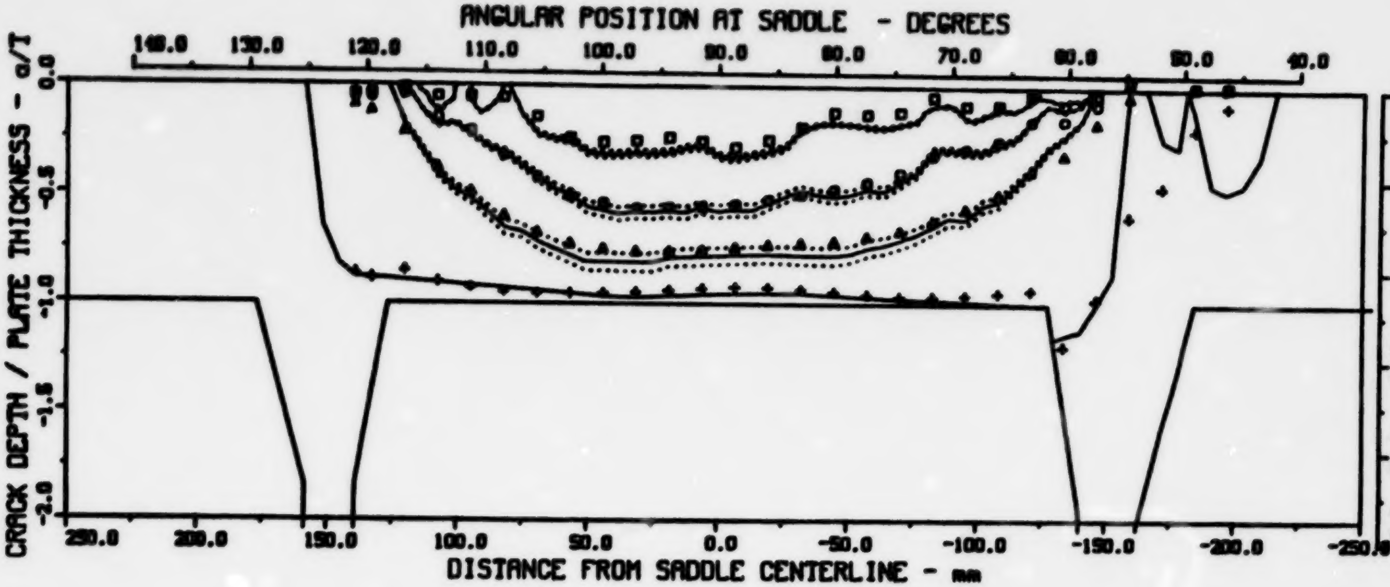

(TB4)

FIGURE 80 CRACK DEPTH VERSUS POSITION
COMPARISON OF DCPD RESULTS AND INKSTAIN / BEACHMARK DATA
STIFFENED TUBULAR T-JOINT *** OUT-OF-PLANE BENDING
R-RATIO - 0.05 *** HOT-SPOT STRESS RANGE- 245.6 MPa

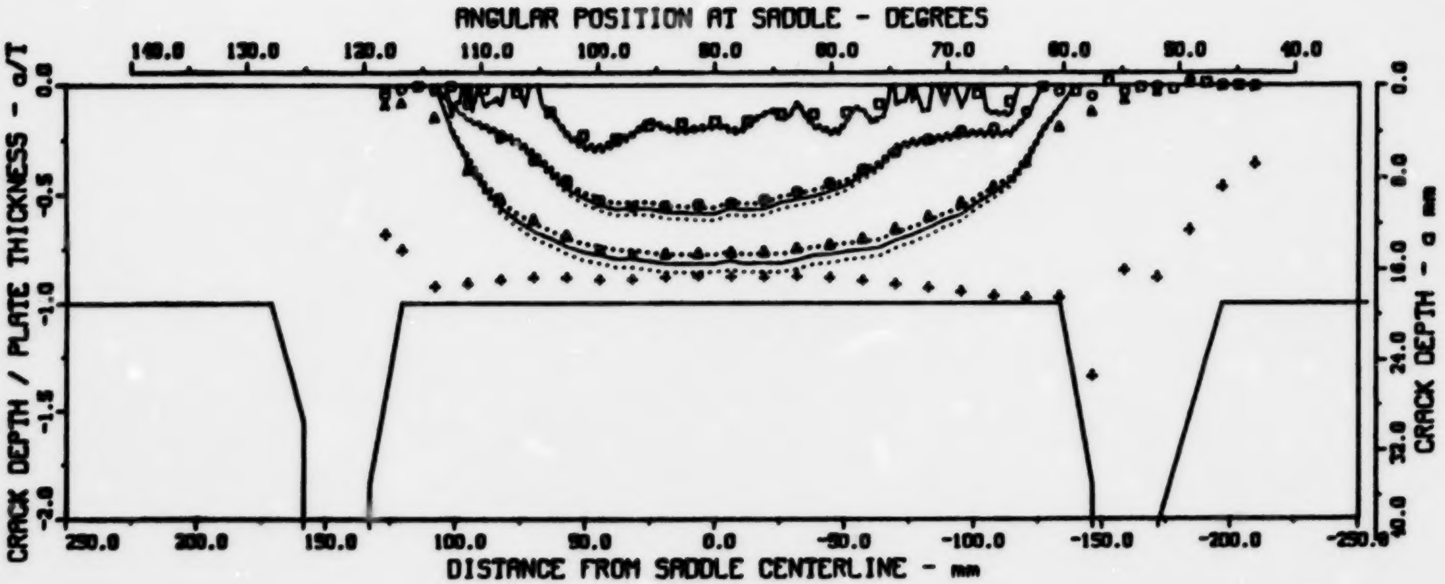

FIGURE 81 CRACK DEPTH VERSUS POSITION (TB5)
COMPARISON OF DCPD RESULTS AND INKSTAIN / BEACHMARK DATA
STIFFENED TUBULAR T-JOINT *** OUT-OF-PLANE BENDING
R-RATIO - 0.05 *** HOT-SPOT STRESS RANGE- 157 MPa

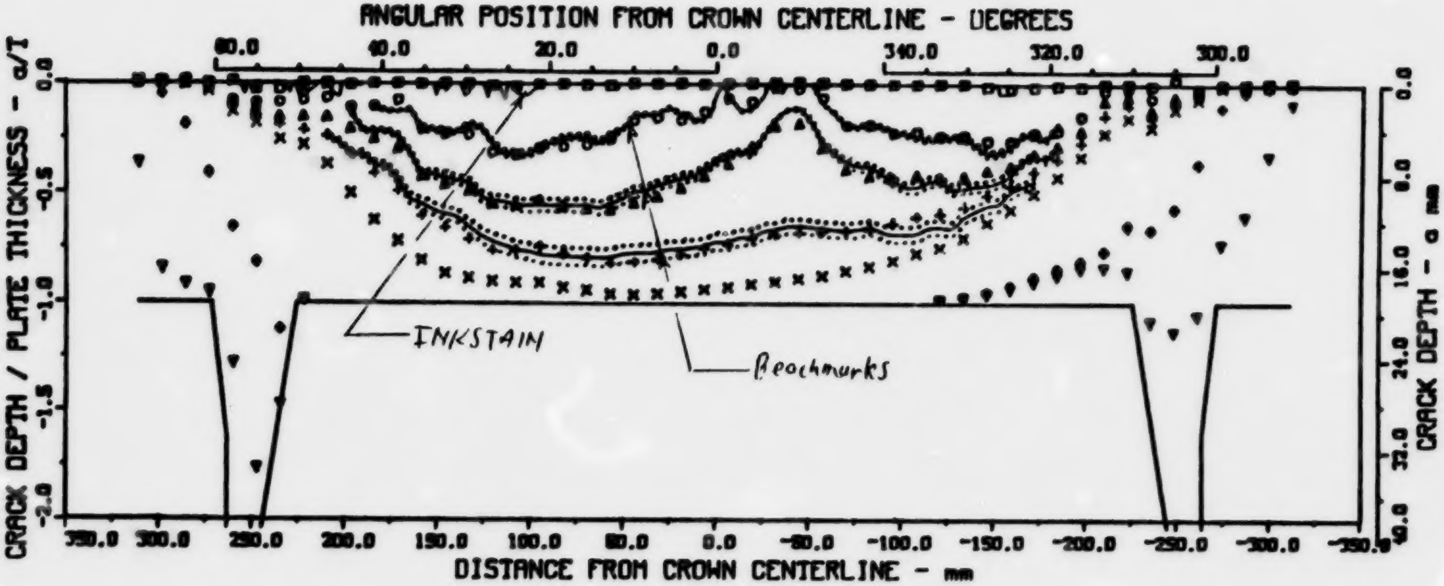

FIGURE 82 CRACK DEPTH VERSUS POSITION (TB6)
COMPARISON OF DCPD RESULTS AND INKSTAIN / BEACHMARK DATA
STIFFENED TUBULAR T-JOINT *** IN-PLANE BENDING
R-RATIO - 0.05 *** HOT-SPOT STRESS RANGE- 163.0 MPa

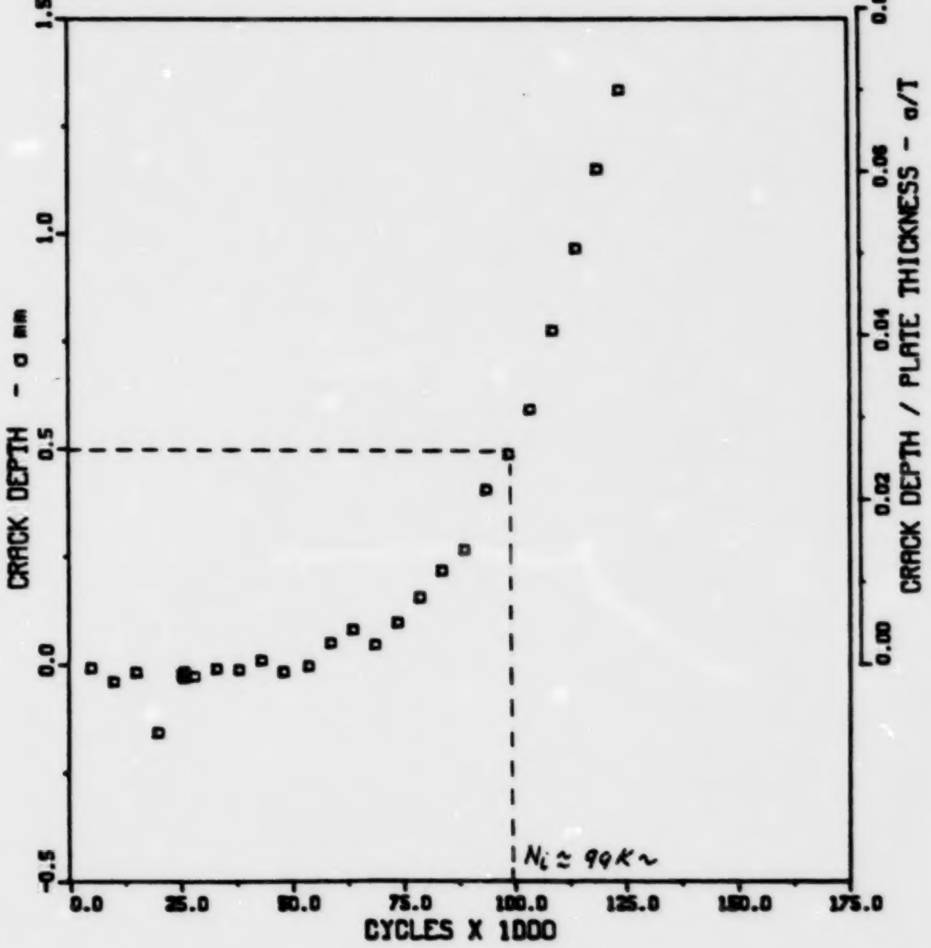

FIGURE 83 DCPD RESULTS *** CRACK DEPTH VERSUS CYCLES (TB1)
UNSTIFFENED TUBULAR T-JOINT *** IN-PLANE BENDING
R-RATIO - 0.05 *** HOT-SPOT STRESS RANGE - 248 MPa
DISTANCE FROM CROWN CENTERLINE - +25.40 mm

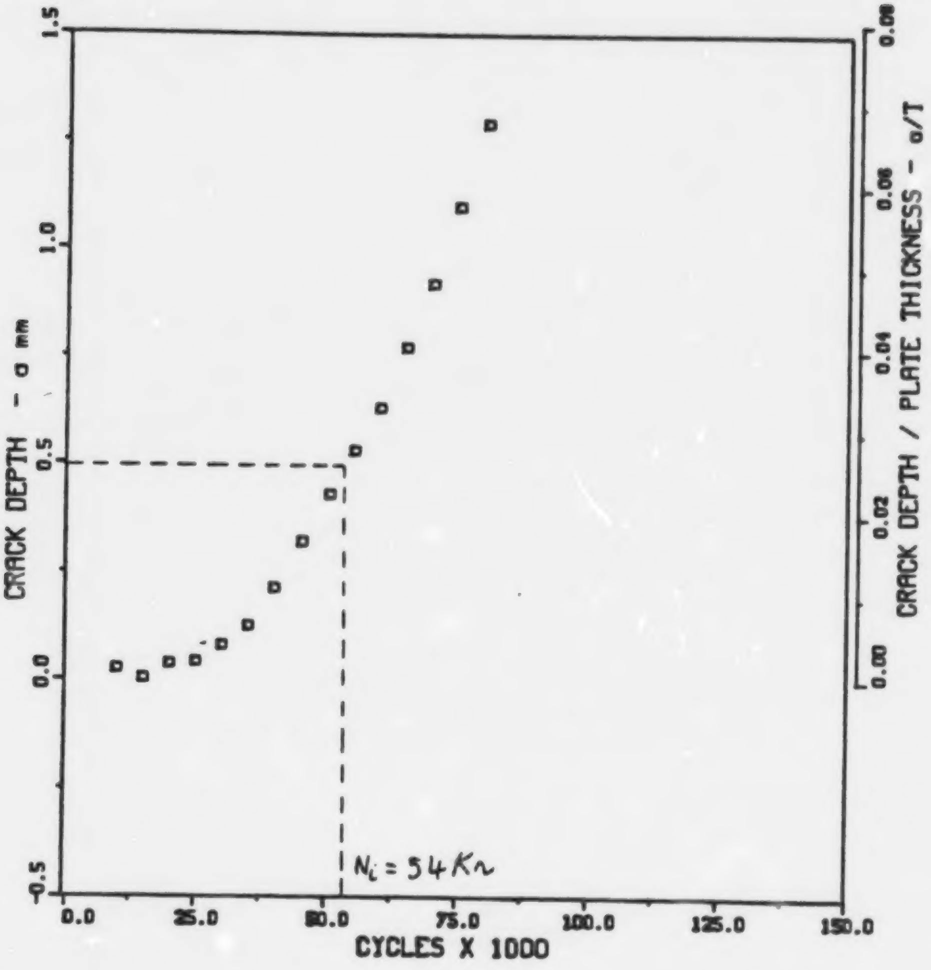

FIGURE 84 DCPD RESULTS *** CRACK DEPTH VERSUS CYCLES (TB2)
STIFFENED TUBULAR T-JOINT *** IN-PLANE BENDING
R-RATIO - 0.05 *** HOT-SPOT STRESS RANGE - 246 MPa
DISTANCE FROM CROWN CENTERLINE - -83.00 mm

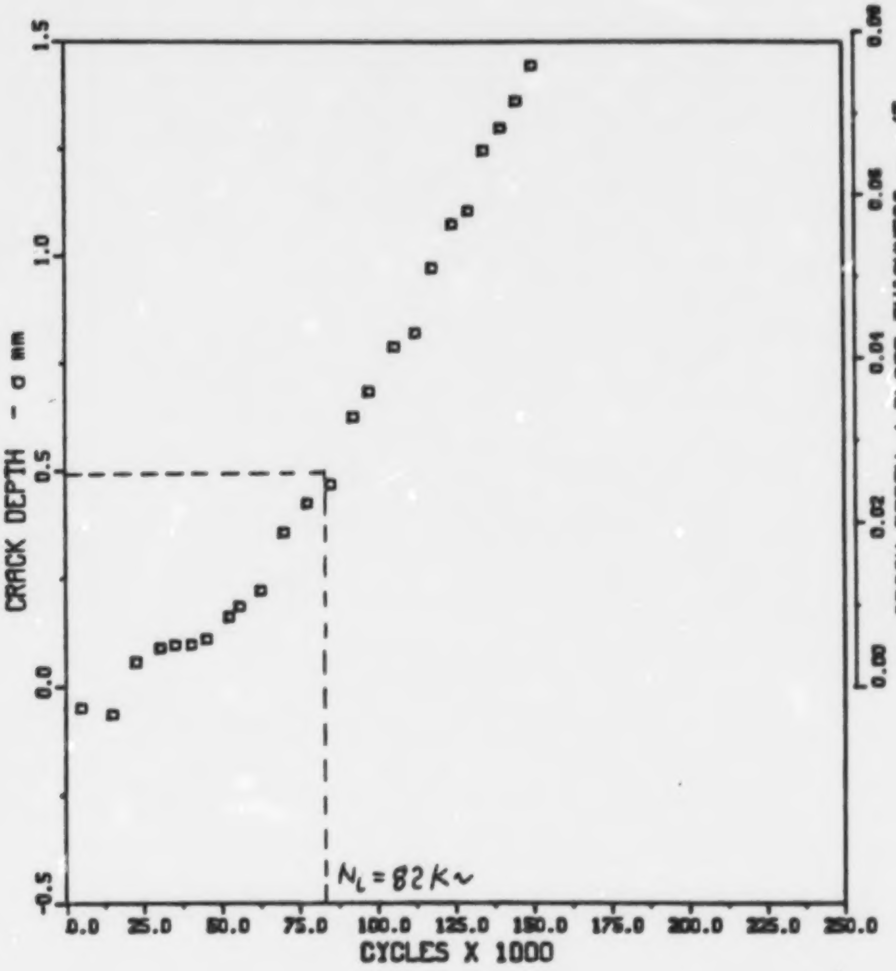

FIGURE 85 DCPD RESULTS *** CRACK DEPTH VERSUS CYCLES (TB3 |
STIFFENED TUBULAR T-JOINT *** IN-PLANE BENDING
R-RATIO - 0.05 *** HOT-SPOT STRESS RANGE - 160.0 MPa
DISTANCE FROM CROWN CENTERLINE - +146.00 mm

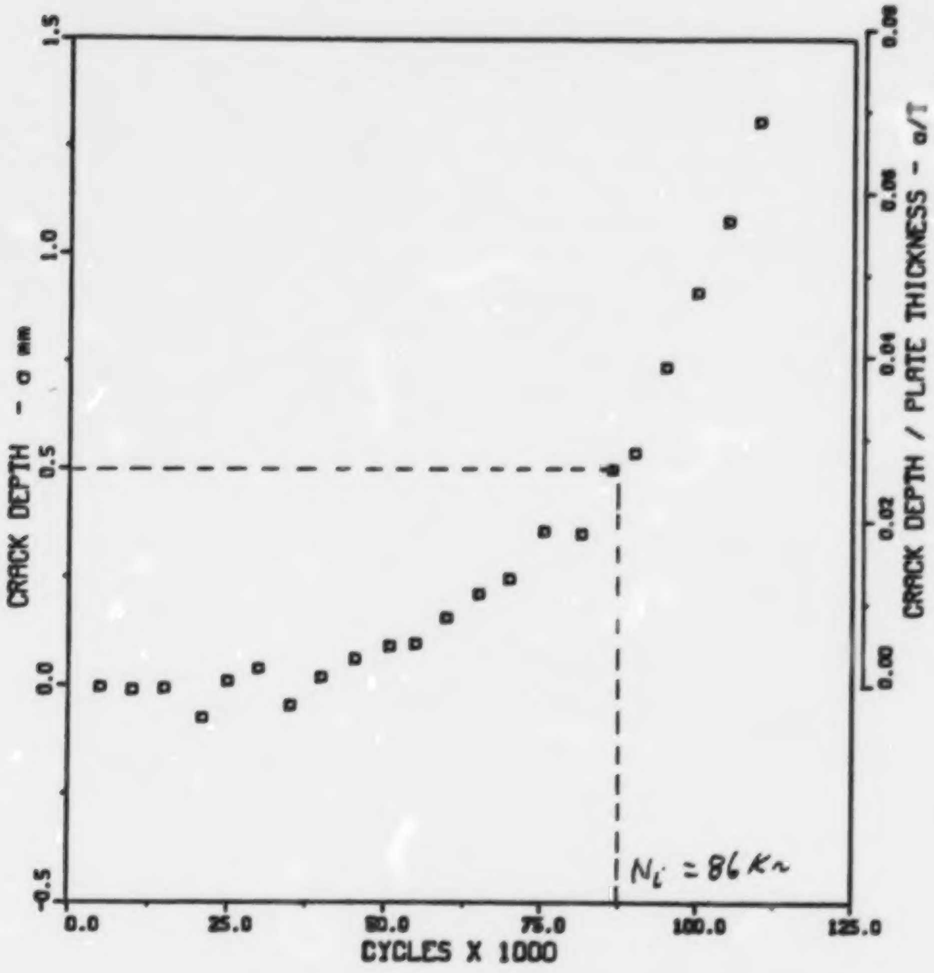

FIGURE 86 DCPD RESULTS ××× CRACK DEPTH VERSUS CYCLES (TB4)
STIFFENED TUBULAR T-JOINT ××× OUT-OF-PLANE BENDING
R-RATIO - 0.05 ××× HOT-SPOT STRESS RANGE - 245.6 MPa
DISTANCE FROM SADDLE CENTERLINE - +00.00 mm

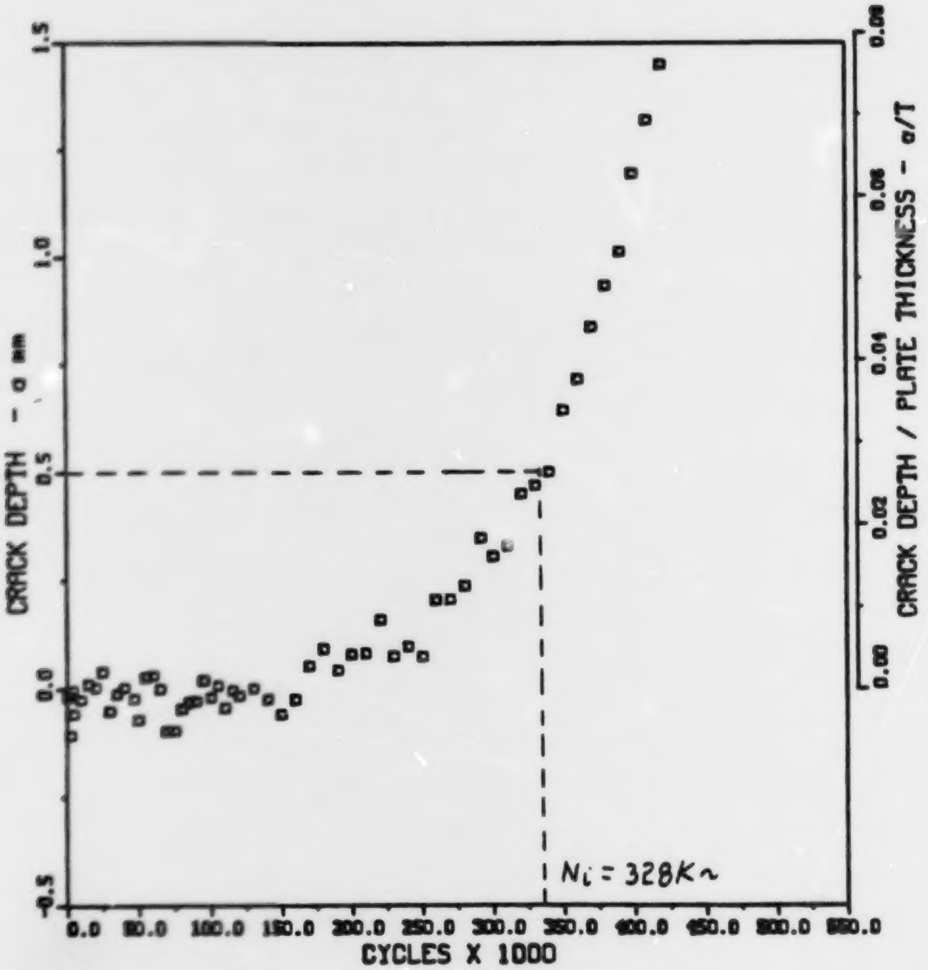

FIGURE 87 DCPD RESULTS *** CRACK DEPTH VERSUS CYCLES (TB5)
STIFFENED TUBULAR T-JOINT *** OUT-OF-PLANE BENDING
R-RATIO - 0.05 *** HOT-SPOT STRESS RANGE - 157 MPa
DISTANCE FROM SADDLE CENTERLINE - +44.45 mm

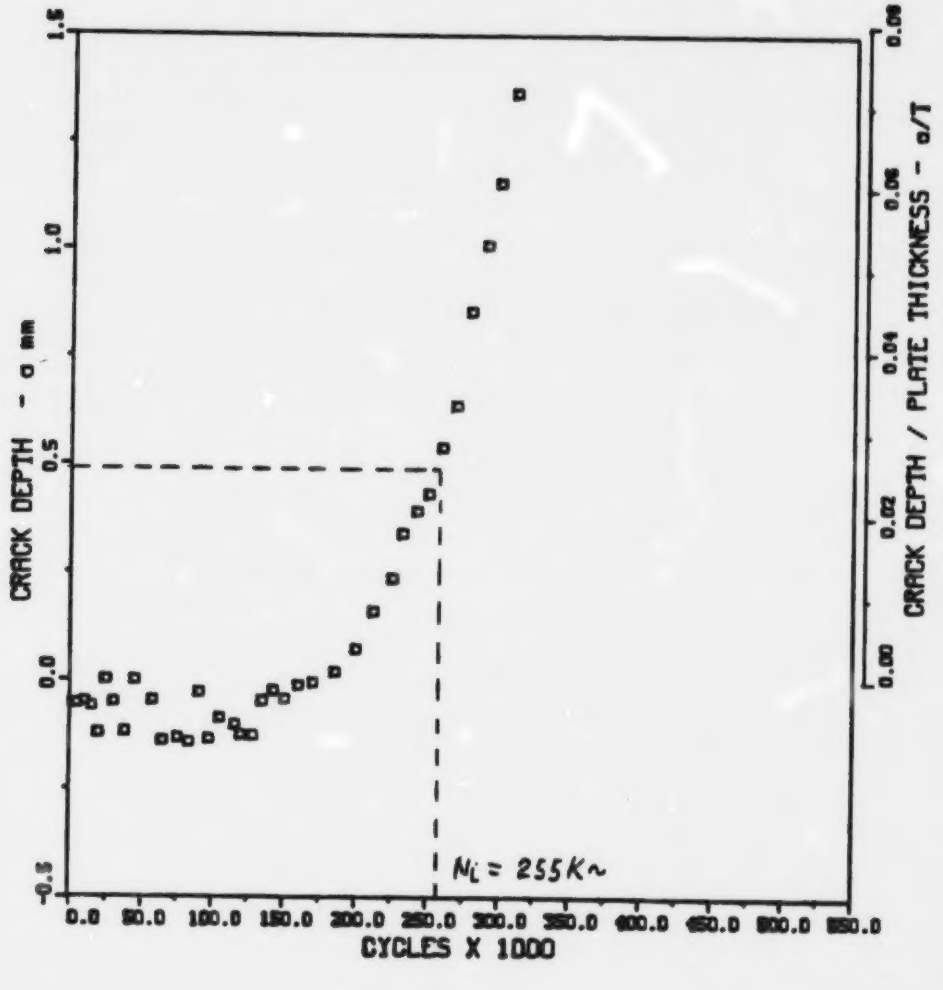

(TB6)

FIGURE 88 DCPD RESULTS *** CRACK DEPTH VERSUS CYCLES
STIFFENED TUBULAR T-JOINT *** IN-PLANE BENDING
R-RATIO - 0.05 *** HOT-SPOT STRESS RANGE - 163.0 MPa
DISTANCE FROM CROWN CENTERLINE - +108.00 mm

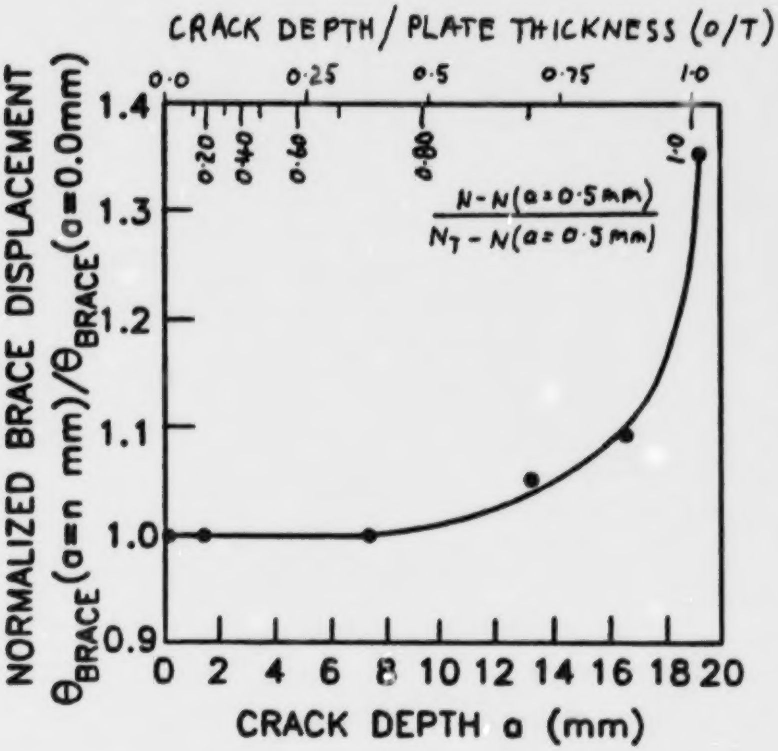

Figure 89: Normalized brace displacement unstiffened tubular t-joint in-plane bending (TB1)
R-ratio = 0.05
Hot spot stress range = 248 MPa

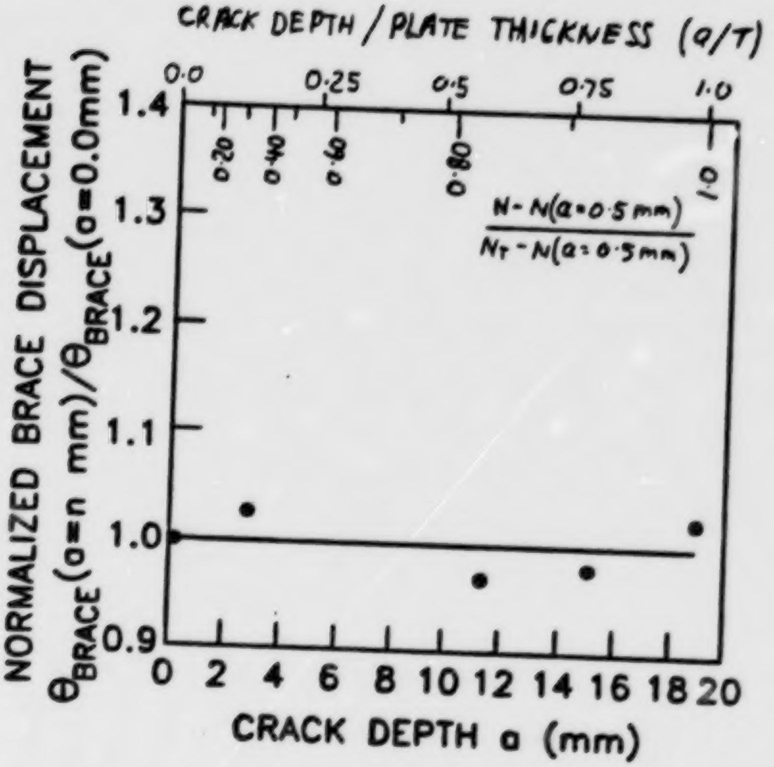

Figure 90: Normalized brace displacement stiffened tubular T-joint in-plane bending (TB2)
R-ratio = 0.05
Hot spot stress range = 246 MPa.

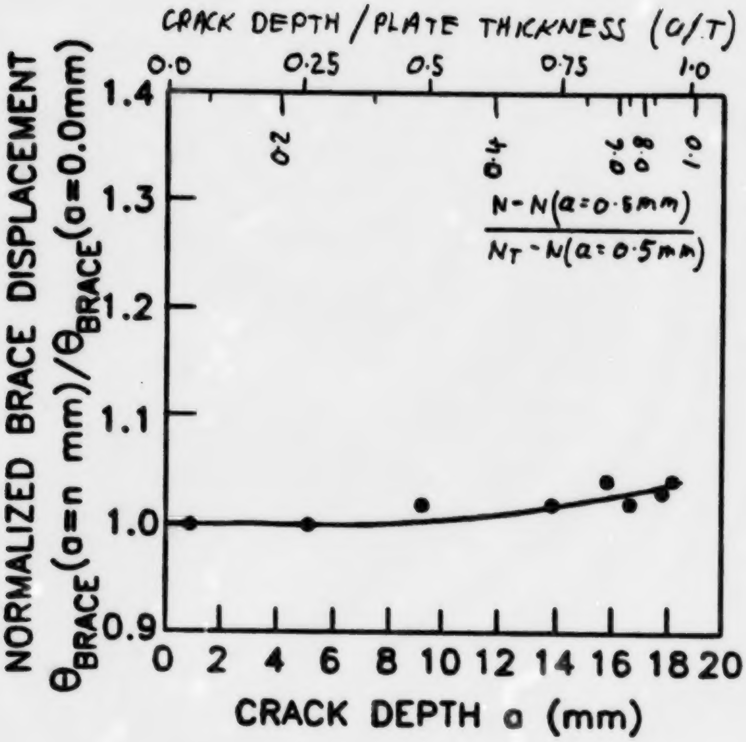

Figure 91: Normalized brace displacement stiffened tubular T-joint out-of-plane bending (TB4)
R - ratio = 0.05
Hot spot stress range = 246 MPa.

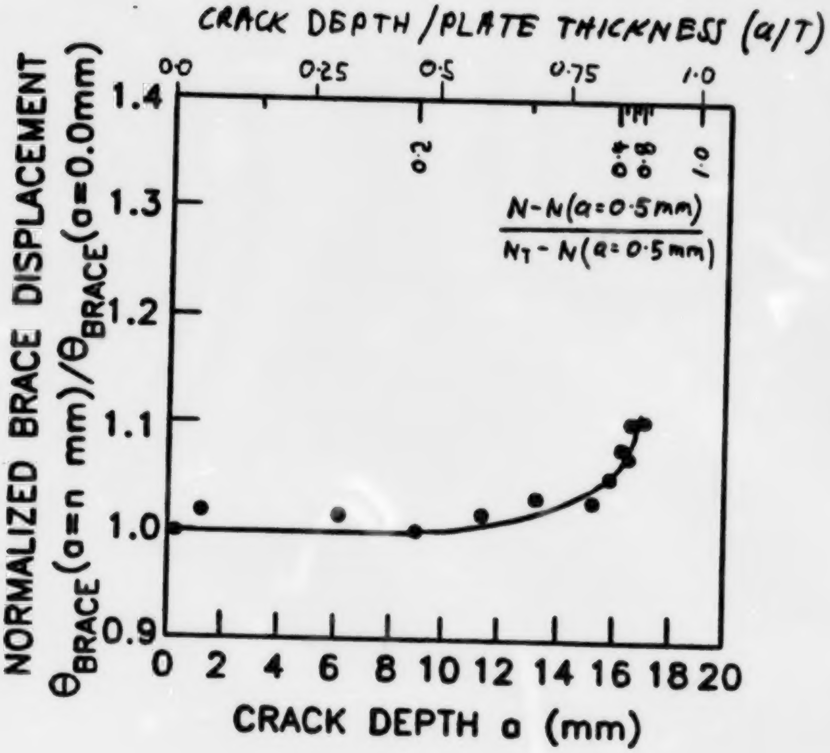

Figure 92: Normalized brace displacement stiffened tubular T-joint out-of-plane bending (TB5)
R-ration = 0.05
Hot spot stress range = 157 MPa.

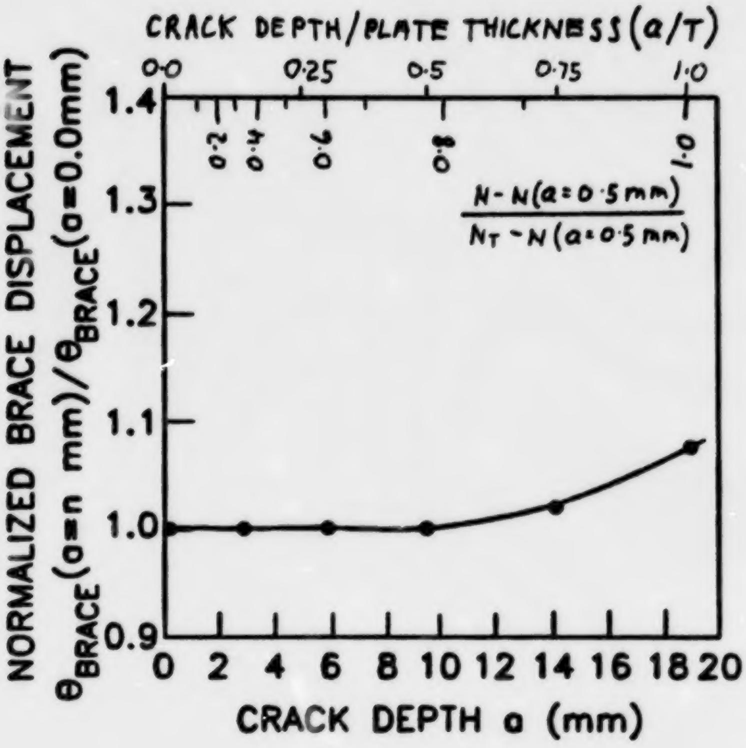

Figure 93: Normalized brace deflection stiffened tubular T-joint in-plane bending (TB6)
R-ratio = 0.05
Hot spot stress range = 163 MPa.

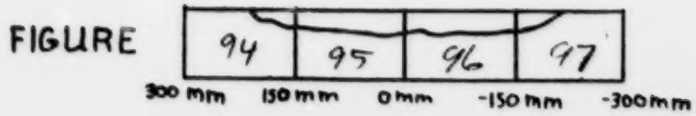
FIGURE
94
95
96
97
300 mm
150 mm
0 mm
-150 mm
-300 mm

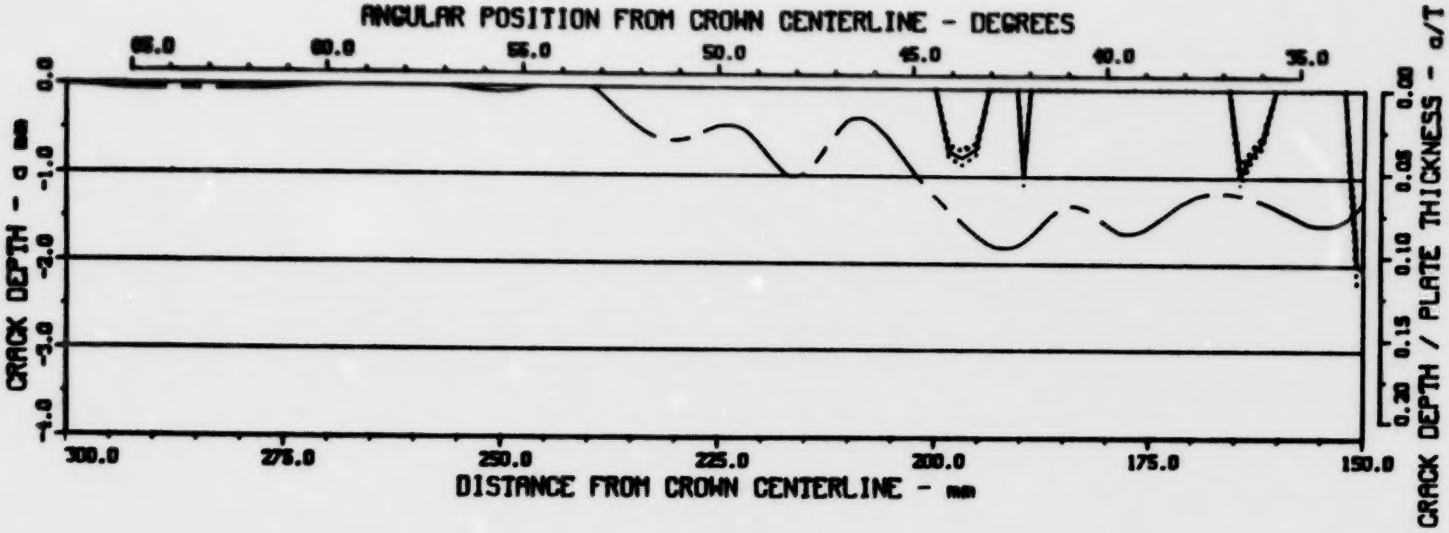

FIGURE 94 CRACK DEPTH VERSUS POSITION (TB1)
COMPARISON OF DCPD RESULTS AND INKSTAIN DATA
UNSTIFFENED TUBULAR T-JOINT *** IN-PLANE BENDING
R-RATIO - 0.05 *** HOT-SPOT STRESS RANGE- 248 MPa

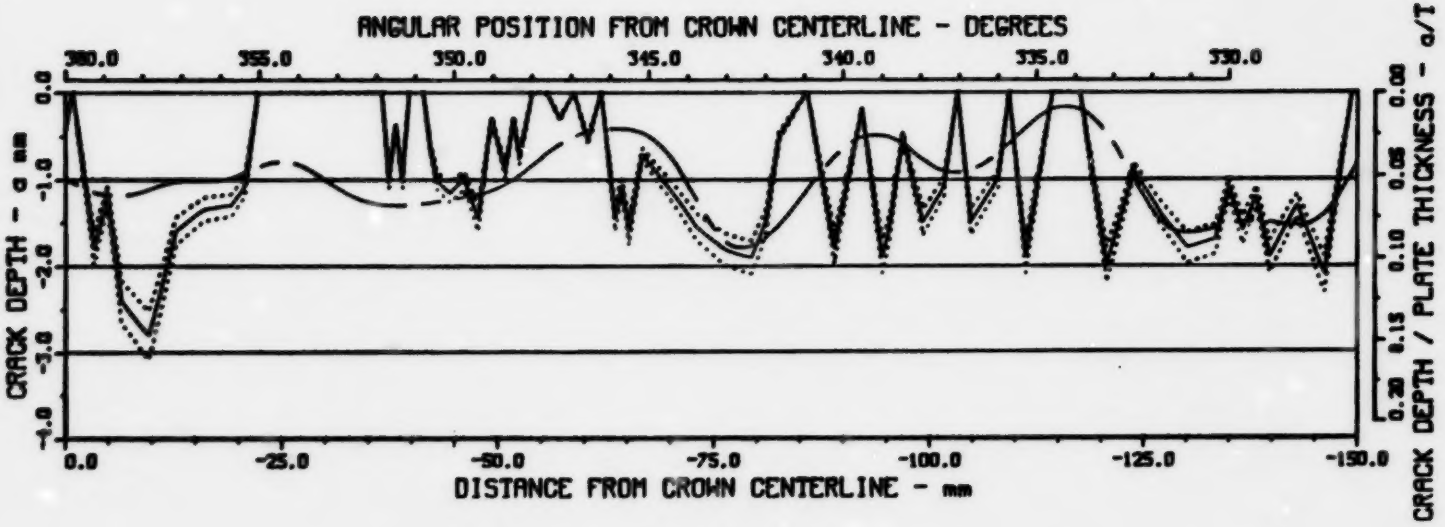

FIGURE 95 CRACK DEPTH VERSUS POSITION (TB1)
COMPARISON OF DCPD RESULTS AND INKSTAIN DATA
UNSTIFFENED TUBULAR T-JOINT *** IN-PLANE BENDING
R-RATIO - 0.05 *** HOT-SPOT STRESS RANGE- 248 MPa

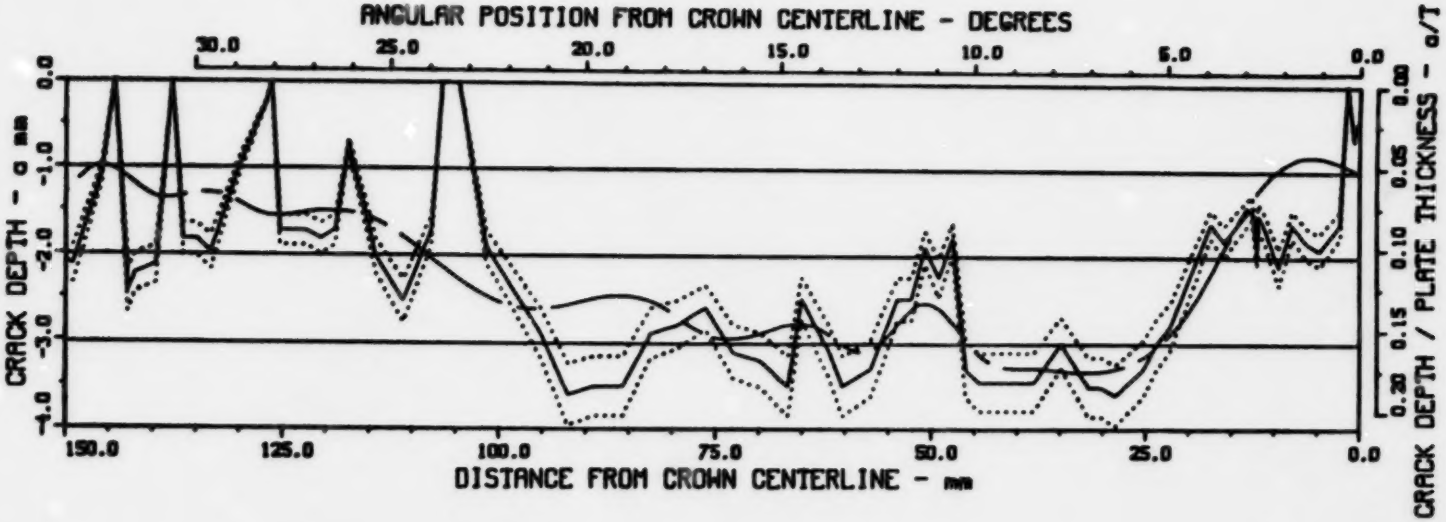

FIGURE 96 CRACK DEPTH VERSUS POSITION (TB1)
COMPARISON OF DCPD RESULTS AND INKSTAIN DATA
UNSTIFFENED TUBULAR T-JOINT *** IN-PLANE BENDING
R-RATIO - 0.05 *** HOT-SPOT STRESS RANGE-248 MPa

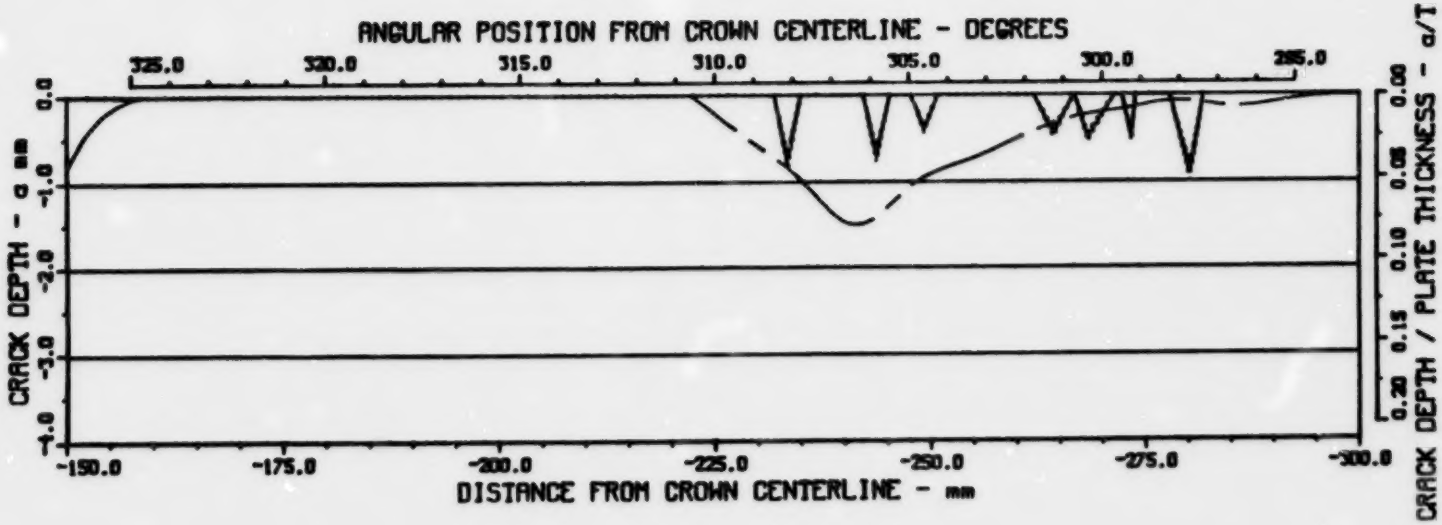

FIGURE 97 CRACK DEPTH VERSUS POSITION (TB1)
COMPARISON OF DCPD RESULTS AND INKSTAIN DATA
UNSTIFFENED TUBULAR T-JOINT *** IN-PLANE BENDING
R-RATIO - 0.05 *** HOT-SPOT STRESS RANGE 248 MPa

FIGURE

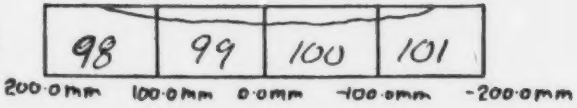
98
99
100
101
200·0mm
100·0mm
0·0mm
-100·0mm
-200·0mm

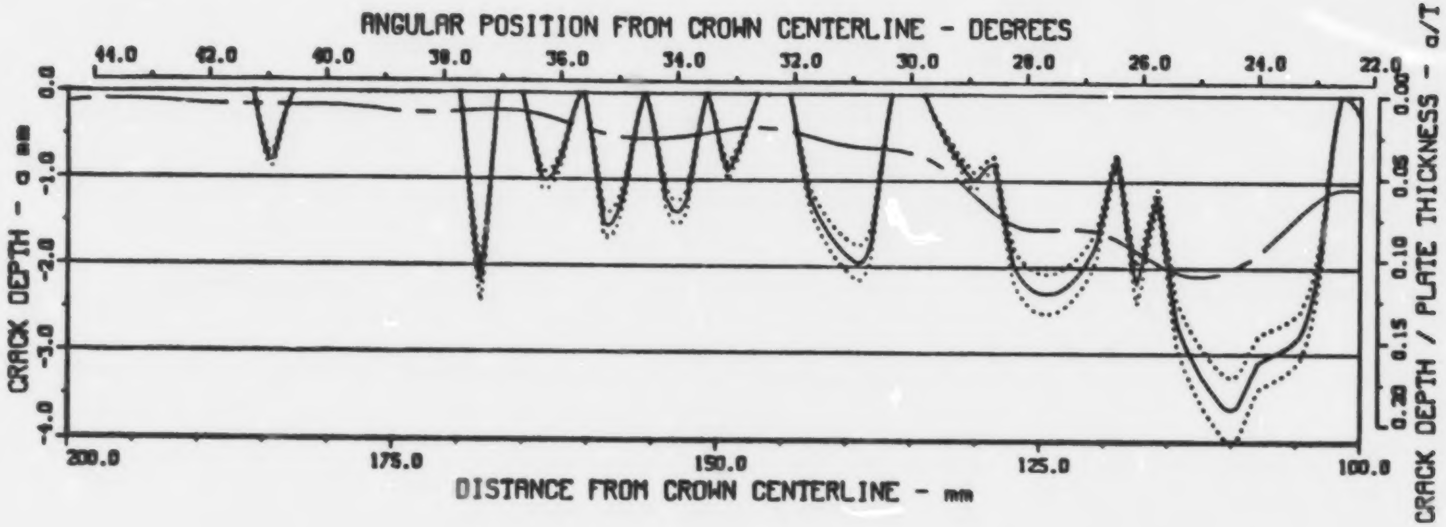

FIGURE 98 CRACK DEPTH VERSUS POSITION (TB2)
COMPARISON OF DCPD RESULTS AND INKSTAIN DATA
STIFFENED TUBULAR T-JOINT *** IN-PLANE BENDING
R-RATIO - 0.05 *** HOT-SPOT STRESS RANGE- 246 MPa

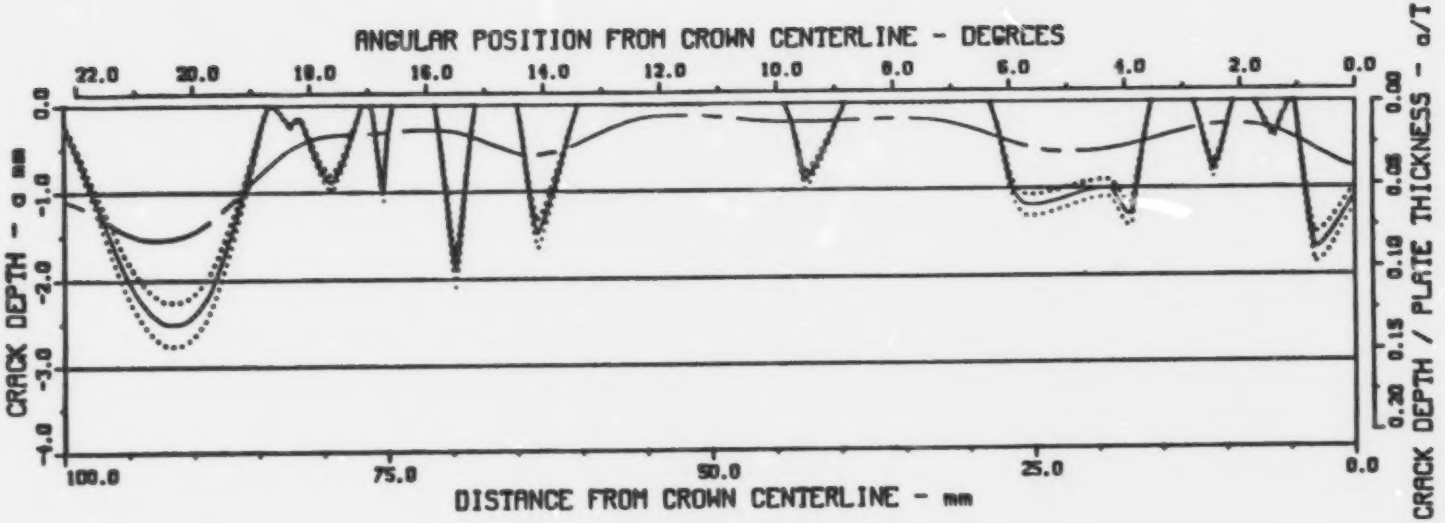

FIGURE 99 CRACK DEPTH VERSUS POSITION (TB2)
COMPARISON OF DCPD RESULTS AND INKSTAIN DATA
STIFFENED TUBULAR T-JOINT *** IN-PLANE BENDING
R-RATIO - 0.05 *** HOT-SPOT STRESS RANGE- 246 MPa

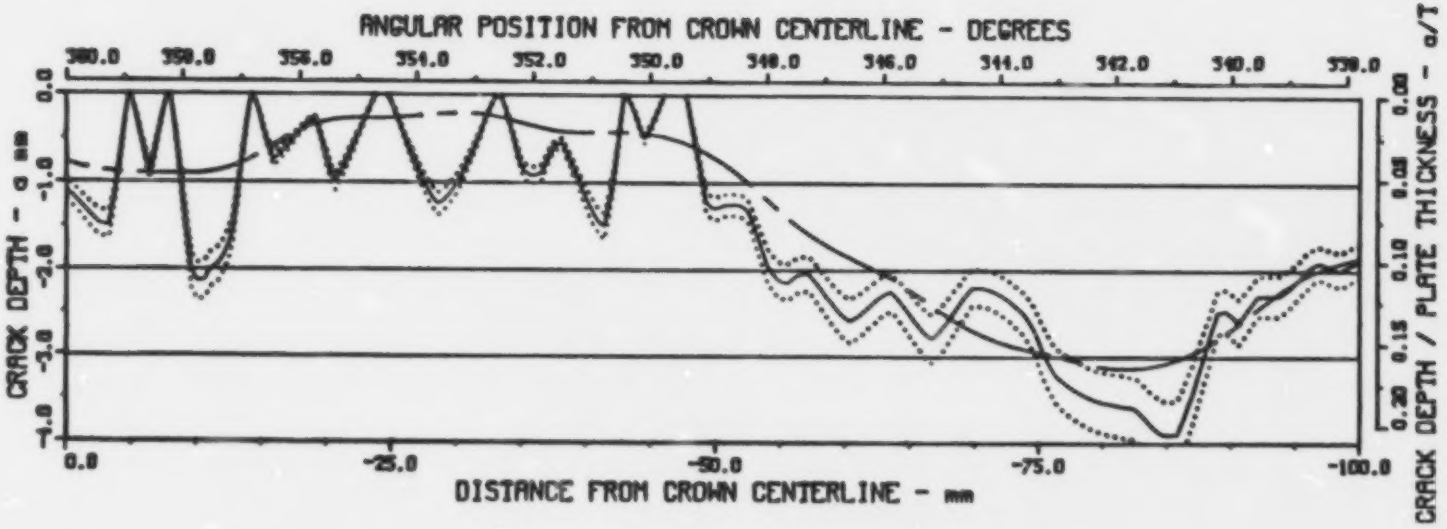

FIGURE 100 CRACK DEPTH VERSUS POSITION (TB2)
COMPARISON OF DCPD RESULTS AND INKSTAIN DATA
STIFFENED TUBULAR T-JOINT *** IN-PLANE BENDING
R-RATIO - 0.05 *** HOT-SPOT STRESS RANGE- 246 MPa

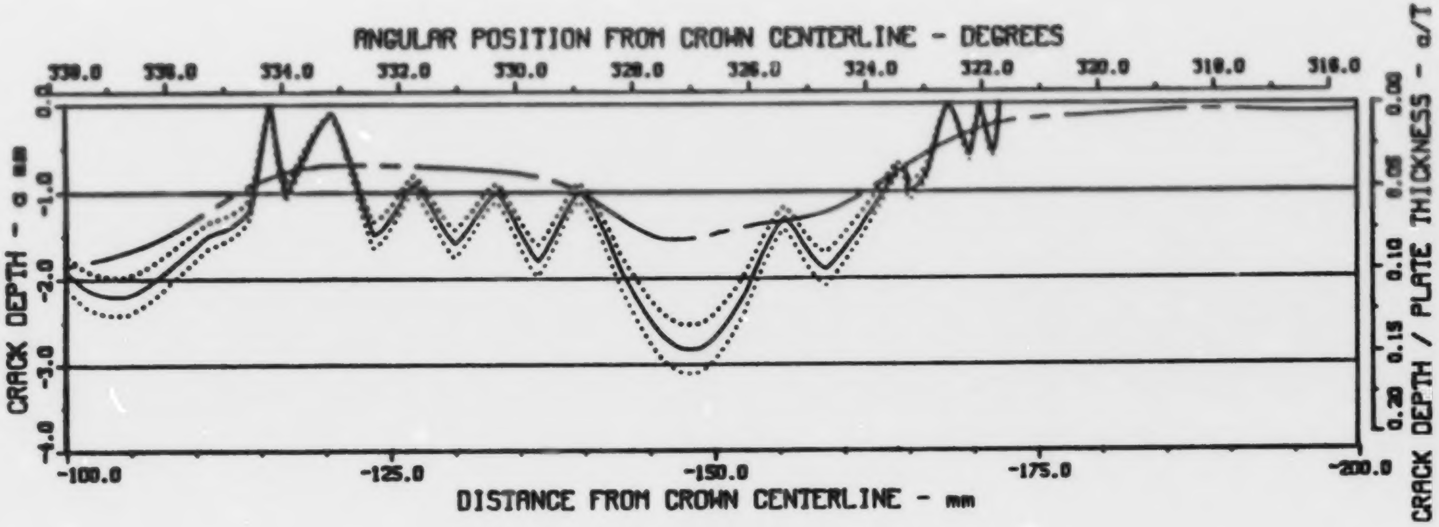

FIGURE 101 CRACK DEPTH VERSUS POSITION (TB2)
COMPARISON OF DCPD RESULTS AND INKSTAIN DATA
STIFFENED TUBULAR T-JOINT *** IN-PLANE BENDING
R-RATIO - 0.05 *** HOT-SPOT STRESS RANGE- 246 MPa

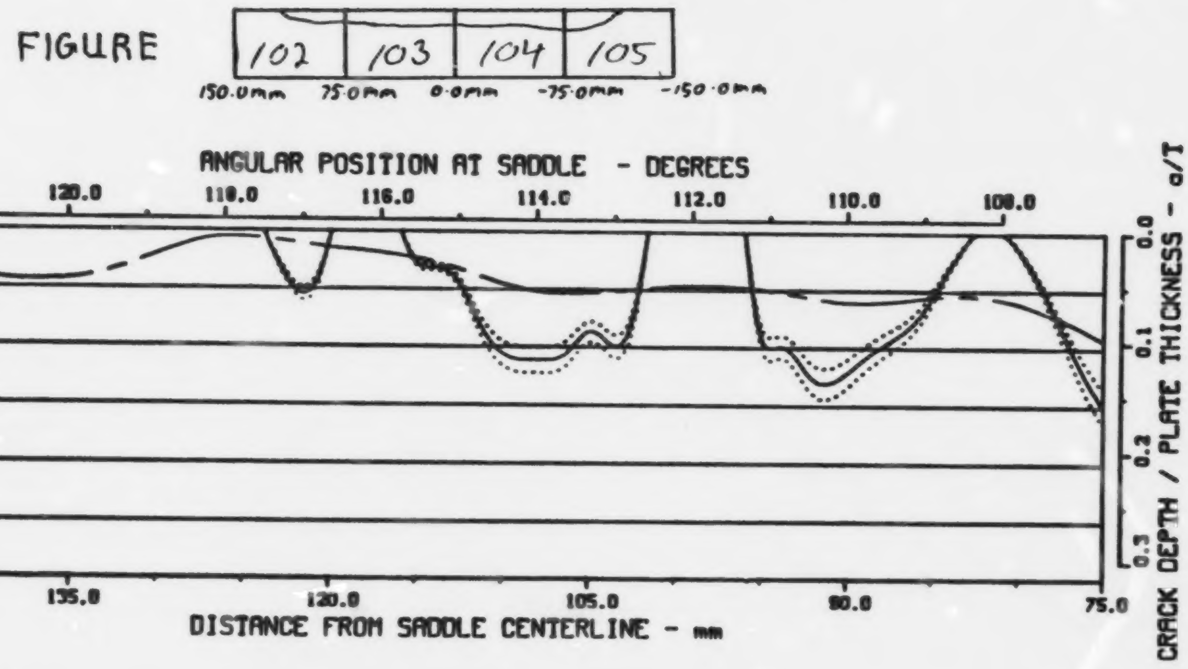

FIGURE 102 CRACK DEPTH VERSUS POSITION (TB4)
COMPARISON OF DCPD RESULTS AND INKSTAIN DATA
STIFFENED TUBULAR T-JOINT *** OUT-OF-PLANE BENDING
R-RATIO - 0.05 *** HOT-SPOT STRESS RANGE- 245.6 MPa

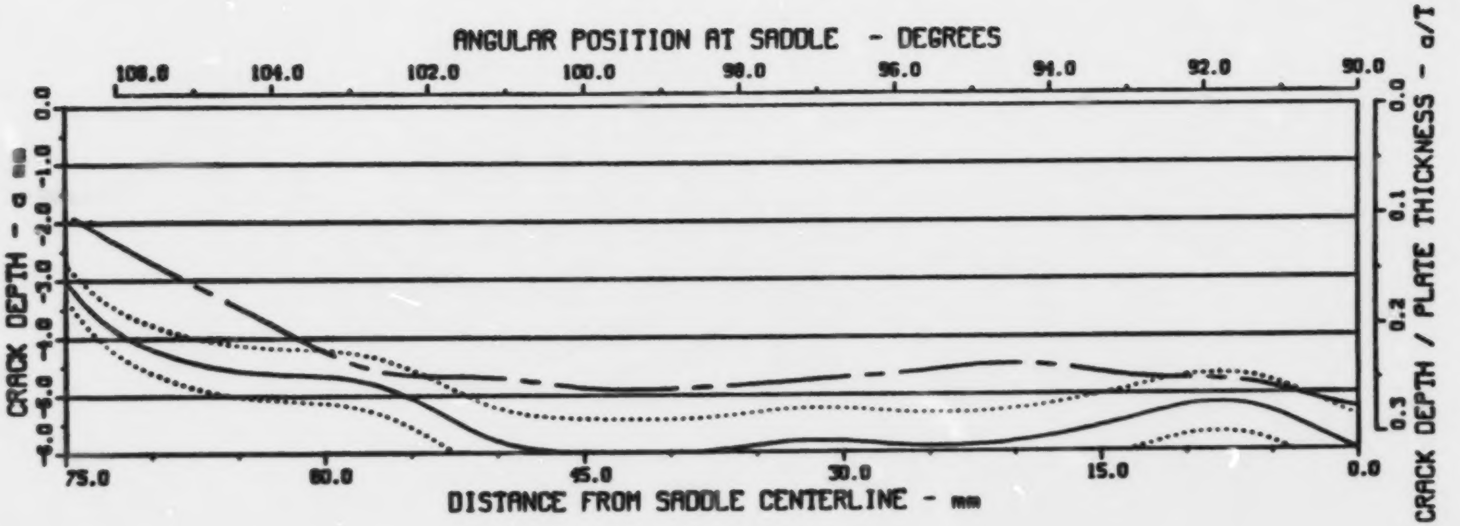

FIGURE 103 CRACK DEPTH VERSUS POSITION (TB4)
COMPARISON OF DCPD RESULTS AND INKSTAIN DATA
STIFFENED TUBULAR T-JOINT *** OUT-OF-PLANE BENDING
R-RATIO - 0.05 *** HOT-SPOT STRESS RANGE- 245.6 MPa

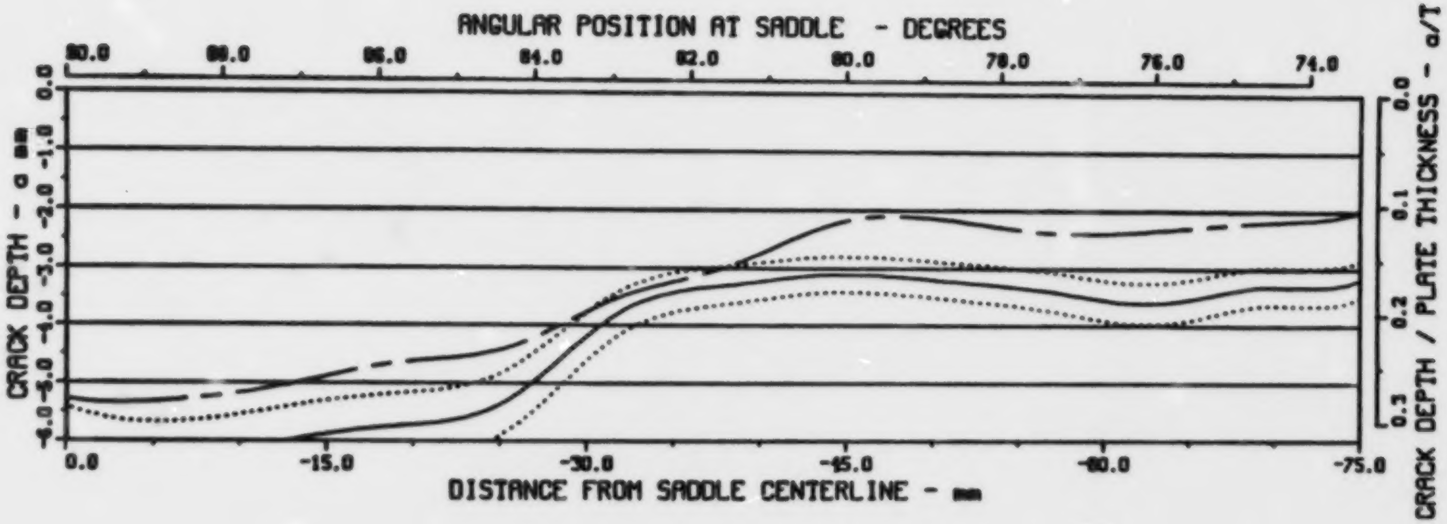

FIGURE 104 CRACK DEPTH VERSUS POSITION (TB4)
COMPARISON OF DCPD RESULTS AND INKSTAIN DATA
STIFFENED TUBULAR T-JOINT *** OUT-OF-PLANE BENDING
R-RATIO - 0.05 *** HOT-SPOT STRESS RANGE- 245.6 MPa

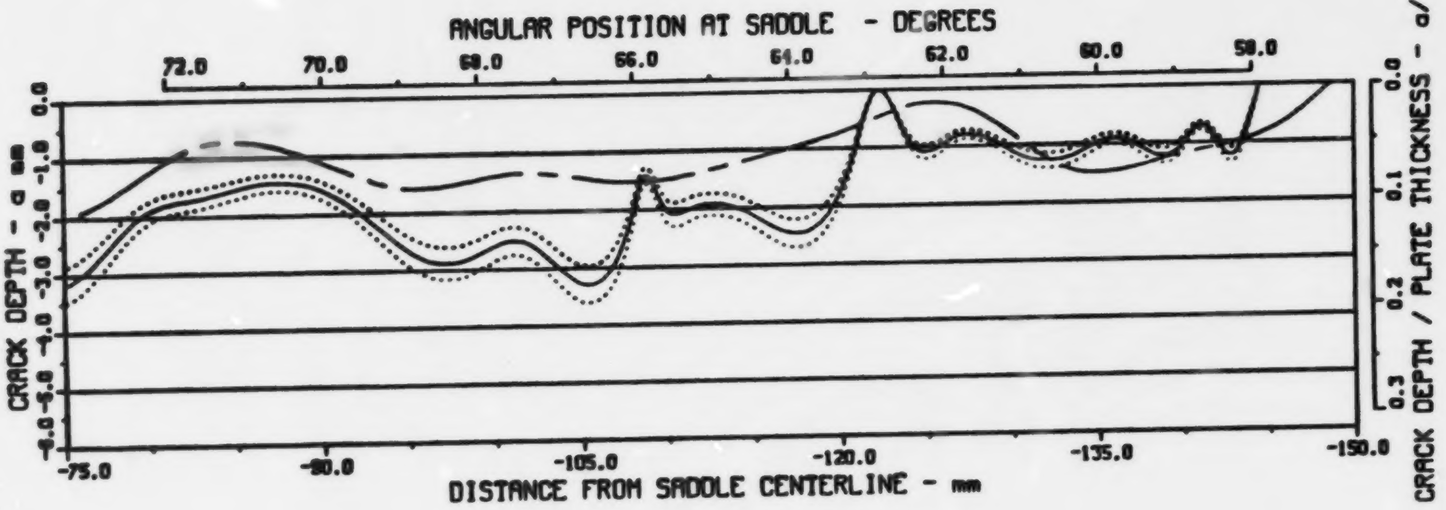

FIGURE 105 CRACK DEPTH VERSUS POSITION (TB4)
COMPARISON OF DCPD RESULTS AND INKSTAIN DATA
STIFFENED TUBULAR T-JOINT *** OUT-OF-PLANE BENDING
R-RATIO - 0.05 *** HOT-SPOT STRESS RANGE- 245.6 MPa

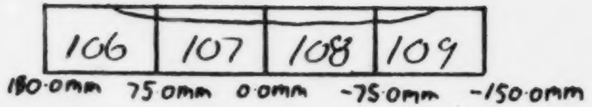
106
107
108
109
150·0mm
75·0mm
0·0mm
-75·0mm
-150·0mm

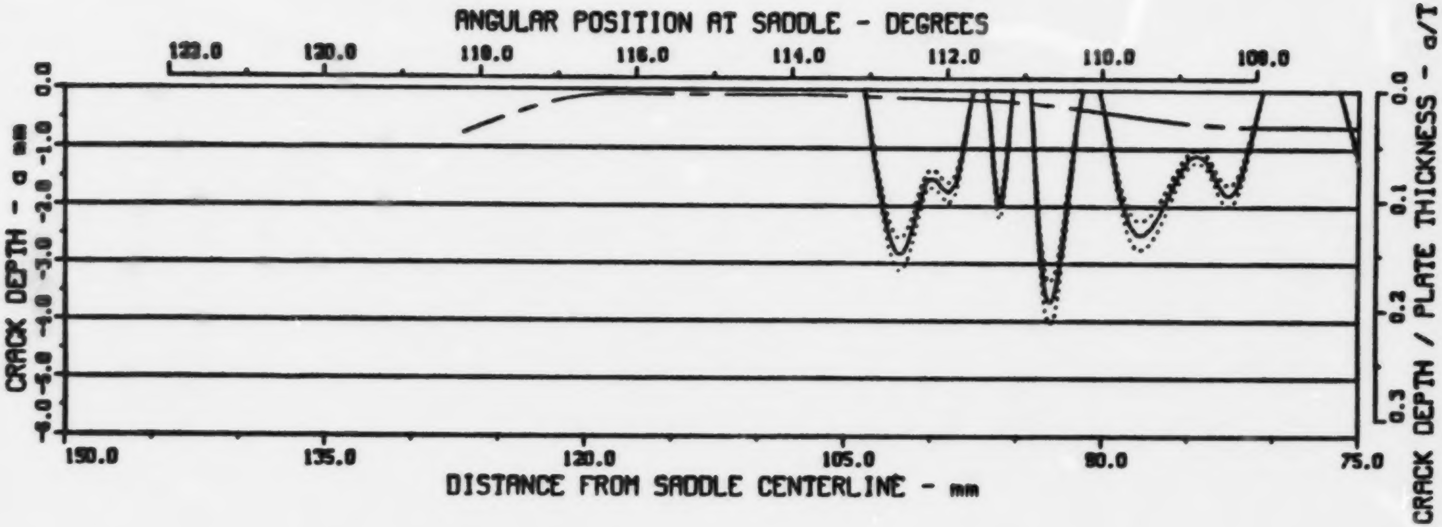

FIGURE 106 CRACK DEPTH VERSUS POSITION (TB5)
COMPARISON OF DCPD RESULTS AND INKSTAIN DATA
STIFFENED TUBULAR T-JOINT *** OUT-OF-PLANE BENDING
R-RATIO - 0.05 *** HOT-SPOT STRESS RANGE- 157 MPa

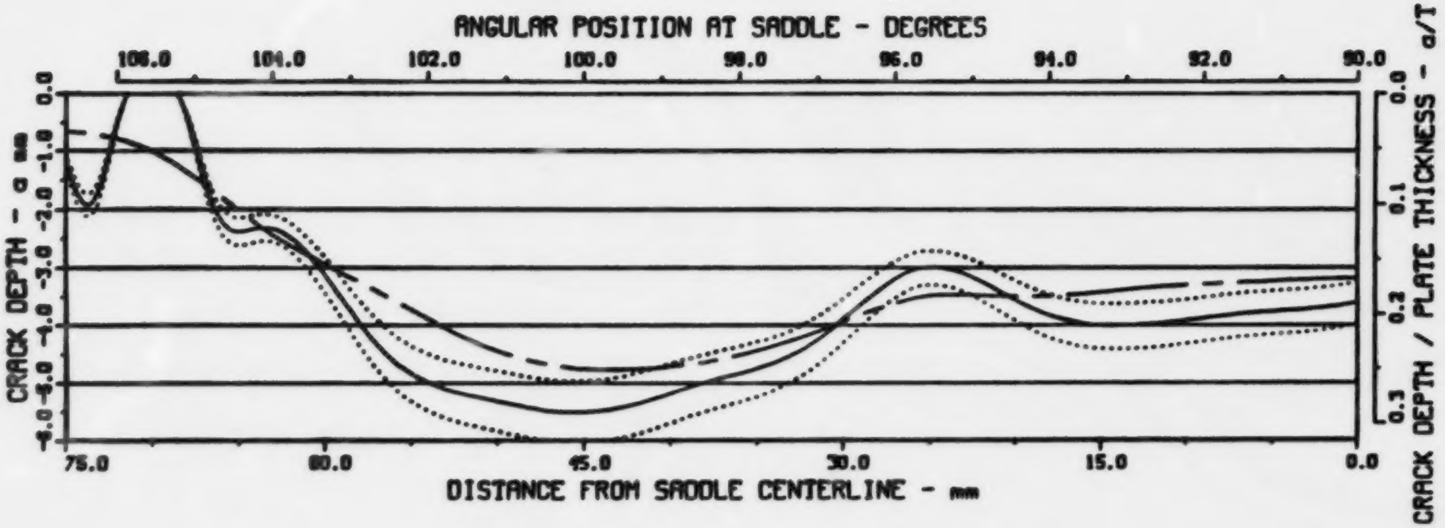

FIGURE 107 CRACK DEPTH VERSUS POSITION (TB5)
COMPARISON OF DCPD RESULTS AND INKSTAIN DATA
STIFFENED TUBULAR T-JOINT *** OUT-OF-PLANE BENDING
R-RATIO - 0.05 *** HOT-SPOT STRESS RANGE- 157 MPa

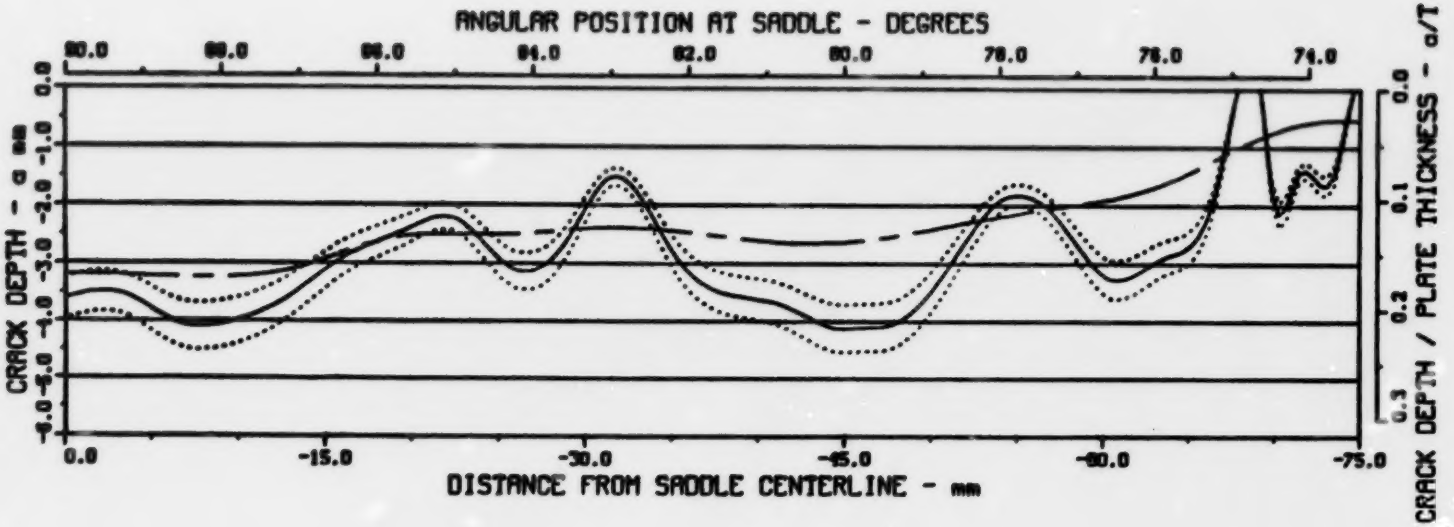

FIGURE 108 CRACK DEPTH VERSUS POSITION (TB5)
COMPARISON OF DCPD RESULTS AND INKSTAIN DATA
STIFFENED TUBULAR T-JOINT *** OUT-OF-PLANE BENDING
R-RATIO - 0.05 *** HOT-SPOT STRESS RANGE- 157 MPa

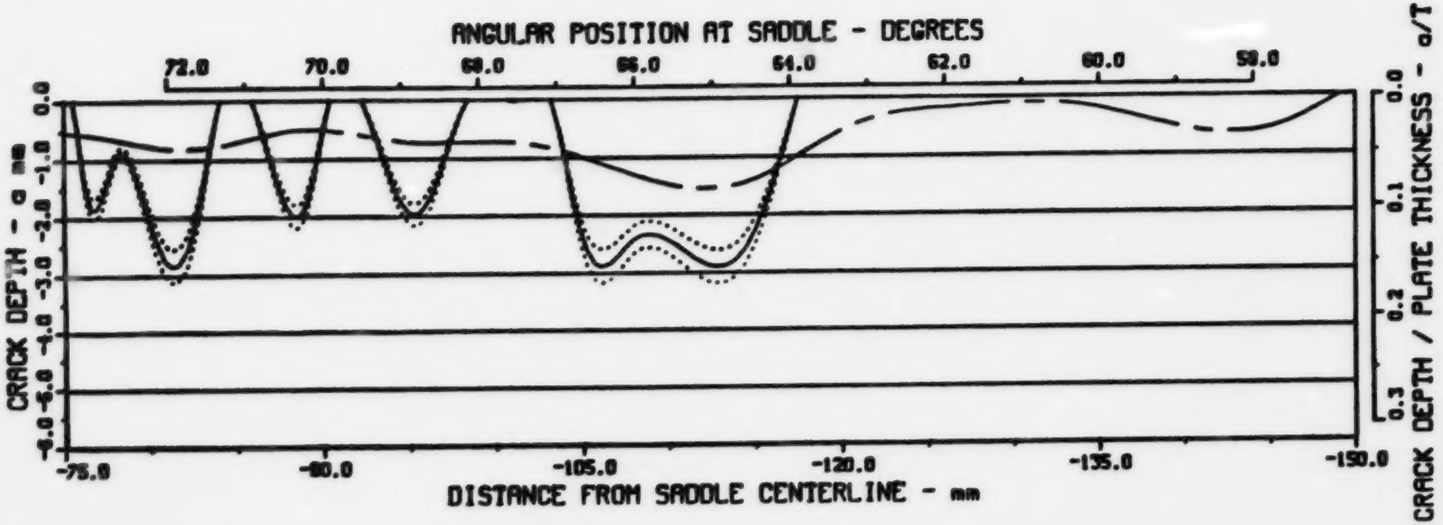

FIGURE 109 CRACK DEPTH VERSUS POSITION (TB5)
COMPARISON OF DCPD RESULTS AND INKSTAIN DATA
STIFFENED TUBULAR T-JOINT *** OUT-OF-PLANE BENDING
R-RATIO - 0.05 *** HOT-SPOT STRESS RANGE- 157 MPa

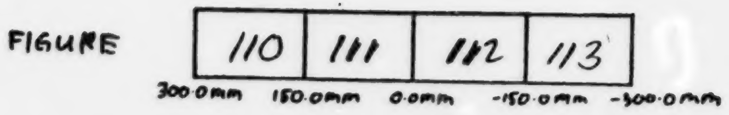
FIGURE
110
111
112
113
300.0mm
150.0mm
0.0mm
-150.0mm
-300.0mm

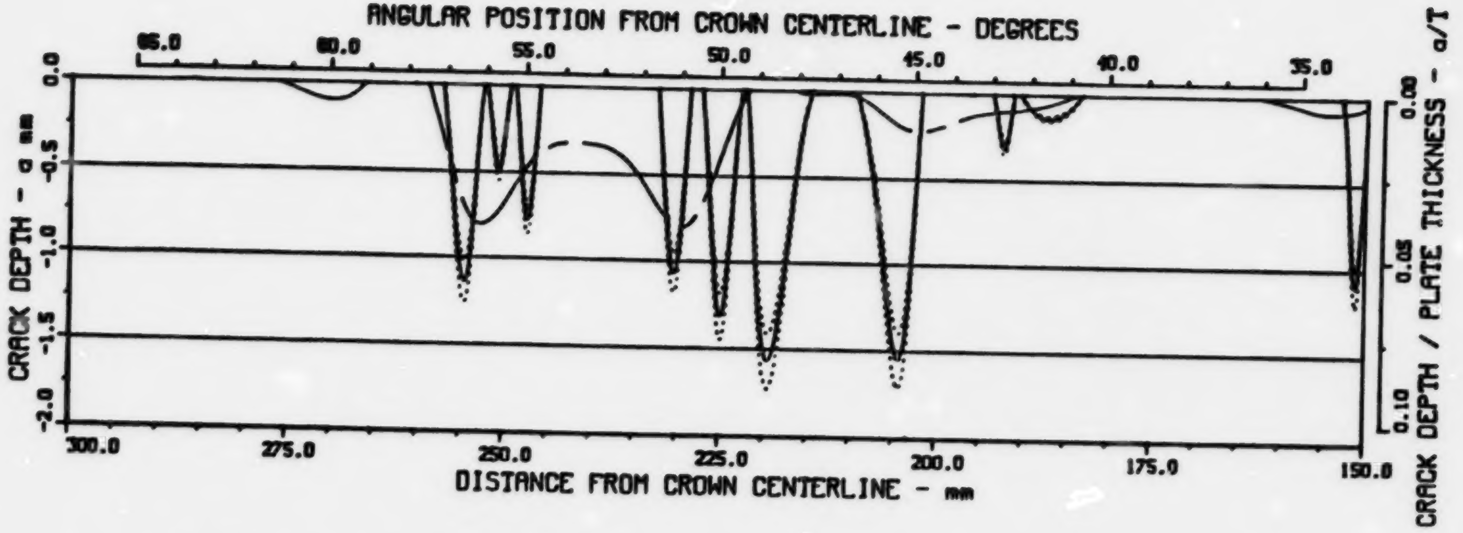

FIGURE 110 CRACK DEPTH VERSUS POSITION (TB6)
COMPARISON OF DCPD RESULTS AND INKSTAIN DATA
STIFFENED TUBULAR T-JOINT *** IN-PLANE BENDING
R-RATIO - 0.05 *** HOT-SPOT STRESS RANGE- 163.0 MPa

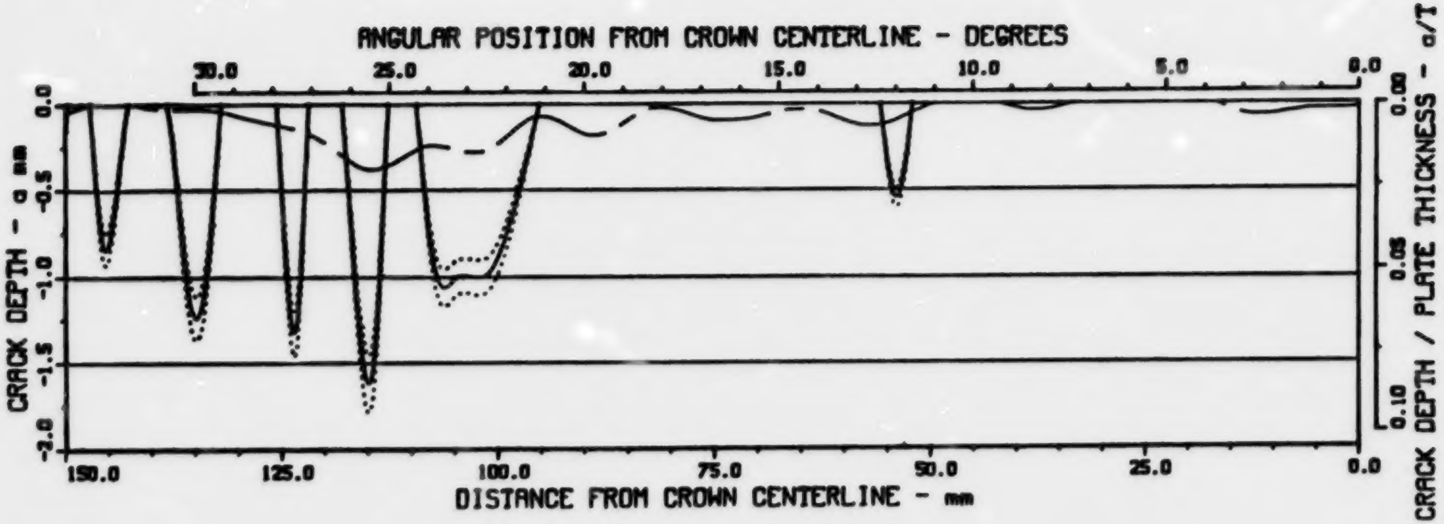

FIGURE 111 CRACK DEPTH VERSUS POSITION (TB6)
COMPARISON OF DCPD RESULTS AND INKSTAIN DATA
STIFFENED TUBULAR T-JOINT *** IN-PLANE BENDING
R-RATIO - 0.05 *** HOT-SPOT STRESS RANGE- 163.0 MPa

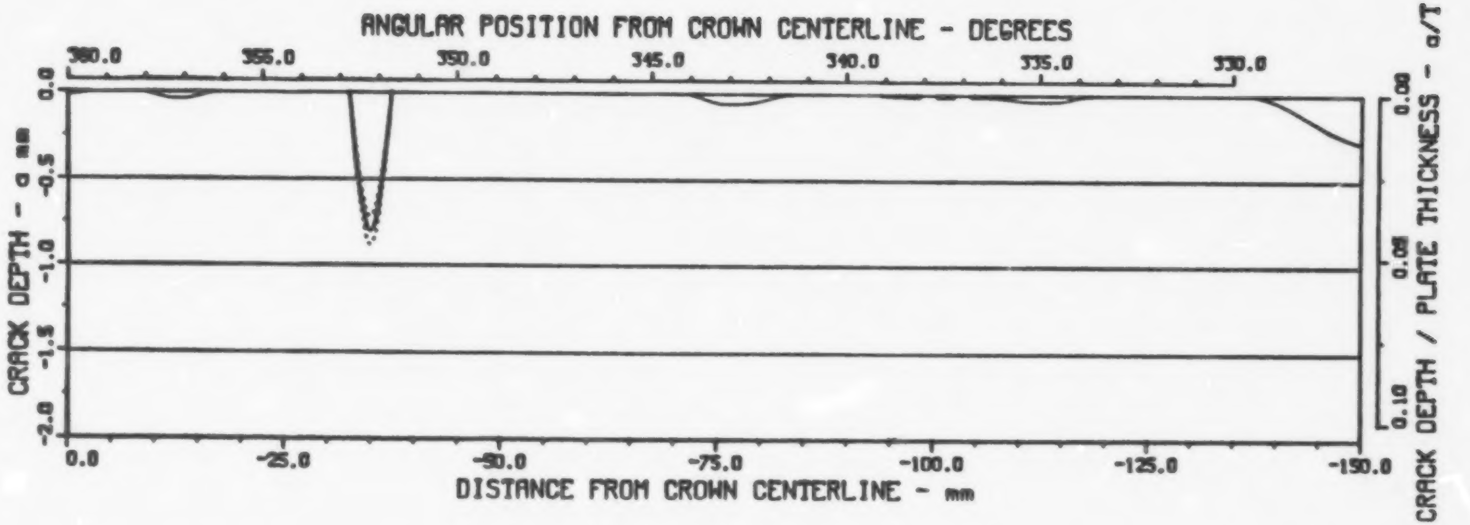

FIGURE 112 CRACK DEPTH VERSUS POSITION (TB6)
COMPARISON OF DCPD RESULTS AND INKSTAIN DATA
STIFFENED TUBULAR T-JOINT *** IN-PLANE BENDING
R-RATIO - 0.05 *** HOT-SPOT STRESS RANGE- 163.0 MPa

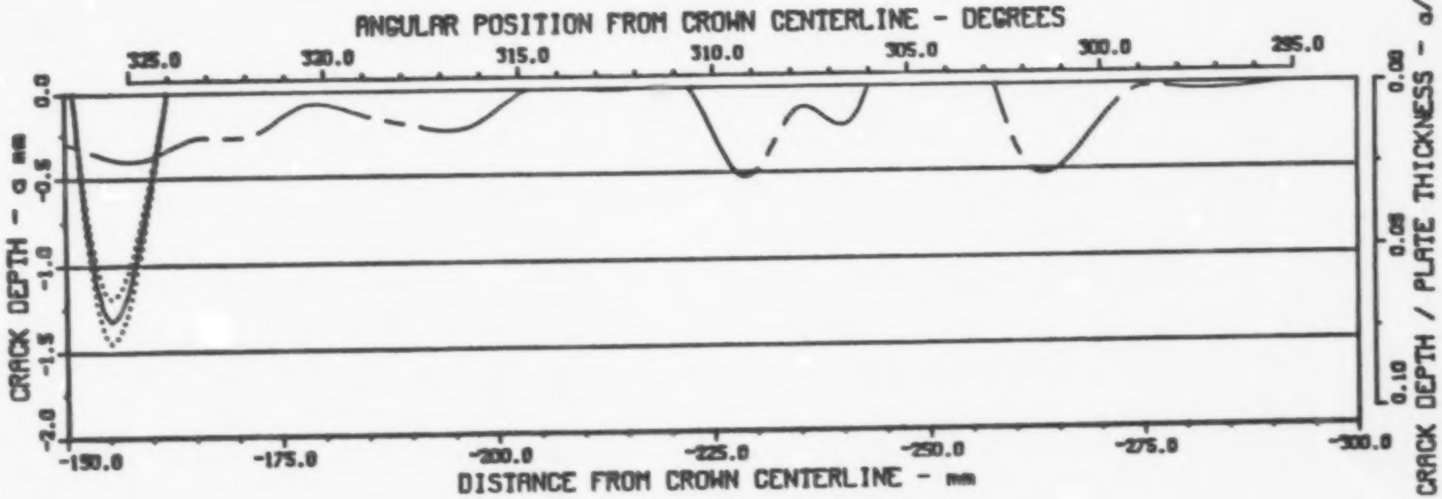

FIGURE 113 CRACK DEPTH VERSUS POSITION (TB6)
COMPARISON OF DCPD RESULTS AND INKSTAIN DATA
STIFFENED TUBULAR T-JOINT *** IN-PLANE BENDING
R-RATIO - 0.05 *** HOT-SPOT STRESS RANGE- 163.0 MPa

$N(a_1) = 78{\cdot}6\ K\sim$ $N(a_5) = 178{\cdot}2\ K\sim$

CURVES PLOTTED AT ≈ 25 K ∼ INTERVALS

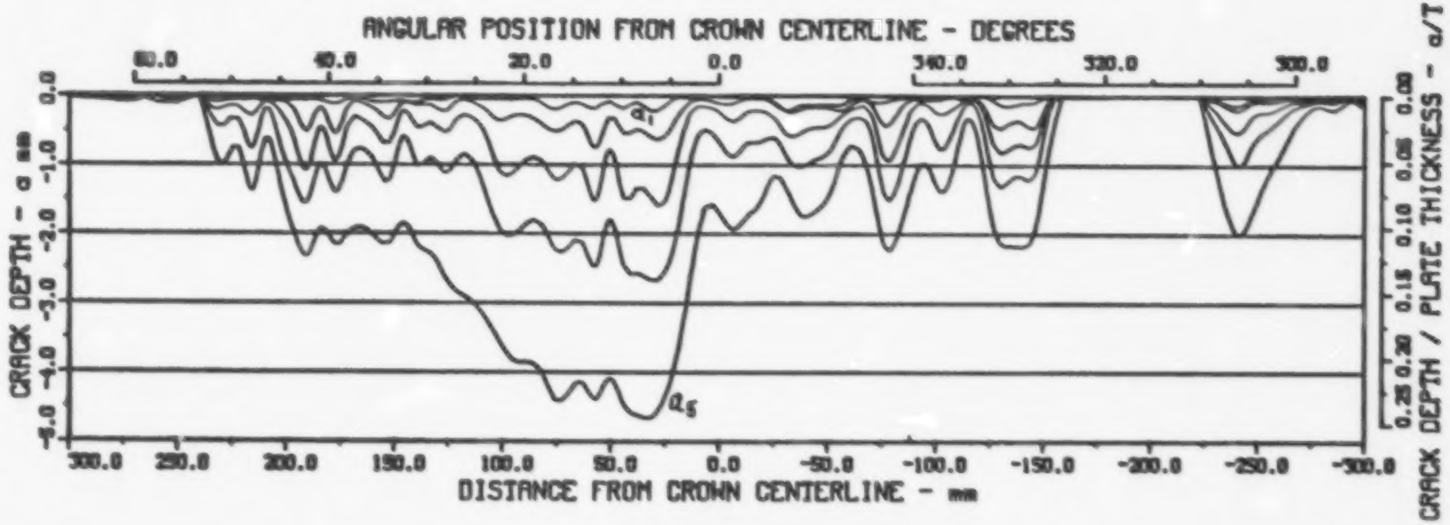

FIGURE 114 DCPD RESULTS *** CRACK DEPTH VERSUS POSITION (TB1)
UNSTIFFENED TUBULAR T-JOINT *** IN-PLANE BENDING
R-RATIO - 0.05 *** HOT-SPOT STRESS RANGE- 248 MPa

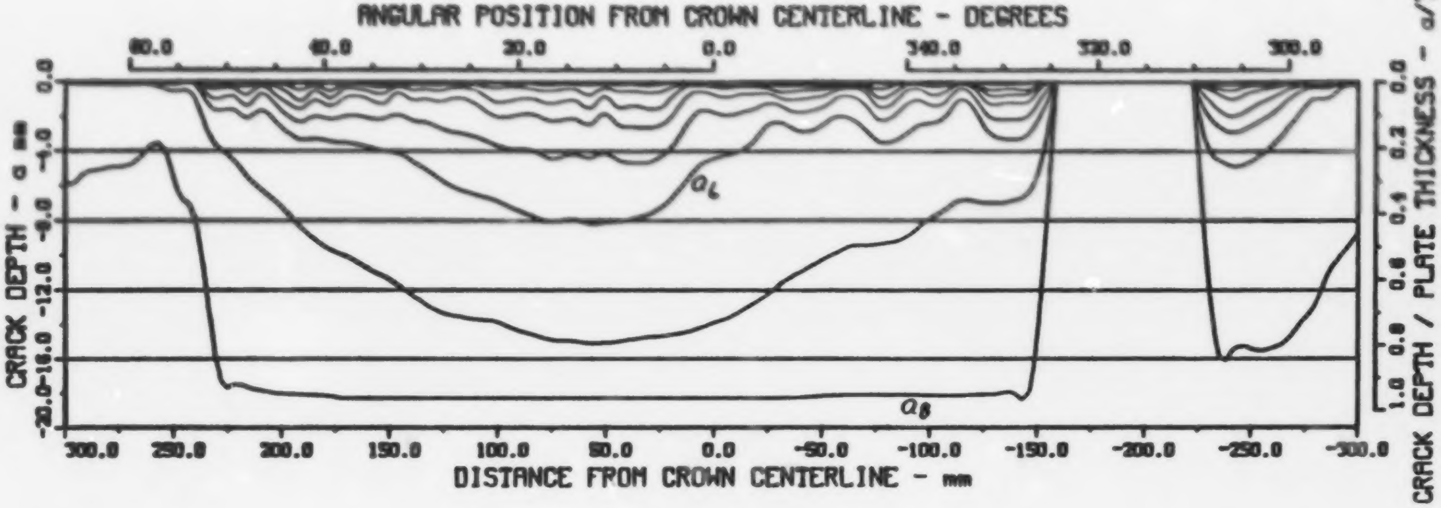

$N(a_L) = 200K\sim$ $N(a_B) = 250K\sim$ $N_T = 235.3K\sim$

CURVES PLOTTED AT ≈ 25K ~ INTERVALS

FIGURE 115 DCPD RESULTS ☒☒☒ CRACK DEPTH VERSUS POSITION (TB1)
UNSTIFFENED TUBULAR T-JOINT ☒☒☒ IN-PLANE BENDING
R-RATIO - 0.05 ☒☒☒ HOT-SPOT STRESS RANGE- 248 MPa

$N(a_1)$= 50·2 K~ $N(a_4)$= 125·6 K~

CURVES PLOTTED AT ≈ 25 K~ INTERVALS

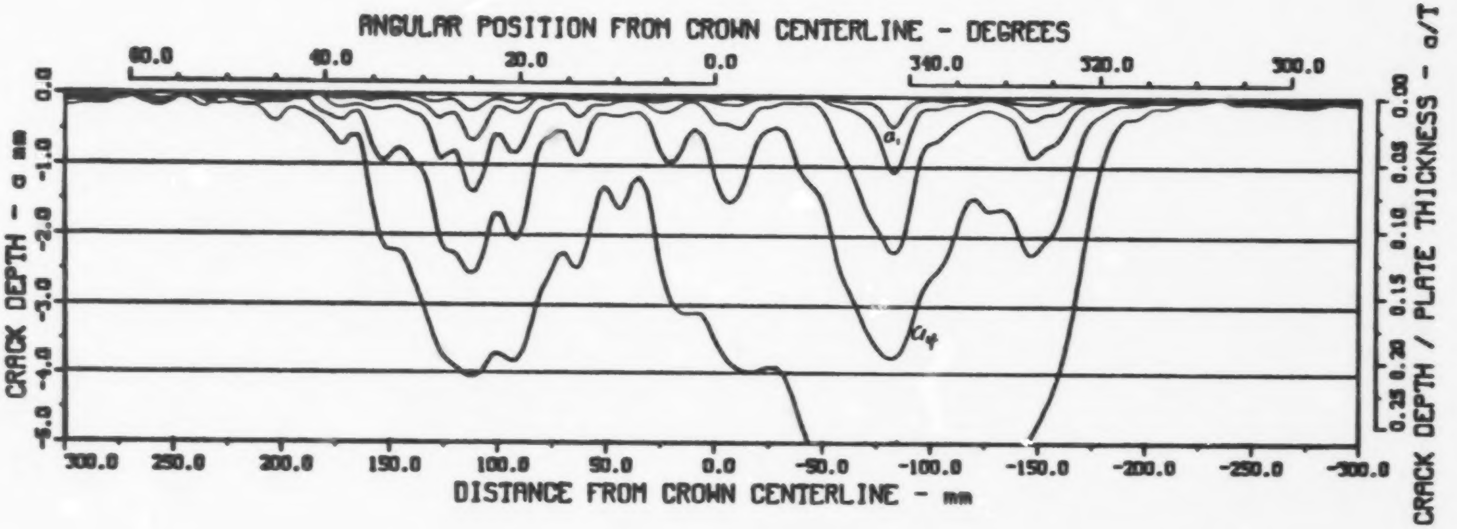

FIGURE 116 DCPD RESULTS *** CRACK DEPTH VERSUS POSITION (TB2)
STIFFENED TUBULAR T-JOINT *** IN-PLANE BENDING
R-RATIO - 0.05 *** HOT-SPOT STRESS RANGE- 246 MPa

$N(a_5) = 150\,K\sim$ $N(a_7) = 202.5\,K\sim$

CURVES PLOTTED AT ≈ 25 K ~ INTERVALS

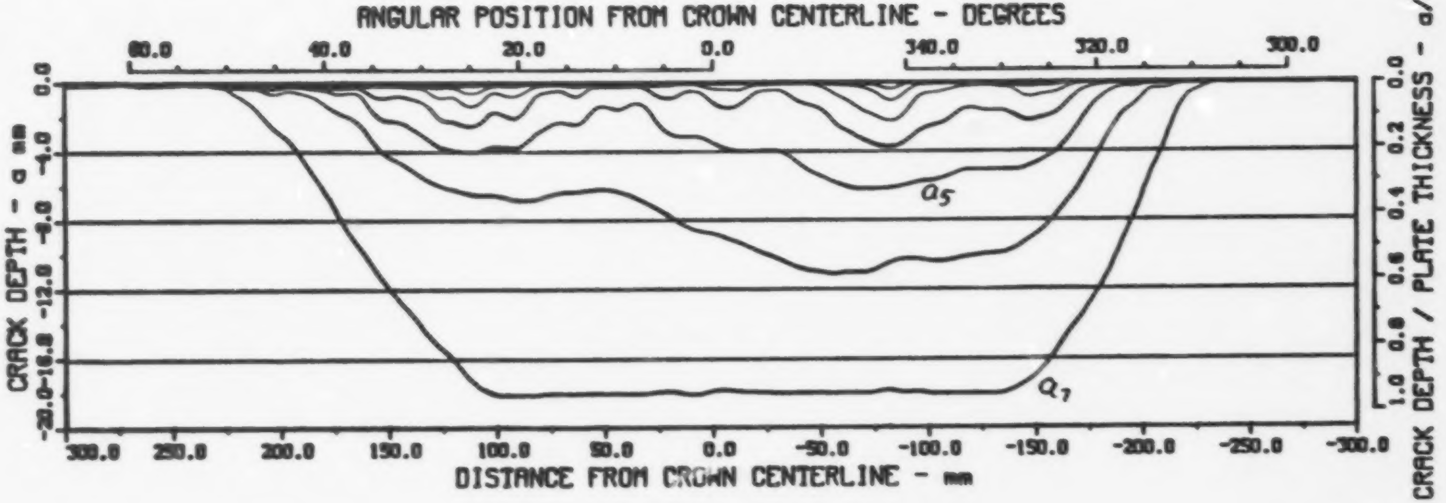

FIGURE 117 DCPD RESULTS *** CRACK DEPTH VERSUS POSITION (TB2)
STIFFENED TUBULAR T-JOINT *** IN-PLANE BENDING
R-RATIO - 0.05 *** HOT-SPOT STRESS RANGE- 246 MPa

$N(a_1) = 97.5\,K\sim$ $N(a_7) = 250\,K\sim$

CURVES PLOTTED AT ≈ 25K~ INTERVALS

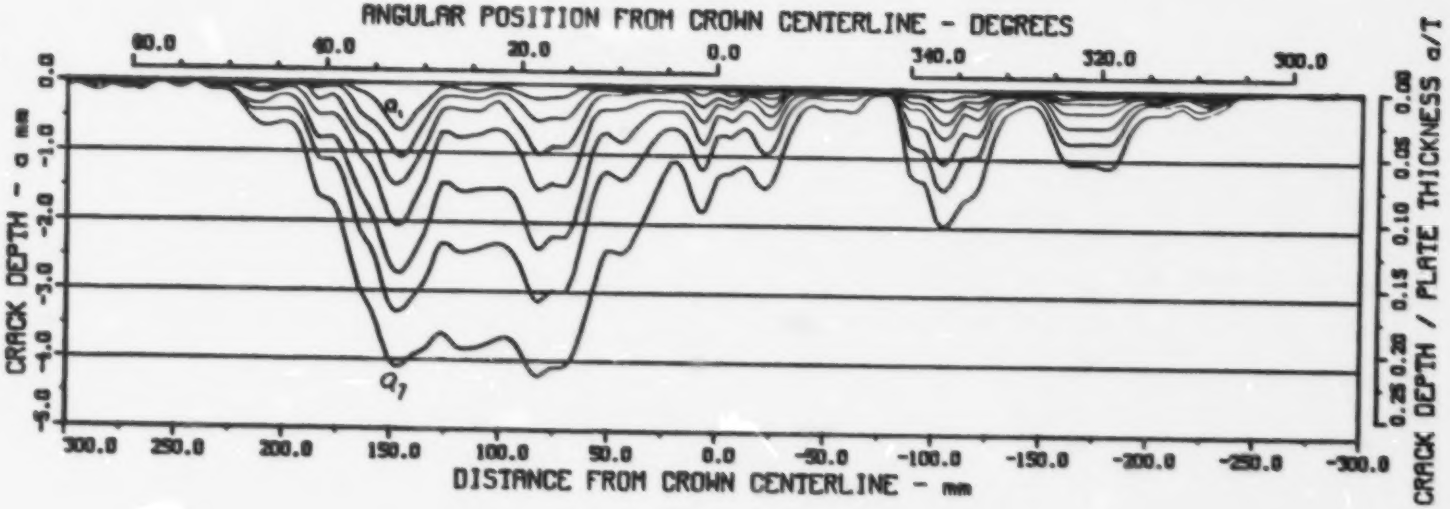

FIGURE 118 DCPD RESULTS *** CRACK DEPTH VERSUS POSITION (TB3)
STIFFENED TUBULAR T-JOINT *** IN-PLANE BENDING
R-RATIO - 0.05 *** HOT-SPOT STRESS RANGE- 160.0 MPa

$N(a_1) = 75 \cdot 5K\sim$ $N(a_4) = 150K\sim$
CURVES PLOTTED AT ≈ 25K~ INTERVALS

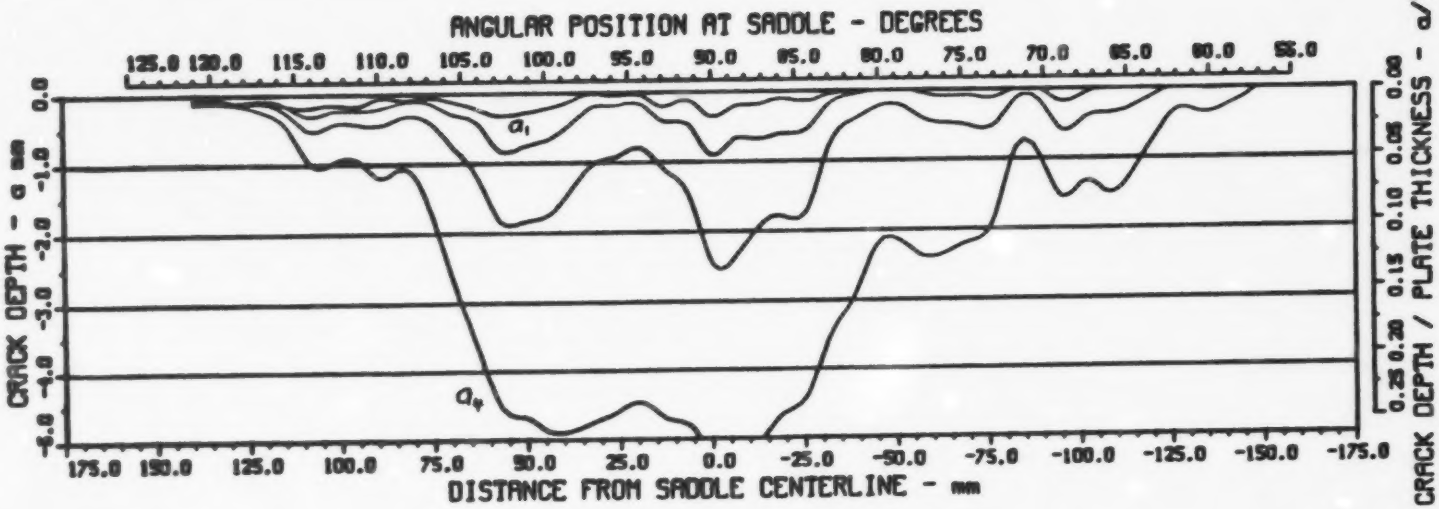

FIGURE 119 DCPD RESULTS *** CRACK DEPTH VERSUS POSITION (TB4)
STIFFENED TUBULAR T-JOINT *** OUT-OF-PLANE BENDING
R-RATIO - 0.05 *** HOT-SPOT STRESS RANGE- 245.6 MPa

$N(a_5) = 175K\sim \qquad N(a_{11}) = 325K\sim$
CURVES PLOTTED AT ≈ 25K~ INTERVALS

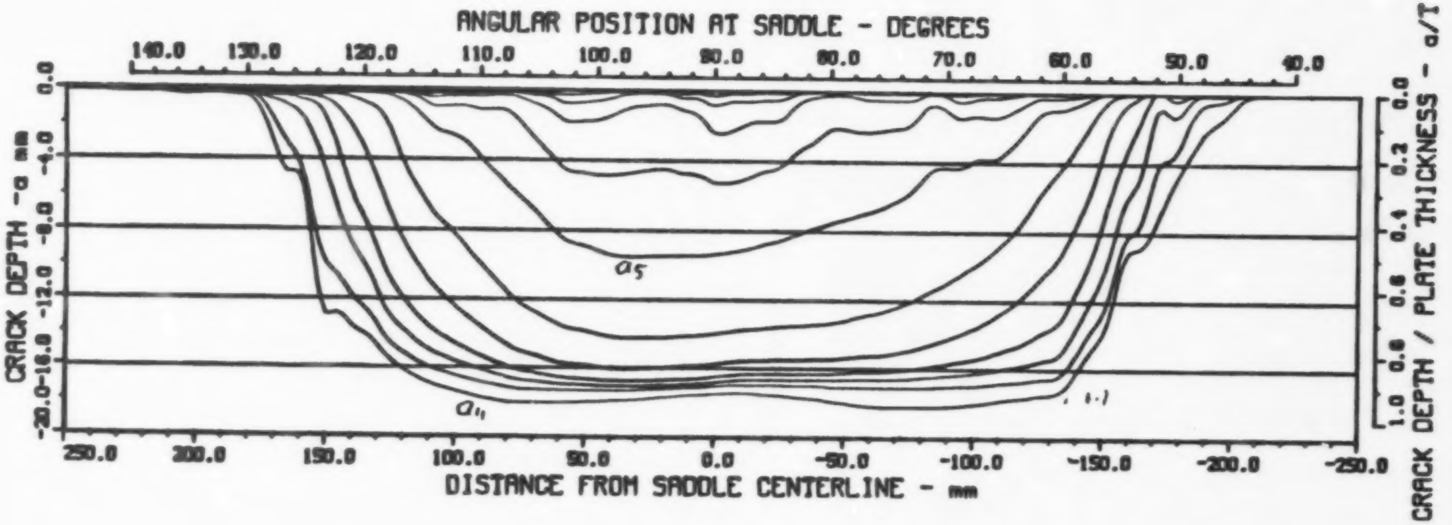

FIGURE 120 DCPD RESULTS ••• CRACK DEPTH VERSUS POSITION (TB4)
STIFFENED TUBULAR T-JOINT ••• OUT-OF-PLANE BENDING
R-RATIO - 0.05 ••• HOT-SPOT STRESS RANGE- 245.6 MPa

$N(a_1) = 350K\sim$ $N(a_4) = 650K\sim$
CURVES PLOTTED AT ≈ 100K ~ INTERVALS

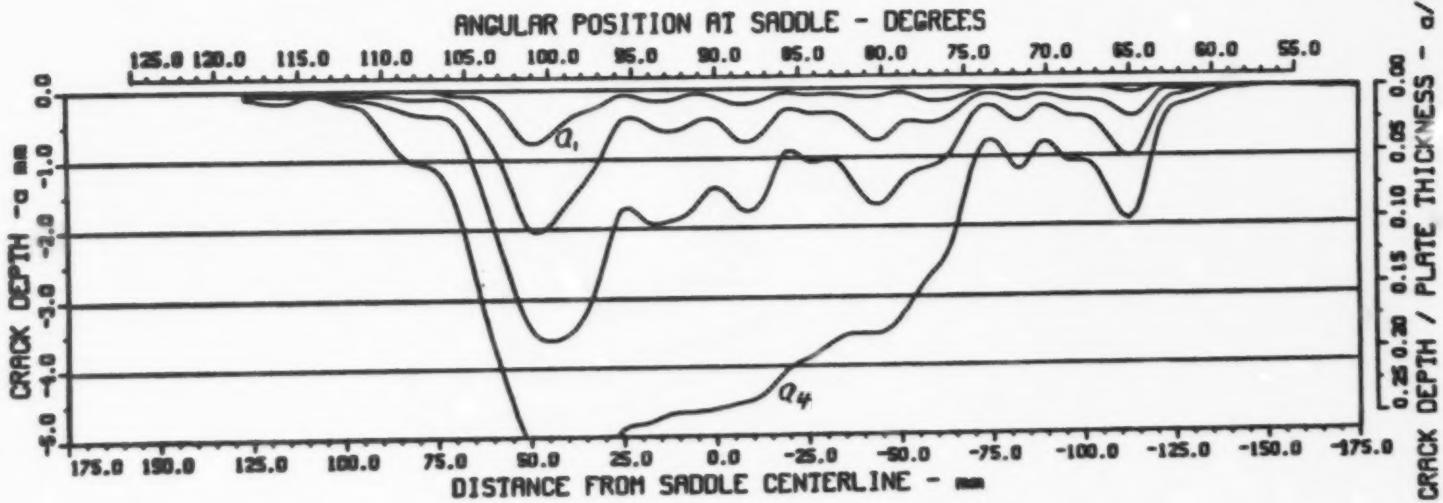

FIGURE 121 DCPD RESULTS *** CRACK DEPTH VERSUS POSITION (TB5)
STIFFENED TUBULAR T-JOINT *** OUT-OF-PLANE BENDING
R-RATIO - 0.05 *** HOT-SPOT STRESS RANGE- 157 MPa

$N(a_5)$= 750K~ $N(a_{18})$= 2110 K~ N_T = 2110 K~

CURVES PLOTTED AT ≈ 100K~ INTERVALS

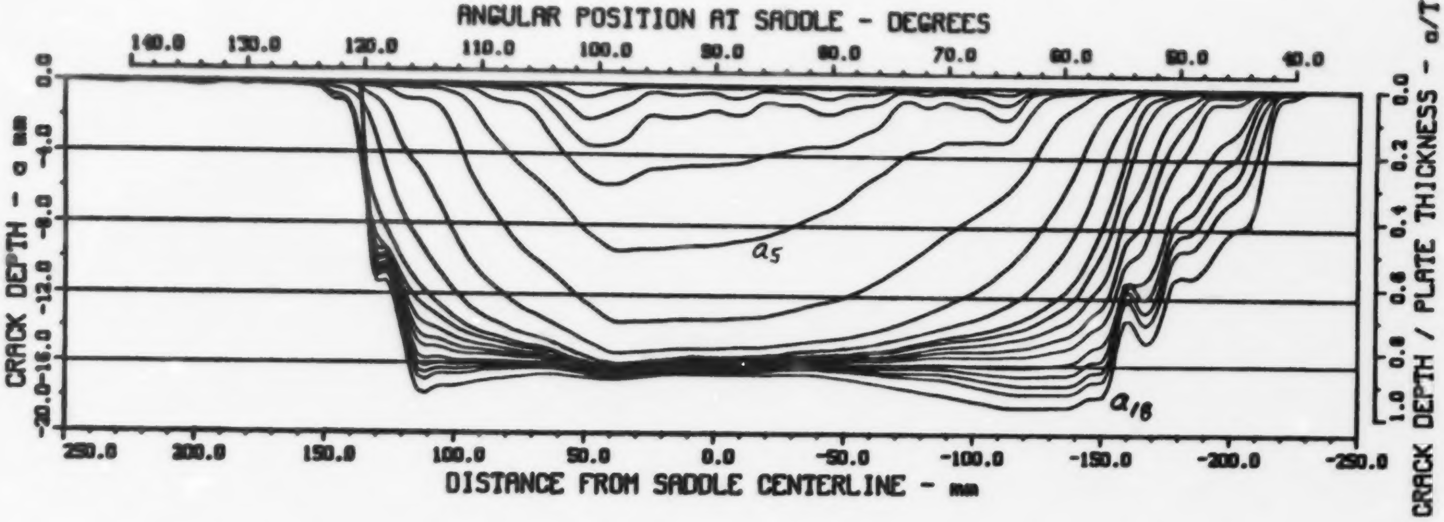

FIGURE 122 DCPD RESULTS ••• CRACK DEPTH VERSUS POSITION (TB5)
STIFFENED TUBULAR T-JOINT ••• OUT-OF-PLANE BENDING
R-RATIO - 0.05 ••• HOT-SPOT STRESS RANGE- 157 MPa

$N(a_1) = 251$ K~ $N(a_6) = 500$ K~
CURVES PLOTTED AT ≈ 50 K~ INTERVALS

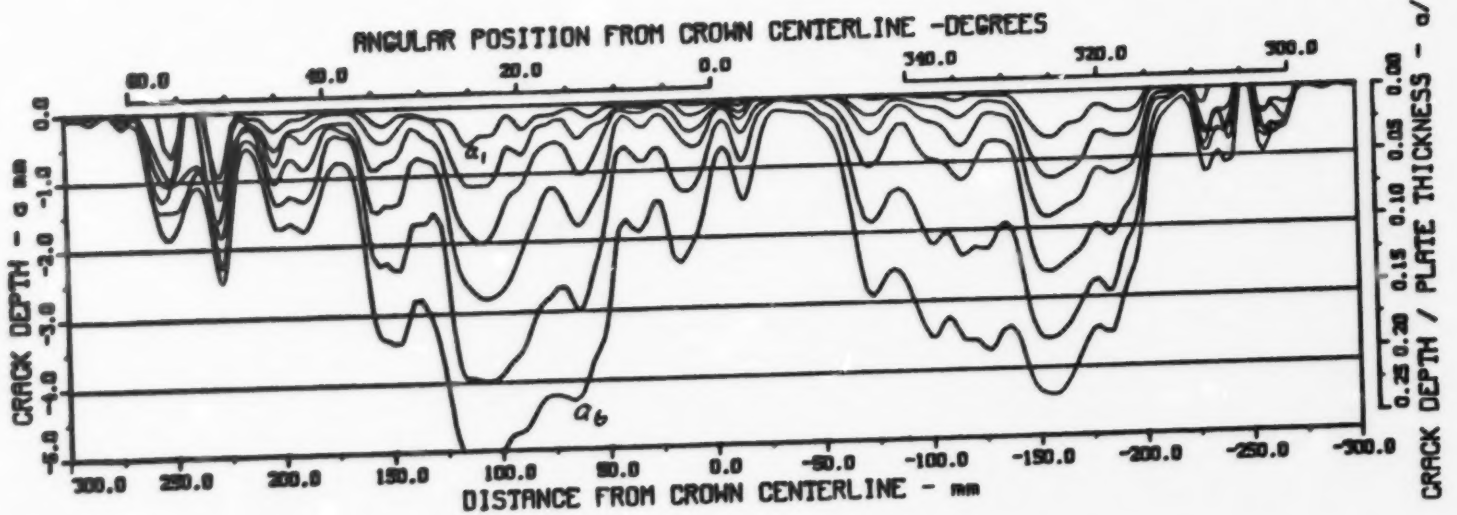

FIGURE 123 DCPD RESULTS *** CRACK DEPTH VERSUS POSITION (TB6)
STIFFENED TUBULAR T-JOINT *** IN-PLANE BENDING
R-RATIO - 0.05 *** HOT-SPOT STRESS RANGE- 163.0 MPa

$N(a_7) = 550K\sim$ $N(a_{10}) = 700K\sim$ $N_T = 690K\sim$
CURVES PLOTTED AT ≈ 50K ~ INTERVALS

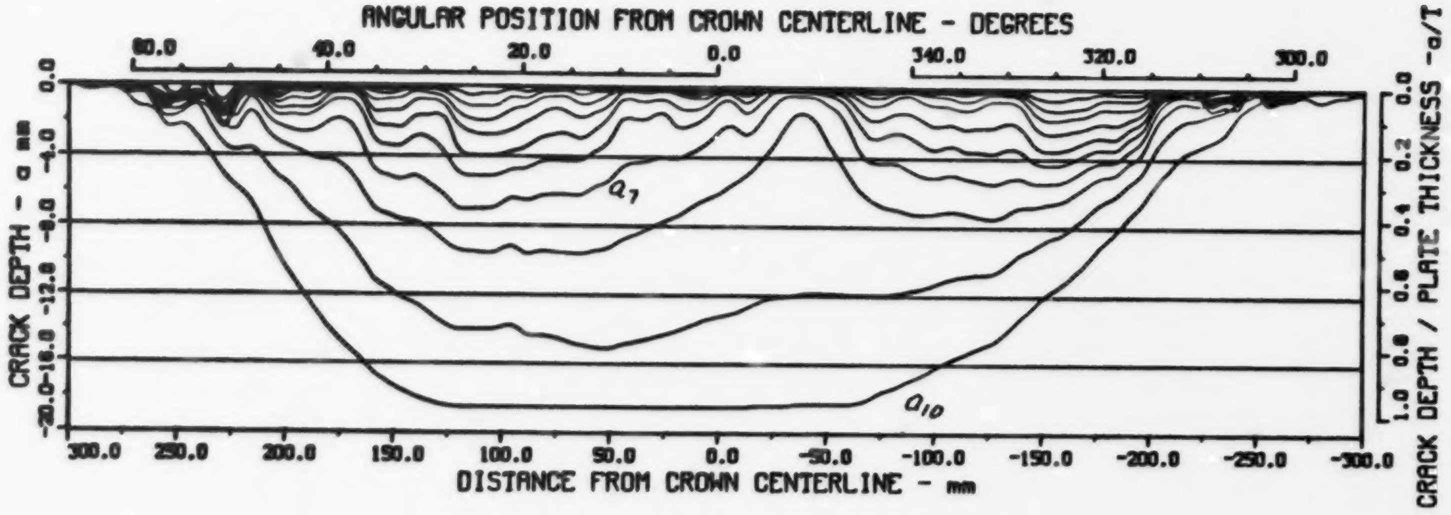

FIGURE 124 DCPD RESULTS *** CRACK DEPTH VERSUS POSITION (TB6)
STIFFENED TUBULAR T-JOINT *** IN-PLANE BENDING
R-RATIO - 0.05 *** HOT-SPOT STRESS RANGE- 163.0 MPa

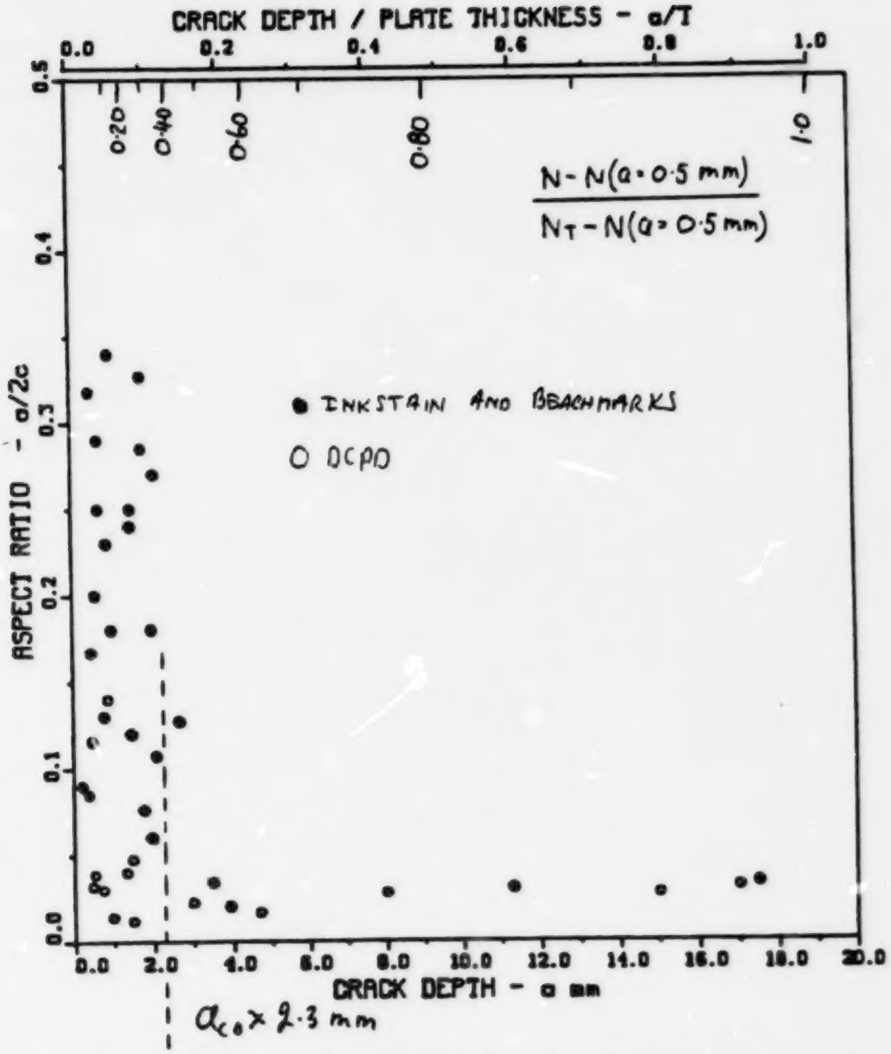

FIGURE 125 CRACK SHAPE (ASPECT RATIO) DEVELOPMENT (TB1)
INKSTAIN, BEACHMARK AND DCPD RESULTS
UNSTIFFENED TUBULAR T-JOINT *** IN-PLANE BENDING
R-RATIO - 0.05 *** HOT-SPOT STRESS RANGE - 248 MPa

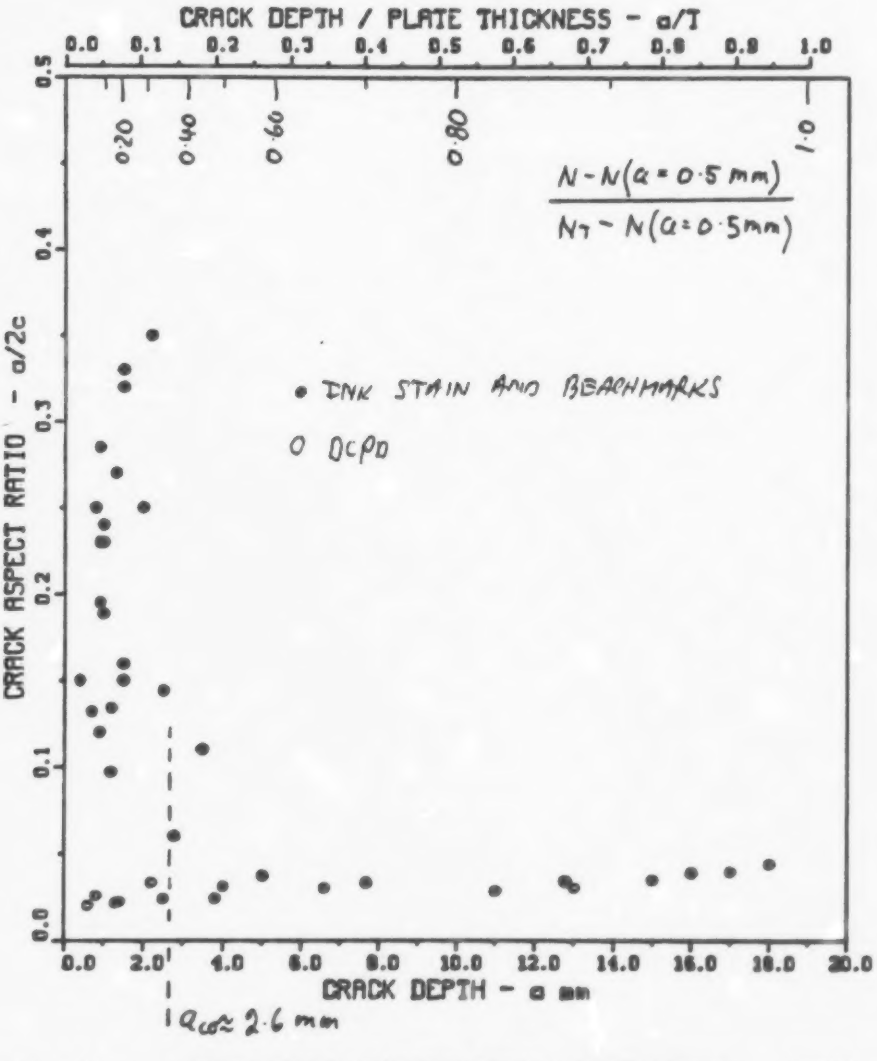

FIGURE 126 CRACK SHAPE (ASPECT RATIO) DEVELOPMENT (TB2)
INKSTAIN, BEACHMARK AND DCPD RESULTS
STIFFENED TUBULAR T-JOINT ■■■ IN-PLANE BENDING
R-RATIO - 0.05 ■■■ HOT-SPOT STRESS RANGE - 246 MPa

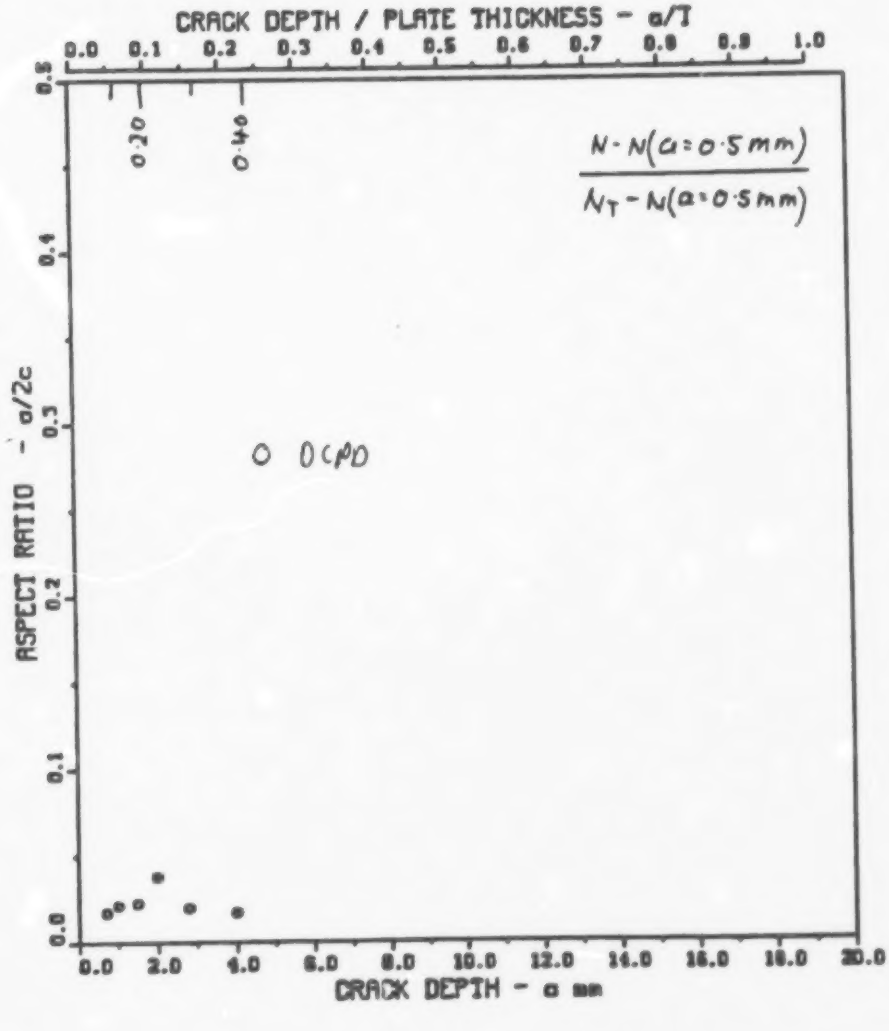

FIGURE 127 CRACK SHAPE (ASPECT RATIO) DEVELOPMENT (TB3)
INKSTAIN, BEACHMARK AND DCPD RESULTS
STIFFENED TUBULAR T-JOINT **** IN-PLANE BENDING
R-RATIO - 0.05 **** HOT-SPOT STRESS RANGE - 160.0 MPa

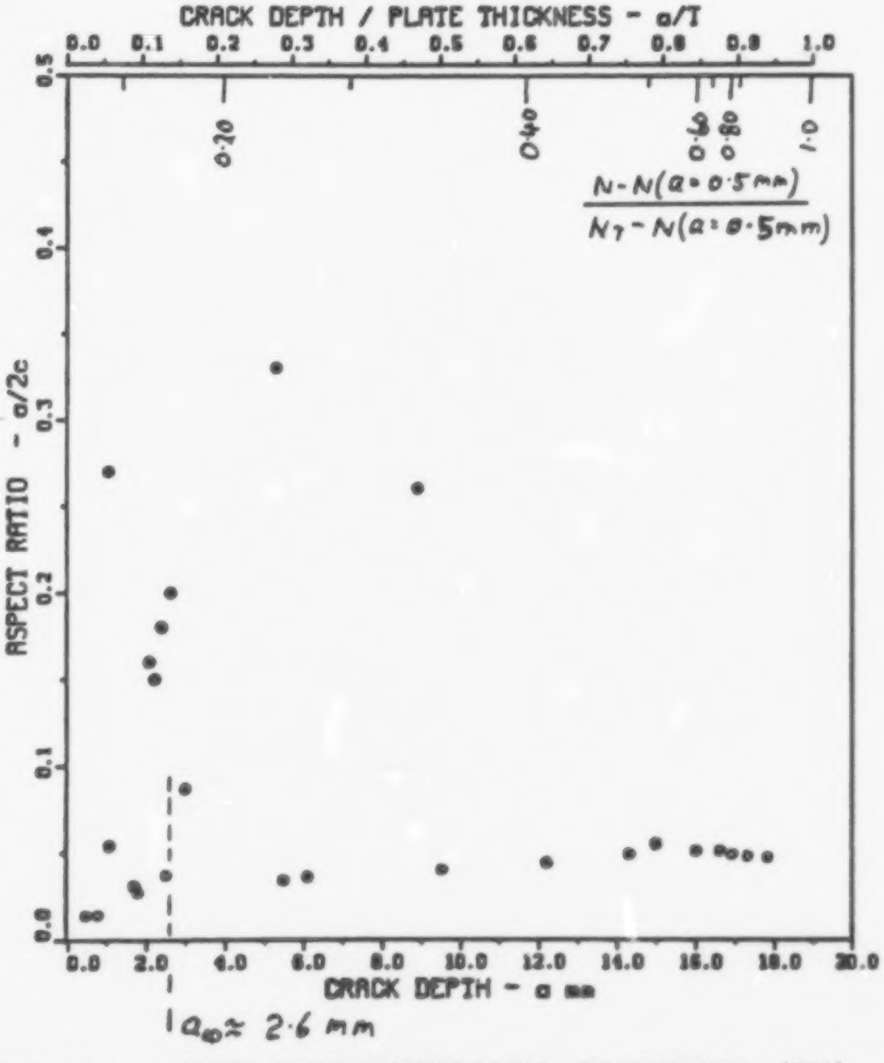

FIGURE 128 CRACK SHAPE (ASPECT RATIO) DEVELOPMENT (TB4)
INKSTAIN, BEACHMARK AND DCPD RESULTS
STIFFENED TUBULAR T-JOINT *** OUT-OF-PLANE BENDING
R-RATIO - 0.05 *** HOT-SPOT STRESS RANGE - 245.6 MPa

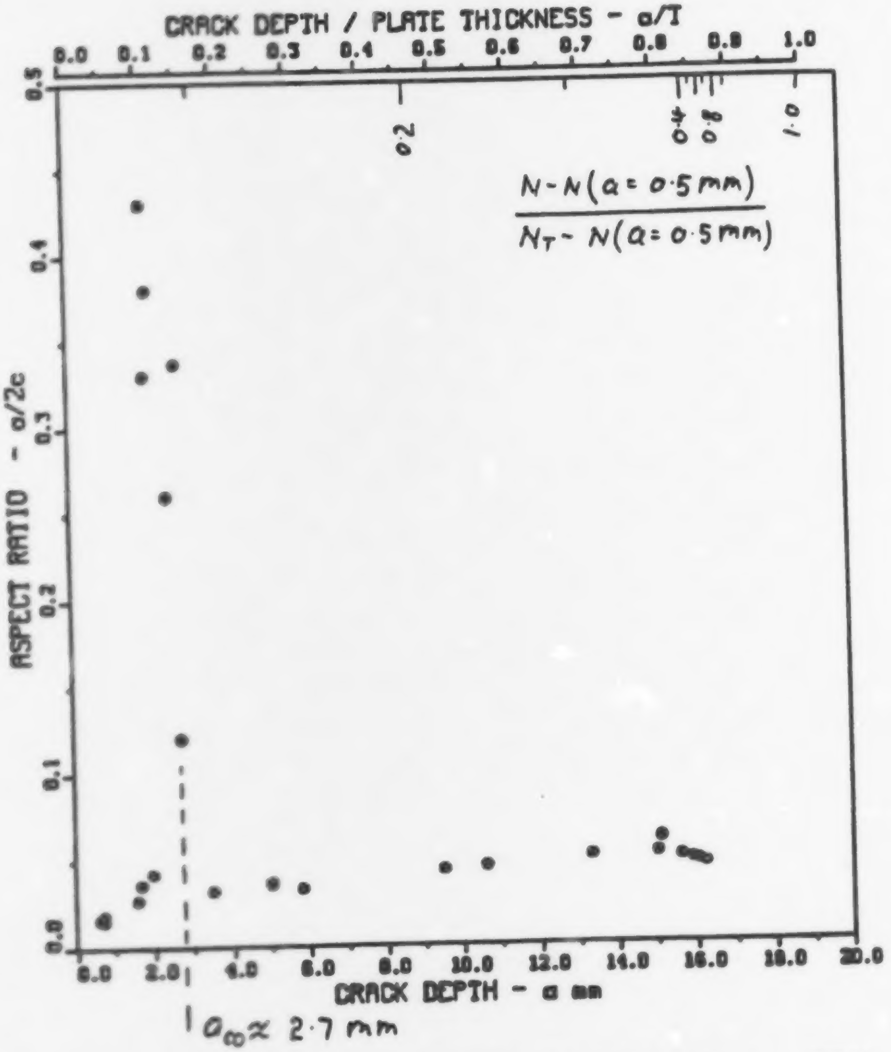

FIGURE 129 CRACK SHAPE (ASPECT RATIO) DEVELOPMENT (TB5)
INKSTAIN, BEACHMARK AND DCPD RESULTS
STIFFENED TUBULAR T-JOINT ■■■ OUT-OF-PLANE BENDING
R-RATIO - 0.05 ■■■ HOT-SPOT STRESS RANGE - 157 MPa

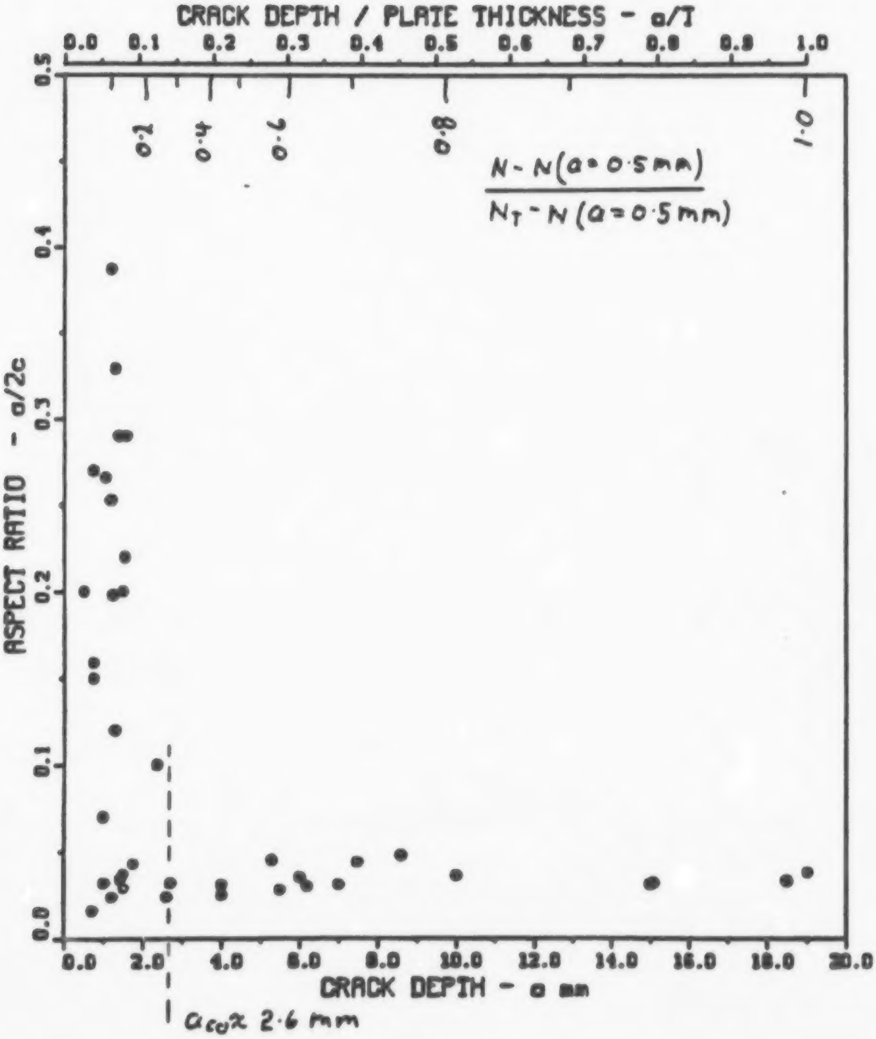

FIGURE 130 CRACK SHAPE (ASPECT RATIO) DEVELOPMENT (TB6)
INKSTAIN, BEACHMARK AND DCPD RESULTS
STIFFENED TUBULAR T-JOINT — IN-PLANE BENDING
R-RATIO - 0.05 — HOT-SPOT STRESS RANGE - 163.0 MPa

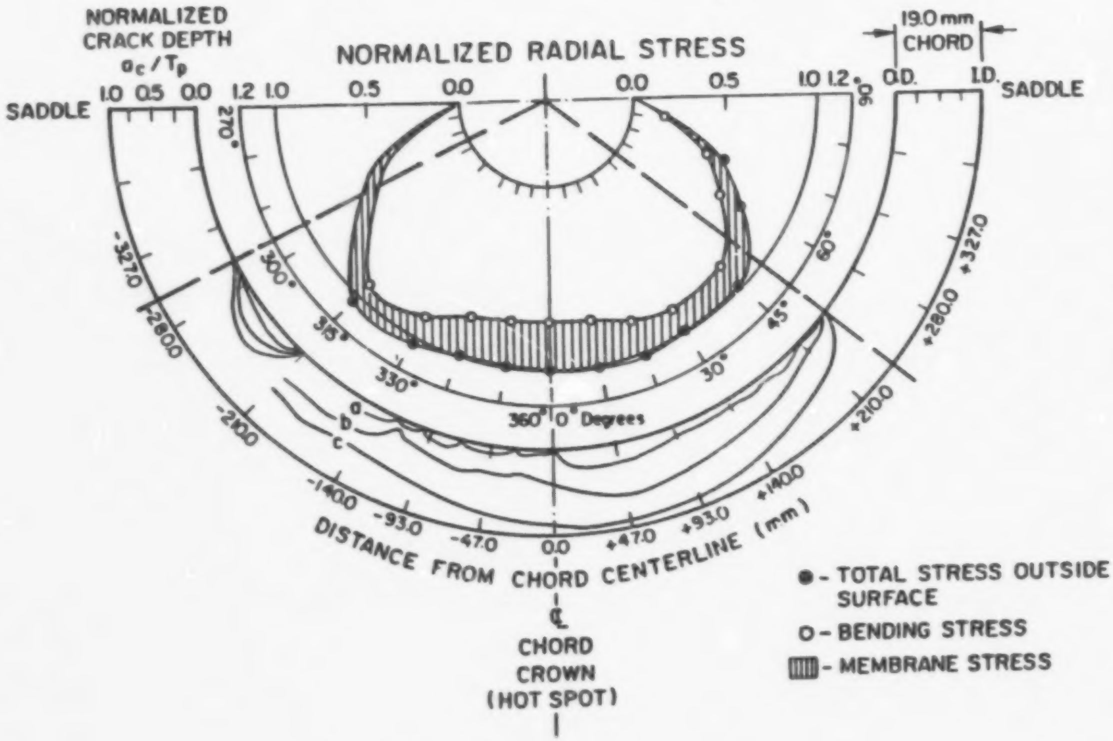

Figure 131: TB1 - Unstiffened Tubular T-Joint - IPB ($\Delta\sigma_{HS} = 248$ MPa). D.C. Potential Drop Crack Depth Measurements Correlated with the Normalized Radial Stress (Extrapolated to the Weld TOE) in the Chord.

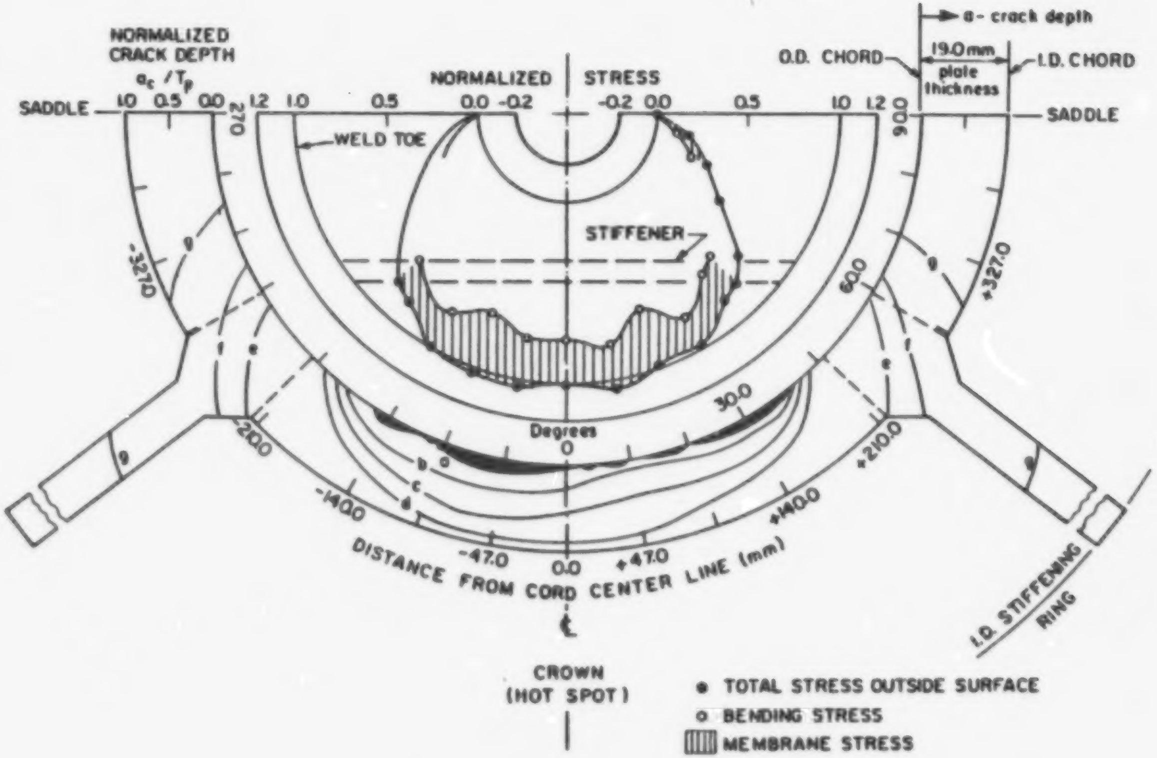
NORMALIZED CRACK DEPTH
a_c / T_p
SADDLE
1.0 0.5 0.0
270
1.2 1.0 0.5 0.0 -0.2
NORMALIZED STRESS
-0.2 0.0 0.5 1.0 1.2
90.0
SADDLE
O.D. CHORD
I.D. CHORD
19.0 mm plate thickness
a - crack depth
WELD TOE
STIFFENER
-327.0
+327.0
60.0
30.0
Degrees
0
-210.0
+210.0
-140.0
+140.0
-47.0
0.0
+47.0
DISTANCE FROM CORD CENTER LINE (mm)
a
b
c
d
e
f
g
I.D. STIFFENING RING
CROWN (HOT SPOT)
● TOTAL STRESS OUTSIDE SURFACE
○ BENDING STRESS
▥ MEMBRANE STRESS

Figure 132: TB2 - Stiffened Tubular T-Joint - IPB ($\Delta\sigma_{HS} = 246$ MPa). D.C. Potential Drop Crack Depth Measurements Correlated with the Normalized Radial Stress (Extrapolated to the Weld TOE) in the Chord.

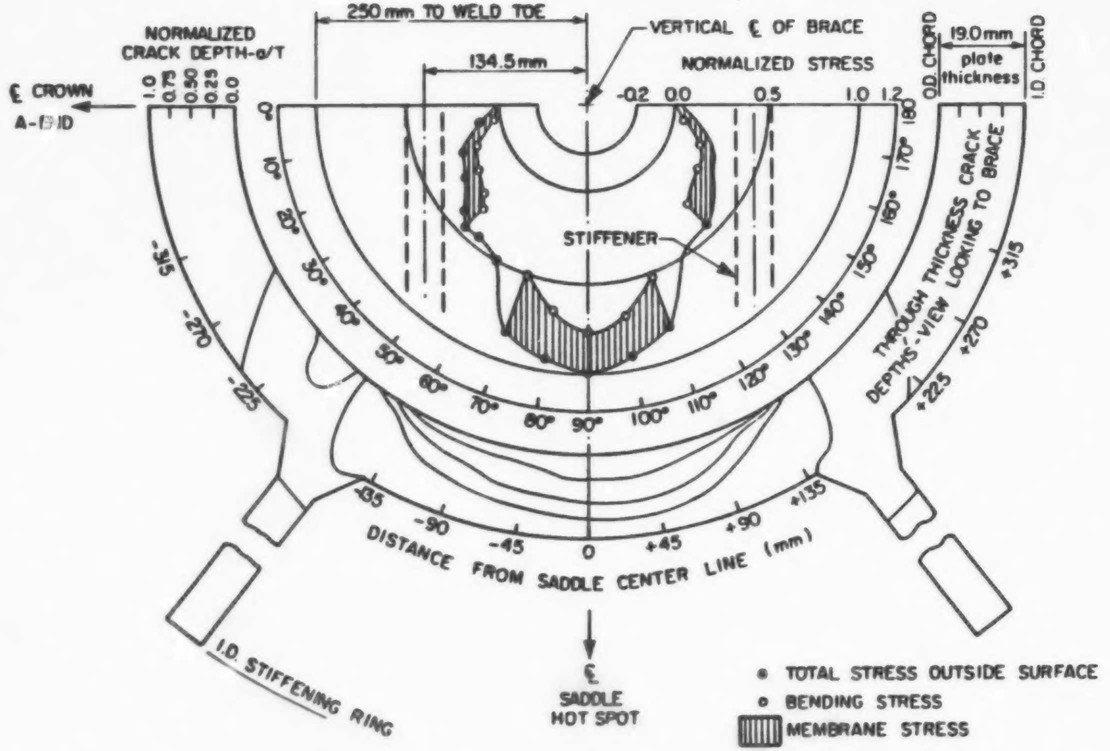
250 mm TO WELD TOE
134.5 mm
VERTICAL ℄ OF BRACE
NORMALIZED STRESS
-0.2 0.0 0.5 1.0 1.2
NORMALIZED CRACK DEPTH-a/T
1.0 0.75 0.50 0.25 0.0
℄ CROWN
A-END
O.D. CHORD
19.0 mm
plate thickness
I.D. CHORD
0° 10° 20° 30° 40° 50° 60° 70° 80° 90° 100° 110° 120° 130° 140° 150° 160° 170° 180
STIFFENER
THROUGH THICKNESS CRACK DEPTHS - VIEW LOOKING TO BRACE
-315 -270 -225 +225 +270 +315
-135 -90 -45 0 +45 +90 +135
DISTANCE FROM SADDLE CENTER LINE (mm)
℄ SADDLE HOT SPOT
I.D. STIFFENING RING
● TOTAL STRESS OUTSIDE SURFACE
○ BENDING STRESS
▥ MEMBRANE STRESS

Figure 133: TB4 - Stiffened Tubular T-Joint - IPB ($\Delta\sigma_{HS} = 256$ MPa). D.C. Potential Drop Crack Depth Measurements Corrolated with the Normalized Radial Stress (Extrapolated to the Weld TOE) in the Chord.

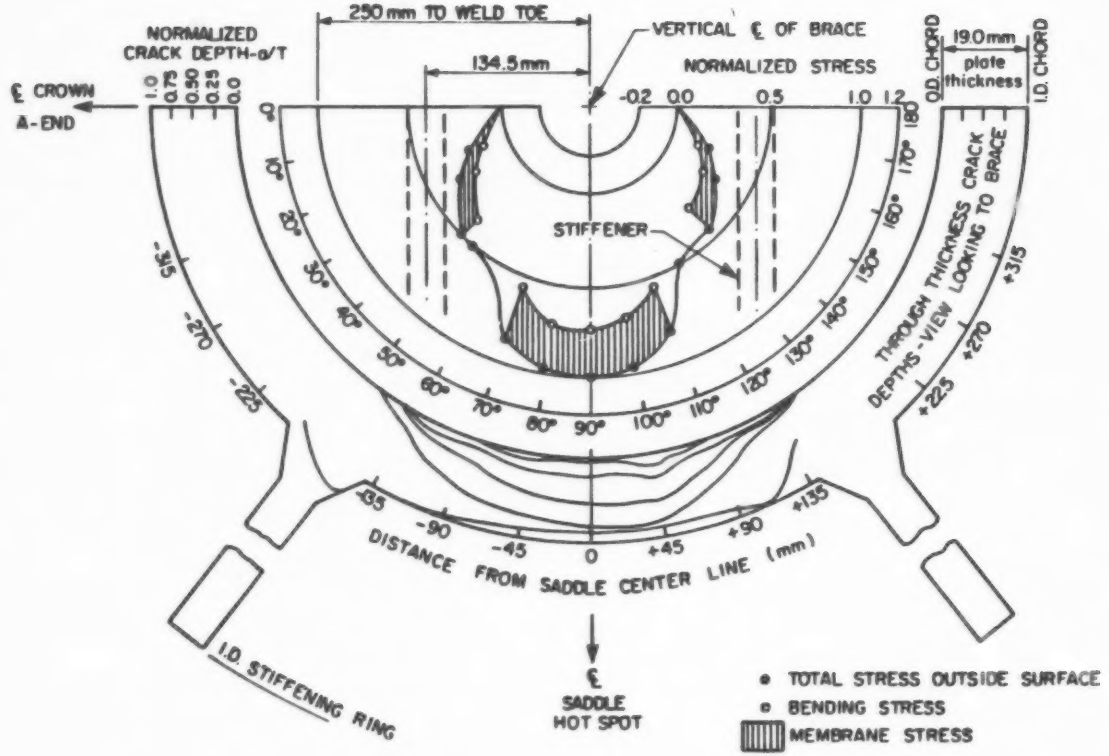
250 mm TO WELD TOE
134.5 mm
VERTICAL ℄ OF BRACE
NORMALIZED STRESS
-0.2 0.0 0.5 1.0 1.2
NORMALIZED CRACK DEPTH-a/T
1.0 0.75 0.50 0.25 0.0
℄ CROWN A-END
O.D. CHORD
19.0 mm
plate thickness
I.D. CHORD
0° 10° 20° 30° 40° 50° 60° 70° 80° 90° 100° 110° 120° 130° 140° 150° 160° 170° 180°
STIFFENER
THROUGH THICKNESS CRACK DEPTHS - VIEW LOOKING TO BRACE
-315 -270 -225 +225 +270 +315
-135 -90 -45 0 +45 +90 +135
DISTANCE FROM SADDLE CENTER LINE (mm)
I.D. STIFFENING RING
℄ SADDLE HOT SPOT
● TOTAL STRESS OUTSIDE SURFACE
○ BENDING STRESS
▥ MEMBRANE STRESS

Figure 134: TB5 - Stiffened Tubular T-Joint - IPB ($\Delta\sigma_{HS} = 157$ MPa). D.C. Potential Drop Crack Depth Measurements Correlated with the Normalized Radial Stress (Extrapolated to the Weld TOE) in the Chord.

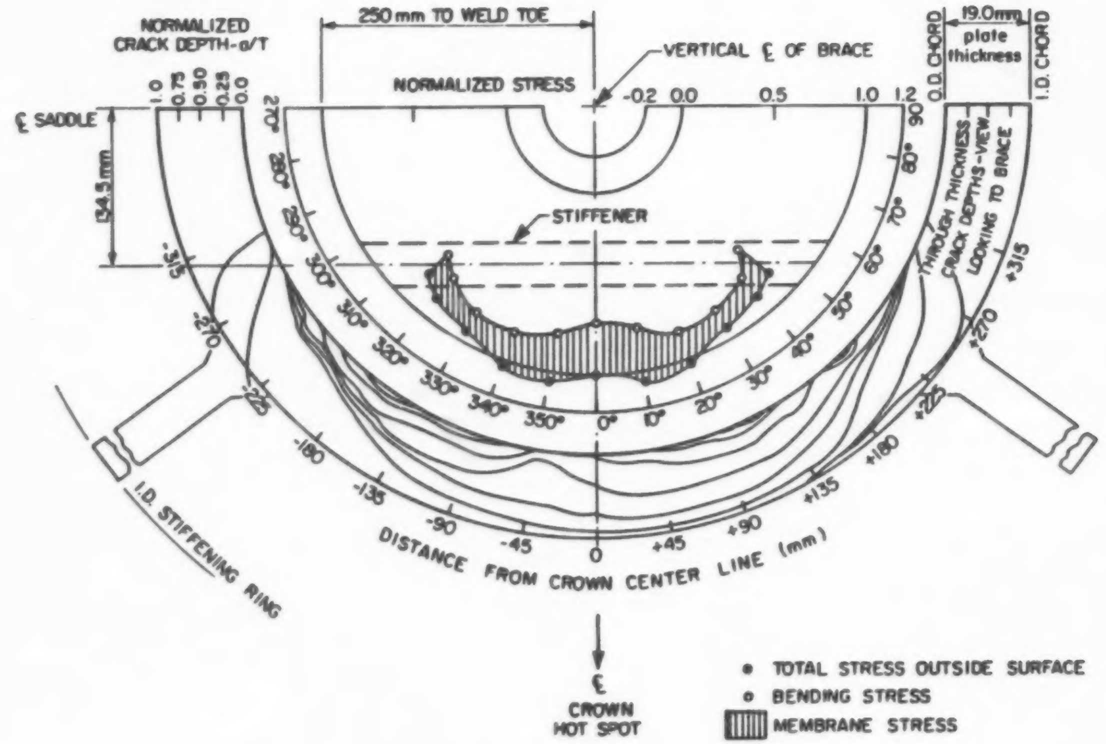
NORMALIZED CRACK DEPTH-a/T
1.0
0.75
0.50
0.25
0.0
250 mm TO WELD TOE
VERTICAL ℄ OF BRACE
NORMALIZED STRESS
-0.2 0.0
0.5
1.0 1.2
O.D. CHORD
19.0mm plate thickness
I.D. CHORD
℄ SADDLE
134.5mm
STIFFENER
THROUGH THICKNESS CRACK DEPTHS-VIEW LOOKING TO BRACE
270°
280°
290°
300°
310°
320°
330°
340°
350°
0°
10°
20°
30°
40°
50°
60°
70°
80°
90
-315
-270
-225
-180
-135
-90
-45
0
+45
+90
+135
+180
+225
+270
+315
DISTANCE FROM CROWN CENTER LINE (mm)
I.D. STIFFENING RING
℄ CROWN HOT SPOT
TOTAL STRESS OUTSIDE SURFACE
BENDING STRESS
MEMBRANE STRESS

Figure 135: TB6 - Stiffened Tubular T-Joint - IPB ($\Delta\sigma_{HS} = 163$ MPa). D.C. Potential Drop Crack Depth Measurements Correlated with the Normalized Radial Stress (Extrapolated to the Weld TOE) in the Chord.

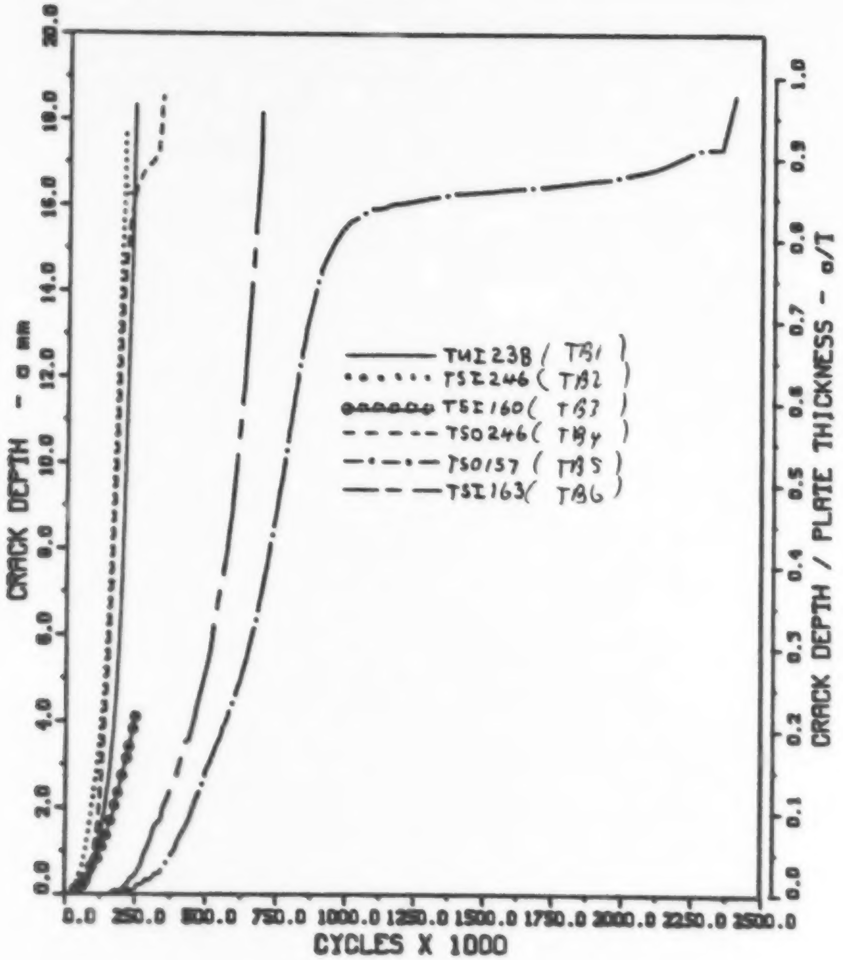

Figure 136: Total life. Specimens TB1, TB2, TB3, TB4, TB5 and TB6.

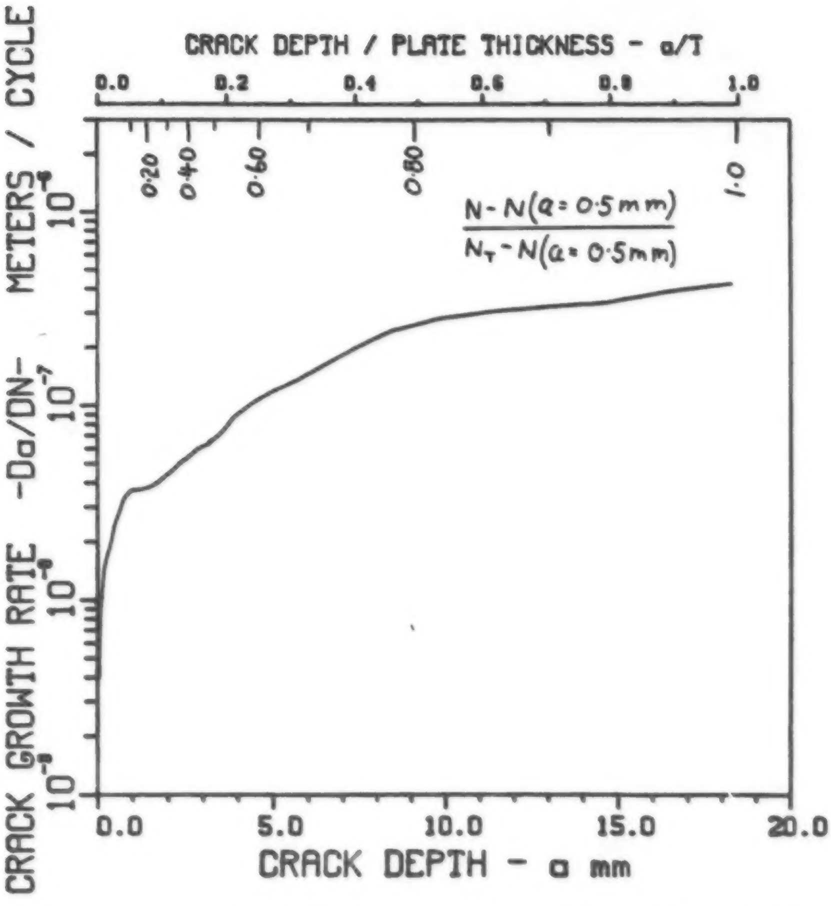

FIGURE 137 DCPD RESULTS *** CRACK GROWTH RATE VERSUS CRACK DEPTH
UNSTIFFENED TUBULAR T-JOINT *** IN-PLANE BENDING
R-RATIO -0.05 *** HOT-SPOT STRESS RANGE - 248 MPa (TB1)
DISTANCE FROM CROWN CENTERLINE - +25.4 mm

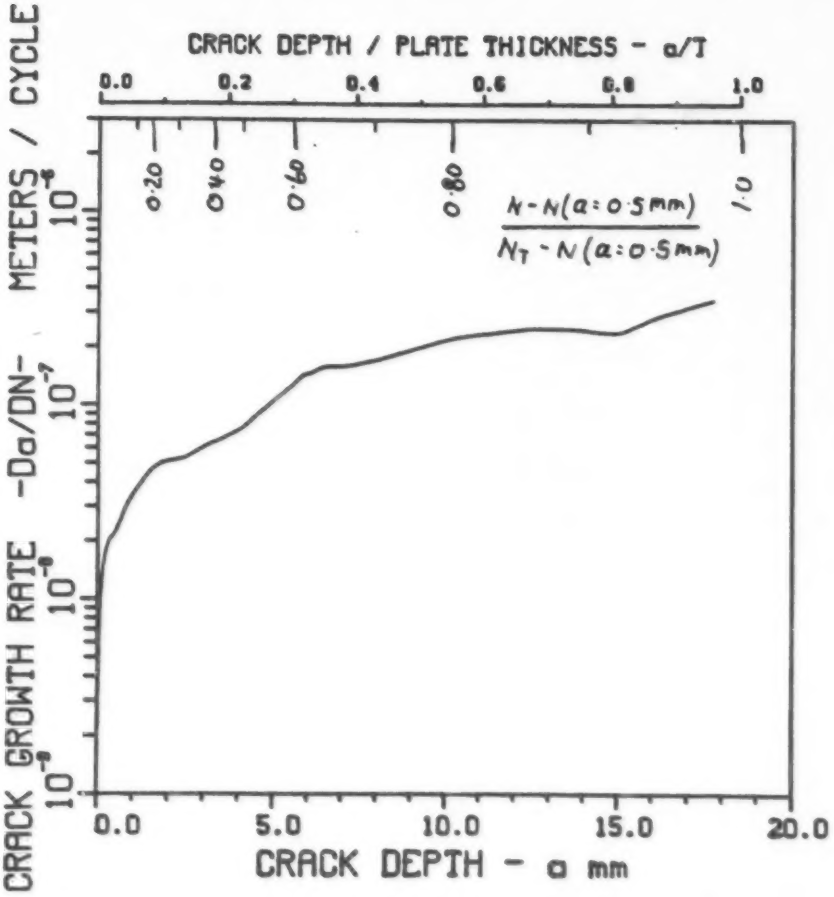

FIGURE 138 DCPD RESULTS **** CRACK GROWTH RATE VERSUS CRACK DEPTH
STIFFENED TUBULAR T-JOINT **** IN-PLANE BENDING (TB2)
R-RATIO -0.05 **** HOT-SPOT STRESS RANGE - 246 MPa
DISTANCE FROM CROWN CENTERLINE - -83.00 mm

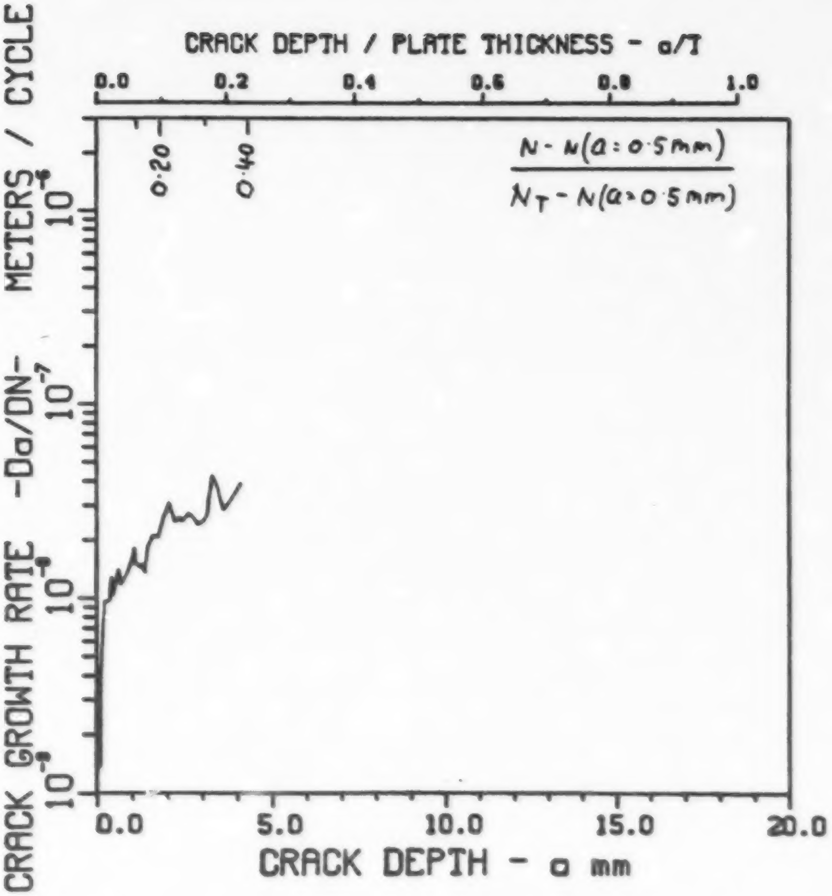

FIGURE 139 DCPD RESULTS *** CRACK GROWTH RATE VERSUS CRACK DEPTH
STIFFENED TUBULAR T-JOINT *** IN-PLANE BENDING (TB3)
R-RATIO -0.05 *** HOT-SPOT STRESS RANGE - 160.0 MPa
DISTANCE FROM CROWN CENTERLINE - +146.0 mm

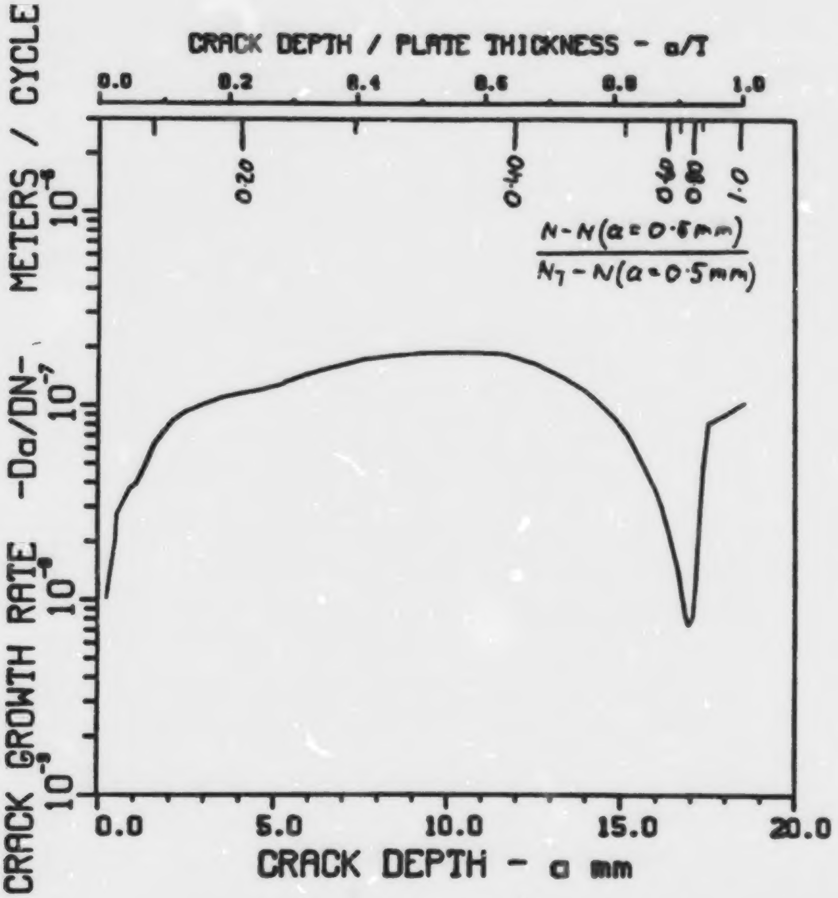

FIGURE 140 DCPD RESULTS *** CRACK GROWTH RATE VERSUS CRACK DEPTH
STIFFENED TUBULAR T-JOINT *** OUT-OF-PLANE BENDING (TB4)
R-RATIO -0.05 *** HOT-SPOT STRESS RANGE - 245.6 MPa
DISTANCE FROM CROWN CENTERLINE - +00.00 mm

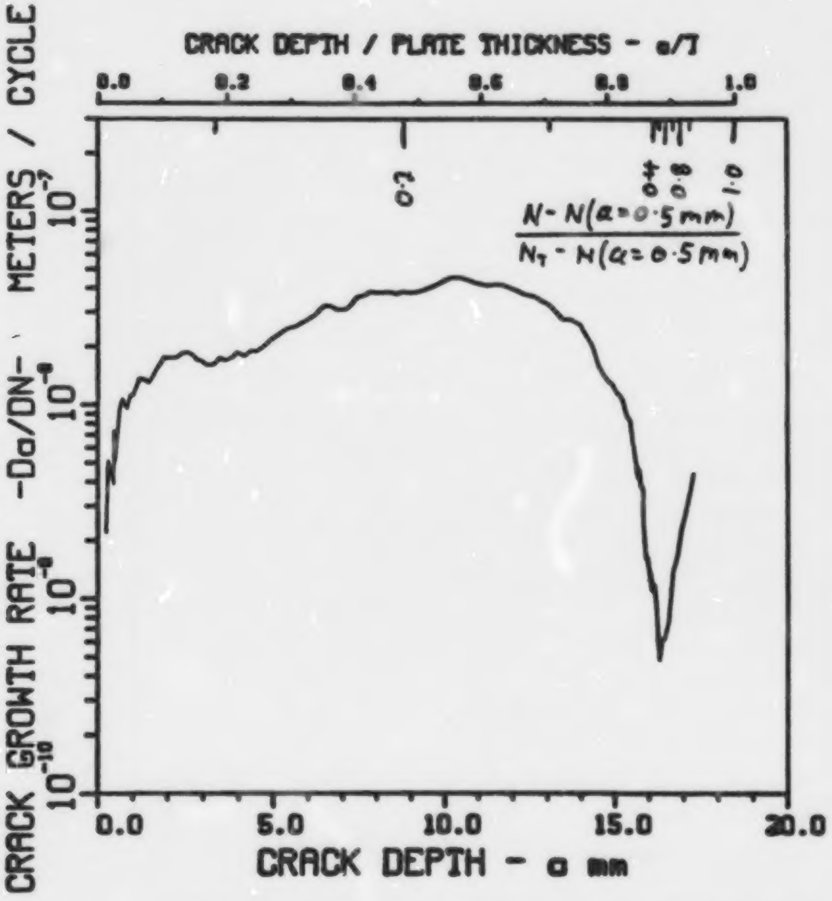

FIGURE 141 DCPD RESULTS ---- CRACK GROWTH RATE VERSUS CRACK DEPTH
STIFFENED TUBULAR T-JOINT ---- OUT-OF-PLANE BENDING (TB5)
R-RATIO -0.05 ---- HOT-SPOT STRESS RANGE - 157 MPa
DISTANCE FROM CROWN CENTERLINE - +44.45 mm

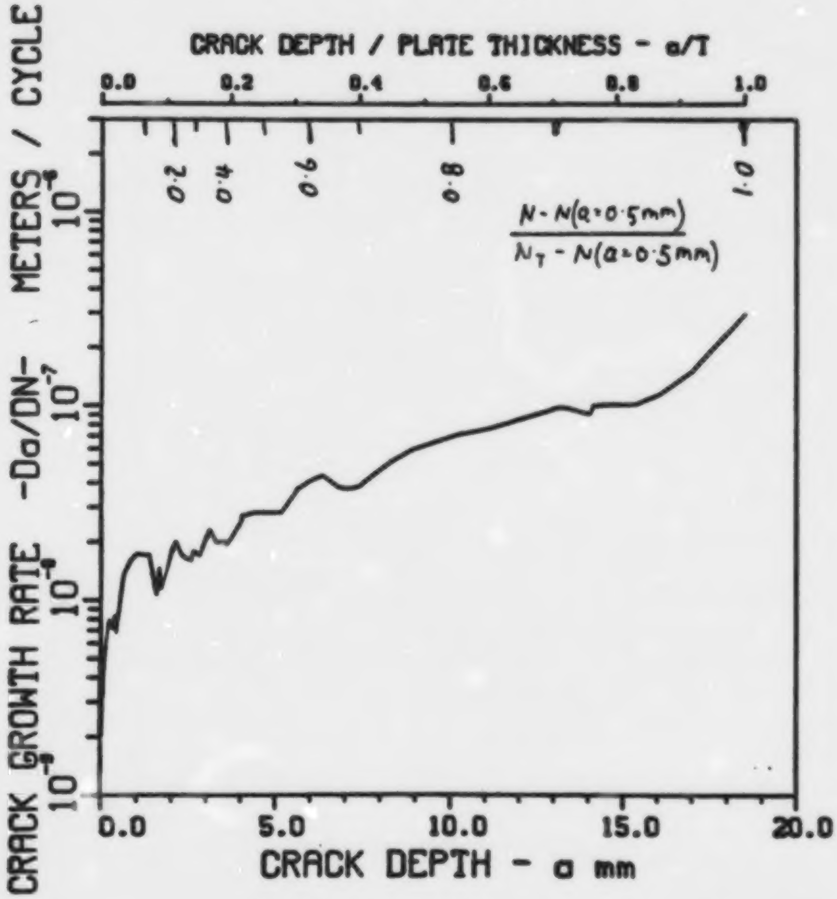

FIGURE 143 DCPD RESULTS *** CRACK GROWTH RATE VERSUS CRACK DEPTH
STIFFENED TUBULAR T-JOINT *** IN-PLANE BENDING (TB6)
R-RATIO -0.05 *** HOT-SPOT STRESS RANGE - 163.0 MPa
DISTANCE FROM CROWN CENTERLINE - +108.0 mm

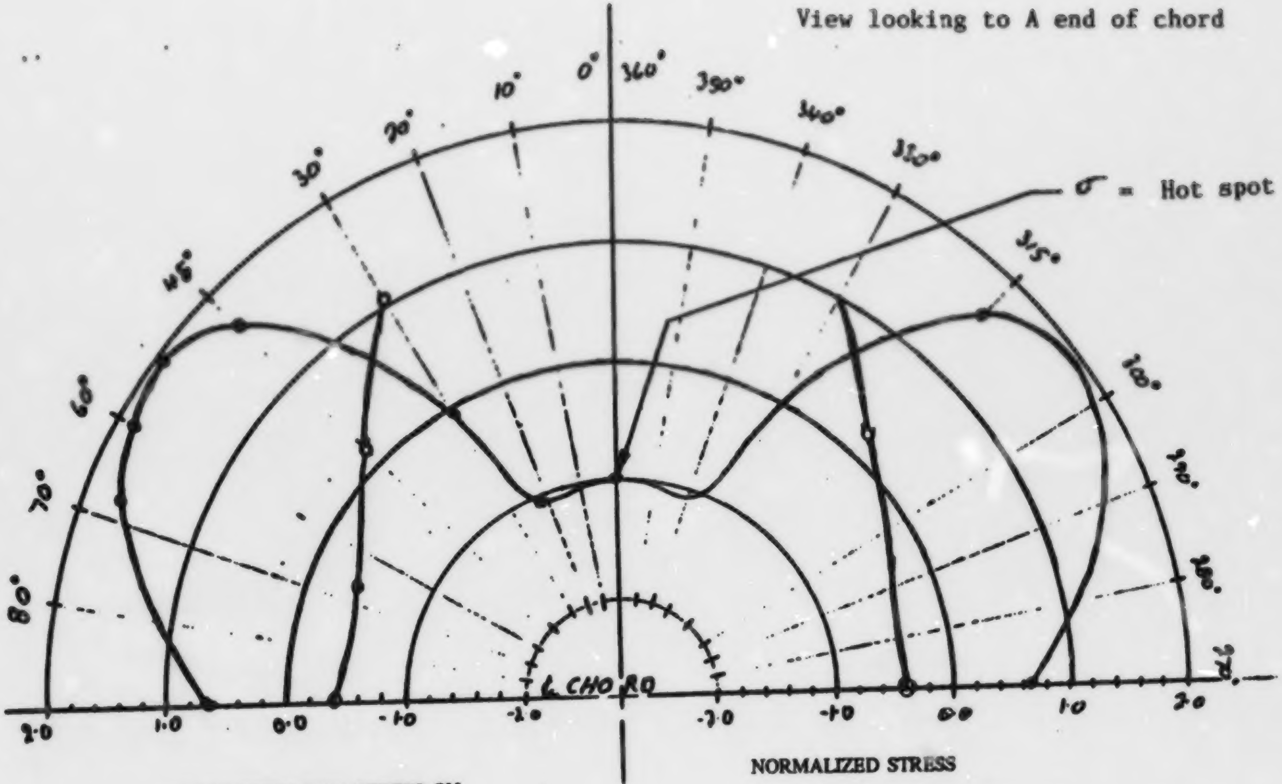

● CIRCUMFERENTIAL STRESS ON INSIDE DIAMETER OF THE STIFFENING RING

○ CIRCUMFERENTIAL STRESS ON OUTSIDE DIAMETER OF CHORD CENTERED OVER THE STIFFENING RING

STIFFENING RING STRESSES
MODE OF LOADING: IN PLANE BENDING
JOINT DESIGN CATEGORY: DOUBLE RING STIFFENING T-JOINT (TB2)

Figure 143 STRAIN GAUGE RESULTS

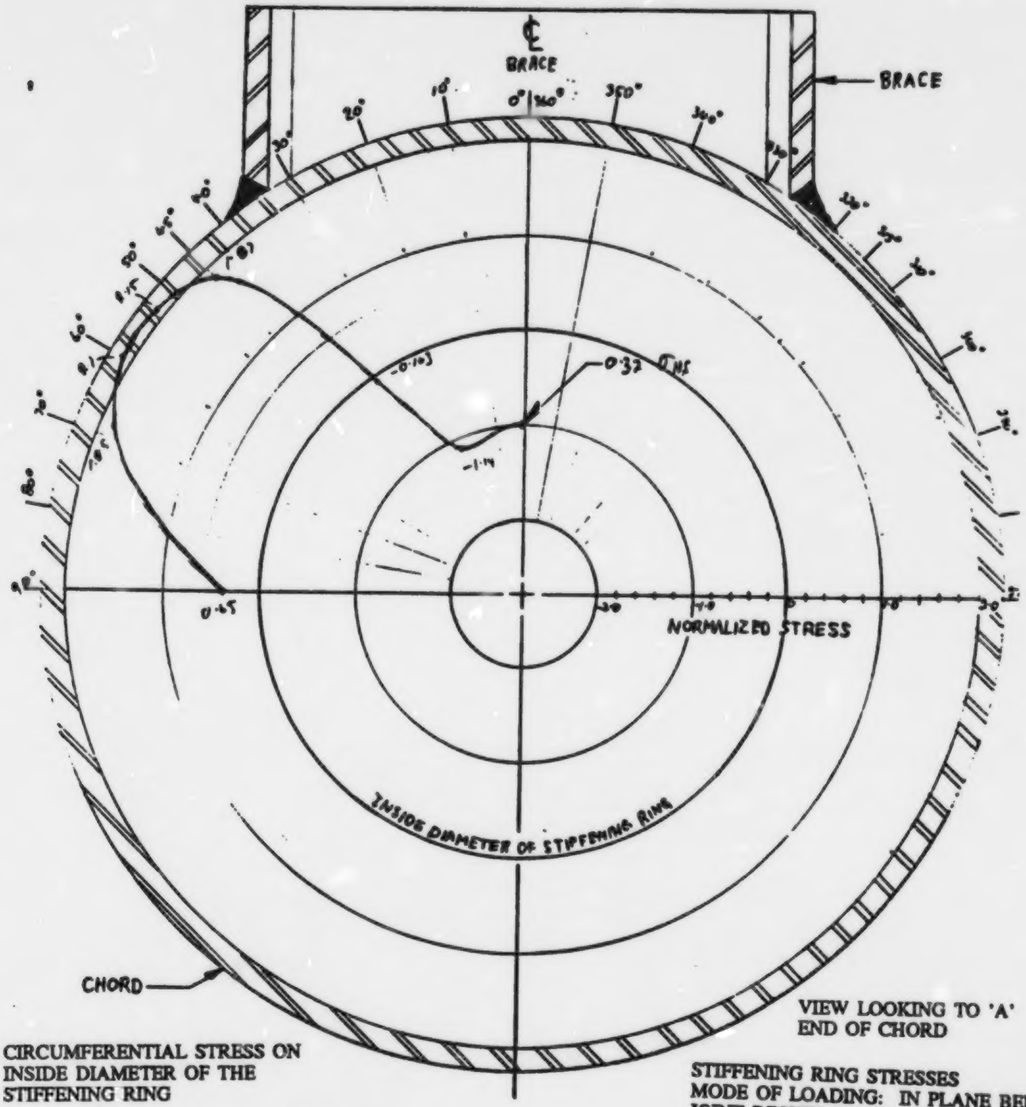

VIEW LOOKING TO 'A'
END OF CHORD

- CIRCUMFERENTIAL STRESS ON INSIDE DIAMETER OF THE STIFFENING RING

STIFFENING RING STRESSES
MODE OF LOADING: IN PLANE BENDING
JOINT DESIGN CATEGORY: DOUBLE RING STIFFENING T-JOINT (TB3)

° CIRCUMFERENTIAL STRESS ON OUTSIDE DIAMETER OF CHORD CENTERED OVER THE STIFFENING RING

Figure 144 STRAIN GAUGE RESULTS

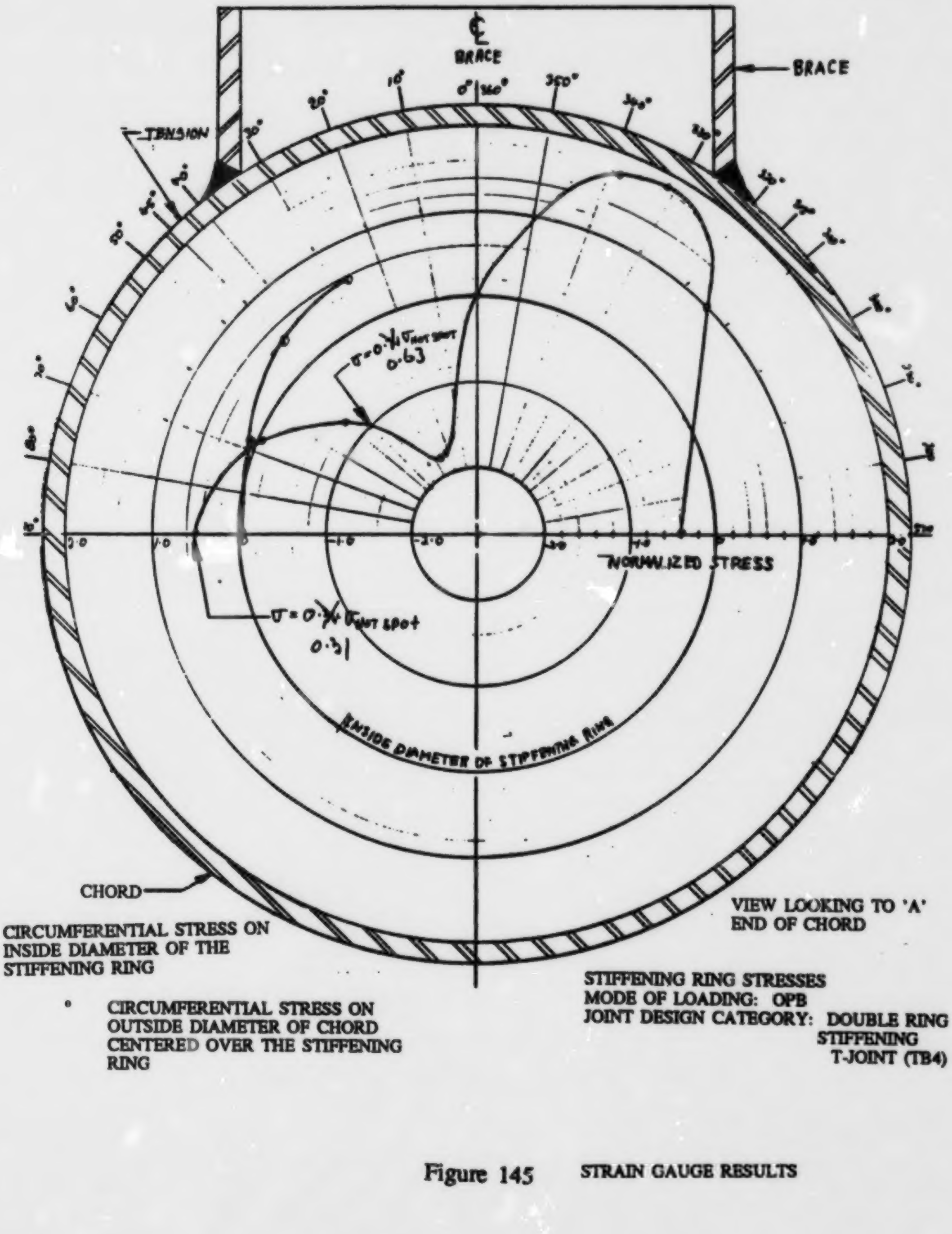

- CIRCUMFERENTIAL STRESS ON INSIDE DIAMETER OF THE STIFFENING RING

° CIRCUMFERENTIAL STRESS ON OUTSIDE DIAMETER OF CHORD CENTERED OVER THE STIFFENING RING

VIEW LOOKING TO 'A' END OF CHORD

STIFFENING RING STRESSES
MODE OF LOADING: OPB
JOINT DESIGN CATEGORY: DOUBLE RING STIFFENING T-JOINT (TB4)

Figure 145 STRAIN GAUGE RESULTS

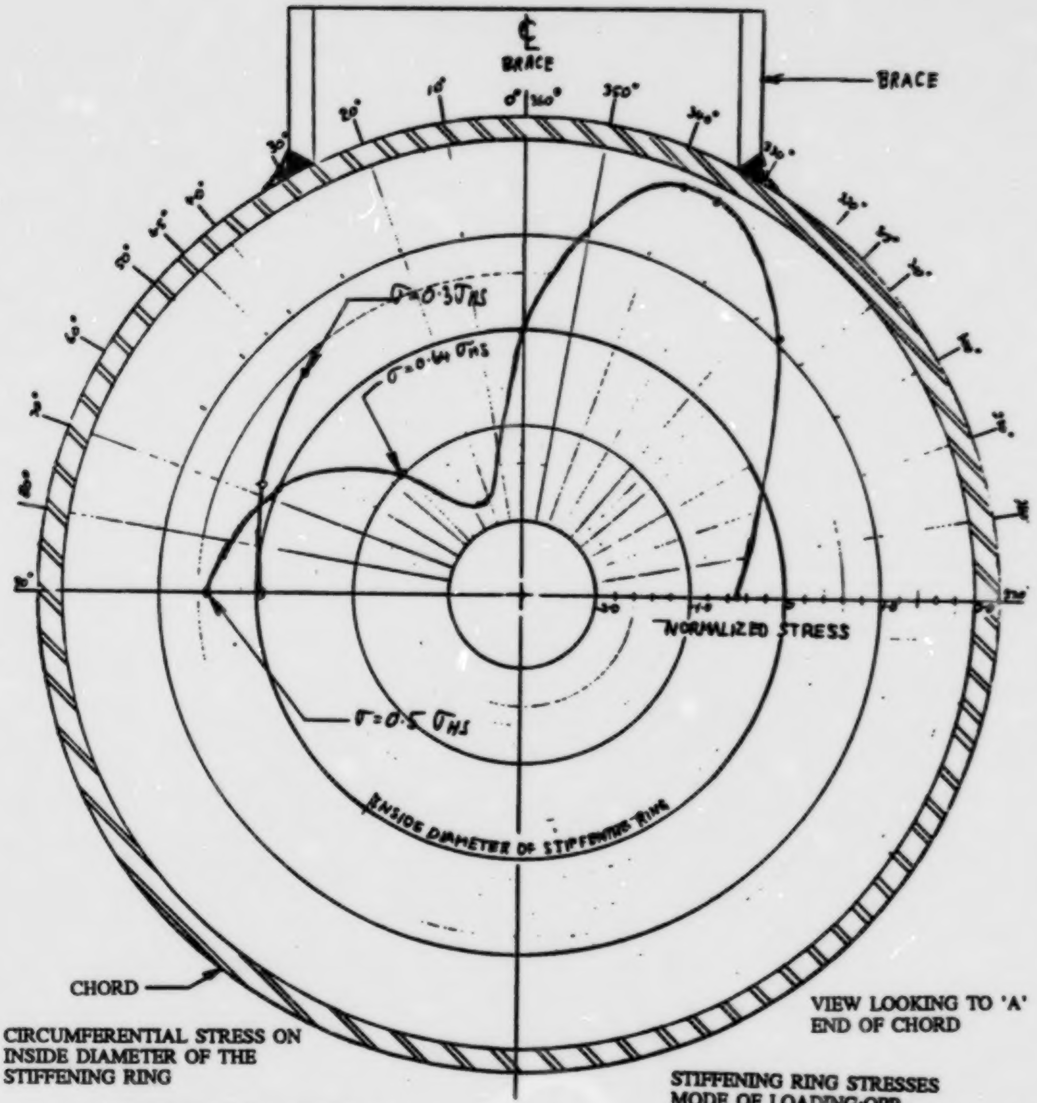

• CIRCUMFERENTIAL STRESS ON INSIDE DIAMETER OF THE STIFFENING RING

° CIRCUMFERENTIAL STRESS ON OUTSIDE DIAMETER OF CHORD CENTERED OVER THE STIFFENING RING

VIEW LOOKING TO 'A' END OF CHORD

STIFFENING RING STRESSES
MODE OF LOADING:OPB
JOINT DESIGN CATEGORY: DOUBLE RING STIFFENING T-JOINT (TB5)

Figure 146 STRAIN GAUGE RESULTS

APPENDIX 1

DEFINITIONS OF THE SPOT STRESSES AND STRESS CONCENTRATION FACTORS

Appendix 1 – Definitions of the Spot Stresses and Stress Concentration Factors

Nominal Stress and Strain Range

Nominal stress range is defined as the ratio of the load range on the brace to the standardized area of the cross section of the brace.

$$\Delta\sigma_{nom} = \Delta F/A \qquad [1-1]$$

where

ΔF = load range on the brace
A = standardized cross-section of the brace

The nominal strain is derived from the above mentioned

$$\begin{aligned}&\Delta\sigma_{nom}\\ \Delta\epsilon_{nom} &= \Delta\sigma_{nom}/E\end{aligned}$$

where,

E = Young's modulus of elasticity = 210,000 N/mm^2

Hot Spot Strain Range

The actual maximum strain at the weld toe, ie, at the hot spot of the tubular joint is affected by (a) the geometry of the joint (t, T, D, d, L, l), the ratio of the diameters of the brace and the chord, and the ratio of wall thickness of the brace and the chord (geometrical effects); and (b) the local geometry, weld profile, radius of the weld toe and defects of the weld toe (local effects).

Only the geometrical effects are reproducible because the local effects depend on the weld profile which varies for each joint. For this reason only the geometrical effects are considered in the analysis of test results and also in the design of tubular joints.

Some distance away from the weld toe, the local effects are negligible and the stress gradient is often linear. This linear region was chosen to obtain the hot spot stress or strain ranges. The geometrical hot spot stress/strain range is now defined as the linearly extrapolated strain range to the weld toe through the measuring points A_n and

B_n located at specified distances from the weld toe as shown in Figure A1. The location of strain gauges correspond to the distances computed above.

Hot Spot Stress Range

For example, the hot spot location for axial and out of plane bending is situated on line 4 (Figure A1). Radial strain range (strain range perpendicular to the weld toe) $\Delta\epsilon_1$ and Tangential strain range (strain range parallel to the weld toe) $\Delta\epsilon_2$ are extrapolated to the weld toe separately, according to the method agreed upon by the Working Group III of ECSC (also shown in Figure 21). The hot spot stress range can be obtained from the extrapolated radial hot spot strain range $\Delta\epsilon_{1HS}$ and tangential hot spot strain range $\Delta\epsilon_{2HS}$ using the following formula,

$$\Delta\sigma_{1HS} = \frac{E}{(1-\nu^2)}(\Delta\epsilon_{1HS} + \nu\Delta\epsilon_{2HS}) \qquad [1-2]$$

where,

E = Young's modulus of elasticity, ν = poisson ratio

Stress and Strain Concentration Factors

The maximum stress concentration factor is defined as the ratio of the maximum hot spot stress range in the specimen to the nominal stress range in the brace.

$$SCF = \frac{\Delta\sigma_{1HS}}{\Delta\sigma_{nom}} \qquad [1-3]$$

The maximum strain concentration factor (SNCF) is defined as the ratio of the hot spot strain range in the specimen to the nominal strain range in the brace, viz.,

$$SNCF = \frac{\Delta\epsilon_{1HS}}{\Delta\epsilon_{nom}} \qquad [1-4]$$

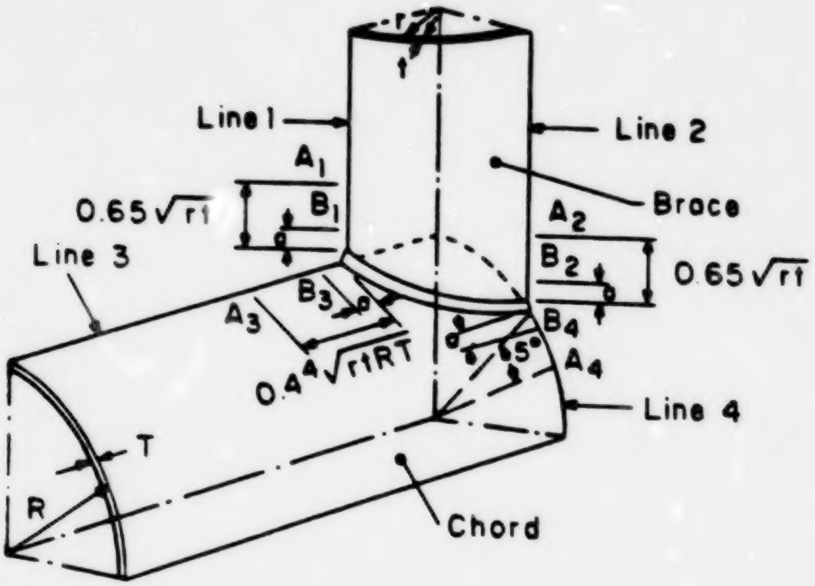
r
t
Line 1
Line 2
A$_1$
B$_1$
$0.65\sqrt{rt}$
a
Brace
A$_2$
B$_2$
$0.65\sqrt{rt}$
a
Line 3
B$_3$
a
A$_3$
$0.4\sqrt[4]{rtRT}$
B$_4$
a
5°
A$_4$
Line 4
T
R
Chord

Fig 1-A Definition of regions of stress linearity for welded tubular T and X joints. $a = 0.2\sqrt{rt}$ but not smaller than 4mm

[Ref. P.F. Pozzolini, "Tests on Tubular Joints", Plenary Sessions, Steel in Marine Structures, Paris, France, Oct. 1981].

$R = 457$ mm, $r = 228.5$ mm, $T = t = 19.0$ mm

$a = 13.20$ mm

$0.4\sqrt{rtRt} = 31.34$ mm

Distance for 5° (on the chord surface) = 39.88 mm

APPENDIX 2

FABRICATION OF TUBULARS FOR FATIGUE TESTING IN AIR AND SEAWATER

APPENDIX 2

Fabrication of Tubulars for Fatigue Testing in Air and Seawater

The fabrication of the tubulars was reported in detail with all historical information compiled in AMCA International Report No. 2-185-066/A. This report was submitted to the Federal Government in November 1986.

This appendix describes briefly some of the more important aspects of this fabrication and produces as reference some of the key fabrication documents.

The tubulars were manufactured to the drawing given in Section 2-BB of this appendix by Dominion Bridge, Toronto, Ontario. Non Destructive Evaluation was performed by CB-Non Destructive Testing Ltd. of Oakville, Ontario with Project Management being performed by AMCA International. The specimen chords and stiffeners were fabricated in steel conforming to CSA G40.21 Grade 350WT in 19mm thickness, a typical breakdown of chemical analysis and properties being given in Table A.

The method of fabrication was essentially the same as that performed in the UKORSP program, however there were two important differences with respect to the stiffeners themselves and these are detailed as follows:

1. In order to prevent fatigue initiation and propagation from the internal edges of the stiffener, these were machined and the sharp edges broken by grinding. In the UKORSP work, the internal edges were flame cut.

2. The weld attaching the stiffeners to the chord was a full penetration weld with reinforcing fillets and the undercut at the toe of the fillet was restricted to 0.5mm maximum. In the UKORSP work, the stiffeners were attached by simple fillets with no additional toe requirements.

The above precautions prevented any fatigue initiation at the stiffeners throughout the experimental program.

The weld in question, chord to brace, was fabricated using E48018 type electrodes of both 3.2 and 4.0mm diameter using stringer beads with the toe of the weld being subject to the dime test as illustrated in Figure 2-A.

All other details of fabrications are given in the referenced fabrication documents as listed herein.

Table 2-A - Chemical Composition and Mechanical Properties

Chemical Composition	Plate Thickness 19mm
C	0.15
Mn	1.36
Si	0.29
S	0.004
P	0.010
Ni	0.26
V	0.08
Mechanical Properties	
Yield Strength (MPa)	370
UTS (MPa)	521
Elongation (%)	29
CVN (joules)(L) -45°	107
(T) -45°	55

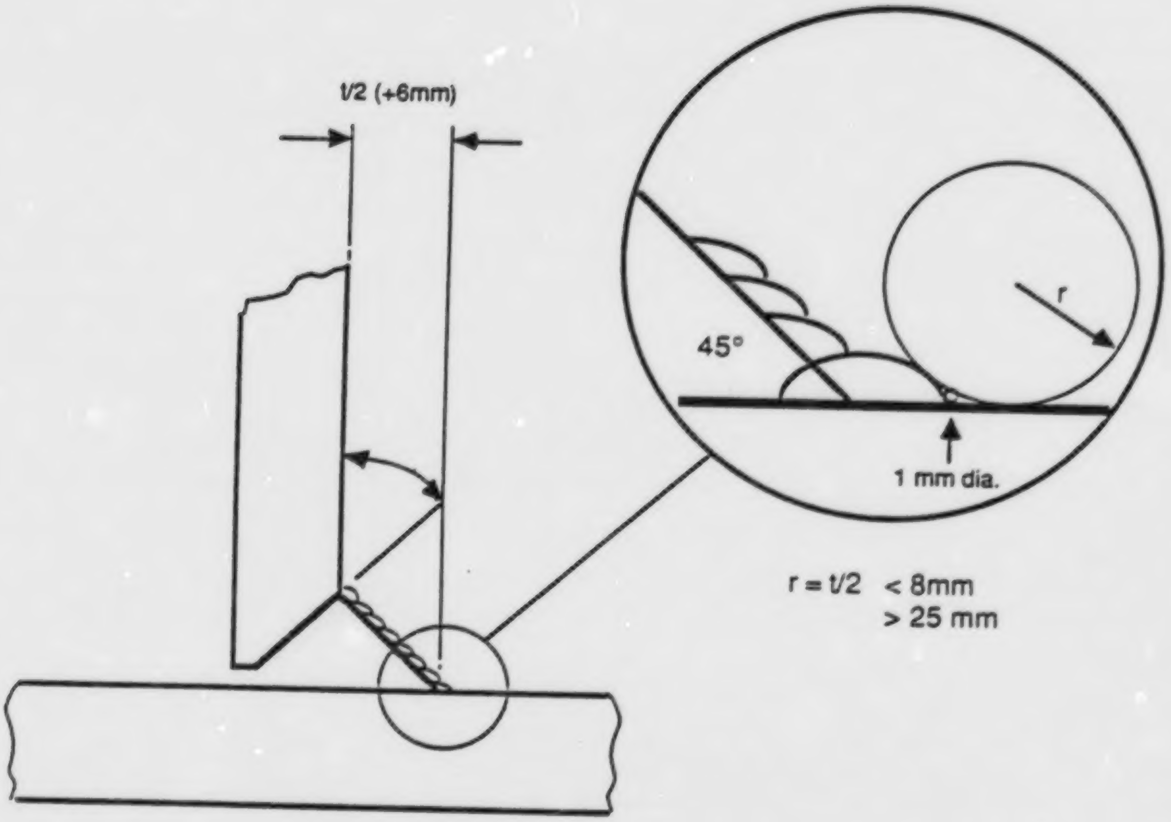
t/2 (+6mm)
45°
r
1 mm dia.
r = t/2 < 8mm
> 25 mm

Dime Test

Figure 2-A

ITEM	TITLE
2-AA	Technical Specification BN2
2-BB	Drawing F638, Issue 1, Rev. 9
2-CC	Approved Welding Data Sheets
2-DD	Manufacturing Procedure, Inspection and Test Plan - Revision 2

ITEM 2-AA

TECHNICAL SPECIFICATION - BN2 - REVISION 2

AMCA INTERNATIONAL LIMITED
RESEARCH AND TECHNOLOGY CENTRE
KANATA, ONTARIO

CANMET TUBULARS - TECHNICAL APPENDIX BN2 - REVISION 2

Drawing Number 2-185-066-099 - Number 1 - Revision 2

T1.0 Scope

T1.1 The 'Fabricator' who must must be certified to the requirements of CSA W47.1 Division 1, shall be responsible for carrying out all the necessary manufacture, testing and transportation described in this Technical Appendix. 1

T2.0 Tolerances

T2.1 The Fabricator shall fabricate, assemble and machine within the tolerances stated on the relevant drawings.

T3.0 Manufacturing and Testing Standards

Manufacturing and testing shall be carried out generally in accordance with the relevant clauses of the following Canadian Standards. In the event of conflict, then the more demanding standard shall apply. In all cases, the issue current at the date of contract shall apply.

T3.1 Canadian Standard	Title
CSA W48.1 - M1980	Mild Steel Covered Arc Welding Electrodes.

CSA W48.5 - M1983	Mild Steel Electrodes for Flux Cored Arc Welding.
CSA W48.6-M1980	Bare Mild Steel Electrodes and Fluxes for Submerged Arc Welding.
CSA W59 - 1982	Welded Steel Construction.
CSA G40.21 - 1981	Weldable Structural Steels.
CSA 47.1 - 1983	Certification of Companies for Fusion Welding of Steel Structures.

T4.0 Manufacture

T4.1 Steel for the chords and stiffeners, which is to CSA G40.21 Grade 350 WT, will be supplied free issue. △1

T4.2 The Fabricator shall carry out all the necessary manufacturing operations to the satisfaction of the 'Project Coordinator'*, in accordance with the related drawings and this specification.

T4.3 Prior to commencement of manufacture, the Fabricator shall submit to the 'Project Coordinator' for approval two copies of the 'Quality Plan'. The Quality Plan shall be to the satisfaction of the 'Project Coordinator'.

* The selected Research Contractor will appoint a 'Project Coordinator' responsible for all administration and coordination of the Research Project.

T4.4 Prior to commencement of manufacture the Fabricator shall satisfy himself that the material provided 'free issue' is received at his works in such a condition that is satisfactory for him to carry out the work required. In the event of any doubt about the condition of any of this material, then the Fabricator shall consult with the 'Project Coordinator'.

T4.5 The Fabricator shall preserve the identity of all materials used throughout the course of manufacture to the satisfaction of the 'Project Coordinator'. Material identification should be maintained by paint stencil or by any other acceptable means other than hard stamping.

T4.6 Welding

T4.6.1 Prior to commencement of manufacture, the Fabricator shall submit to the 'Project Coordinator' for approval two copies of the weld procedures the Contractor proposes to use in the manufacture of these specimens. All weld procedures shall be to the satisfaction of the 'Project Coordinator'.

T4.6.2 All welds between braces and chords shall be in accordance with those on the relevant drawing being of the single sided full penetration type.

T4.6.3 Welding shall be performed using approved welding processes to the satisfaction of the 'Project Coordinator' or his Inspector'. The brace to chord weld must be performed by the shielded metal arc process. △1

T4.6.4 The welding procedures, which shall be approved by the 'Project Coordinator' prior to commencement of manufacture, shall be strictly maintained and no variation shall be permitted without written approval.

T4.6.5 Attention shall be paid to the adequacy of the facilities and the welding processes at the Fabricator's works to ensure that the work is protected from accidental sudden temperature changes and adverse weather conditions.

T4.6.6 The welding of temporary attachments to the components shall be avoided as far as possible, but when used the weld shall be remote from principal joints and shall be made in accordance with this specification. Such welds shall be evenly made with the minimum of penetration into the parent metal to avoid excessive dilution and the possibility of cracking. The Fabricator shall carry out such repairs and testing as may be required by the 'Project Coordinators' Inspector, after removal of temporary attachments.

T4.6.7 Where temporary attachments are to be removed, they shall be removed by grinding, care being taken not to "undercut" the parent metal.

T4.6.8 The position and detail of all temporary attachments shall be agreed with the 'Project Coordinator' prior to commencement of manufacture.

T4.6.9 Prior to commencement of manufacture, the Fabricator shall demonstrate, to the satisfaction of the 'Project Coordinator' or his Inspector, using suitable test plates, the capability of the welding operators to consistently achieve a one sided full penetration joint similar to the chord to brace joint. Only approved welders shall be employed on this contract. Any welder who consistently fails to satisfy the 'Project Coordinators' Inspector during the course of manufacture shall not be employed on this Contract. △1

T4.6.10 The 'Project Coordinator' or his Inspector shall have the right to call for such welder qualification and weld procedure tests as he may require. △1

T4.7 Welding Consumables

T4.7.1 All the welding consumables shall be provided by the Fabricator. Test certification and analyses of the consumables shall be provided in duplicate by the Fabricator. All test certification shall be to the satisfaction of the 'Project Coordinator'. △1

T4.7.2 All welding consumables shall be in accordance with the CSA W48 series. Shielded metal arc consumables shall be in accordance with CSA W48.1 and shall be supplied in sealed, moisture proof containers and stored in a dry location where a temperature of 20°C to 30°C is maintained. Once the containers have been opened, they shall be stored in a heated cabinet at a temperature of not less than 120°C. In all events, the maximum period of electrode exposure to atmospheric conditions permitted by the manufacturer of the electrodes as consistent with maintaining the low hydrogen characteristics must not be exceeded. All electrodes shall be inspected and any deemed unsuitable shall not be used. Identification of electrodes must be maintained at all times, those that cannot be identified shall not be used.

T4.8 Preheating

T4.8.1 Preheat requirements will be as per CSA W59-1982.

T4.8.2 Where necessary, the welding procedures shall specify the method of preheat to be used. All proven standard methods of preheating are acceptable provided that care is taken by the Fabricator so as to ensure that all areas to be joined are at the same temperature.

T5.0 Surface Finishes

T5.1 Surface finishes of components shall be as follows, except where specified otherwise on the drawings:

(a) Machined surfaces - not coarser than 125 micro inches.
(b) Plate - as rolled.
(c) Tube - as drawn.

T5.2 The surface of welds (apart from those joining the brace of the chord) shall be of regular contour, dressed smooth or ground flush only where necessary for weld testing techniques and/or to meet dimensional tolerances. All burrs and sharp edges shall be removed.

T5.3 The brace to chord weld profiles shall be in accordance with the relevant drawings. No grinding shall be carried out on the brace to chord weld.

T6.0 Inspection and Testing

T6.1 Inspection will be carried out at the Fabricators' works.

T6.2 The 'Project Coordinator' and his Inspector shall be allowed free access to the Fabricators' works at any reasonable time to witness or review any process used in the manufacture of these test specimens.

T6.3 All welds shall be inspected by the Fabricator; those found to contain unacceptable defects shall either be repaired or replaced to the satisfaction of the Inspector at Contractor's expense. (See Clause T6.13). △2

T6.4 Non-destructive examinations shall be carried out by the Fabricator in accordance with written procedures approved by the 'Project Coordinator' using all Non Destructive Evaluation (NDE) methods or combination of methods, coincidental with acceptable fabrication techniques, within the guide lines and acceptance levels laid down in this specification. Particular attention shall be given to each joint configuration when proposing examination procedures, utilizing the proper combination of NDE to give the optimum confidence level.

T6.5 All welds shall be inspected by the magnetic particle and ultrasonic or radiographic methods as specified in this specification.

T6.6 Magnetic particle inspection shall be carried out in such a manner as to prevent arcing on the material surface. In the event of damage due to arcing then the Fabricator shall carry out such repairs as the 'Project Coordinators' Inspector may require.

T6.7 Non-destructive Testing shall be carried out by the Fabricator to the satisfaction of the Inspector in accordance with CSA W59 and acceptance standards for all welds other than the brace to chord weld, and the stiffener to chord weld shall be to CSA W59 Section 11. Additional surface requirements for brace to chord and stiffener to chord welds are given in T6.8, 6.9 and 6.10.

T6.8 Undercut at the Stiffener to Chord weld is restricted to 0.5mm.

T6.9 For the brace to chord weld, the weld profile shall conform to the profile as shown on the relevant drawings. Particular attention should be paid to the weld toe angle for the chord to brace weld, such that the last capping run of weld in the toe region conforms to the "dime test", i.e., when a disc of the appropriate diameter is placed, perpendicular to the parent plate, on the last weld run and the parent plate then a 1mm dia. wire shall not pass through the gap in the region of the weld toe and undercut shall be restricted to 0.25mm. △1 The acceptance standard for magnetic particle and Ultrasonic Testing shall be to CSA W59, Section 11.

T6.10 For the cases of full penetration single sided welding for the △1 brace to chord weld, any defect outside the acceptance standard found within the first 25% (4.mm) of the weld root depth, measured from the inside surface of the brace, shall not be an immediate cause for rejection of the weld. However, any defects found in this area shall be recorded and reported to the 'Project Coordinator' and his Inspector for information and analysis.

T6.11 If areas are found which, although being within the above cri- △1 teria, give rise for concern, these shall be reported to the 'Project Coordinator' or his Inspector for further investigation.

T6.12 All labour, materials and equipment required to carry out the NDE tests shall be provided by the Fabricator.

T6.13 There shall be no rectification of defective work without the △1 prior permission, in writing, of the 'Project Coordinator'.

T7.0 Delivery

T7.1 Delivery of specimens as per your estimate dated January 8, 1985. △1

T8.0 Drawings, Specifications, Weld Procedures and Quality Plan

T8.1 Prior to commencement of manufacture and at dates to be agreed by the 'Project Coordinator', the Fabricator shall submit for approval by the 'Project Coordinator' the following:

(a) Two copies of all manufacturing specifications and weld procedures.

(b) Two copies of the Quality Plan.

(c) Two copies of any drawings which have been prepared to suit the Contractor's own manufacturing techniques and which differ in detail from the authority's drawings. These drawings shall include all weld preparations.

T8.2 One copy of all manufacturing specifications, weld procedures, Quality Plan and drawings so submitted will be returned to the Contractor marked "Approved" or will be approved subject to agreed modifications being incorporated. All of these documents shall be in such detail as the 'Project Coordinator' may require. All work shall be carried out to the approved manufacturing specifications, weld procedures, Quality Plan and drawings, and the Fabricator shall not amend any of the details without the prior approval of the 'Project Coordinator', in writing.

T8.3 Approval of drawings and documents by the 'Project Coordinator' is required to ensure that the Fabricator is meeting the general requirements and not for the approval of details, tolerances, etc.

T8.4 On completion of manufacture, the Fabricator shall provide updated drawings showing the "as built" dimensions of each specimen.

T9.0 Documentation

T9.1 On completion of fabrication, the Fabricator shall supply two copies of a comprehensive report covering all stages of manufacture of each test assembly. The report shall record the history of manufacture and any difficulties encountered and how they were overcome, finished dimensions and any concessions granted to ease manufacture. △1

T9.2 The Fabricator shall supply two certified copies of all test certificates to the 'Project Coordinator' to show that all materials of construction and components comply with the requirements of this specification. The certificates shall contain sufficient information to clearly identify each component or material to which the certification refers and to enable the material to be traced throughout every stage of manufacture. △1

T9.3 The format and contents of all documentation and test certification shall be to the satisfaction of the 'Project Coordinator'. △1

T10.0 Identification

T10.1 Each specimen shall be marked with a reference number, the contract number and the gross weight of the specimen for identification. This marking, which shall be in an approved paint in letters not less than 25mm high, shall be carried out to the satisfaction of the Inspector.

T11.0 Lifting Instructions, Transport and Delivery

T11.1 The Fabricator shall be responsible for off-loading at his works of all materials supplied by the Department of Energy Mines and Resources of the Federal Government.

T11.2 The Fabricator shall be responsible for delivering the completed test specimens to the selected Research Establishment. Details of this establishment will be notified at a later date. The selected Research Establishment will be responsible for off loading of the specimens.

T11.3 The Fabricator shall clearly indicate all necessary lifting instructions on the specimens. All lifting instructions shall be to the satisfaction of the 'Project Coordinators' Inspector.

T11.4 All machined faces, flanges, etc., shall be protected by the Fabricator, by greasing the machined parts, and by fitting wooden blanks on flange faces. All protection shall be to the satisfaction of the 'Project Coordinators' Inspector.

T11.5 No item shall be dispatched without the prior permission of the 'Project Coordinators' Inspector.

T12.0 Meetings

T12.1 During the period of the work, the Fabricator shall provide a responsible representative/s to attend meetings, when requested by the 'Project Coordinator', at intervals of approximately one month. Such representative/s shall be empowered to take decisions arising from the business of the meetings. These meetings will normally take place at the Fabricators' works.

ITEM 2-BB

DRAWING NO. F638, ISSUE 1, REVISION 9

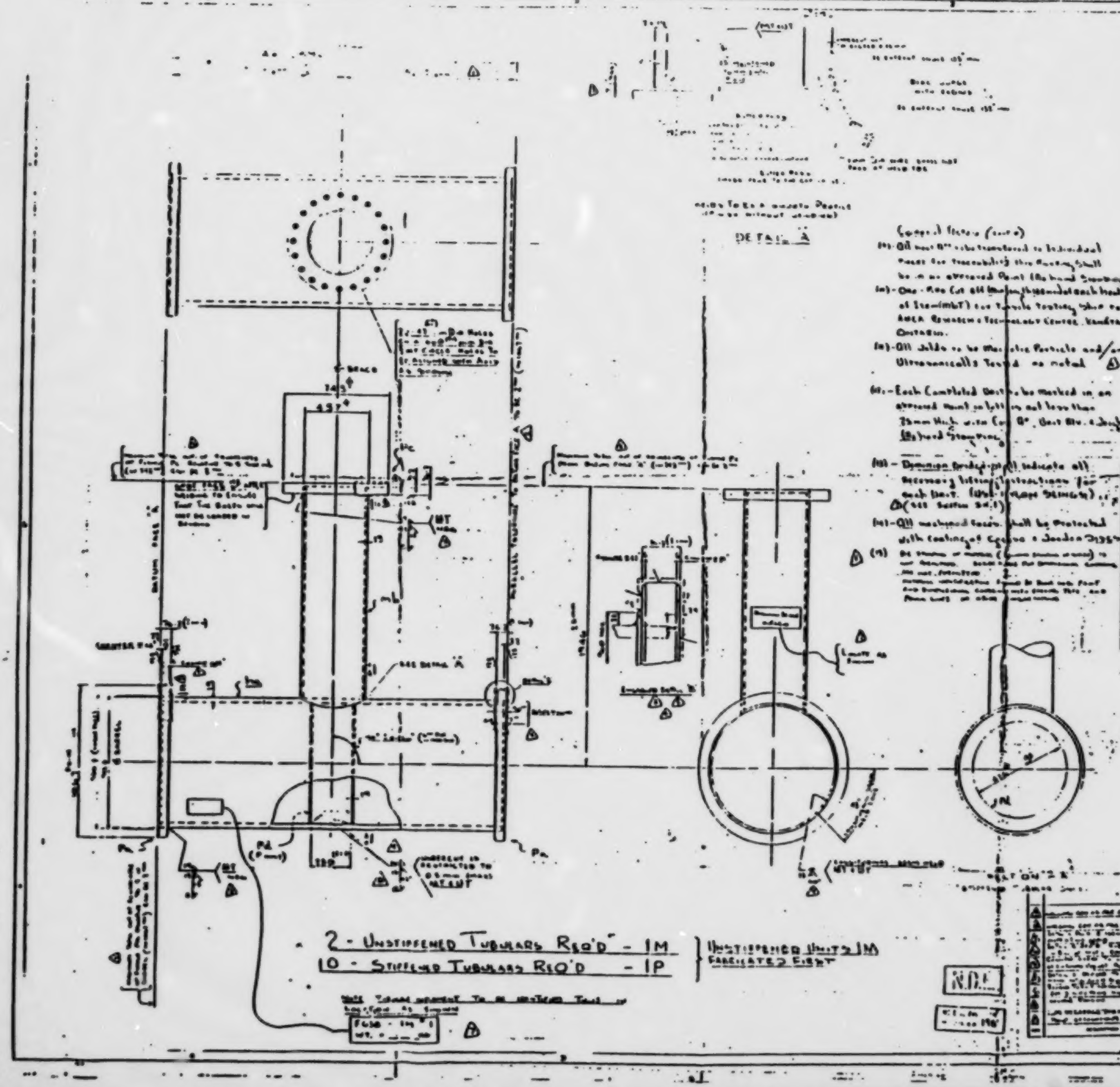
DETAIL "A"
SECTION "2-2"
2 - UNSTIFFENED TUBULARS REQ'D - 1M
10 - STIFFENED TUBULARS REQ'D - 1P
UNSTIFFENED UNITS 1M FABRICATED FIRST
N.D.E.
457
143
Pa
Pb
BT
F638

GENERAL NOTES

Fabrication is to be carried out in accordance with Request for Quotation Document/Sec. 1 [illegible]

FABRICATION TOLERANCES

1) The diameter of any section shall not be more than [illegible] from the nominal [illegible] for [illegible]

2) Straightness variation of the [illegible] from a straight line is to be not greater than [illegible] of the length measured from a reference point with a maximum variation of [illegible] The reference point shall be the intersection of the brace and vessel center lines

3) The intersection of the tube [illegible] is to be within [illegible] of the nominal point of the intersection

4) Where applicable the ends of all pipe sections and spools shall be perpendicular to the longitudinal axis to within [illegible] across any face

5) All machined and flange faces are to be protected with grease and wooden blanks for shipping

6) The thickness of the brace at the [illegible] is to be measured at [illegible] points. If less than the nominal [illegible] no welding is to be performed without the consent of the project coordinator

7) General fabrication tolerance to be [illegible] unless noted

8) Tolerance on the roundness of [illegible] to be [illegible]

General Notes (cont'd)

(9) - All [illegible] to be transferred to individual [illegible] for traceability; the [illegible] shall be in an approved [illegible]

(10) - One [illegible] for tensile testing [illegible] Research & Technology Centre, [illegible] Ontario.

(11) - All welds to be Magnetic Particle and/or Ultrasonically Tested as noted

(12) - Each completed unit to be marked in an approved [illegible] not less than [illegible] high [illegible]

(13) - [illegible] indicate all necessary [illegible] for each unit. [illegible] (see Section 24.1)

(14) - All machined faces shall be protected with coating of [illegible]

(15) [illegible]

MATERIAL

1) Flanges from plate material [illegible]

2) Barrel and stiffener plate material [illegible] (see [illegible])

3) Brace seamless tube to be [illegible] minimum yield [illegible] certificate required. Supply [illegible] to [illegible] International [illegible] Ontario for confirmatory tensile tests

[illegible]

ITEM 2-CC

APPROVED WELDING DATA SHEETS

DOMINION BRIDGE - ONTARIO
A UNIT OF AMCA INTERNATIONAL LIMITED
WELDING PROCEDURE SPECIFICATION

[illegible]

CONTRACT DESCRIPTION: Corrosion Fatigue of Off-Shore Structures

CUSTOMER: AMCA - Kanata

CUSTOMER CONTRACT NO.: 4032

D.B. - ONTARIO CONTRACT NO.: F638

SCOPE: *This Welding Procedure Specification covers welding and related processes for the fabrication of:*

12 Tubular Weldments

Approved
M. J. Pikes 11/6/85
AMCA Int. R&T Centre

FABRICATION DATA

1.0 *FABRICATION CODES AND SPECIFICATIONS:*

(a). W59 and W47.1
(b). AMCA Technical Appendix BN2
(c).
(d).

2.0 *POST WELD HEAT TREATMENT:*

None

SPECIFICATION NO.	*ISSUED*	*REVISED*	*CONTRACT*	*PAGE NO.*
198	May 31, 1985		F638	1 of 3

DOMINION BRIDGE - ONTARIO   A UNIT OF AMCA INTERNATIONAL LIMITED

3.0 WELDING PROCEDURE SPECIFICATION SUMMARY

WELD PROCESS	PROCESS SPEC.	F-No.	PQR	QUALIFIED CONSUMABLES	BRAND NAME	APPLICATION	DATA SHEETS
SMAW	C1-M	4		E7018		Fillet welds Stiffener to Chord	0-1G-1, 0-2G-1 T4-2G-2
				E7018	18 Plus LH 75	Brace to Chord	T4-2G-3a
SAW	C1-S	6		F72-EM12K	L61 860	Chord Long Seam Fillet Welds Flange to Tube Stiffener to Chord	2-1G-12, 2-1G-1 0-1G-2, 0-2G-2, 0-2G-1 PTC4-1G-11 4-2G-1
FCAW	C1-F	6		E70T-9	LA T-9	Fillets Flange to Tube	0-1G-2, 0-2G-3 PT4-1G-1
GTAW							[illegible] 16/7/85

SPECIFICATION NO.	ISSUED	REVISED	CONTRACT	PAGE NO.
198	May 31, 1985	June 27/85	F638	2 of 3

4.0 *MATERIAL SPECIFICATION (RELATED TO WELDING)*

DESCRIPTION	*SPECIFICATION*	*THICKNESS*
Chord	G40.21 - 350WT	19 mm
Brace	A106 - Grade B	19 mm
Flange	G40.21 - 300W	90 mm

5.0 *WELDER'S QUALIFICATION IN ACCORDANCE WITH:*

☐ *(A) A.S.M.E. BOILER AND PRESSURE VESSEL CODE, SECTION IX*

☒ *(B) C.S.A. STANDARD W47.1-1973*

6.0 *SPECIAL REQUIREMENTS:*

6.1 The brace to chord weld must be performed by SMAW.

6.2 Prior to commencement of manufacture, the fabricator shall demonstrate to the satisfaction of the "Project Co-Ordinator" the capability of the welders to consistantly achieve a one-sided full penetration joint using the test assembly of AWS Clause 5.21 except that the bevel angle shall be 45°.

6.3 Only welding consumables supplied with a letter of conformance from the consumable manufacturer may be used.

SPECIFICATION NO.	*ISSUED*	*REVISED*	*CONTRACT*	*PAGE NO.*
198	May 31, 1985		F638	3 of 3

6.0 SPECIAL REQUIREMENTS - Continued

6.4 Grinding on the final layer of the brace to chord weld is not permitted. Previous layers may be repaired by grinding.

6.5 See contract drawing for details of the brace to chord weld profile.

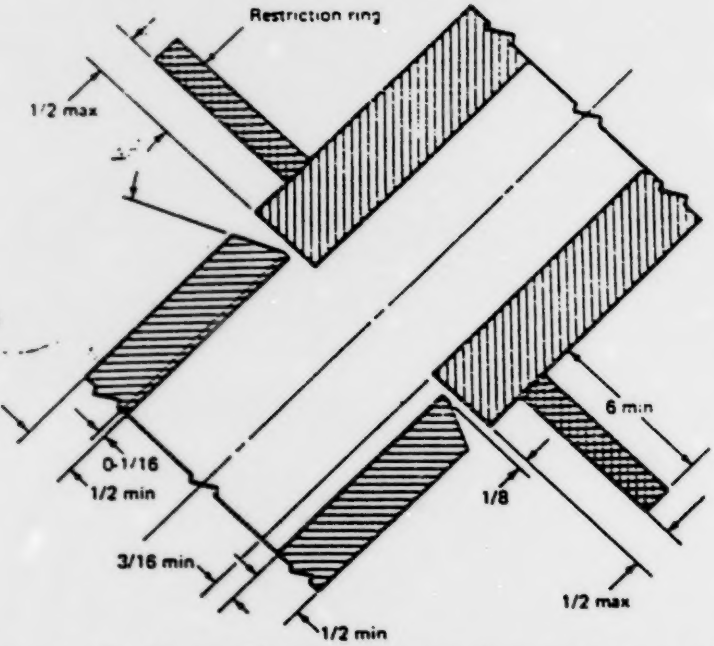

Fig. 5.21—Test joint for T-, K-, and Y-connections on pipe or square or rectangular tubing—welder qualification

VOLUME:	W 6
DATA SHEET	CI - S 4-2G-1

DOMINION BRIDGE COMPANY, LIMITED

- WELDING DATA SHEET -

BASE METAL	See Spec'n: CI - S
WELD PROCESS	Submerged Arc
△1 POSITION	2G - Horizontal
FILLER MATERIAL	AWS Group "F7x -Exxxx"
PRE HEAT	See Spec'n CI - S
POLARITY	DC + ve

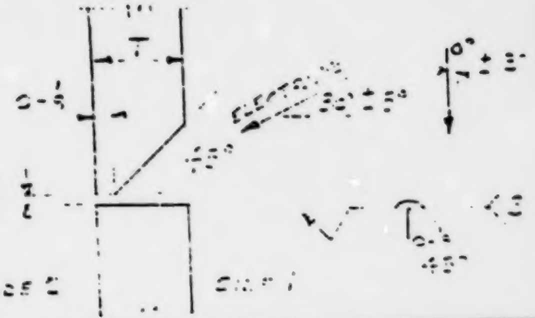

DOMINION BRIDGE COMPANY LIMITED

T	A°	GAP	SIDE	LAYER NO	BEAD NO	WIRE DIA	AMPS	VOLTS	SPEED		ESO		
3/8	45	0-1/8	1	1	1	3/32	350	30	16		1		
			1	2	2	"	"	"	16		"		
			2	3	3	"	"	"	16		"		
1/2	45	0-1/8	1	1	1	3/32	350	30	16		1		
			1	2	2	"	425	32	17		"		
			1	3	3, 4	"	"	"	21		"		
			2	4	5	"	"	"	14		"		
5/8	45	0-1/8	1	1	1	3/32	350	30	16		1		
			1	2	2	"	425	32	17		"		
			1	3, 4	3-6	"	"	"	21		"		
			2	5	7	"	"	"	14		"		
3/4	45	0-1/8	1	1	1	3/32	350	30	16		1		
			1	2	2	"	425	32	17		"		
			1	3-5	3-8	"	"	"	20		"		
			2	6	9	"	"	"	14		"		

C.W.B. APPROVED
DEC 9 1977

D.B.Co. APPROVED	DATE	TEST PLATE REF NO
Rev. △1 JG Breakell	10 Nov. 1977.	PQR - S - PI - 123

DOMINION BRIDGE COMPANY LIMITED
- WELDING DATA SHEET -

VOLUME: W 6

DATA SHEET: CI - S / 0-2G-2

BASE METAL	See Spec'n: CI - S
WELD PROCESS	Submerged Arc
POSITION	Horizontal
FILLER MATERIAL	AWS Group "F7x -Exxxx"
PRE HEAT	See Spec'n: CI - S
POLARITY	DCSP (DC-)

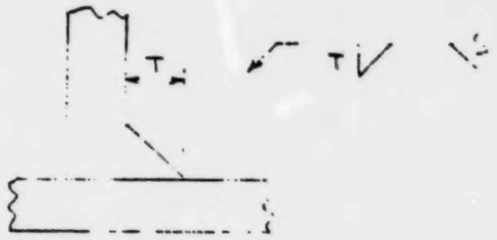

T	A°	GAP	SIDE	LAYER NO.	BEAD NO.	WIRE DIA	AMPS	VOLTS	SPEED		E.S.O.		
3/16				1	1	5/32	500	30	49		1½		
1/4				1	1	5/32	650	30	45		1½		
5/16				1	1	5/32	700	32	30		1½		
3/8				1	1	5/32	650	30	45		1½		
				2	2	"	"	32	45		"		
1/2				1	1	5/32	700	30	30		1½		
				2	2,3	"	"	32	39		"		

APPROVED
MAY [illegible] 1972
C.W.B.

D B Co APPROVED: Morton S. Tipleman

DATE: APR 24 1972

TEST PLATE REF NO.

PREQUALIFIED

TO CODES:	D1·0	D2·0	W59

VOLUME: W 6

DATA SHEET: CI - S / 0-2G-1

DOMINION BRIDGE COMPANY LIMITED

- WELDING DATA SHEET -

BASE METAL	See Spec'n.: CI - S
WELD PROCESS	Submerged Arc
POSITION	Horizontal (2G)
FILLER MATERIAL	AWS Group "F7x -Exxxx"
PRE HEAT	See Spec'n.: CI - S
POLARITY	AC or DCRP (DC+)

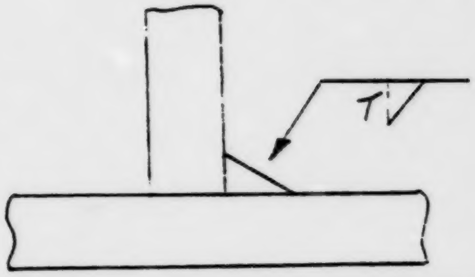

DOMINION BRIDGE COMPANY LIMITED

T	Δ°	GAP	SIDE	LAYER NO.	BEAD NO.	WIRE DIA	AMPS	VOLTS	SPEED		E.S.O.
3/16				1	1	5/32	500	30	35		1¼
1/4				1	1	"	650	30	30		1¼
5/16				1	1	"	700	32	20		1¼
3/8				1	1	"	650	30	30		1¼
				2	2	"	650	32	30		
1/2				1	1	"	700	30	20		1¼
				2	2,3	"	700	32	26		
5/8				1	1	"	700	30	17		1¼
				2	2,3,4	"	700	32	17		
3/4				1	1	"	700	30	18		1¼
				2	2,3	"	700	32	18		1¼
				3	4-6	"	700	32	18		1¼

Welding Procedure Data Sheet
CWB Approved to CSA W47.1
83 02 08

D.B.Co. APPROVED

DATE Jan.26,1983.

TEST PLATE

PREQUALIFIED

DOMINION BRIDGE COMPANY LIMITED

- WELDING DATA SHEET -

VOLUME: W 6

DATA SHEET: CI - S / 0-1G-2

BASE METAL	See Spec'n: CI - S
WELD PROCESS	Submerged Arc
POSITION	Flat (1G)
FILLER MATERIAL	AWS Group "F7x -Exxxx"
PRE HEAT	See Spec'n: CI - S
POLARITY	DCSP (DC⁻)

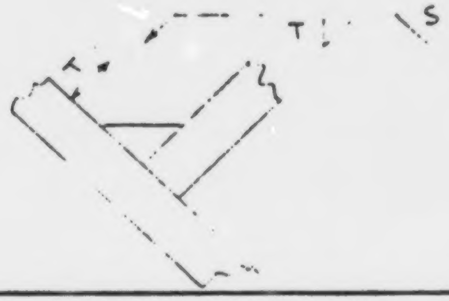

T	A°	GAP	SIDE	LAYER NO.	BEAD NO.	WIRE DIA	AMPS	VOLTS	SPEED		E.S.O.		
1/4			1	1	1	5/32	650	30	43		1 1/4		
5/16			1	1	1	5/32	700	31	32		1 1/4		
3/8			1	1	1	5/32	750	32	25		1 1/4		
1/2			1	1	1	3/16	900	34	15½		1 1/4		
5/8			1	1	1	3/16	1000	35	11½		1 1/4		
3/4			1	1	1	3/16	1000	35	8½		1 1/4		

APPROVED
MAY 11 1972
C.W.B.

D B Co APPROVED	DATE	TEST PLATE REF. NO	PREQUALIFIED TO CODES:
Martin S. Tilleman	APR 24 1972		D1-0 D2-0 W59

DOMINION BRIDGE COMPANY LIMITED

DOMINION BRIDGE COMPANY, LIMITED

- WELDING DATA SHEET -

VOLUME:	W 6
DATA SHEET	CI - S 2-1G-12

BASE METAL	See Spec'n.: CI - S
WELD PROCESS	Submerged Arc
POSITION	Flat (1G)
FILLER MATERIAL	AWS Group "F7x -Exxxx"
PRE HEAT	See Spec'n.: CI - S
POLARITY	DC +ve

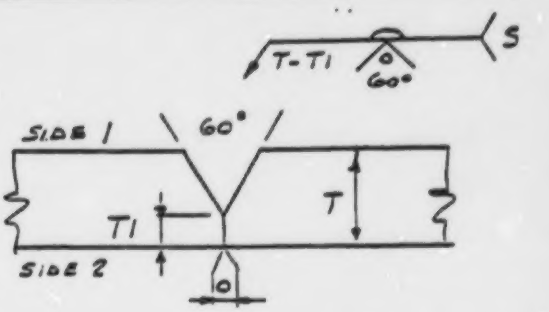

DOMINION BRIDGE COMPANY, LIMITED

T	A°	GAP	SIDE	LAYER NO.	BEAD NO.	WIRE DIA.	AMPS	VOLTS	SPEED		E.S.O.		T.
1/2	60	0	1	1	1	3/32	450/500	28/32	15/17		1½		1/
			2	2	2	"	"	"	9/10		"		
3/4	60	0	1	1	1	3/32	450/500	28/32	13/15		1½		1/
			1	2	2	"	500/550	33/36	6/7		"		
			2	3	3	"	"	"	10/11		"		
1	60	0	1	1	1	3/32	500/550	33/36	14/16		1½		5/1
			1	2	2	"	"	"	6/7		"		
			1	3	3,4	"	"	"	12/13		"		
			2	4	5	"	"	"	7/8		"		
1½	60	0	1	1	1	3/32	500/550	33/36	14/16		1½		7/1
			1	2	2	"	"	"	10/11		"		
			1	3	3,4	"	"	"	13/14		"		
			1	4	5,6	"	"	"	10/11		"		
			2	5,6	7,8	"	"	"	10/11		"		
1½	60	0	1	1	1	3/32	500/550	33/36	14/16		1½		1/
			1	2	2	"	"	"	6/7		"		
			1	3	3,4	"	"	"	8/9		"		
			1	4	5-7	"	"	"	9/10		"		
			2	5,6	8,9	"	"	"	8/9		"		

Welding Procedure Data Sheet
CWB Accepted to CSA W47.1
80 05 C

D.B.Co. APPROVED	DATE	TEST PLATE REF. NO.	PREQUALIFIED TO CODES:	D1·1		W59
J. Brakell	April 7, 1980					

DOMINION BRIDGE COMPANY LIMITED

- WELDING DATA SHEET -

VOLUME: W 6

DATA SHEET } CI - S / 2-1G-1

BASE METAL	See Spec'n: CI - S
WELD PROCESS	Submerged Arc
POSITION	Flat (1G)
FILLER MATERIAL	AWS Group "F7x -Exxxx"
PRE HEAT	See Spec'n: CI - S
POLARITY	AC or DCRP (DC+)

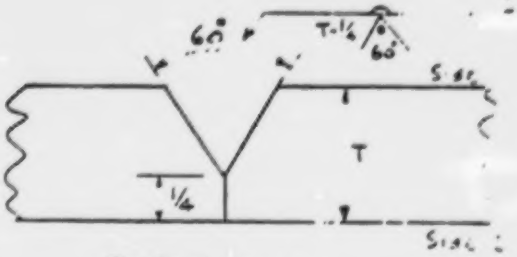

Back Groove

T	A°	GAP	SIDE	LAYER NO.	BEAD NO.	WIRE DIA	AMPS	VOLTS	SPEED		E.S.O	
9/16	60	0	1	1	1	5/32	600	30	6½		1¼	
			2	2	2	"	750	35	12			
3/4	60	0	1	1	1	5/32	600	30	8		1¼	
			1	2	2	"	700	35	10			
			2	3	3	"	750	35	12			
1	60	0	1	1	1	5/32	600	30	8		1¼	
			1	2	2	"	600	32	8			
			2	3	3	"	750	35	12			
			1	4	4,5	"	700	33	10			

APPROVED
OCT 13 1971
C.W.B.

D B Co APPROVED	DATE	TEST PLATE REF. NO }	PREQUALIFIED TO CODES: D1·0 D2·0 W59
Morton S. Tickleman	SEP 30 1971		

VOLUME:	W6
DATA SHEET	CI - F 0-1G-2

DOMINION BRIDGE COMPANY LIMITED

- WELDING DATA SHEET -

BASE METAL	See Spec'n: CI - F
WELD PROCESS	FLUX-CORE
POSITION	1G Flat
FILLER MATERIAL	See Spec'n: CI - F
PRE HEAT	See Spec'n: CI - F
SHIELDING GAS	Welding Grade CO_2
POLARITY	DC +ve

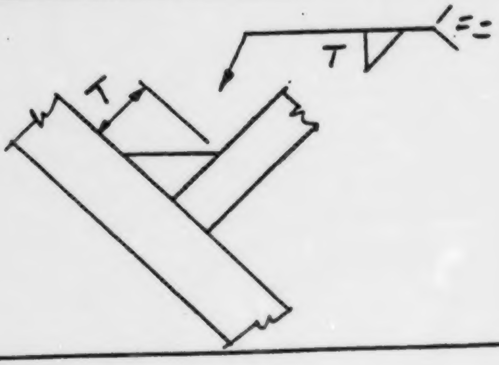

T	A°	ROOT FACE	GAP	SIDE	LAYER	BEAD	WIRE DIA	AMPS	VOLTS	SPEED	GAS C.F.H	E.S.C	[illegible]
3/16				1	1	1	5/64	325	31	30	40	1	[illegible]
1/4				1	1	1	5/64	325	31	17	40	1	[illegible]
5/16				1	1	1	5/64	325	31	12	40	1	[illegible]
3/8				1	1	1	5/64	325	31	8	40	1	[illegible]
1/2				1	1	1	5/64	325	31	12	40	1	[illegible]
				1	2	2,3	"	"	"	16	"	"	[illegible]
5/8				1	1	1	5/64	325	31	8	40	1	[illegible]
				1	2	2,3	"	"	"	10	"	"	[illegible]
3/4				1	1	1	5/64	325	31	12	40	1	[illegible]
				1	2	2,3	"	"	"	13	"	"	[illegible]
				1	3	4,5	"	"	"	9	"	"	[illegible]

Welding Procedure Data Sheet
[illegible]
80 05 02

D.B.Co. APPROVED J. Breakell	DATE April 25,1980	TEST PLATE REF. NO.	PREQUALIFIED TO CODES: D1.1 W59

DOMINION BRIDGE COMPANY LIMITED

- WELDING DATA SHEET -

VOLUME: W 6

DATA SHEET: CI - F / 0-2G-3

BASE METAL	See Spec'n.: CI - F
WELD PROCESS	FLUX-CORE
POSITION	2G Horizontal
FILLER MATERIAL	See Spec'n: CI - F
PRE HEAT	See Spec'n: CI - F
SHIELDING GAS	Welding Grade CO_2
POLARITY	DC +ve

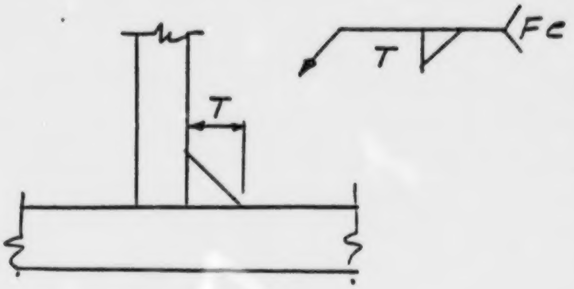

T	A°	ROOT FACE	GAP	SIDE	LAYER	BEAD	WIRE DIA	AMPS	VOLTS	SPEED	GAS C.F.H	E.S.O.	W.F.S. in.mi
3/16				1	1	1	5/64	325	31	30	40	1	225
1/4				1	1	1	5/64	325	31	17	40	1	225
5/16				1	1	1	5/64	325	31	12	40	1	225
3/8				1	1	1	5/64	325	31	8	40	1	225
		OR											
				1	1	1,2	5/64	325	31	15/17	40	1	225
1/2				1	1	1	5/64	325	31	12	40	1	225
				1	2	2,3	"	"	"	15/17	"	"	"
5/8				1	1	1	5/64	325	31	12	40	1	225
				1	2	2-4	"	"	"	12/14	"	"	"
3/4				1	1	1	5/64	325	31	12	40	1	225
				1	2	2,3	"	"	"	15/17	"	"	"
				1	3	4-6	"	"	"	13/15	"	"	"

Welding Procedure Data Sheet
CWB Approved to CSA W47.1
30 05 [illegible]

D.B. Co. APPROVED
J. Breakell

DATE
April 25,1980

TEST PLATE REF. NO.

PREQUALIFIED
TO CODES: D1·1 | | W59

DOMINION BRIDGE COMPANY LIMITED

DOMINION BRIDGE COMPANY LIMITED

DOMINION BRIDGE COMPANY LIMITED

- WELDING DATA SHEET -

VOLUME: W6

DATA SHEET: CI - F / PT4-1G-1

BASE METAL	See Spec'n:	CI - F
WELD PROCESS	FLUX - CORE	
POSITION	Flat (1G)	
FILLER MATERIAL	See Spec'n	CI - F
PRE HEAT	See Spec'n	CI - F
SHIELDING GAS	CO_2	
POLARITY	DCRP (DC+)	

Partial Penetration:

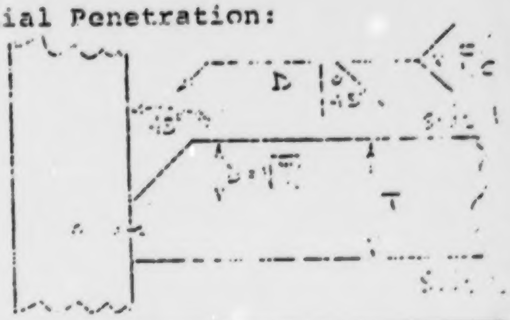

T	A°	ROOT FACE	GAP	SIDE	LAYER	BEAD	WIRE DIA	AMPS	VOLTS	SPEED	GAS CFH	[illegible]	[illegible]
½ - ¾	45		0	1	1	1	3/32	450	27	17	45	1	3/8
				1	2	2	"	500	30	16	"	"	
13/16 - 1	45		0	1	1	1	3/32	450	27	13	45	1	7/1
				1	2	2	"	500	30	13	"	"	
1 1/16 - 1 1/2	45		0	1	1	1	3/32	450	27	11	45	1	[illegible]
				1	2	2	"	500	30	9	"	"	
1 9/16 - 2 1/2	45		0	1	1	1	3/32	450	27	9	45	1	[illegible]
				1	2	2	"	500	30	6	"	"	
2 5/8 - 3 1/2	45		0	1	1	1	3/32	450	27	9	45	1	3/4
				1	2	2	"	500	30	7	"	"	
				1	3	3.4	"	"	30	12	"	"	

CHECKED / APPROVED Morton S. Tikleman	DATE OCT 10 1972	TEST PLATE REF NO	PREQUALIFIED TO CODES: D1.0 / [illegible] / W59

DOMINION BRIDGE COMPANY LIMITED

- WELDING DATA SHEET -

VOLUME: W 6

DATA SHEET: CI - M / 0-1C-1

BASE METAL	See Spec'n.: CI - M
WELD PROCESS	Shielded MANUAL Metal Arc
POSITION	Flat
FILLER MATERIAL	AWS Group "F- 4" (EXX18)
PRE HEAT	See Spec'n: CI - M

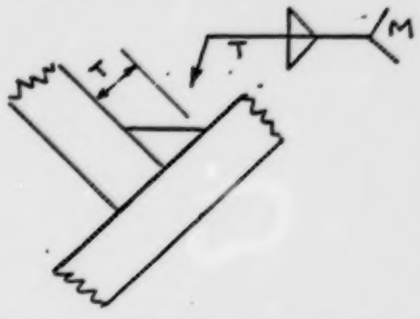

T	A°	GAP	SIDE	LAYER	BEAD	WIRE DIA.	AMPS	VOLTS	SPEED				
3/16			1	1	1	7/32	280		12				
1/4			1	1	1	7/32	280		9				
5/16			1	1	1	1/4	360		8				
3/8			1	1	1	1/4	360		5½				
1/2			1	1	1	1/4	360		7				
			1	2	2	1/4	360		7				

C.W.B. APPROVED
APP [illegible]
TO W47.1 - W59.1

DOMINION BRIDGE COMPANY LIMITED

REV. △ MARCH 11, 1975

D.B.Co. - APPROVED	DATE	TEST PLATE REF. NO.
Morton S. Titleman	July 1971	

PREQUALIFIED

TO CODES:	D1-0	D2-0	W59

DOMINION BRIDGE COMPANY LIMITED

- WELDING DATA SHEET -

VOLUME W 6

DATA SHEET CI - M / T4-2G-2

BASE METAL	See Spec'n: CI - M
WELD PROCESS	Shielded MANUAL Metal Arc
POSITION	Horizontal
FILLER MATERIAL	AWS Group "F- 4"
PRE HEAT	See Spec'n: CI - M

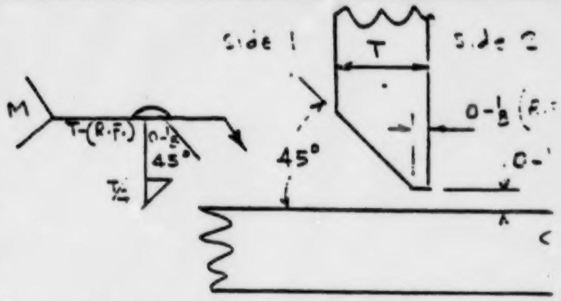

Fillet Reinforcement = T/2

T	A°	GAP	SIDE	LAYER	BEAD	WIRE DIA.	AMPS	VOLTS	SPEED				
1/4			1	1	1	5/32	165		6				
			1	2	2-3	5/32	165		7½				
			2	3	4	5/32	165		7½				
3/8			1	1	1	5/32	165		6				
			1	2	2-4	5/32	165		5				
			2	3	5	5/32	165		7½				
1/2			1	1	1	5/32	165		6				
			1	2	2-3	5/32	165		5				
			1	3	4-6	5/32	165		5				
			2	4	7	5/32	165		7½				
5/8			1	1	1	5/32	165		6				
			1	2	2-3	5/32	165		5				
			1	3	4-5	5/32	165		5				
			1	4	6-8	5/32	165		4½				
			2	5	9	5/32	165		7½				
3/4			1	1	1	5/32	165		6				
			1	2	2-3	5/32	165		5				
			1	3-4	4-10	5/32	165		4½				
			2	5	11	5/32	165		7½				

APPROVED
JUL 21 1971
C. W. B.

D & Sc APPROVED Morton S. Titleman	DATE July 1971	TEST PLATE REF. NO.	PREQUALIFIED TO CODES: D1·0 D2·0 W59

DOMINION BRIDGE COMPANY LIMITED

- WELDING DATA SHEET -

VOLUME: W 6

DATA SHEET: CI - M / 0-2G-1

BASE METAL	See Spec'n.: CI - M
WELD PROCESS	Shielded MANUAL Metal Arc
POSITION	Horizontal
FILLER MATERIAL	AWS Group "F-4" (EXX18)
PRE HEAT	See Spec'n.: CI - M

△1

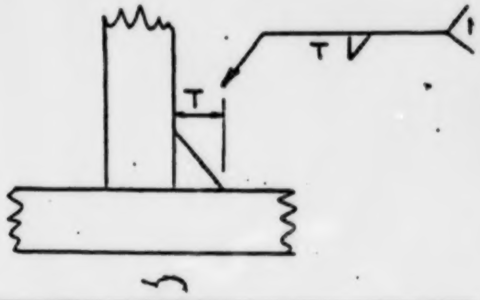

T	A°	GAP	SIDE	LAYER	BEAD	WIRE DIA.	AMPS	VOLTS	SPEED				
3/16			1	1	1	3/16	250		12				
1/4			1	1	1	7/32	280		9				
5/16			1	1	1	1/4	360		8				
3/8			1	1	1	1/4	360		11				
			1	1	2	1/4	360		11				
1/2			1	1	1	1/4	360		10				
			1	2	2	1/4	360		10				
			1	2	3	1/4	360		10				

C.W.B. APPROVED

APR 7 [illegible]

To W47.1 - W59.1

C.W.B. APPROVED Morton S. Titleman

DATE July 1971

TEST PLATE REF. NO.

PREQUALIFIED

TO CODES:	D1·0	D2·0	W59

DOMINION BRIDGE COMPANY LIMITED

REV. △1 MARCH 11, 1975

VOLUME	W 6
DATA SHEET	CI - S PTC4-1G-11

DOMINION BRIDGE COMPANY. LIMITED

- WELDING DATA SHEET -

BASE METAL	See Spec'n.: CI - S
WELD PROCESS	Submerged Arc
POSITION	1G Flat
FILLER MATERIAL	AWS Group "F7x -Exxxx"
PRE HEAT	See Spec'n.: CI - S
POLARITY	DC +ve

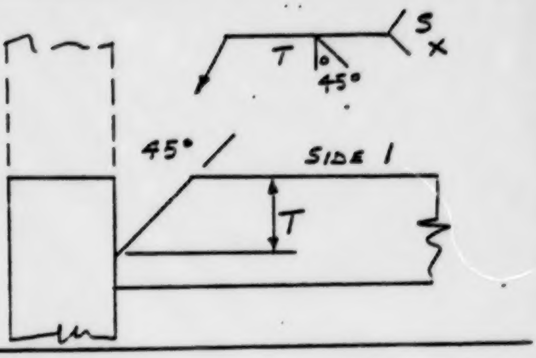

T	A°	GAP	SIDE	LAYER NO.	BEAD NO.	WIRE DIA.	AMPS	VOLTS	SPEED		E.S.O.		
3/8	45	0	1	1	1	5/32	450	29	13		1½		
			1	2	2	"	600/650	30/32	15/16		"		
1/2	45	0	1	1	1	5/32	450	29	13		1½		
			1	2	2	"	600/650	30/32	8/9		"		
3/4	45	0	1	1	1	5/32	450	29	13		1½		
			1	2	2	"	600/650	30/32	8/11		"		
			1	3	3,4	"	"	"	8/11		"		
1	45	0	1	1	1	5/32	450	29	13		1½		
			1	2	2	"	600/650	30/32	8/11		"		
			1	3	3,4	"	"	"	7/10		"		
			1	4	5,6	"	"	"	7/10		"		

Welding Procedure Data Sheet
CWB Approved to CSA W47.1
800502

D B Co APPROVED J. Breakell	DATE April 25, 1980	TEST PLATE REF. NO. L227/S-44-1

DOMINION BRIDGE COMPANY LIMITED
- WELDING DATA SHEET -

VOLUME: W 6

DATA SHEET: CI - M
T4-2G-3a

BASE METAL	See Spec'n: CI - M
WELD PROCESS	Shielded MANUAL Metal Arc
POSITION	HORIZONTAL
FILLER MATERIAL	AWS Group "F-4"
PRE HEAT	See Spec'n: CI - M
CONSUMABLES	CL4- 18 PLUS- 1ST THREE PASSES, LINCOLN LH-75 REMAINDER
ROOT PASS	STOP-STARTS TO BE TAPERED BY GRINDING

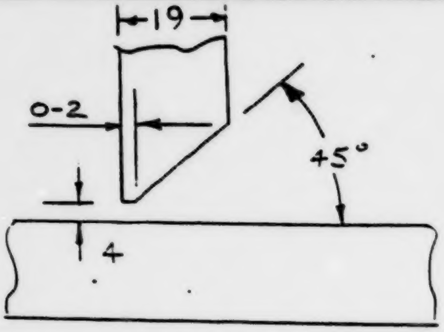

T	∠°	GAP	SIDE	LAYER	BEAD	WIRE DIA	AMPS	VOLTS	SPEED			
			1		1-36	1/8	135	22	4-7			

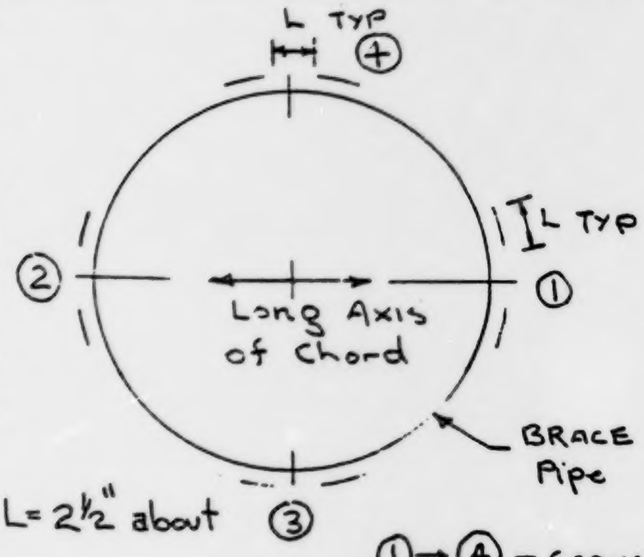
L TYP
④
L TYP
②
①
Long Axis of Chord
BRACE Pipe
③

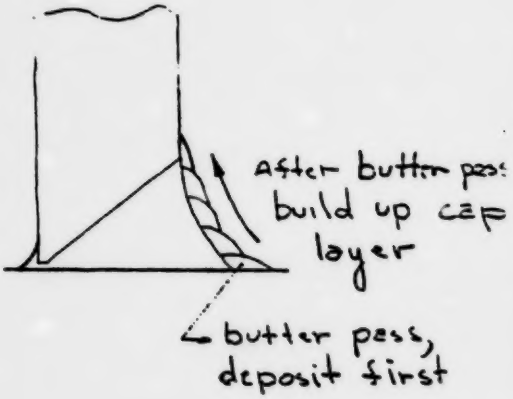
After butter pass build up cap layer
butter pass, deposit first

L = 2½" about

① → ④ – sequence for depositing root pass
Remainder to be balanced by welding opposite sides.
Fill passes to be also balanced.

Approved
16/7/85

D.B.Co. APPROVED

DATE June 27/85

TEST PLATE REF NO: PRE-QUALIFIED TO AWS D1.1

3.0 WELDING PROCE[illegible] SPECIFICATION SUMMARY

WELD PROCESS	PROCESS SPEC.	F-No.	PQR	QUALIFIED CONSUMABLES	BRAND NAME	APPLICATION	DATA SHEETS
SMAW	C1-M	4		E7018		Fillet welds Stiffener to Chord	0-1G-1, 0-2G-1 T4-2G-2
				E7018	18 Plus LH 75	Brace to Chord	T4-2G-3a
SAW	C1-S	6		F72-EM12K	L61 860	Chord Long Seam Fillet Welds Flange to Tube Stiffener to Chord	2-1G-12, 2-1G-1 0-1G-2, 0-2G-2, 0-2G-1 PTC4-1G-11 4-2G-1
FCAW	C1-F	6		E70T-9	LA T-9	Fillets Flange to Tube	0-1G-2, 0-2G-3 PT4-1G-1
					LA T-91	Stiffener to Chord	T4-1G-1 4-1G-2
GTAW							Approved

SPECIFICATION NO.	ISSUED	REVISED	CONTRACT	PAGE NO.
198	May 31, 1985	June 27, 1985 Feb. 5. 1986	F638	2 of 3

DOMINION BRIDGE COMPANY LIMITED

- WELDING DATA SHEET -

VOLUME: W 6

DATA SHEET CI - F / T4-1G-1

BASE METAL	See Spec'n: CI - F
WELD PROCESS	FLUX-CORE
POSITION	Flat (1G)
FILLER MATERIAL	See Spec'n. CI - F
PRE HEAT	See Spec'n. CI - F
SHIELDING GAS	CO_2
POLARITY	DCRP (DC+)

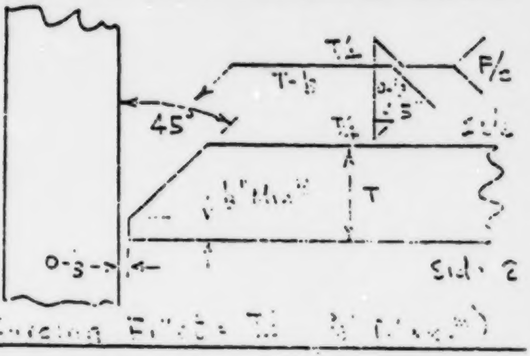

T	A°	ROOT FACE	GAP	SIDE	LAYER	BEAD	WIRE DIA	AMPS	VOLTS	SPEED	GAS CFH	[illegible]
1/2	45	1/8	0-1/8	1	1	1	3/32	450	27	16	45	1
				1	2	2	"	500	29	11	"	"
				2	3	3	"	"	30	14	"	"
3/4	45	1/8	0-1/8	1	1	1	3/32	450	27	13	45	1
				1	2	2	"	500	29	8	"	"
				1	3	3,4	"	"	30	16	"	"
				2	4	5	"	"	30	12	"	"
1	45	1/8	0-1/8	1	1	1	3/32	450	27	13	45	1
				1	2	2	"	500	29	8	"	"
				1	3	3,4	"	"	30	11	"	"
				1	4	5,6	"	"	30	10	"	"
				2	5	7	"	"	30	11	"	"
1-1/4	45	1/8	0-1/8	1	1	1	3/32	450	27	13	45	1
				1	2	2	"	500	29	8	"	"
				1	3	3,4	"	"	30	11	"	"
				1	4	5,6	"	"	30	8	"	
				1	5	7,8	"	"	32	10	"	"
				1	6	9	"	"	32	8	"	
				2	7	10	"	"	30	10	"	

APPROVED
NOV 1 1972
C.W.B.

APPROVED Martin S. Tikleman	DATE OCT 10 1972	TEST PLATE REF NO.	PREQUALIFIED TO CODES: D1-0 D2-0 W59

VOLUME: W 6

DATA SHEET } CI - F / 4-1G-2

DOMINION BRIDGE COMPANY LIMITED

- WELDING DATA SHEET -

BASE METAL	See Spec'n: CI - F
WELD PROCESS	FLUX-CORE
POSITION	1G Flat
FILLER MATERIAL	See Spec'n: CI - F
PRE HEAT	See Spec'n: CI - F
SHIELDING GAS	Welding Grade CO_2
POLARITY	DC + ve

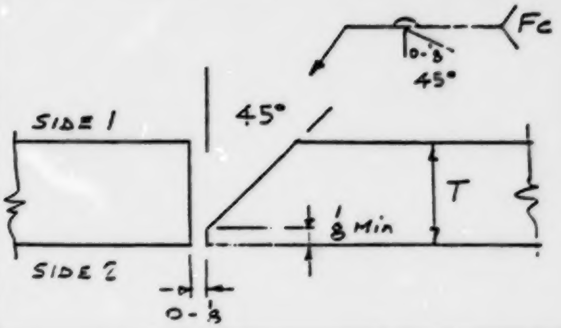

T	A°	ROOT FACE	GAP	SIDE	LAYER	BEAD	WIRE DIA	AMPS	VOLTS	SPEED	GAS CFH	ESO
1/4	45	0-1/8	0-1/8	1	1	1	1/16	300	28	21	45	1
				2	2	2	"	"	"	20	"	"
3/8	45	0-1/8	0-1/8	1	1	1	1/16	300	28	11	45	1
				2	2	2	"	"	"	13	"	"
1/2	45	0-1/8	0-1/8	1	1	1	1/16	300	28	15	45	1
				1	2	2	"	"	"	9	"	"
				2	3	3	"	"	"	13	"	"
3/4	45	0-1/8	0-1/8	1	1	1	1/16	300	28	15	45	1
				1	2	2	"	"	"	10	"	"
				1	3	3.4	"	"	"	10	"	"
				2	4	5	"	"	"	13	"	"
1	45	0-1/8	0-1/8	1	1	1	1/16	300	28	15	45	1
				1	2	2	"	"	"	10	"	"
				1	3	3.4	"	"	"	14	"	"
				1	4	5.6	"	"	"	11	"	"
				1	5	7.8	"	"	"	13	"	"
				2	6	9	"	"	"	13	"	"

C.W.B. APPROVED
AUG 8 1977

D.B.Co. APPROVED J.F. Breakell	DATE August 4, 1977	TEST PLATE REF NO }	Prequalified to Codes: W59.1 & D1.1

Nyp
17/2

ITEM 2-DD

MANUFACTURING PROCEDURE AND INSPECTION AND TEST PLAN, REVISION 2

DOMINION BRIDGE - ONTARIO
A Unit Of AMCA International Limited

MANUFACTURING PROCEDURE & INSPECTION AND TEST PLAN

CSA Z299.2 QUALITY CONTROL PROGRAM

NO.: 1
ISSUE: 2
DATE: May 23, 1985

REVISIONS: △1 Sept. 10/85 - pg.3, △2 Oct. 28/85 page 1.

SUBJECT: 12 Tubular Weldments

CONTRACT NO.: F638 CUSTOMER: AMCA Corporate Engineering

CUSTOMER REF.: P.O. No. 4032, Tech. Appendix BN2, and Drg. No. 2-185-C66-099

SCOPE: To describe the preparation, sub-assembly and assembly of a tubular weldment - including inspection and testing requirements.

CODE REFERENCE: CSA W59-1982

ONTARIO I.D. NO.: N/A C.R.N.: N/A

WELDING PROCEDURE SPECIFICATION NO.: 198

LEGEND:
◆ Q.C. HOLD POINTS, FOR INSPECTIONS OR TESTS
△ Q.C. INSPECTION POINTS

Also refer to the Standard Inspection and Test Plan for the Contract

Approved 18/6/85
M. J. Pakes
AMCA R&T
Centre

Approval for Rev △2 4/11/85
M. J. Pakes

DISTRIBUTION:

H. Wismayer
J. Chudobiak (2)
C. Storey (2)
G. Startup
G. Mansour
J. Reiman
Customer (2)

PREPARED BY: Mike Laidlaw

MANUFACTURING ENG. APPROVAL: Mike Laidlaw
(M. Laidlaw)

QUALITY CONTROL APPROVAL: G. Startup
(G. Startup)

ENGINEERING APPROVAL: J. Reiman
(J. Reiman)

AUTHORIZED INSPECTOR ACCEPTANCE: N/A

File 066 – Approved Docs

MANUFACTURING PROCEDURE

DOMINION BRIDGE - ONTARIO

CONTRACT	DRAWING(S)	DESCRIPTION	SHEET
F638	1	12 Tubular Weldments	1 OF 4

OPER. NO.	DEPT.	DESCRIPTION OF OPERATION	Q.C. INSPECTION
		PREPARATION	
	26	1. Burn plates ha to width (leave overage on length for rolling.) Layout length.	◆ Receiving inspection req' on plates ha (Ref. to I & T Plan).
	26	2. Pipe mb to be contour cut and bevelled at outside machinist. After machining square cut other end.	◆ Receiving inspection req' on pipes mb (Ref. to I & T Plan.) (Receiving inspection report to identify bevelled end)
	26	3. Burn flange plates pa and pc with machining allowances. Burn bevel on the inside diameter of flanges. Layout and drill holes full size in flange pc. Machining to be done in final assembly.	△ Subject to in process inspection by Q.C.
	26 & Sub.	4. Burn plates pd, burn cut out with machining allowance. Prepare bevelled edge. Machine △2 inside edge at sublet machine shop.	
		SUB - ASSEMBLY	
		(i) Barrel	
	26	1. Pre-bend plate ha.	
		2. Trim plate to exact length and bevel ends for longitudinal weld seam.	
		3. Complete rolling of plate to form barrel.	
		4. Weld longitudinal seam complete.	
		5. Re-roll barrel if necessary.	◆ Q.C. Dept to check barrel for tolerances. Refer to I & T Plan and drawings.
		ASSEMBLY	
	31	1. Fit one stiffener plate pd to barrel ha and △2 make interior fillet weld. Ensure that machined edge is fully protected with wood covers.	△ Subject to in process inspection by Q.C.

MANUFACTURING PROCEDURE

DOMINION BRIDGE - ONTARIO

CONTRACT	DRAWING(S)	DESCRIPTION	SHEET
F638	1	12 Tubular Weldments	2 OF 4

OPER. NO.	DEPT.	DESCRIPTION OF OPERATION	Q.C. INSPECTION
		ASSEMBLY - Continued	
	31	2. Fit second stiffener plate pd and make interior fillet weld.	
		3. Complete all welding of stiffener plates to the barrel.	
		4. Perform N.D.E. on welds.	◆ N.D.E. required by Q.C. Dept.
		5. Check straightness of barrel. If correction is required, advise Q.C./Eng.Dept. for repair procedures.	
		6. Fit flanges pa to barrel ha and tack weld. (Note: Make allowance for machining).	
		7. Check alignment of flanges to centre line of barrel. (No centre punching or scrib lines allowed.)	
		8. Weld flanges complete. Perform N.D.E. on welds.	◆ N.D.E. required by Q.C. Dept.
		9. Fit flange pc to pipe section mb and tack weld. Ensure proper alignment of holes to contoured end.	
		10. Weld flange pc to pipe mb complete. Perform N.D.E. testing on weld.	◆ N.D.E. required by Q.C. Dept.
	82	11. Fit pipe mb to barrel ha. Provide temporary bracing angles for alignment. See Sketch #1. Tack weld pipe to barrel. (Note: Use minimal tack welds on bracing members to pipe and barrel.)	◆ Hold for customer and Q.C. Inspection of fit-up and preparations. (ref. to I & T Plan)
		12. Check alignment of flange surfaces prior to welding.	△ Q.C. Dept. to check
		13. Weld pipe mb to barrel complete. Perform N.D.E. testing on welds.	◆ N.D.E. required by Q.C. Dept.
		14. Remove temporary braces by grinding only. No hammering, burning or gouging of tack weld permitted.	

MANUFACTURING PROCEDURE AND
INSPECTION AND TEST PLAN

DOMINION BRIDGE - ONTARIO

CONTRACT		DRAWING(S)	DESCRIPTION	SHEET
F638		1	12 Tubular Weldments	3 OF 4
OPER. NO.	DEPT.	DESCRIPTION OF OPERATION		Q.C. INSPECTION

① 85-09-10 M.L.

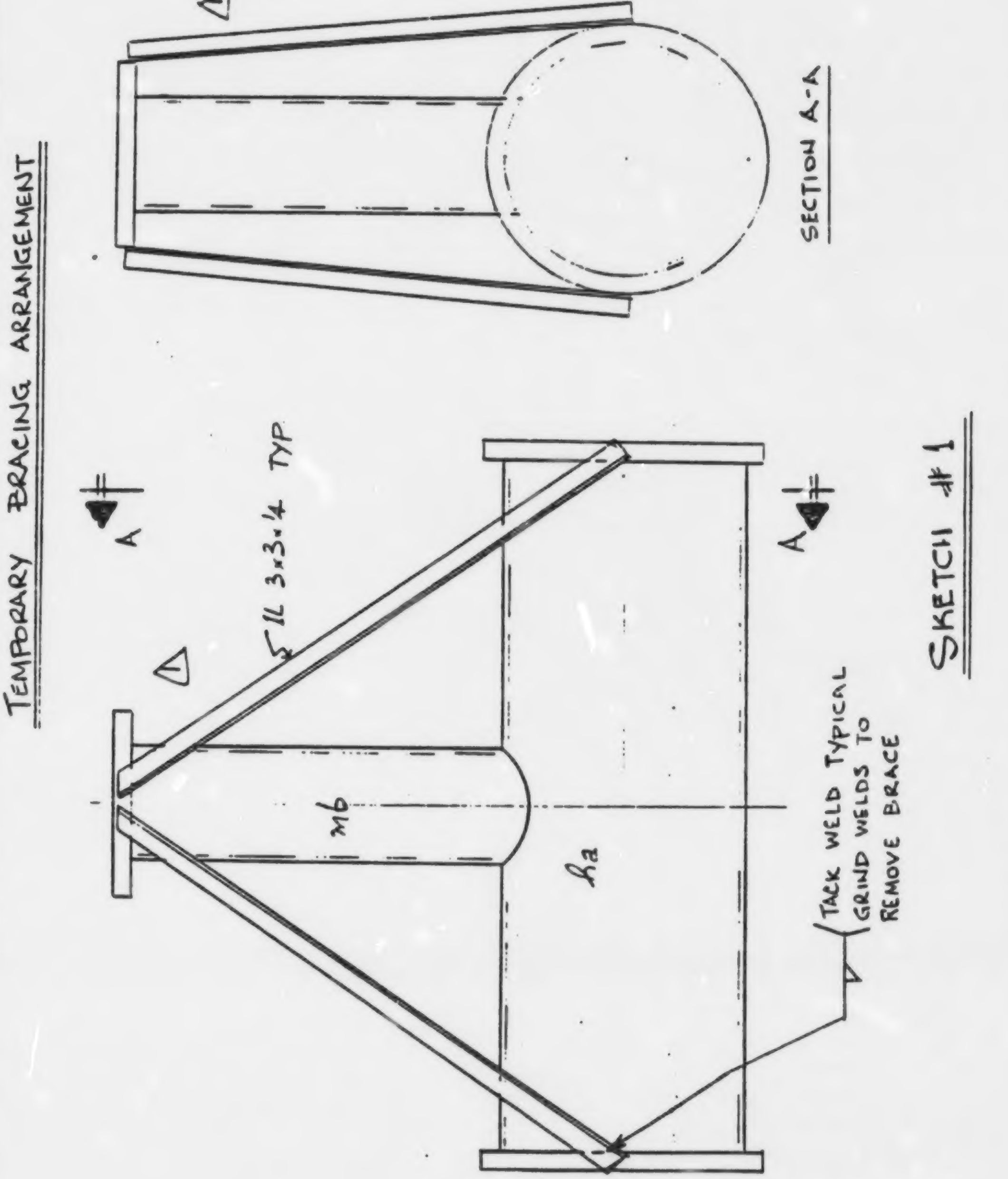
TEMPORARY BRACING ARRANGEMENT
SECTION A-A
SKETCH #1
L 3×3×¼ TYP
A
A
9b
8a
TACK WELD TYPICAL GRIND WELDS TO REMOVE BRACE

MANUFACTURING PROCEDURE

DOMINION BRIDGE - ONTARIO

CONTRACT	DRAWING(S)	DESCRIPTION	SHEET
F638	1	12 Tubular Weldments	4 OF 4

OPER. NO.	DEPT.	DESCRIPTION OF OPERATION	Q.C. INSPECTION
		ASSEMBLY - Continued	
		15. Q.C. Dept. to check assemblies to tolerances Release for outside machining.	◆ Q.C. Dept. to check. (Refer to I & T Plan)
		16. Mark assemblies as per drawings.	
		17. Send for outside machining of flanges.	
		18. Q.C. Dept. to check machining tolerances at outside machine shop.	◆ Q.C. Dept. check (refer to I & T Plan)
		19. Apply grease coating and wooden covers to machined surfaces at outside machine shop.	
		20. Final Q.C. inspection.	◆ Obtain shipping release form from Q.C. to ship items.

APPENDIX 3

PROCEDURE OF MEASURING CRACK DEPTH BY ACPD TECHNIQUE

APPENDIX 3

PROCEDURE FOR MEASURING CRACK DEPTH BY ACPD TECHNIQUE

3.1 General

Procedure for setup of ACPD technique for sizing of cracks in welded joints.

1. Field connections
2. Probe connections
3. Instrument setup
4. Crack depth measurement

3.2 Field Connections

1. Field connection should be at least at a distance of 150 mm on either side of defect
2. Multiple field connections may be used.
3. Attempts should be made to obtain a uniform field, by careful positioning of the field input connections.
4. For tubular joints the field connections are normally positioned approximately 300 to 400 mm from the weld toe.
5. For very large specimens, i.e., tubular joints where the total impedance of the sample is relatively large, it may be necessary to switch the field on and off for different crack locations around the intersection.

3.3 Probe Connections

1. The optimum probe configuration for weld toe applications consists of the following arrangement.

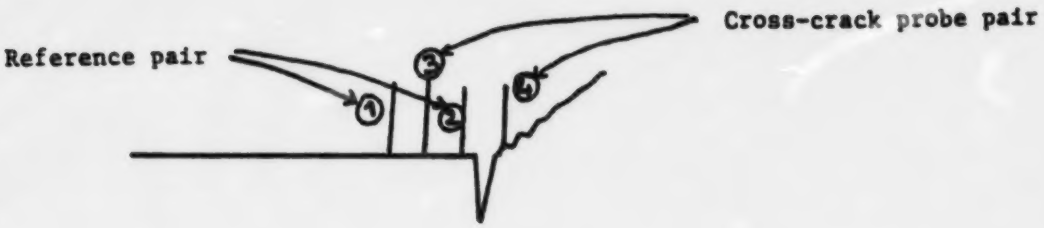

2. Probe No. 4 should be placed as close to the weld toe as possible, but should always straddle the crack. Probe No. 2 should be placed approximately 1 mm from the crack edge.
3. The optimum probe spacing is 10 mm for reference pair ((1) and (2)) and cross-crack probe pair ((3) and (4))
4. The worst case accuracy that can be expected from the probe spacing measurement is ± 1 mm.
5. The reference spacing can normally be measured quite easily. To measure the cross-crack spacing a strip of graph paper, or other methods should be used. The measured cross-crack spacing can also be checked by using the initial, no crack reading with the known reference spacing obtained from

$$\frac{V_r}{V_c} = \frac{\Delta_r}{\Delta_c}$$

where

V_r = reference voltages
V_c = cross-crack voltages
Δ_r = reference probe spacing
Δ_c = cross-crack probe spacing

This equation should only be used as a check on Δ_c; in all cases the measured values of Δ_r and Δ_c should be used.

6. Every attempt should be made to minimize the probe loop areas; this requires that the wires be laid as close to the metal surface as possible
7. Every care should be taken to ensure that the field wire does not interfere with the probe wires; a good check is to gently move the probe wires around. This should not result in any major change in the microgauge reading.

3.4 Instrument Setup

1. The balancing of the instrument is the most important feature to ensure accurate results.
2. The instrument should be balanced again in the following cases:

    (a) set-up new test
    (b) new material tested
    (c) field connections changed

3. The best and most accurate balancing technique is to measure the voltage near the crack using a hand held probe, i.e., at the reference site, and rotate the probe unit through 180°. The magnitude of the readings should be similar (within 2% difference).
4. The instrument is now balanced and balance should be confirmed by using the probe polarity switch.
5. The balance should also be checked at other locations of the weld.

3.5 Crack Depth Measurement

1. The crack depths can be interpreted from the following relationship:

$$\frac{V_c'}{V_r'} = \frac{\Delta_c + 2a}{\Delta_r}$$

where

$V_c' =$ cross-crack voltage

$V_r' =$ reference voltage

$\Delta_c =$ cross-crack probe spacing

$\Delta_r =$ reference probe spacing, and

$a =$ crack depth

2. Line contacts should be identified by looking at the cross-crack and reference voltage signals and the data in this region, approximately 2a on either side, should be ignored.
3. For cracks of high aspect ratios, corrections to account for the shape should be used.

APPENDIX 4

STRAIN GAUGE DATA SHEETS MEMORIAL AND WATERLOO

4M - MEMORIAL DATA
4W - WATERLOO DATA

Table M1 Data Sheet for Tubular T-Joint TA1

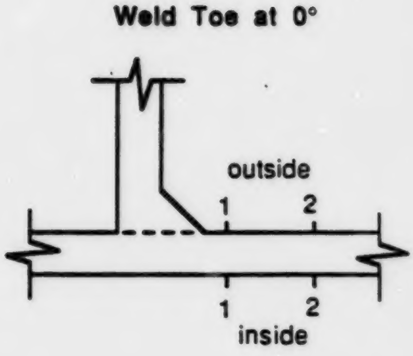

1. Specimen: TA1-Unstiffened
2. Mode of Loading: Axial
3. Maximum Load: 315.00 kN
4. Cross-sectional Area:
   $0.026144\ m^2$ (Nominal)
   $0.025960\ m^2$ (Measured & Computed)
5. Young's Modulus: 214.00 GPa
6. Strain Gauge Data at Hot Spot (Saddle) - Uncracked Section / Load: 315.00 kN

Gauge No. & Angular Position	Radial Strain ε_r ($\mu\varepsilon$)	Radial Stress σ_r (MPa)	Tangential Strain ε_θ ($\mu\varepsilon$)	Tangential Stress σ_θ (MPa)
1 (outside) - 0°	974.80	242.00	249.30	125.00
2 (outside) - 0°	489.70	128.10	218.00	84.22
1 (inside) - 0°	-669.30	-156.60	-30.57	-53.39
2 (inside) - 0°	-279.20	-66.78	-33.93	-27.16
31 (outside) - 180°	937.30	231.60	221.60	116.00
32 (outside) - 180°	506.70	132.20	220.00	85.86
31 (inside) - 180°	-748.10	-173.30	-10.03	-54.10
32 (inside) - 180°	-262.50	-62.39	-26.17	-24.21

7. Brace Strain Gauge Readings (at every 45°) / Load: 315.00 kN

Strain Gauge Readings ($\mu\varepsilon$)								Strain ($\mu\varepsilon$)		Stress (MPa)	
0°	45°	90°	135°	180°	225°	270°	315°	Average Measured Strain	Computed From Load	From Measured Strain	Computed From Load
65	56	46	66	80	63	42	54	59.00	56.30 Nominal Area	12.63	12.05 Nominal Area
									56.70 Computed Area		12.13 Computed Area

Table M1 Data Sheet for Tubular T-Joint TA1 (cont'd)

8. Extrapolated Hot Spot Stress at the Saddle Weld Toe (outside)	0°	298.25 MPa
	180°	280.58 MPa
9. Stress Concentration Factor (Nominal computed stress used)	0°	24.77
	180°	23.28
10. Extrapolated Stress on the Inside (below the hot spot on the outside)	0°	-201.04 MPa
	180°	-228.17 MPa
11. Extrapolated Hot Spot Bending Stress σ_b	0°	± 249.65 MPa
	180°	± 254.38 MPa
12. Extrapolated Hot Spot Membrane Stress σ_m	0°	48.60 MPa
	180°	26.20 MPa
13. Hot Spot Stress Range (R = 0.16)	0°	250.53 MPa
	180°	235.69 MPa
14. Extrapolated Hot Spot Strain at the Weld Toe (outside)	0°	1214.80 $\mu\varepsilon$
	180°	1150.34 $\mu\varepsilon$
15. Strain Concentration Factor (Nominal computed strain used)	0°	21.58
	180°	20.43
16. $\frac{\sigma_b}{(\sigma_b + \sigma_m)}$	0°	0.837
	180°	0.907
17. $\frac{\sigma_m}{(\sigma_b + \sigma_m)}$	0°	0.163
	180°	0.0934

Table M2 Data Sheet for Tubular T-Joint TA2

1. Specimen: TA2-Stiffened

2. Mode of Loading: Axial

3. Maximum Load: 1085.00 kN

4. Cross-sectional Area:
   0.026144 m^2 (Nominal)
   0.026256 m^2 (Measured & Computed)

5. Young's Modulus: 214.00 GPa

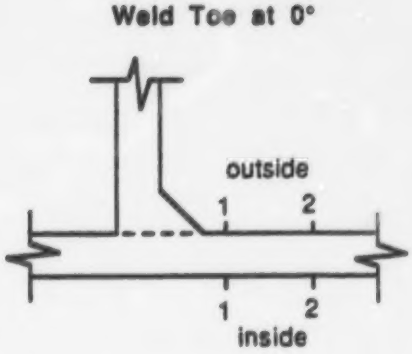

6. Strain Gauge Data at Hot Spot (Saddle) - Uncracked Section / Load: 950.00 kN

Gauge No. & Angular Position	Radial Strain ε_r ($\mu\varepsilon$)	Radial Stress σ_r (MPa)	Tangential Strain ε_θ ($\mu\varepsilon$)	Tangential Stress σ_θ (MPa)
1 (outside) - 0°	684.70	182.30	350.90	128.40
2 (outside) - 0°	263.50	81.60	300.50	87.60
1 (inside) - 0°	-301.90	-62.20	107.40	3.90
2 (inside) - 0°	47.20	18.60	110.70	28.80
36 (outside) - 180°	645.30	171.10	320.20	118.60
37 (outside) - 180°	277.20	83.30	279.30	83.60
36 (inside) - 180°	-245.90	-50.00	98.10	5.60
37 (inside) - 180°	60.10	31.60	111.70	29.90

7. Brace Strain Gauge Readings (at every 45°) / Load: 450.00 kN

Strain Gauge Readings ($\mu\varepsilon$)								Strain ($\mu\varepsilon$)		Stress (MPa)	
0°	45°	90°	135°	180°	225°	270°	315°	Average Measured Strain	Computed From Load	From Measured Strain	Computed From Load
- -	98.1	40.3	99.1	110.1	105.1	- -	- -	90.54	80.43 Nominal Area	19.38	17.21 Nominal Area
									80.09 Computed Area		17.14 Computed Area

Table M2 Data Sheet for Tubular T-Joint TA2 (cont'd)

8. Extrapolated Hot Spot Stress at the Saddle Weld Toe (outside)	0°	266.81 MPa
	180°	245.03 MPa
9. Stress Concentration Factor (Nominal computed stress used)	0°	6.43
	180°	5.90
10. Extrapolated Stress on the Inside (below the hot spot on the outside)	0°	-116.56 MPa
	180°	-97.56 MPa
11. Extrapolated Hot Spot Bending Stress σ_b	0°	± 191.76 MPa
	180°	± 171.30 MPa
12. Extrapolated Hot Spot Membrane Stress σ_m	0°	75.06 MPa
	180°	73.73 MPa
13. Hot Spot Stress Range (R = 0.05)	0°	253.47 MPa
	180°	232.78 MPa
14. Extrapolated Hot Spot Strain at the Weld Toe (outside)	0°	1020.00 $\mu\varepsilon$
	180°	945.00 $\mu\varepsilon$
15. Strain Concentration Factor (Nominal computed strain used)	0°	5.260
	180°	4.873
16. $\dfrac{\sigma_b}{(\sigma_b + \sigma_m)}$	0°	0.719
	180°	0.699
17. $\dfrac{\sigma_m}{(\sigma_b + \sigma_m)}$	0°	0.281
	180°	0.301

Table M3 Data Sheet for Tubular T-Joint TA3

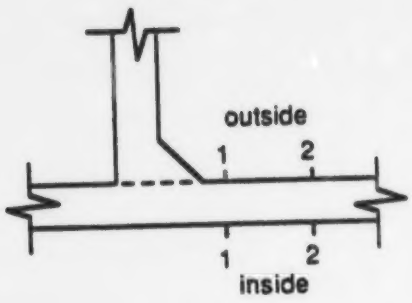
Weld Toe at 0°

1. Specimen: TA3-Stiffened
2. Mode of Loading: Axial
3. Maximum Load: 630.00 kN
4. Cross-sectional Area: 0.026144 m^2 (Nominal)
5. Young's Modulus: 214.00 GPa
6. Strain Gauge Data at Hot Spot (Saddle) - Uncracked Section / Load: 570.00 kN

Gauge No. & Angular Position	Radial Strain ε_r ($\mu\varepsilon$)	Radial Stress σ_r (MPa)	Tangential Strain ε_θ ($\mu\varepsilon$)	Tangential Stress σ_θ (MPa)
1 (outside) - 0°	469.90	122.20	199.30	78.50
2 (outside) - 0°	200.70	59.50	191.20	58.00
1 (inside) - 0°	-227.50	-47.40	74.10	1.30
2 (inside) - 0°	72.00	73.60	24.00	23.20
36 (outside) - 180°	414.10	109.20	197.30	74.20
37 (outside) - 180°	170.30	51.70	179.50	53.20
36 (inside) - 180°	-214.80	-44.90	67.70	0.80
37 (inside) - 180°	68.30	71.40	20.70	21.20

7. Brace Strain Gauge Readings / Load: 630.00 kN

(Computed from Load and Nominal Area)

Strain ($\mu\varepsilon$)	Stress (MPa)
112.604	24.10

Table M3 Data Sheet for Tubular T-Joint TA3 (cont'd)

8. Extrapolated Hot Spot Stress at the Saddle Weld Toe (outside)	0°	169.35 MPa
	180°	152.14 MPa
9. Stress Concentration Factor (Nominal computed stress used)	0°	7.03
	180°	6.31
10. Extrapolated Stress on the Inside (below the hot spot on the outside)	0°	-118.56 MPa
	180°	-113.22 MPa
11. Extrapolated Hot Spot Bending Stress σ_b	0°	± 143.96 MPa
	180°	± 132.68 MPa
12. Extrapolated Hot Spot Membrane Stress σ_m	0°	25.39 MPa
	180°	19.46 MPa
13. Hot Spot Stress Range ($R = 0.05$)	0°	160.88 MPa
	180°	144.53 MPa
14. Extrapolated Hot Spot Strain at the Weld Toe (outside)	0°	666.57 $\mu\varepsilon$
	180°	591.01 $\mu\varepsilon$
15. Strain Concentration Factor (Nominal computed strain used)	0°	5.919
	180°	5.249
16. $\dfrac{\sigma_b}{(\sigma_b + \sigma_m)}$	0°	0.850
	180°	0.872
17. $\dfrac{\sigma_m}{(\sigma_b + \sigma_m)}$	0°	0.150
	180°	0.128

Table M4 Data Sheet for Tubular T-Joint TA4

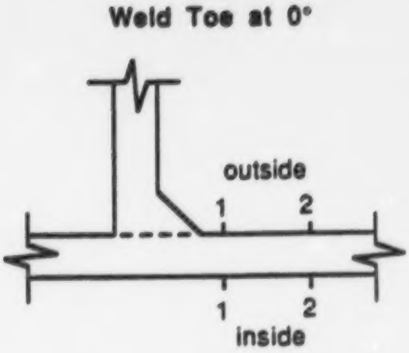

1. Specimen: TA4-Stiffened
2. Mode of Loading: Axial
3. Maximum Load: 1125.00 kN
4. Cross-sectional Area: 0.026144 m^2 (Nominal)
5. Young's Modulus: 214.00 GPa
6. Strain Gauge Data at Hot Spot (Saddle) - Uncracked Section / Load: 975.00 kN

Gauge No. & Angular Position	Radial Strain ε_r ($\mu\varepsilon$)	Radial Stress σ_r (MPa)	Tangential Strain ε_θ ($\mu\varepsilon$)	Tangential Stress σ_θ (MPa)
1 (outside) - 0°	674.50	176.50	301.20	116.20
2 (outside) - 0°	281.30	86.90	317.40	92.70
1 (inside) - 0°	-402.60	-83.80	131.80	2.50
2 (inside) - 0°	21.80	14.10	131.00	31.70
36 (outside) - 180°	698.80	185.40	348.40	128.80
37 (outside) - 180°	293.70	89.80	318.30	93.80
36 (inside) - 180°	-364.40	-76.00	117.00	1.80
37 (inside) - 180°	67.50	23.80	119.10	32.20

7. Brace Strain Gauge Readings / Load: 1125.00 kN

(Computed from Load and Nominal Area)

Strain ($\mu\varepsilon$)	Stress (MPa)
201.079	43.03

Table M4 Data Sheet for Tubular T-Joint TA4 (cont'd)

8. Extrapolated Hot Spot Stress at the Saddle Weld Toe (outside)	0°	254.80 MPa
	180°	268.80 MPa
9. Stress Concentration Factor (Nominal computed stress used)	0°	5.92
	180°	6.25
10. Extrapolated Stress on the Inside (below the hot spot on the outside)	0°	-152.56 MPa
	180°	-144.67 MPa
11. Extrapolated Hot Spot Bending Stress σ_b	0°	± 203.69 MPa
	180°	± 206.59 MPa
12. Extrapolated Hot Spot Membrane Stress σ_m	0°	51.11 MPa
	180°	61.91 MPa
13. Hot Spot Stress Range (R = 0.05)	0°	242.06 MPa
	180°	255.36 MPa
14. Extrapolated Hot Spot Strain at the Weld Toe (outside)	0°	1002.73 $\mu\varepsilon$
	180°	1037.57 $\mu\varepsilon$
15. Strain Concentration Factor (Nominal computed strain used)	0°	4.987
	180°	5.160
16. $\frac{\sigma_b}{(\sigma_b + \sigma_m)}$	0°	0.799
	180°	0.769
17. $\frac{\sigma_m}{(\sigma_b + \sigma_m)}$	0°	0.201
	180°	0.231

Table M5 Data Sheet for Tubular T-Joint TA5

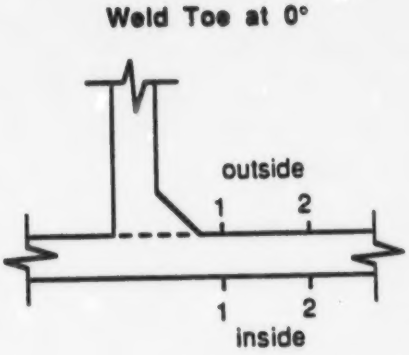

1. Specimen: TA5-Stiffened
2. Mode of Loading: Axial
3. Maximum Load: 660.00 kN
4. Cross-sectional Area:
   0.026144 m^2 (Nominal)
5. Young's Modulus: 214.00 GPa
6. Strain Gauge Data at Hot Spot (Saddle) - Uncracked Section / Load: 660.00 kN

Gauge No. & Angular Position	Radial Strain ε_r ($\mu\varepsilon$)	Radial Stress σ_r (MPa)	Tangential Strain ε_θ ($\mu\varepsilon$)	Tangential Stress σ_θ (MPa)
1 (outside) - 0°	460.70	121.10	213.20	81.10
2 (outside) - 0°	185.50	56.30	194.00	57.60
1 (inside) - 0°	-251.20	-52.60	77.90	0.60
2 (inside) - 0°	54.40	17.80	76.00	21.30
36 (outside) - 180°	504.30	131.70	220.60	85.80
37 (outside) - 180°	193.80	58.00	191.20	57.50
36 (inside) - 180°	-242.60	-53.00	43.40	-6.80
37 (inside) - 180°	21.70	9.30	62.30	15.90

7. Brace Strain Gauge Readings / Load: 660.00 kN

(Computed from Load and Nominal Area)

Strain ($\mu\varepsilon$)	Stress (MPa)
117.97	25.25

Table M6 Data Sheet for Tubular T-Joint TA5 (cont'd)

8. Extrapolated Hot Spot Stress at the Saddle Weld Toe (outside)	0°	151.16 MPa
	180°	168.16 MPa
9. Stress Concentration Factor (Nominal computed stress used)	0°	5.99
	180°	6.66
10. Extrapolated Stress on the Inside (below the hot spot on the outside)	0°	-87.43 MPa
	180°	-83.82 MPa
11. Extrapolated Hot Spot Bending Stress σ_b	0°	± 119.30 MPa
	180°	± 125.99 MPa
12. Extrapolated Hot Spot Membrane Stress σ_m	0°	31.86 MPa
	180°	42.17 MPa
13. Hot Spot Stress Range (R = 0.05)	0°	143.60 MPa
	180°	159.75 MPa
14. Extrapolated Hot Spot Strain at the Weld Toe (outside)	0°	597.16 $\mu\varepsilon$
	180°	657.92 $\mu\varepsilon$
15. Strain Concentration Factor (Nominal computed strain used)	0°	5.062
	180°	5.577
16. $\dfrac{\sigma_b}{(\sigma_b + \sigma_m)}$	0°	0.789
	180°	0.749
17. $\dfrac{\sigma_m}{(\sigma_b + \sigma_m)}$	0°	0.211
	180°	0.251

4W - TB1

STRAIN GAUGE RESULTS AND EXPERIMENTAL STRESSES (ALL RESULTS AT MAXIMUM LOAD)

SPECIMEN: TB1
UNSTIFFENED T-JOINT
MODE OF LOADING: In-Plane Bending
APPLIED LOAD: 171 KN-m

Gauge No.	Radial Strain ϵ_r $\times 10^{-6}$	Tangential Strain ϵ_θ $\times 10^{-6}$	Shear Strain $\gamma_{r\theta}$ $\times 10^{-6}$	Radial Stress σ_r MPa	Tangential Stress σ_θ MPa	Shear Stress $\sigma_{r\theta}$ MPa	σ_θ / σ_r
7	-321	-31.6	13.6	-74.2	-22.9	1.1	0.31
8	-26.7	-79.3	15.8	-11.6	-20.1	1.3	1.7
9	285	-239	26.3	49.2	-35.4	2.1	0.72
10	294	-345	18.2	43.7	-59.3	1.5	1.4
35	357	-11.6	0	81.6	22.0	0	0.27
36	54.4	68	0	17.3	19.4	0	1.12
43	805	437	-2.5	216	157	-0.2	0.73
44	544	417	-10.9	154	134	-0.9	0.87
45	269	304	0	83.2	88.7	0	1.07
46	207	170	0	59.5	53.6	0	0.91
71	-797	-445	-7.4	-215	-158	-0.6	0.74
72	-534	-419	-12.9	-152	-134	-1.1	0.88
75	89.8	107	-10.5	28.1	30.9	-0.8	1.1
76	304	241	-14.0	86.8	76.7	-1.1	0.9
79	-96.8	-121	-10.5	-30.7	-34.6	-0.8	1.1
80	-376	-252	-13.4	-104	-84.1	-1.1	0.81
82	297	–	–	61.4	–	–	–
84	-297	–	–	-61.4	–	–	–

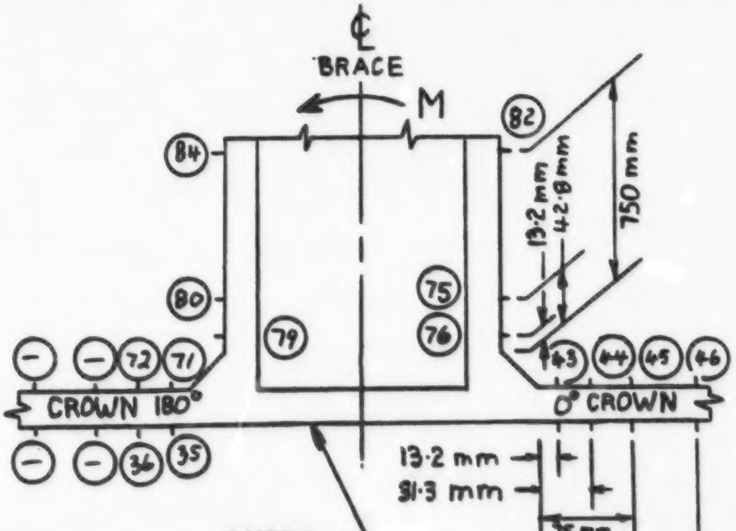
℄
BRACE
M
82
84
13·2 mm
42·8 mm
750 mm
80
75
79
76
–
–
72
71
43
44
45
46
CROWN 180°
0° CROWN
–
–
36
35
13·2 mm
91·3 mm
75 mm
150 mm
CHORD
7
8
9
10

STRAIN GAUGE RESULTS AND EXPERIMENTAL STRESSES (ALL RESULTS AT MAXIMUM LOAD)

SPECIMEN: TB1
UNSTIFFENED T-JOINT
MODE OF LOADING: In-Plane Bending
APPLIED LOAD: 171 KN-m

Gauge No.	Radial Strain ϵ_r $\times 10^{-6}$	Tangential Strain ϵ_θ $\times 10^{-6}$	Shear Strain $\gamma_{r\theta}$ $\times 10^{-6}$	Radial Stress σ_r MPa	Tangential Stress σ_θ MPa	Shear Stress $\sigma_{r\theta}$ MPa	σ_θ/σ_r
1	-72.9	28.4	-1578	-14.9	1.47	-128	–
2	-18.6	-12.6	-1514	-5.2	-4.2	-123	–
32	38.9	23.9	1549	10.6	8.2	126	–
33	10.5	12.3	1497	3.3	3.6	121	–
34	0	0	1227	0	0	99.1	–
37	49.8	15.8	197	12.6	7.0	15.9	–
38	41	16.8	170	10.6	6.7	13.8	–
68	-72.5	-17.2	-207	-17.9	-8.9	-16.7	–
69	-12.8	-6.6	-169	-10.8	-4.7	-13.7	–
70	0	0	-279	0	0	-22.5	–
73	0	0	131	0	0	10.6	–
74	24.2	24.2	248	7.3	7.3	20.1	–
77	-10.5	-27.7	-142	-4.3	-7.1	-11.4	–
78	-48.4	-3.9	-252	-11.4	-4.2	-20.3	–
81	0	–	–	0	–	–	–
83	0	–	–	0	–	–	–

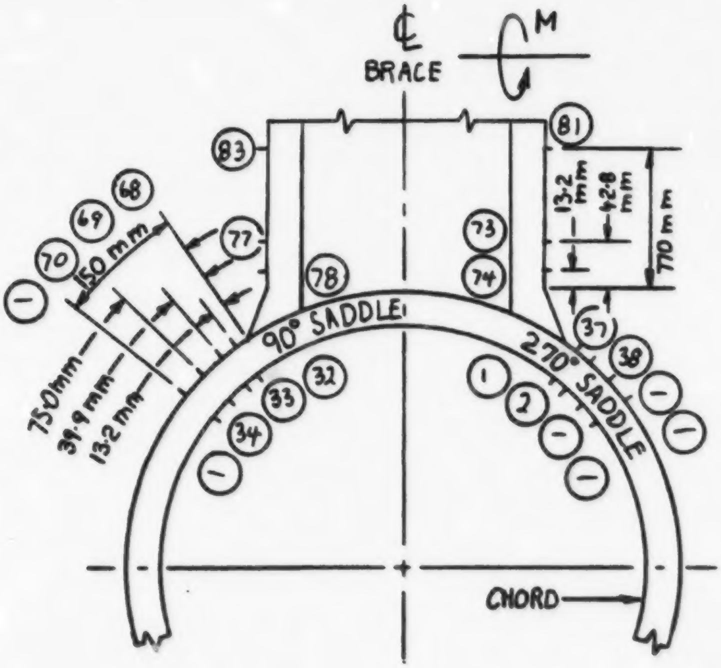

℄ BRACE
M
83
81
68
69
70
150 mm
77
78
73
74
13.2 mm
42.8 mm
110 mm
90° SADDLE
270° SADDLE
37
38
75.0mm
39.9mm
13.2mm
32
33
34
1
2
CHORD
℄

STRAIN GAUGE RESULTS AND EXPERIMENTAL STRESSES (ALL RESULTS AT MAXIMUM LOAD)

SPECIMEN: TB1
UNSTIFFENED T-JOINT
MODE OF LOADING: Out-of-Plane Bending
APPLIED LOAD: 13.6 KN-m

Gauge No.	Radial Strain ϵ_r $\times 10^{-6}$	Tangential Strain ϵ_θ $\times 10^{-6}$	Shear Strain $\gamma_{r\theta}$ $\times 10^{-6}$	Radial Stress σ_r MPa	Tangential Stress σ_θ MPa	Shear Stress $\sigma_{r\theta}$ MPa	σ_θ / σ_r
1	-239	-7.5	8.9	-55.7	-18.3	.72	0.33
2	-132	0.3	-1.6	-30.3	-9.04	-0.1	0.30
32	249	5.1	0	57.7	18.4	0	0.32
33	139	-1.0	-5.9	32	9.4	-0.5	0.30
34	50.8	-11.4	-5.8	10.9	0.9	-0.5	0.10
37	289	67	-4.2	71.4	35.5	0	0.49
38	183	67	-2.3	46.8	28.2	-0.2	0.60
68	-291	-79	-1.8	-72.2	-38.3	-0.2	0.53
69	-193	-66	0	-49.1	-28.6	0	0.58
70	-99.6	-57	0	-26.9	-20	0	0.74
73	25.6	37.4	0	8.5	10.4	0	1.22
74	100	49	0	26.6	18.3	0	0.69
77	-45	-39.5	0	-13.2	-12.3	0	0.93
78	-124	-60	0	-32.8	-22.4	0	0.68
81	24	–	–	4.9	–	–	–
83	-24	–	–	-4.9	–	–	–

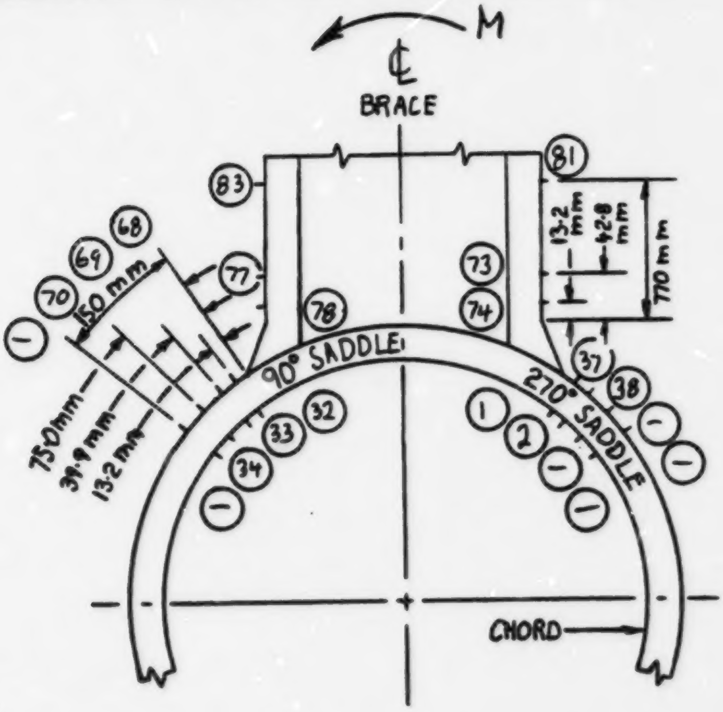
M
℄
BRACE
81
83
68
69
70
77
78
73
74
150 mm
13.2 mm
42.8 mm
770 mm
90° SADDLE
270° SADDLE
750mm
39.9mm
13.2mm
32
33
34
37
38
1
2
CHORD

STRAIN GAUGE RESULTS AND EXPERIMENTAL STRESSES (ALL RESULTS AT MAXIMUM LOAD)

SPECIMEN: TB1
UNSTIFFENED T-JOINT
MODE OF LOADING: Out-of-Plane Bending
APPLIED LOAD: 13.6 KN-m

Gauge No.	Radial Strain ϵ_r $\times 10^{-6}$	Tangential Strain ϵ_θ $\times 10^{-6}$	Shear Strain $\gamma_{r\theta}$ $\times 10^{-6}$	Radial Stress σ_r MPa	Tangential Stress σ_θ MPa	Shear Stress $\sigma_{r\theta}$ MPa	σ_θ / σ_r
7	0.8	0.4	50.8	0.2	0.2	4.11	–
8	-0.2	1.2	56	0	0	4.5	–
9	-1.2	0.8	65	0	0	5.3	–
10	0	0	65.2	0	0	5.3	–
35	0	0	-50.4	0	0	-4.1	–
36	0	0	-55	0	0	-4.5	–
43	0	0	-44	0	0	-3.6	–
44	0	0	-33	0	0	-2.7	–
45	0	0	-16	0	0	-1.3	–
46	0	0	0	0	0	0	–
71	0	0	41.3	0	0	3.3	–
72	0	0	31.5	0	0	2.6	–
75	0	0	-29	0	0	-2.3	–
76	0	0	-41.3	0	0	-3.3	–
79	–	–	–	–	–	–	–
80	0	0	45.2	0	0	3.7	–
82	0	–	–	0	–	–	–
84	0	–	–	0	–	–	–

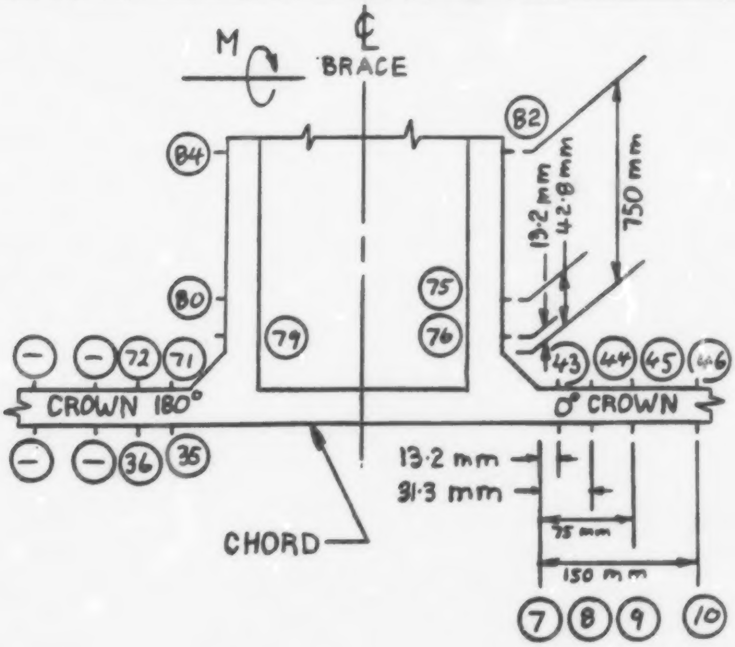
M
℄
BRACE
82
84
13·2 mm
42·8 mm
750 mm
80
75
79
76
—
—
72
71
43
44
45
46
CROWN 180°
0° CROWN
—
—
36
35
13·2 mm
31·3 mm
75 mm
150 mm
CHORD
7
8
9
10

STRAIN GAUGE RESULTS AND EXPERIMENTAL STRESSES (ALL RESULTS AT MAXIMUM LOAD)

SPECIMEN: TB1
UNSTIFFENED T-JOINT
MODE OF LOADING: AXIAL
APPLIED LOAD: 89 KN

Gauge No.	Radial Strain ϵ_r $\times 10^{-6}$	Tangential Strain ϵ_θ $\times 10^{-6}$	Shear Strain $\gamma_{r\theta}$ $\times 10^{-6}$	Radial Stress σ_r MPa	Tangential Stress σ_θ MPa	Shear Stress $\sigma_{r\theta}$ MPa	σ_θ / σ_r
1	-188	-3.6	0	-43.7	-13.9	0	0.32
2	-73.1	-1.6	0	-17.0	-5.4	0	0.32
32	-210	-1.3	0	-48.7	-14.9	0	0.31
33	-818	0	0	-20.2	-6.1	0	0.30
34	11.9	3.7	0	3.0	1.7	0	0.57
37	249	65	0	62	32.3	0	0.52
38	138	60.4	0	36.0	23.5	0	0.65
68	273	73.7	0	68	35.9	0	0.53
69	155	66.2	0	40.4	26	0	0.64
70	53.2	46.1	0	15.5	14.3	0	0.92
73	31.5	30.5	0	9.4	9.2	0	0.98
74	89.6	50.1	0	24.1	17.8	0	0.74
77	39.3	39.5	0	11.8	11.8	0	1.0
78	116	62.8	0	31.2	22.6	0	0.72
81	16.4	-4.9	0	3.4	0	0	0
83	16.4	-4.9	0	3.4	0	0	0

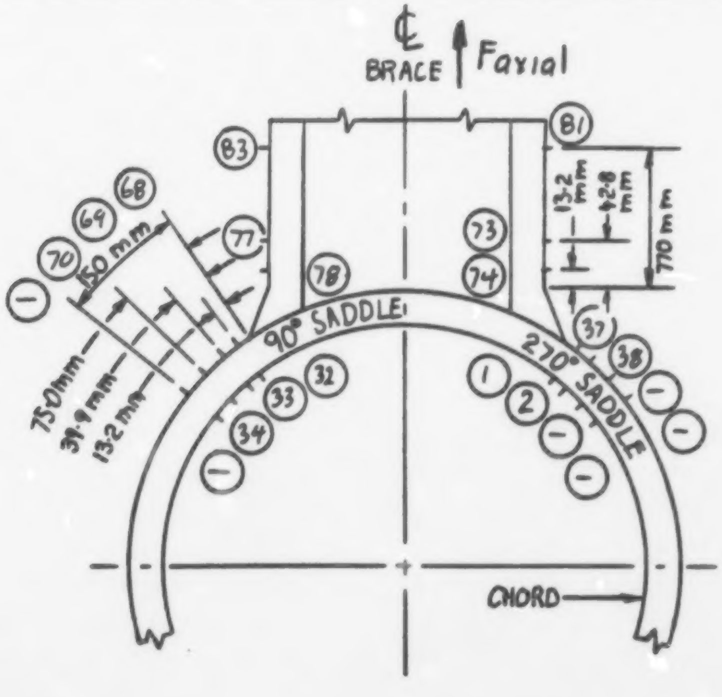
℄ BRACE
Faxial
83
81
68
69
70
150 mm
77
73
74
78
13.2 mm
42.8 mm
110 mm
90° SADDLE
270° SADDLE
37
38
75.0mm
39.9 mm
13.2 mm
32
33
34
1
2
CHORD

STRAIN GAUGE RESULTS AND EXPERIMENTAL STRESSES (ALL RESULTS AT MAXIMUM LOAD)

SPECIMEN: TB1
UNSTIFFENED T-JOINT
MODE OF LOADING: AXIAL
APPLIED LOAD: 89 KN

Gauge No.	Radial Strain ϵ_r $\times 10^{-6}$	Tangential Strain ϵ_θ $\times 10^{-6}$	Shear Strain $\gamma_{r\theta}$ $\times 10^{-6}$	Radial Stress σ_r MPa	Tangential Stress σ_θ MPa	Shear Stress $\sigma_{r\theta}$ MPa	σ_θ / σ_r
7	29.9	-14.8	0	5.9	1.4	0	70.24
8	42	-22.6	0	8.1	-2.3	0	0.28
9	101	-86.6	0	17.3	-12.9	0	0.75
10	53.4	-54.9	0	8.6	-8.94	0	1.04
35	28	-16.2	0	5.3	-1.79	0	0.34
36	40	-21.6	0	7.7	-2.22	0	0.29
43	86	14.7	1.9	20.9	9.3	0.2	0.45
44	79	16.3	0	19.4	9.2	0	0.47
45	70.7	19.2	0	17.7	9.3	0	0.53
46	64.2	24.6	0	16.5	10.1	0	0.61
71	98.3	16.8	0	23.9	10.7	0	0.45
72	84.5	17.9	0	20.7	10.0	0	0.48
75	-7.9	13.8	0	-0.9	2.6	0	2.9
76	3.9	14.7	0	1.9	3.7	0	1.9
79	-3.9	9.8	0	-0.2	2.0	0	-
80	12.8	17.7	0	4.2	5.0	0	1.2
82	16.4	-4.9	0	3.4	0	–	0
84	16.4	-4.9	0	3.4	0	0	0

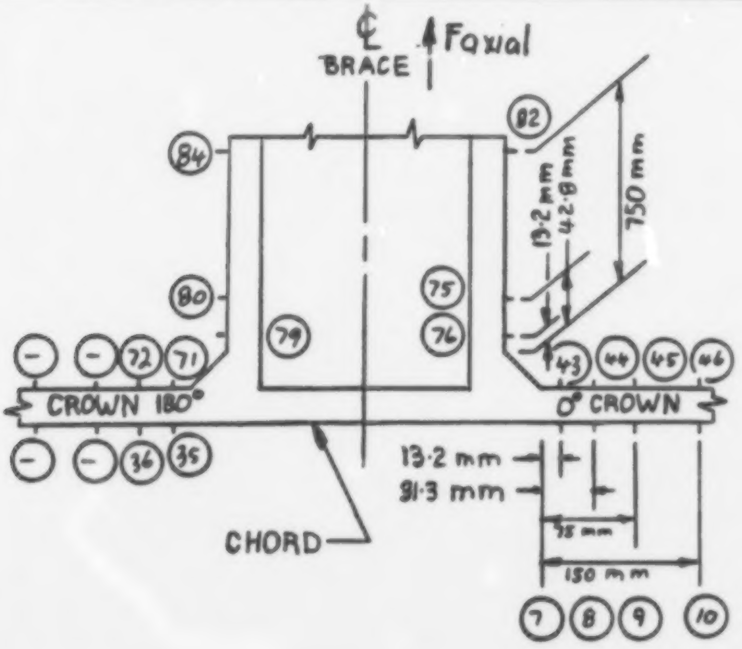

℄ BRACE
F axial
82
84
750 mm
13.2 mm
42.8 mm
80
75
79
76
–
–
72
71
43
44
45
46
CROWN 180°
0° CROWN
–
–
36
35
13.2 mm
31.3 mm
75 mm
150 mm
CHORD
7
8
9
10

4W - TB2

STRAIN GAUGE RESULTS AND EXPERIMENTAL STRESSES (ALL RESULTS AT MAXIMUM LOAD)

SPECIMEN: TB2
RING STIFFENED T-JOINT
MODE OF LOADING: In-Plane Bending
APPLIED LOAD: 236 KN-m

Gauge No.	Radial Strain ϵ_r $\times10^{-6}$	Tangential Strain ϵ_θ $\times10^{-6}$	Shear Strain $\gamma_{r\theta}$ $\times10^{-6}$	Radial Stress σ_r MPa	Tangential Stress σ_θ MPa	Shear Stress $\sigma_{r\theta}$ MPa	σ_θ/σ_r
3	-350	89.4	22.5	-74.5	-3.6	1.8	0.05
4	-26.7	-79.3	15.8	-11.6	-20.1	1.3	1.73
5	287	-219	0	54.0	-20.7	0	0.38
6	296	-287	0	48.3	-45.8	0	0.95
42	372	-185	0	73.1	17.0	0	0.23
53	763	443	0	207	155	0	0.75
54	462	416	0	136	128	0	0.94
55	189	277	0	62.8	77.0	0	1.23
56	169	99.3	0	45.9	34.6	0	0.75
100	-700	-419	0	-191	-145	0	0.76
108	350	295	0	101	92.5	0	0.92
109	124	144	0	38.6	41.9	0	1.1
124	-350	-295	0	-101	-92.5	0	0.92
126	397	–	–	82.1	–	–	–
128	-430	–	–	88.9	0	–	–

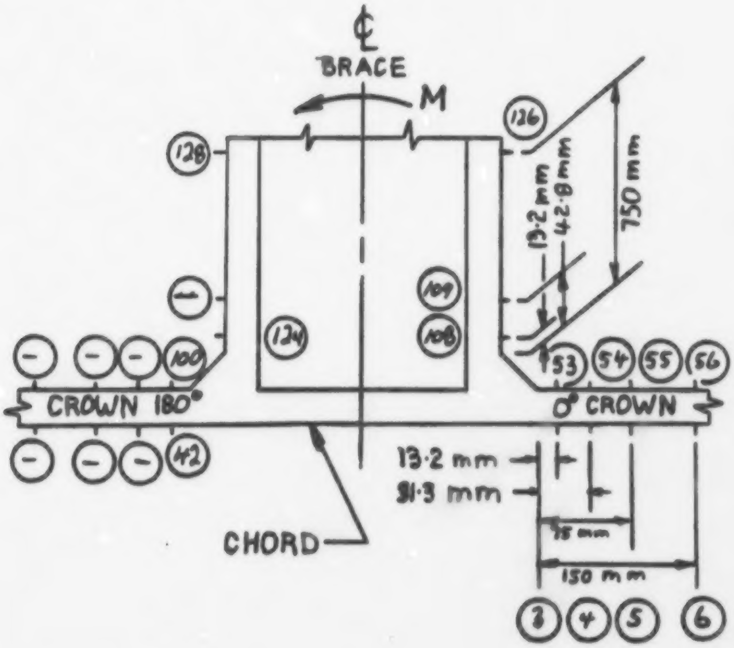
℄
BRACE
M
126
128
750 mm
13·2 mm
42·8 mm
109
108
124
–
–
–
–
100
53
54
55
56
CROWN 180°
0° CROWN
–
–
–
42
13·2 mm
31·3 mm
75 mm
150 mm
CHORD
3
4
5
6

STRAIN GAUGE RESULTS AND EXPERIMENTAL STRESSES (ALL RESULTS AT MAXIMUM LOAD)

SPECIMEN: TB2
RING STIFFENED T-JOINT
MODE OF LOADING: In-Plane Bending
APPLIED LOAD: 236 KN-m

Gauge No.	Radial Strain ϵ_r $\times 10^{-6}$	Tangential Strain ϵ_θ $\times 10^{-6}$	Shear Strain $\gamma_{r\theta}$ $\times 10^{-6}$	Radial Stress σ_r MPa	Tangential Stress σ_θ MPa	Shear Stress $\sigma_{r\theta}$ MPa	σ_θ/σ_r
1	0	0	-1101	0	0	-89	–
39	0	0	1061	0	0	85.7	–
40	0	0	1081	0	0	88	–
41	0	0	1017	0	0	82	–
51	0	0	-478	0	0	-37	–
97	0	0	459	0	0	37	–
98	0	0	415	0	0	33.6	–
99	0	0	442	0	0	35.7	–
106	0	0	-207	0	0	16.7	–
125	0	0	–	0	0	–	–
127	0	–	–	0	–	–	–
122	0	0	212	0	0	17.2	–
123	0	0	97	0	0	7.8	–

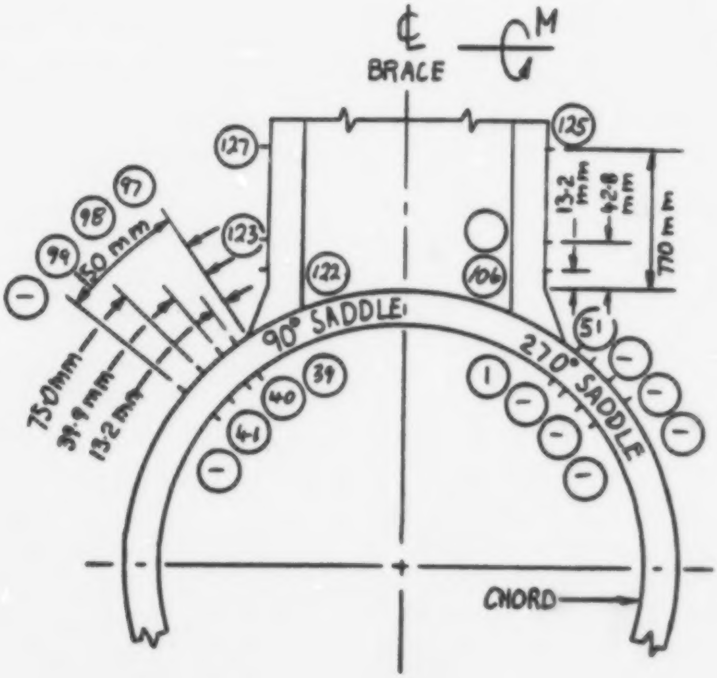

℄
BRACE
M
127
125
97
98
99
–
150 mm
123
122
106
13.2 mm
42.8 mm
110 mm
90° SADDLE
270° SADDLE
51
75.0mm
39.9 mm
13.2 mm
39
40
41
1
–
CHORD

STRAIN GAUGE RESULTS AND EXPERIMENTAL STRESSES (ALL RESULTS AT MAXIMUM LOAD)

SPECIMEN: TB2
STIFFENED T-JOINT
MODE OF LOADING: In-Plane Bending
APPLIED LOAD: 236 KN-m

Gauge No.	Radial Strain ϵ_r $\times 10^{-6}$	Tangential Strain ϵ_θ $\times 10^{-6}$	Shear Strain $\gamma_{r\theta}$ $\times 10^{-6}$	Radial Stress σ_r MPa	Tangential Stress σ_θ MPa	Shear Stress $\sigma_{r\theta}$ MPa	σ_θ / σ_r
43	255	–	–	52.7	–	–	–
44	682	–	–	141	–	–	–
45	661	–	–	137	–	–	–
46	-37.6	–	–	-7.8	–	–	–
47	-427	–	–	-88.3	–	–	–
48	-395	–	–	-81.6	–	–	–
49	669	–	–	138	–	–	–
50	252	–	–	52	–	–	–
82	380	25	-84	69.4	32	-6.8	0.36
101	-81	-163	110	-30	-43.2	8.9	1.44
102	-97.7	-149	191	-32.9	-41.2	15.4	1.25
103	66	53.4	188	18.9	16.9	15.2	0.89
104	84	61	-180	24	20.0	14.6	0.83
135	729	–	–	151	–	–	–
136	704	–	–	146	–	–	–

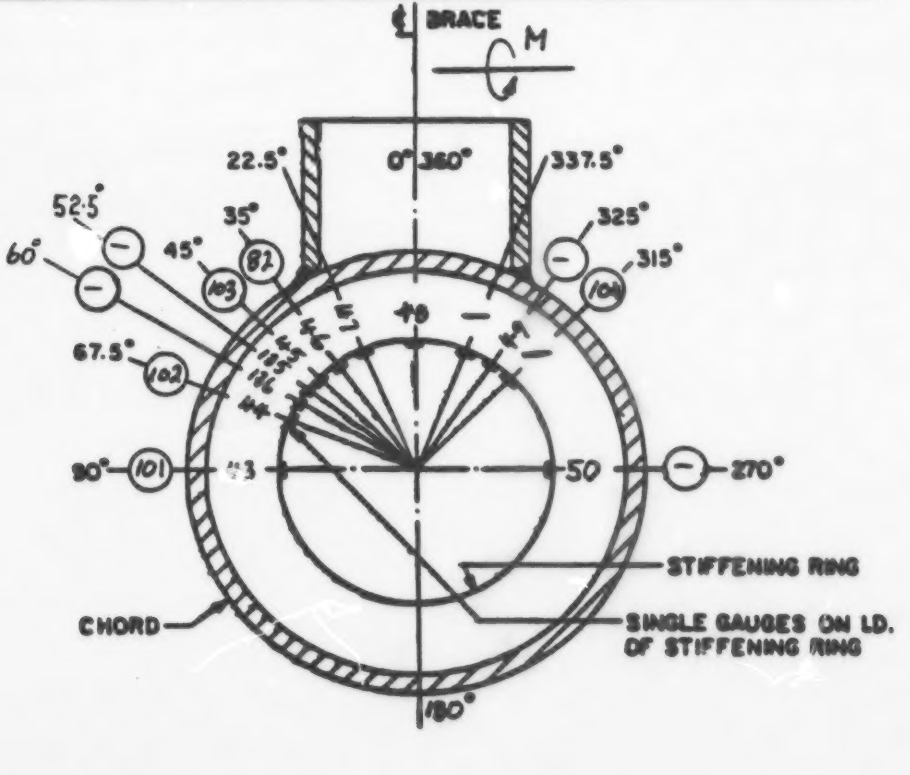
℄ BRACE
M
22.5°
0° 360°
337.5°
52.5°
60°
45°
35°
82
103
325°
315°
104
47
46
45
135
136
44
48
49
67.5°
102
90°
101
43
50
270°
STIFFENING RING
CHORD
SINGLE GAUGES ON I.D. OF STIFFENING RING
180°

STRAIN GAUGE RESULTS AND EXPERIMENTAL STRESSES (ALL RESULTS AT MAXIMUM LOAD)

SPECIMEN: TB2
RING STIFFENED T-JOINT
MODE OF LOADING: AXIAL
APPLIED LOAD: 133 KN

Gauge No.	Radial Strain ϵ_r $\times10^{-6}$	Tangential Strain ϵ_θ $\times10^{-6}$	Shear Strain $\gamma_{r\theta}$ $\times10^{-6}$	Radial Stress σ_r MPa	Tangential Stress σ_θ MPa	Shear Stress $\sigma_{r\theta}$ MPa	σ_θ/σ_r
1	-46.1	15.8	-5.9	-9.54	0.45	-0.5	0
39	-50.2	18.9	-4.1	-10.3	0.9	-0.3	0
40	8.2	19.3	4.7	3.2	5.0	0.4	1.56
41	33.2	23.6	5.1	9.3	7.8	0.4	2.84
51	94	41.2	-1.3	24.5	16	-0.1	0.65
97	94	47	3.0	24.9	17.3	0.2	0.7
98	38.5	44.9	1.9	11.9	13.0	0.2	1.1
99	5.4	32.3	0.9	3.5	7.8	0.1	2.2
106	29	24.6	1.2	8.4	7.7	0.1	0.92
122	36.8	29.5	5.7	10.5	9.4	0.5	0.90
123	9.2	11.8	4.5	2.9	3.4	0.4	1.17
125	24	–	–	5.1	–	–	–
127	28.5	–	–	5.1	–	–	–

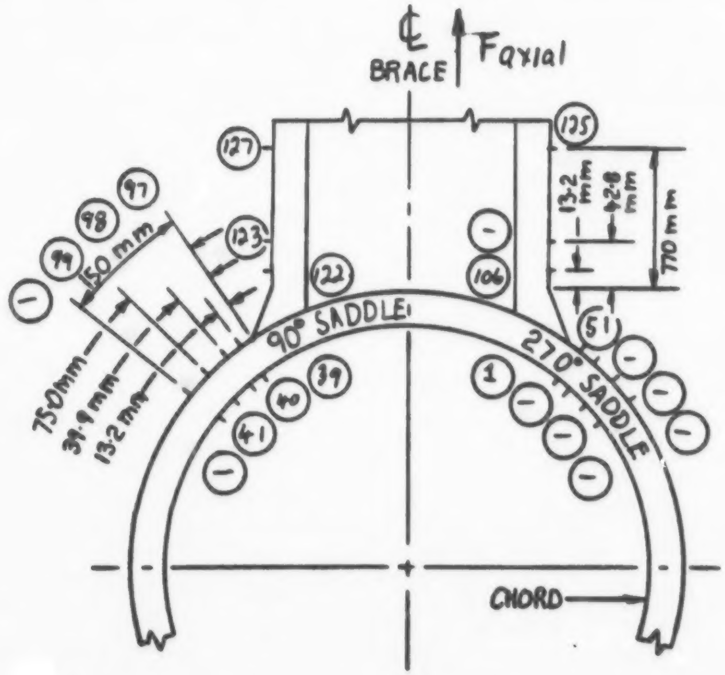
℄
BRACE
Faxial
127
125
97
98
99
50 mm
123
122
106
13.2 mm
42.8 mm
110 mm
51
90° SADDLE
270° SADDLE
75.0mm
39.9mm
13.2mm
1
39
40
41
CHORD

STRAIN GAUGE RESULTS AND EXPERIMENTAL STRESSES (ALL RESULTS AT MAXIMUM LOAD)

SPECIMEN: TB2
RING STIFFENED T-JOINT
MODE OF LOADING: AXIAL
APPLIED LOAD:133 KN

Gauge No.	Radial Strain ϵ_r $\times 10^{-6}$	Tangential Strain ϵ_θ $\times 10^{-6}$	Shear Strain $\gamma_{r\theta}$ $\times 10^{-6}$	Radial Stress σ_r MPa	Tangential Stress σ_θ MPa	Shear Stress $\sigma_{r\theta}$ MPa	σ_θ / σ_r
3	19.2	-3.2	3.0	4.21	0.6	-0.24	0
4	38.3	-10.8	-3.4	8.1	0.2	-0.3	0
5	55.3	-24.1	0.8	11.1	-1.73	0.1	0.16
6	51.2	-31.8	-2.0	9.61	-3.8	-0.2	0.40
42	25.2	4.5	0	6.12	2.8	0	0.46
53	77	19	-10	19.1	9.7	-0.1	0.51
54	60.4	16.5	-8.2	15.1	8.0	-0.7	0.53
55	46.0	7.0	-7.4	11.1	4.8	-0.6	0.43
56	45.7	-1.4	-4.7	10.5	2.9	-0.4	0.28
100	73.6	16.6	-4.2	18.1	8.9	-0.3	0.50
108	27.6	23.6	2.3	8.0	7.4	0.2	0.93
109	-2.6	15.7	-4.5	0.5	3.5	-0.4	–
124	21	23.6	-2.3	6.5	6.9	-0.2	1.06
126	22·5	–	–	5.1	–	–	–
128	22·5	–	0	5.1	0	0	–

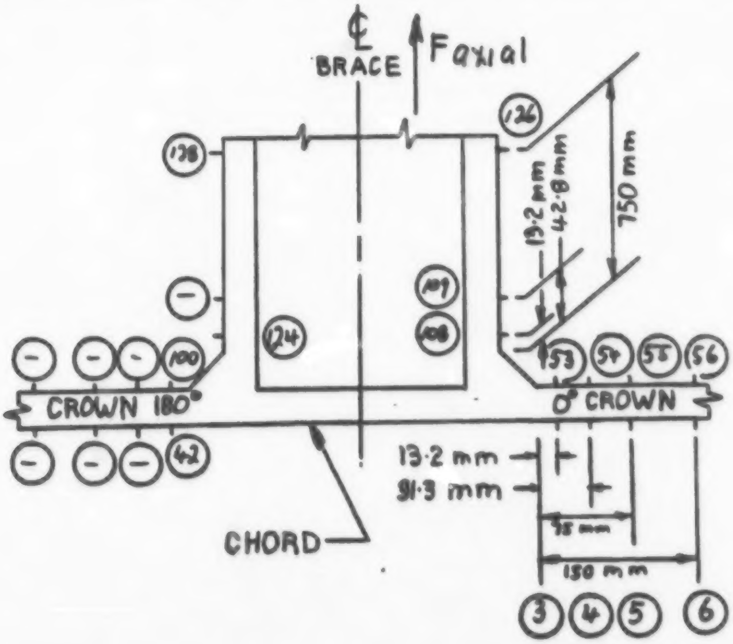

℄ BRACE
Faxial
126
128
750 mm
13·2 mm
42·8 mm
109
108
124
100
42
53
54
55
56
CROWN 180°
0° CROWN
13·2 mm
91·3 mm
75 mm
150 mm
CHORD
3
4
5
6

STRAIN GAUGE RESULTS AND EXPERIMENTAL STRESSES (ALL RESULTS AT MAXIMUM LOAD)

SPECIMEN: TB2
RING STIFFENED T-JOINT
MODE OF LOADING: AXIAL
APPLIED LOAD: 133 KN

Gauge No.	Radial Strain ϵ_r $\times 10^{-6}$	Tangential Strain ϵ_θ $\times 10^{-6}$	Shear Strain $\gamma_{r\theta}$ $\times 10^{-6}$	Radial Stress σ_r MPa	Tangential Stress σ_θ MPa	Shear Stress $\sigma_{r\theta}$ MPa	σ_θ / σ_r
43	147	–	–	30.3	–	–	–
44	148	–	–	30.6	–	–	–
45	37.6	–	–	7.8	–	–	–
46	-97.3	–	–	-20.1	–	–	–
47	-136	–	–	-28.2	–	–	–
48	-121	–	–	-25.0	–	–	–
49	41.8	–	–	5.2	–	–	–
50	147	–	–	30.4	–	–	–
82	51.3	18.5	-27	13.1	7.8	-2.2	0.60
101	-27.2	-22.6	-10.2	-7.9	-7.1	-0.8	0.90
102	-22	-6.9	-13.6	-4.6	-0.1	-1.1	0
103	4.9	44.3	-2.3	4.2	10.6	-0.2	2.52
104	5.9	39.3	7.9	4.1	9.5	0.6	2.3

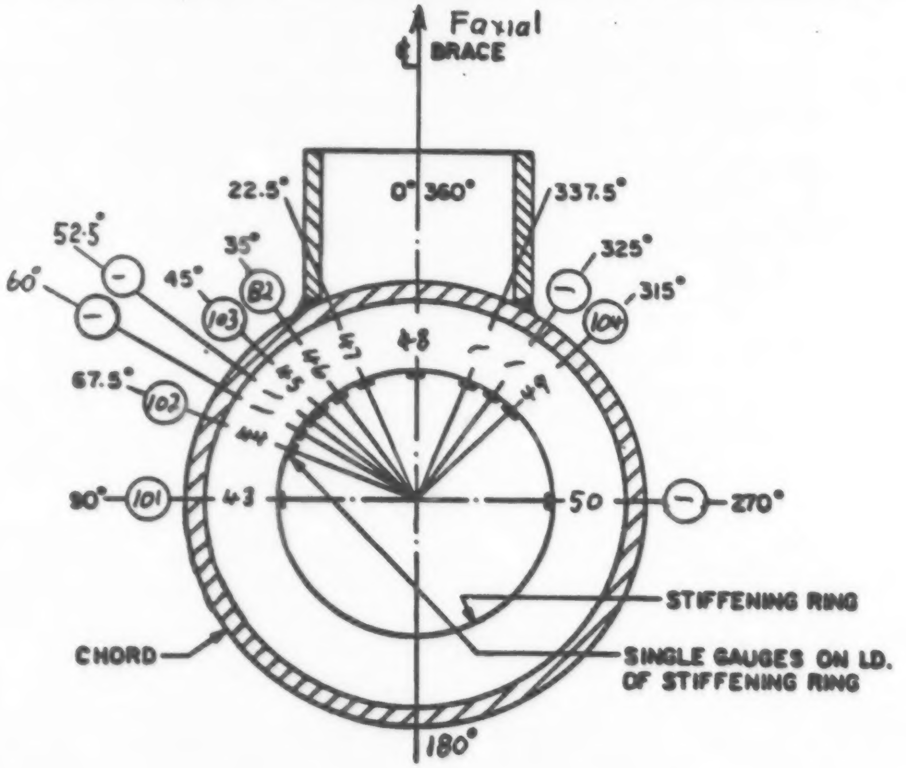
Faxial
℄ BRACE
22.5°
0° 360°
337.5°
52.5°
60°
45°
35°
82
103
325°
315°
104
48
47
46
45
49
67.5°
102
44
90°
101
43
50
270°
STIFFENING RING
CHORD
SINGLE GAUGES ON I.D. OF STIFFENING RING
180°

4W - TB3

STRAIN GAUGE RESULTS AND EXPERIMENTAL STRESSES (ALL RESULTS AT MAXIMUM LOAD)

SPECIMEN: TB3
STIFFENED T-JOINT
MODE OF LOADING: In-Plane Bending
APPLIED LOAD: 149 KN-m

Gauge No.	Radial Strain ϵ_r $\times 10^{-6}$	Tangential Strain ϵ_θ $\times 10^{-6}$	Shear Strain $\gamma_{r\theta}$ $\times 10^{-6}$	Radial Stress σ_r MPa	Tangential Stress σ_θ MPa	Shear Stress $\sigma_{r\theta}$ MPa	σ_θ / σ_r
3	-268	79	0	-55	-0.3	0	0
4	-53.2	18.8	17.8	-11	0	1.4	0
5	189	-107	-4.7	36.3	-11.5	0	0.32
6	–	–	–	–	–	–	–
53	526	295	0	140	103	0	0.74
54	348	283	10.5	99.9	89.5	0	0.9
55	127	192	9.4	42.6	53.2	0.8	1.25
56	110	69.4	6.9	30.1	23.6	0.6	0.78
126	253	–	–	54	–	–	–
128	271	–	–	54	–	–	–
142	463	286	0	125	96.5	0	0.77
143	272	272	0	80.3	80.3		

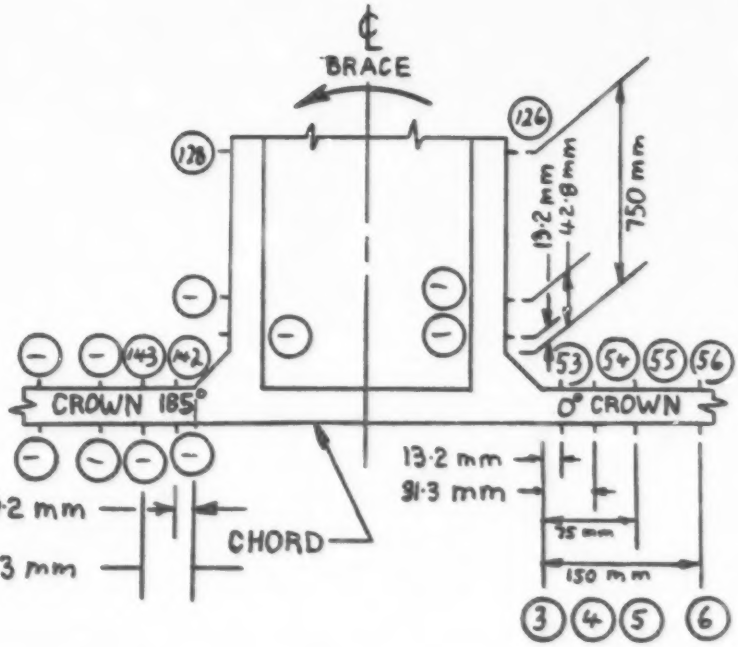
℄
BRACE
128
126
750 mm
13·2 mm
42·8 mm
143
142
53
54
55
56
CROWN 185°
0° CROWN
13·2 mm
91·3 mm
75 mm
150 mm
20·2 mm
38·3 mm
CHORD
3
4
5
6

STRAIN GAUGE RESULTS AND EXPERIMENTAL STRESSES (ALL RESULTS AT MAXIMUM LOAD)

SPECIMEN: TB3
STIFFENED T-JOINT
MODE OF LOADING: In-Plane Bending
APPLIED LOAD: 149 KN-m

Gauge No.	Radial Strain ϵ_r $\times 10^{-6}$	Tangential Strain ϵ_θ $\times 10^{-6}$	Shear Strain $\gamma_{r\theta}$ $\times 10^{-6}$	Radial Stress σ_r MPa	Tangential Stress σ_θ MPa	Shear Stress $\sigma_{r\theta}$ MPa	σ_θ/σ_r
44	424	–	–	87.6	–	–	–
45	428	–	–	88.5	–	–	–
46	-24	–	–	-5	–	–	–
47	-263	–	–	-54.4	–	–	–
48	-231	–	–	-47.7	–	–	–
49	415	–	–	85.8	–	–	–
82	238	5.9	32	55.3	17.8	2.6	0.32
102	-75	-89.5	-135	-23.4	-25.8	-11	1.1
103	38	37.4	-131	11.4	11.3	-10.6	1.0
104	41.6	32.5	125	11.9	10.4	10.1	0.87
135	495	–	–		–	–	–
136	484	–	–		–	–	–

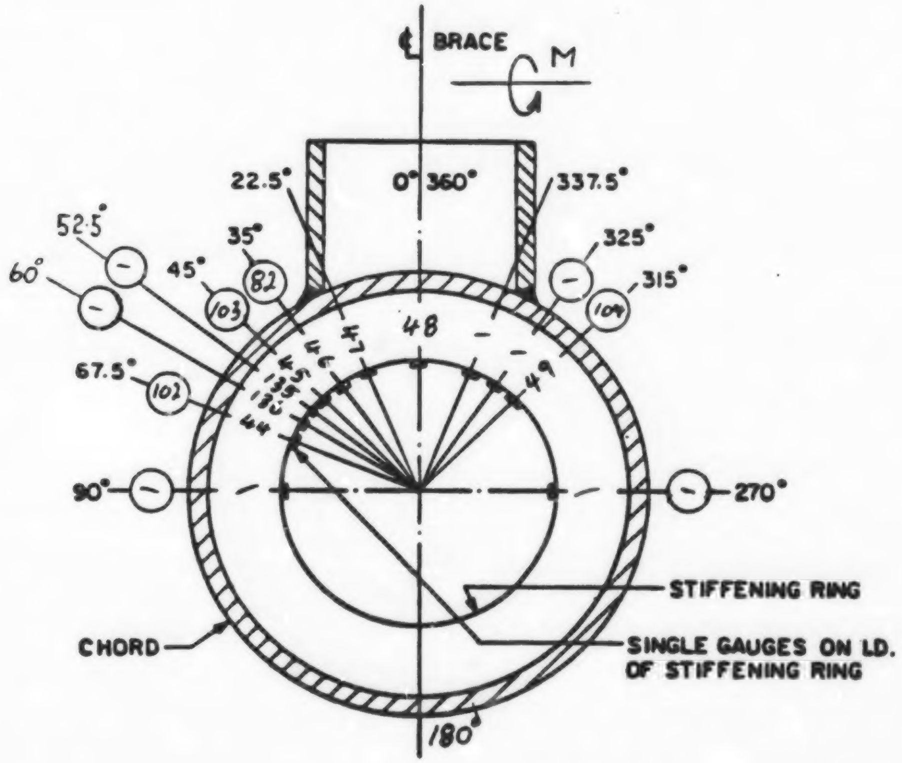
℄ BRACE
M
22.5°
0° 360°
337.5°
52.5°
35°
325°
60°
45°
82
103
104
315°
48
47
46
45
135
136
44
49
67.5°
102
90°
270°
STIFFENING RING
CHORD
SINGLE GAUGES ON I.D. OF STIFFENING RING
180°

4W - TB4

STRAIN GAUGE RESULTS AND EXPERIMENTAL STRESSES (ALL RESULTS AT MAXIMUM LOAD)

SPECIMEN: TB4
STIFFENED T-JOINT
MODE OF LOADING: Out-of-Plane Bending
APPLIED LOAD: 164 KN-m

Gauge No.	Radial Strain ϵ_r $\times10^{-6}$	Tangential Strain ϵ_θ $\times10^{-6}$	Shear Strain $\gamma_{r\theta}$ $\times10^{-6}$	Radial Stress σ_r MPa	Tangential Stress σ_θ MPa	Shear Stress $\sigma_{r\theta}$ MPa	σ_θ/σ_r
1	-861	-146	-49	-209	-93.2	-4.0	0.45
2	-460	-10.4	12.3	-107	-34.2	-1.0	
33	878	145	0	209	92.8	0	0.44
34	450	129	0	110	60	0	0.55
35	186	31	-7.2	45.1	20.0	-0.6	0.44
36	57.7	-129	0	4.3	-25.9	0	6.0
71	368	167	-18	96.5	64	-1.45	0.66
72	183	61.8	6.5	46.4	26.9	0.53	0.58
80	386	108	3.6	96.7	51.6	0.3	0.53
81	-17.4	78.5	-4.1	1.5	16.9	0	11.3
107	-402	-72.9	-29	-97.9	-44.7	-2.3	0.46
108	34.9	-52.7	5.4	4.4	-9.75	0.44	2.2
109	230	4.5	22.4	53.5	16.9	1.8	-0.32
110	237	126	14.2	63.5	45.6	1.2	0.72
140	-245	–	–	-50.6	–	–	–
142	282	–	–	58.3	–	–	–

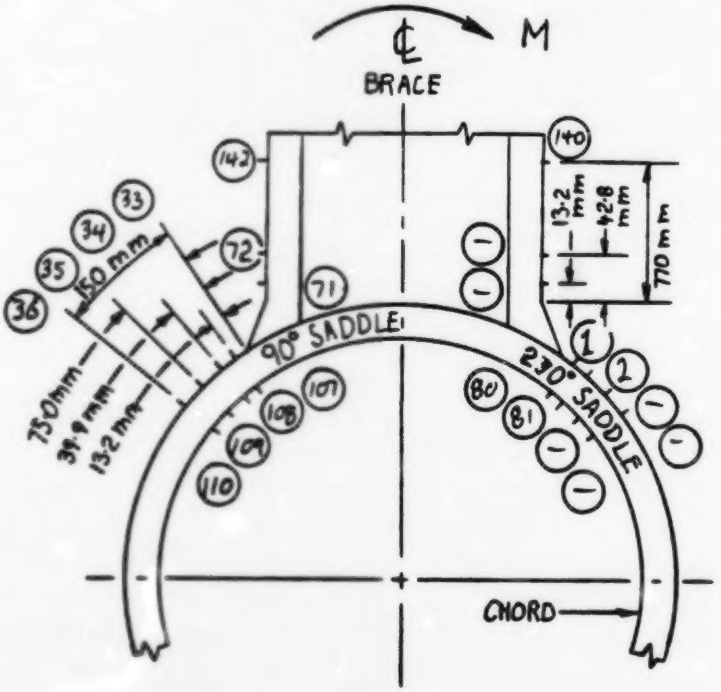
M
℄
BRACE
142
140
33
34
35
36
150 mm
72
71
13.2 mm
42.8 mm
770 mm
90° SADDLE
230° SADDLE
1
2
80
81
107
108
109
110
75.0mm
39.9mm
13.2mm
CHORD

STRAIN GAUGE RESULTS AND EXPERIMENTAL STRESSES (ALL RESULTS AT MAXIMUM LOAD)

SPECIMEN: TB4
STIFFENED T-JOINT
MODE OF LOADING: Out-of-Plane Bending
APPLIED LOAD: 164 KN-m

Gauge No.	Radial Strain ϵ_r $\times10^{-6}$	Tangential Strain ϵ_θ $\times10^{-6}$	Shear Strain $\gamma_{r\theta}$ $\times10^{-6}$	Radial Stress σ_r MPa	Tangential Stress σ_θ MPa	Shear Stress $\sigma_{r\theta}$ MPa	σ_θ/σ_r
3	16.7	9.9	12.1	4.5	3.5	1.0	–
4	13.8	9.9	-7	3.8	3.2	-0.6	–
5	6.0	7.7	-22	1.9	2.2	-1.7	–
41	10.1	9.9	-12	3.04	3.0	-1.0	–
42	9.4	11.3	12.3	2.9	3.3	1.0	–
57	25.6	29.9	162	7.7	8.7	13.1	–
58	171	69.8	-61.6	44.3	27.9	-5.0	–
82	16.2	11.1	-129	4.5	3.6	-10.4	–
83	16.2	16.2	-146	4.9	4.8	-11.8	–
84	21.7	16.9	-146	6.2	5.4	-11.8	–
115	23	14.5	131	6.4	5.0	10.6	–
116	20	20.3	149	6.0	6.1	12.1	–
141	24.2	–	–	5.0	–	–	–
143	9.7	–	–	2.0	–	–	–
144	12.1	-8.9	-151	2.2	-1.2	-12.2	–
145	9.9	-4.8	-101	1.9	-0.4	-8.2	–

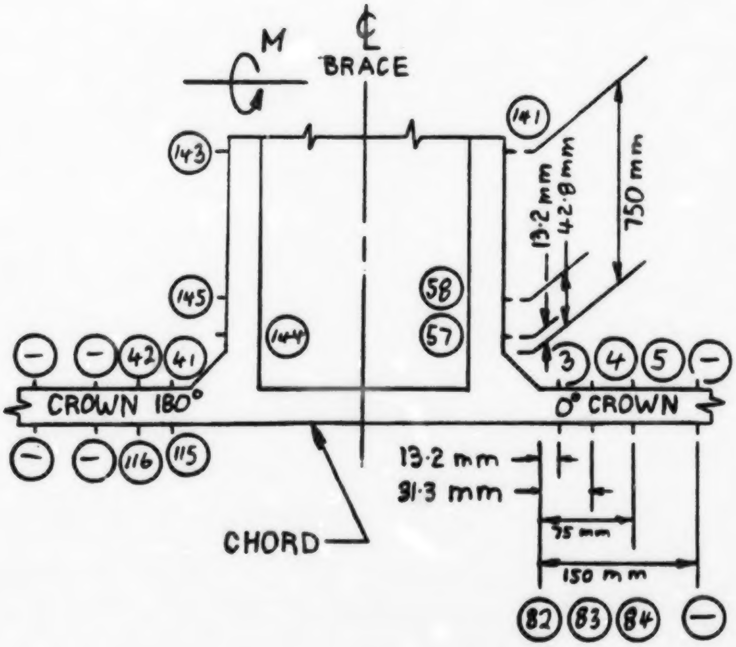
M
℄ BRACE
141
143
750 mm
42.8 mm
13.2 mm
145
58
144
57
–
–
42
41
3
4
5
–
CROWN 180°
0° CROWN
–
–
116
115
13.2 mm
31.3 mm
75 mm
150 mm
CHORD
82
83
84
–

STRAIN GAUGE RESULTS AND EXPERIMENTAL STRESSES (ALL RESULTS AT MAXIMUM LOAD)

SPECIMEN: TB4
STIFFENED T-JOINT
MODE OF LOADING: Out-of-Plane Bending
APPLIED LOAD: 164 KN-m

Gauge No.	Radial Strain ϵ_r $\times 10^{-6}$	Tangential Strain ϵ_θ $\times 10^{-6}$	Shear Strain $\gamma_{r\theta}$ $\times 10^{-6}$	Radial Stress σ_r MPa	Tangential Stress σ_θ MPa	Shear Stress $\sigma_{r\theta}$ MPa	σ_θ / σ_r
46	195	-117	159	101	5.8	12.8	0
75	265	146	-48.3	71.3	52	-3.9	0.73
76	83.1	85	41.1	25.1	25.4	3.3	1.01
77	-44.4	-13.8	23.4	-11.2	-6.3	1.9	0.56
78	-242	-122	-52.2	-64.2	-44.9	-4.3	0.70
79	58	28.7	19.3	15.5	10.7	1.6	0.69
128	-324	–	–	-67	–	–	–
129	825	–	–	171	–	–	–
130	-11.4	–	–	-2.4	–	–	–
131	-1398	–	–	-289	–	–	–
132	-1476	–	–	-305	–	–	–
133	-794	–	–	-164	–	–	–
134	-30.4	–	–	-6.3	–	–	–
135	383	–	–	79.1	–	–	–
146	1461	–	–	302	–	–	–
147	1345	–	–	278	–	–	–

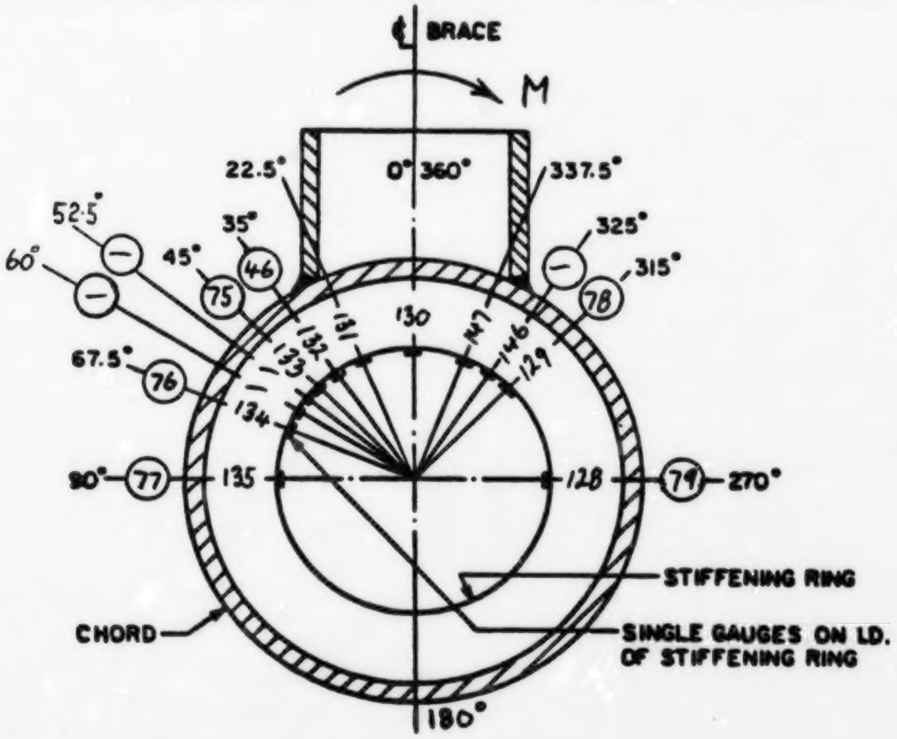

℄ BRACE
M
22.5°
0° 360°
337.5°
52.5°
35°
325°
60°
45°
46
315°
75
78
130
131
132
133
147
146
129
67.5°
76
134
90°
77
135
128
79
270°
STIFFENING RING
CHORD
SINGLE GAUGES ON I.D. OF STIFFENING RING
180°

STRAIN GAUGE RESULTS AND EXPERIMENTAL STRESSES (ALL RESULTS AT MAXIMUM LOAD)

SPECIMEN: TB4
STIFFENED T-JOINT
MODE OF LOADING: AXIAL
APPLIED LOAD: 88.9 KN

Gauge No.	Radial Strain ϵ_r $\times 10^{-6}$	Tangential Strain ϵ_θ $\times 10^{-6}$	Shear Strain $\gamma_{r\theta}$ $\times 10^{-6}$	Radial Stress σ_r MPa	Tangential Stress σ_θ MPa	Shear Stress $\sigma_{r\theta}$ MPa	σ_θ/σ_r
1	63.5	27	1.0	16.5	10.6	0.1	0.64
2	25.7	26.3	-1.4	7.7	7.8	-0.1	1.0
33	67.7	29	0	17.3	11.2	0	0.65
34	27.7	27	0	8.1	8.0	0	1.0
35	4.1	19.0	-1.4	2.3	4.7	-0.11	2.01
36	-8.5	2.0	-2.8	-1.8	-0.1	-0.2	0
71	26.2	20.6	-2.8	7.53	6.6	0.2	0.88
72	6.9	7.1	-1.6	2.1	2.1	-0.1	1.0
80	-32.8	8.7	-1.5	-6.9	-0.3	-0.1	0
81	1.7	8.4	0.3	0.9	2.1	0	2.3
107	-38	10.6	-1.7	-8.0	-0.2	-0.1	0
108	3.4	9.6	2.6	1.4	2.4	0.2	1.7
109	22.2	11.9	3.3	6.0	4.3	0.3	0.72
110	22.2	14.4	3.6	6.1	4.9	0.3	0.8
140	15	–	–	3.1	–	–	–
142	18	–	–	3.7	–	–	–

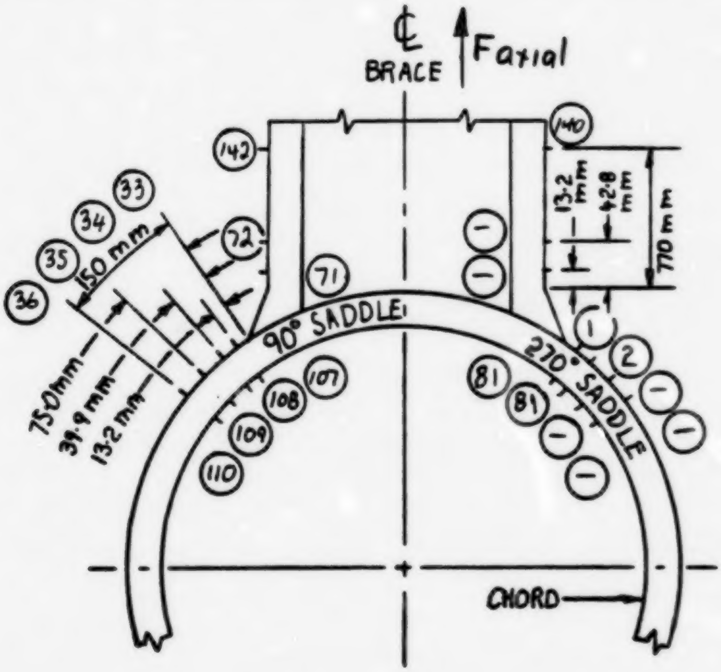

℄
BRACE
Faxial
142
140
33
34
35
36
150 mm
72
71
13.2 mm
42.8 mm
110 mm
90° SADDLE
270° SADDLE
75.0mm
39.9mm
13.2mm
107
108
109
110
81
81
1
2
CHORD

STRAIN GAUGE RESULTS AND EXPERIMENTAL STRESSES (ALL RESULTS AT MAXIMUM LOAD)

SPECIMEN: TB4
STIFFENED T-JOINT
MODE OF LOADING: AXIAL
APPLIED LOAD: 88.9 KN

Gauge No.	Radial Strain ϵ_r $\times 10^{-6}$	Tangential Strain ϵ_θ $\times 10^{-6}$	Shear Strain $\gamma_{r\theta}$ $\times 10^{-6}$	Radial Stress σ_r MPa	Tangential Stress σ_θ MPa	Shear Stress $\sigma_{r\theta}$ MPa	σ_θ/σ_r
3	46.4	11.3	3.0	11.5	5.8	0.2	0.5
4	37.2	10.5	2.8	9.3	5.0	0.2	0.54
5	27.3	5.0	1.7	6.7	3.0	0.1	0.45
41	49.8	11.5	-0.1	12.3	6.1	0	0.50
42	37.3	10.4	5.9	9.3	4.9	0.5	0.53
57	14.7	16.3	0.2	4.5	4.8	0	1.07
58	-1.9	9.3	0.7	0.2	2.01	0	–
82	8.1	-1.6	-1.0	1.77	0.2	-0.1	0
83	20.4	-5.9	-1.7	4.3	0	-0.14	0
84	33.4	-15.0	-2.6	6.7	-1.2	-0.2	0.2
115	10.6	-2.7	-0.6	2.3	0.11	0	0
116	21.7	-7.3	1.2	4.5	-0.2	0.1	0
141	16.5	–	–	3.36	–	–	–
143	16.5	–	–	3.36	–	–	–
144	10.2	13.7	0.8	3.3	3.9	0	1.2
145	-1.7	8.7	-0.7	0.21	1.9	0	–

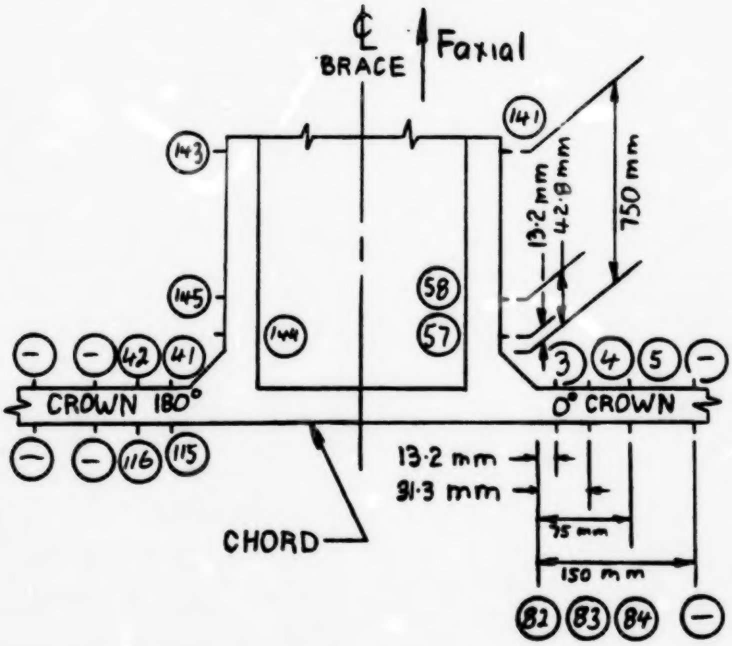
℄ BRACE
Faxial
141
143
750 mm
13·2 mm
42·8 mm
145
58
144
57
−
−
42
41
3
4
5
−
CROWN 180°
0° CROWN
−
−
116
115
13·2 mm
31·3 mm
75 mm
CHORD
150 mm
82
83
84
−

STRAIN GAUGE RESULTS AND EXPERIMENTAL STRESSES (ALL RESULTS AT MAXIMUM LOAD)

SPECIMEN: TB4
STIFFENED T-JOINT
MODE OF LOADING: AXIAL
APPLIED LOAD: 88.9 KN

Gauge No.	Radial Strain ϵ_r $\times 10^{-6}$	Tangential Strain ϵ_θ $\times 10^{-6}$	Shear Strain $\gamma_{r\theta}$ $\times 10^{-6}$	Radial Stress σ_r MPa	Tangential Stress σ_θ MPa	Shear Stress $\sigma_{r\theta}$ MPa	σ_θ / σ_r
46	34	11.5	17.2	8.64	5.0	1.39	0.58
75	4.1	25.3	-2.4	2.7	6.12	-0.2	2.3
76	-16.1	3.8	7.1	-3.45	-0.24	0.57	0
77	-19.6	-14.3	5.5	-5.5	-4.7	0.5	0.85
78	3.1	24.6	3.0	2.4	5.9	0.3	2.5
79	-19.3	-14.2	-8.5	-5.4	-4.6	-0.7	0.85
128	100	–	–	20.7	–	–	–
129	30	–	–	6.2	–	–	–
130	-78.6	–	–	16.2	–	–	–
131	-95.4	–	–	19.7	–	–	–
132	Defective	–	–	–	–	–	–
133	25	–	–	5.2	–	–	–
134	99.4	–	–	20.5	–	–	–
135	95.8	–	–	19.8	–	–	–
146	-73	–	–	15.1	–	–	–
147	-82	–	–	17.0	–	–	–

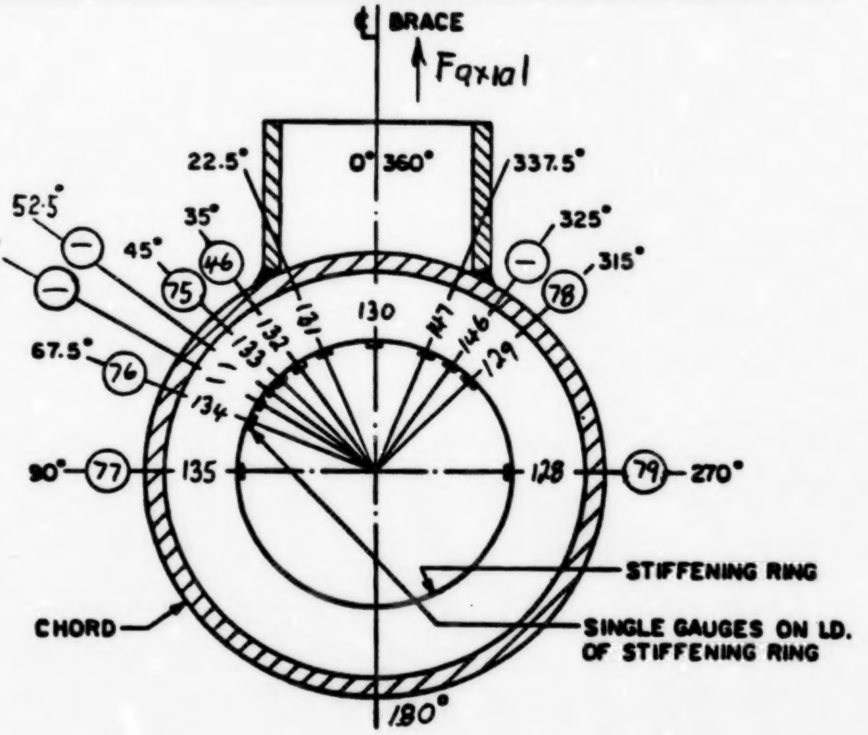
℄ BRACE
Faxial
22.5°
0° 360°
337.5°
52.5°
60°
45°
35°
46
75
325°
315°
78
131
132
133
130
147
146
129
67.5°
76
134
90°
77
135
128
79
270°
STIFFENING RING
CHORD
SINGLE GAUGES ON I.D. OF STIFFENING RING
180°

4W - TB5

STRAIN GAUGE RESULTS AND EXPERIMENTAL STRESSES (ALL RESULTS AT MAXIMUM LOAD)

SPECIMEN: TB5
STIFFENED T-JOINT
MODE OF LOADING: Out-of-Plane Bending
APPLIED LOAD: 110 KN-m

Gauge No.	Radial Strain ϵ_r $\times 10^{-6}$	Tangential Strain ϵ_θ $\times 10^{-6}$	Shear Strain $\gamma_{r\theta}$ $\times 10^{-6}$	Radial Stress σ_r MPa	Tangential Stress σ_θ MPa	Shear Stress $\sigma_{r\theta}$ MPa	σ_θ/σ_r
1	-563	-107	-55	-137.2	-63.6	-4.4	0.46
2	-289	-86	-8.2	-72.6	-39.9	-0.7	0.55
33	551	97.5	3.4	133.8	60.6	0.3	0.45
34	281	77.5	2.7	70.2	37.3	0.2	0.53
35	108	6.8	5.7	25.5	9.1	0.5	0.36
36	37	-97.5	5.5	1.8	-19.9	0.4	–
71	254	111	-3.7	66.2	43	-0.3	0.65
72	128	56.2	-6.8	33.5	21.8	-0.5	0.65
80	15.3	52.5	-3.7	0	11.0	0.3	–
81	230	62	1.77	57.4	30.3	0.1	0.53
107	-219	-52.8	9.9	-54.2	-27.4	0.8	0.51
108	35.2	37.8	18.1	5.5	-6.3	1.5	1.15
109	174	6.9	4.5	40.5	13.6	0.4	0.34
110	139	73.5	6.8	37.2	26.6	0.6	0.72
140	-181	–	–	37.7	–	–	–
142	183	–	–	37.7	–	–	–

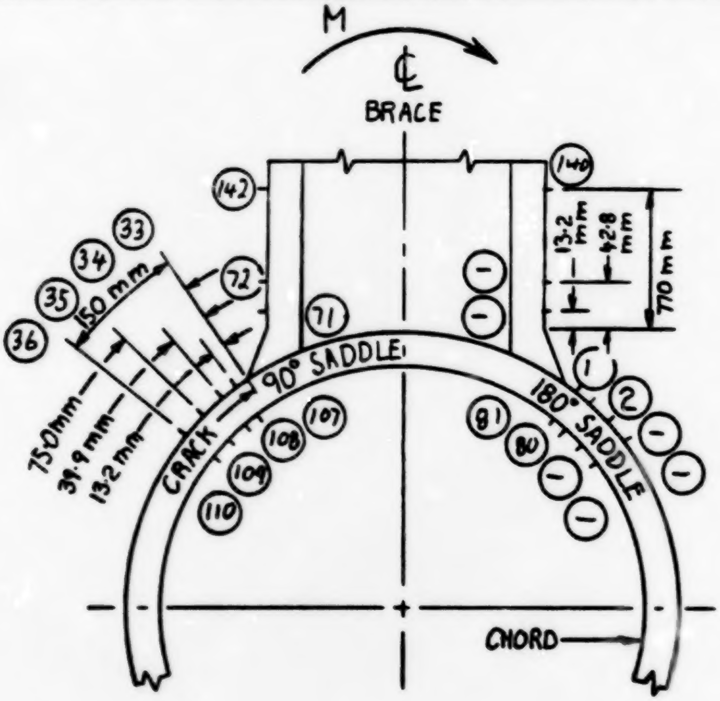
M
℄
BRACE
142
140
33
34
35
36
150 mm
72
71
13.2 mm
42.8 mm
710 mm
1
2
90° SADDLE
180° SADDLE
750mm
39.9mm
13.2mm
CRACK
107
108
109
110
81
80
CHORD

STRAIN GAUGE RESULTS AND EXPERIMENTAL STRESSES (ALL RESULTS AT MAXIMUM LOAD)

SPECIMEN: TB5
STIFFENED T-JOINT
MODE OF LOADING: Out-of-Plane Bending
APPLIED LOAD: 110 KN-m

Gauge No.	Radial Strain ϵ_r $\times 10^{-6}$	Tangential Strain ϵ_θ $\times 10^{-6}$	Shear Strain $\gamma_{r\theta}$ $\times 10^{-6}$	Radial Stress σ_r MPa	Tangential Stress σ_θ MPa	Shear Stress $\sigma_{r\theta}$ MPa	σ_θ / σ_r
75	177	104	4.8	48	36.2	-0.4	0.75
76	53	59	42	16.3	17.3	3.4	1.06
77	-36.2	-14.6	18.7	-9.4	-5.9	1.5	0.63
78	-172	-88.9	-13.8	-45.9	-32.5	-1.1	0.71
79	37.6	17.1	19.1	9.9	6.5	1.5	0.66
128	-258	–	–	-53.3	–	–	–
129	536	–	–	111	–	–	–
130	1.0	–	–	0.21	–	–	–
131	-954	–	–	-197	–	–	–
132	-949	–	–	-196	–	–	–
133	-539	–	–	-111	–	–	–
134	258	–	–	53.3	–	–	–
135	Defective	–	–	–	–	–	–
146	968	–	–	200	–	–	–
147	963	–	–	199	–	–	–

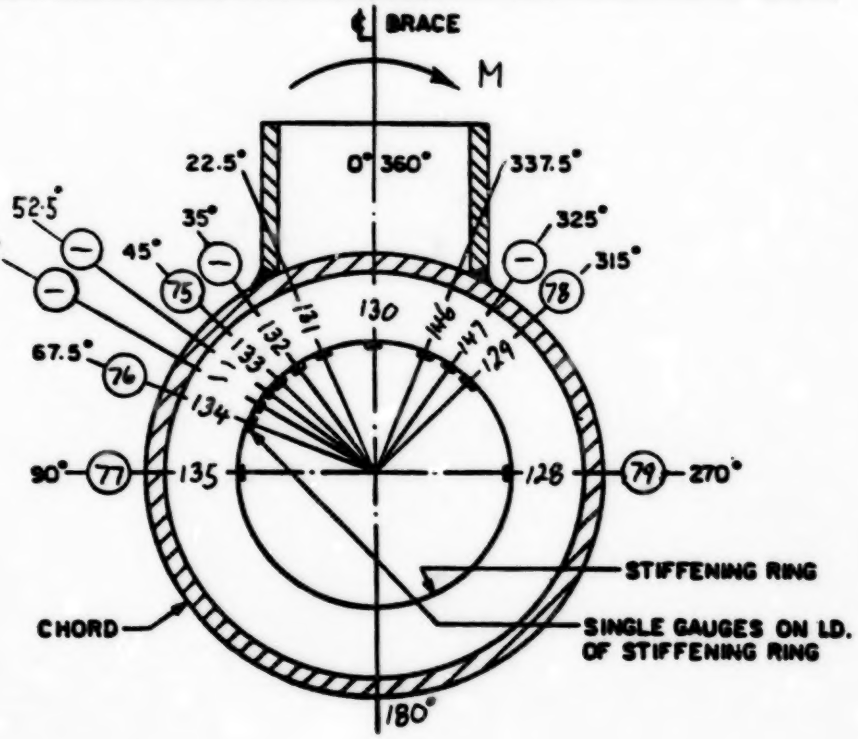

℄ BRACE
M
22.5°
0° 360°
337.5°
52.5°
35°
325°
60°
45°
75
315°
78
131
130
146
147
129
132
133
67.5°
76
134
90°
77
135
128
79
270°
STIFFENING RING
CHORD
SINGLE GAUGES ON I.D. OF STIFFENING RING
180°

STRAIN GAUGE RESULTS AND EXPERIMENTAL STRESSES (ALL RESULTS AT MAXIMUM LOAD)

SPECIMEN: TB5
STIFFENED T-JOINT
MODE OF LOADING: AXIAL
APPLIED LOAD: 88.9 KN

Gauge No.	Radial Strain ϵ_r $\times 10^{-6}$	Tangential Strain ϵ_θ $\times 10^{-6}$	Shear Strain $\gamma_{r\theta}$ $\times 10^{-6}$	Radial Stress σ_r MPa	Tangential Stress σ_θ MPa	Shear Stress $\sigma_{r\theta}$ MPa	σ_θ/σ_r
1	65.1	30.3	5.1	17.1	11.5	0.4	0.67
2	28.0	28.1	0.7	8.4	8.4	0.1	1.0
33	57.3	27.3	-0.8	15.1	10.3	-0.1	0.68
34	22.4	25.8	0.2	6.9	7.5	0	1.1
35	-0.2	16.9	0.6	1.12	3.9	0	3.5
36	-9.8	2.0	-0.9	-2.12	-0.22	-0.1	0
71	23.6	18.0	-1.2	6.7	5.8	-0.1	0.87
72	6.9	7.0	-1.1	2.1	2.1	-0.1	1.0
80	-0.7	9.8	2.3	0.5	2.23	0.2	–
81	-33.8	10.3	4.5	-7.04	0.2	0.4	0
107	-29.3	10.5	2.1	-6.1	0.4	0.2	0
108	4.2	10.2	2.4	1.7	2.6	0.2	1.53
109	23.5	12.7	1.2	6.3	4.6	0.1	0.73
110	20.8	13.8	0.6	5.8	4.6	0.1	0.8
140	15	–	–	3.1	–	–	–
142	18	–	–	3.7	–	–	–

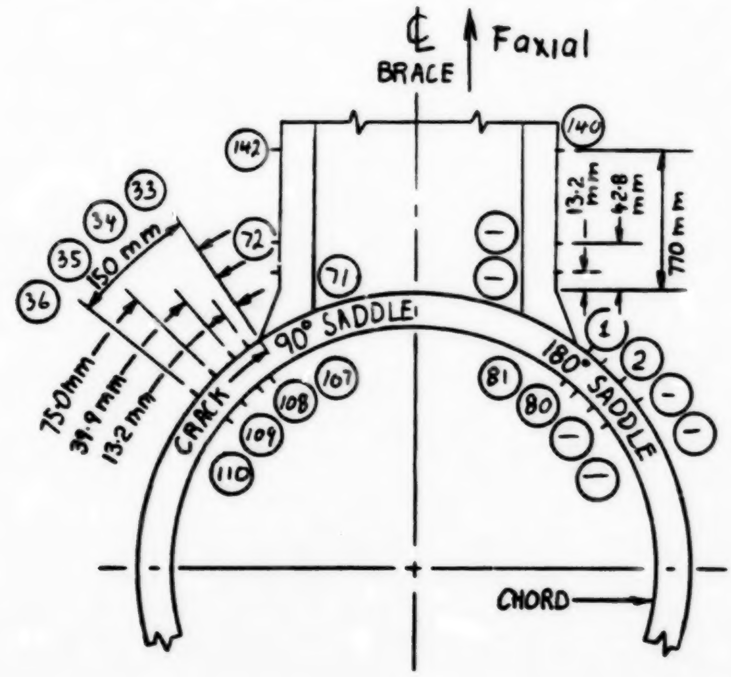
℄ BRACE
Faxial
142
140
33
34
35
36
150 mm
72
71
13.2 mm
42.8 mm
110 mm
1
2
90° SADDLE
180° SADDLE
81
80
107
108
109
110
CRACK
75.0 mm
39.9 mm
13.2 mm
CHORD

STRAIN GAUGE RESULTS AND EXPERIMENTAL STRESSES (ALL RESULTS AT MAXIMUM LOAD)

SPECIMEN: TB5
STIFFENED T-JOINT
MODE OF LOADING: AXIAL
APPLIED LOAD: 88.9 KN

Gauge No.	Radial Strain ϵ_r $\times 10^{-6}$	Tangential Strain ϵ_θ $\times 10^{-6}$	Shear Strain $\gamma_{r\theta}$ $\times 10^{-6}$	Radial Stress σ_r MPa	Tangential Stress σ_θ MPa	Shear Stress $\sigma_{r\theta}$ MPa	σ_θ / σ_r
75	4.0	27.3	1.3	2.8	6.6	0.1	2.4
76	-16.4	4.7	11.0	-3.5	-0.1	0.9	0
77	-20.3	-13.4	6.3	-5.6	-4.5	0.5	0.8
78	4.2	26.4	0.5	2.8	6.4	0.0	2.3
79	-21	-14.5	-4.8	-5.8	-4.8	-0.4	0.83
128	101	-	-	21	-	-	-
129	27	-	-	5.6	-	-	-
130	-78.3	-	-	-16.2	-	-	-
131	-92	-	-	-19	-	-	-
132	-62	-	-	-12.8	-	-	-
133	31	-	-	6.4	-	-	-
134	97.6	-	-	20.2	-	-	-
135	104	-	-	21.5	-	-	-
146	-70.6	-	-	-14.6	-	-	-
147	-95.4	-	-	-19.7	-	-	-

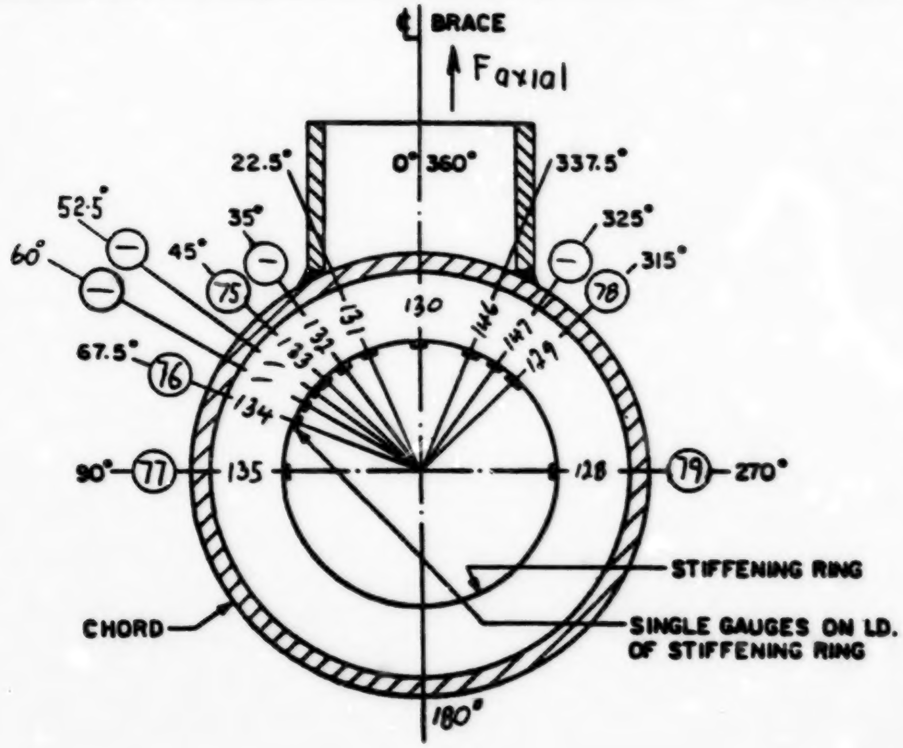
℄ BRACE
Faxial
22.5°
0° 360°
337.5°
52.5°
35°
325°
60°
45°
315°
75
78
130
131
132
133
146
147
129
67.5°
76
134
90°
77
135
128
79
270°
STIFFENING RING
CHORD
SINGLE GAUGES ON I.D. OF STIFFENING RING
180°

4W - TB6

STRAIN GAUGE RESULTS AND EXPERIMENTAL STRESSES (ALL RESULTS AT MAXIMUM LOAD)

SPECIMEN: TB6
STIFFENED T-JOINT
MODE OF LOADING: In-Plane Bending
APPLIED LOAD: 147KN-m

Gauge No.	Radial Strain ϵ_r $\times 10^{-6}$	Tangential Strain ϵ_θ $\times 10^{-6}$	Shear Strain $\gamma_{r\theta}$ $\times 10^{-6}$	Radial Stress σ_r MPa	Tangential Stress σ_θ MPa	Shear Stress $\sigma_{r\theta}$ MPa	σ_θ / σ_r
3	-268	65	-19.6	-57.3	-3.5	-1.6	0.06
4	-60	17.7	0	-12.5	0	0	0
5	178	-108	18.3	33.5	-12.7	1.5	0.40
6	182	-185	0	28.7	-29.6	0	1.03
53	520	270	-15	139	98	-1.2	0.71
54	323	272	2.3	93	85	0.2	0.91
55	127	189	-5	42	52	-0.4	1.24
56	105	75	-2	29.4	25	0	0.85
126	229	–	–	47.3	–	–	–
128	-226	–	–	46.7	–	–	–
137	-186	174	7.9	-55	-53	0.6	0.96
138	-78	-73	5	-23	-22	0.4	1.0
140	237	-58	26.1	50.4	3.0	2.1	0
141	37.8	11	0	9.3	5.1	0	0.55
142	-512	-274	11	-137	-99	0	0.72
143	-319	-275	-3	-93	-86	-0.3	0.93

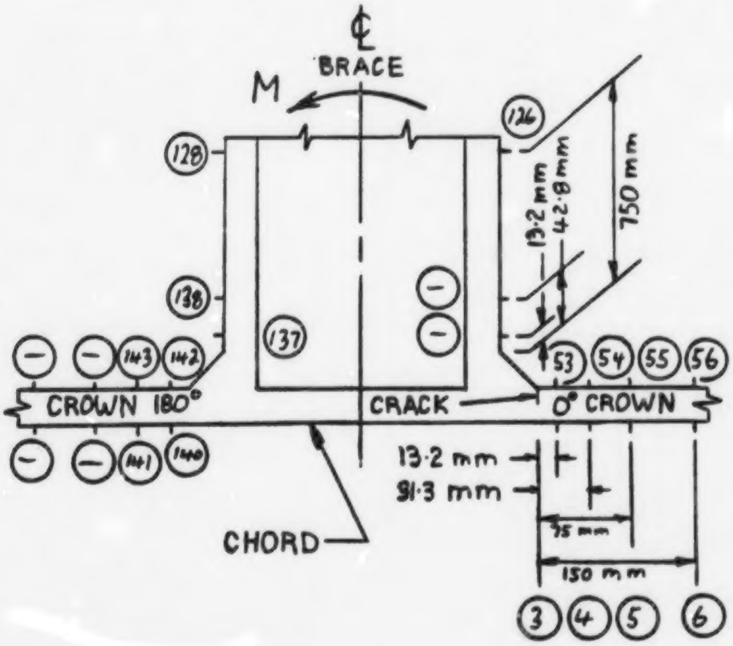
℄
BRACE
M
126
128
13·2 mm
42·8 mm
750 mm
138
137
−
−
−
−
143
142
53
54
55
56
CROWN 180°
CRACK
0° CROWN
−
−
141
140
13·2 mm
91·3 mm
75 mm
150 mm
CHORD
3
4
5
6

STRAIN GAUGE RESULTS AND EXPERIMENTAL STRESSES (ALL RESULTS AT MAXIMUM LOAD)

SPECIMEN: TB6
STIFFENED T-JOINT
MODE OF LOADING: In-Plane Bending
APPLIED LOAD: 147 KN-m

Gauge No.	Radial Strain ϵ_r $\times10^{-6}$	Tangential Strain ϵ_θ $\times10^{-6}$	Shear Strain $\gamma_{r\theta}$ $\times10^{-6}$	Radial Stress σ_r MPa	Tangential Stress σ_θ MPa	Shear Stress $\sigma_{r\theta}$ MPa	σ_θ/σ_r
125	-2	–	–	0	–	–	–
127	-8	–	–	0	–	–	–
144	1.6	1.4	52	0	0	4.2	–
145	2.7	2.8	109	0	0	8.8	–
146	7.6	-3.3	304	1.5	-0.2	25	–
147	0.2	2.8	277	0.2	0.7	22.4	–

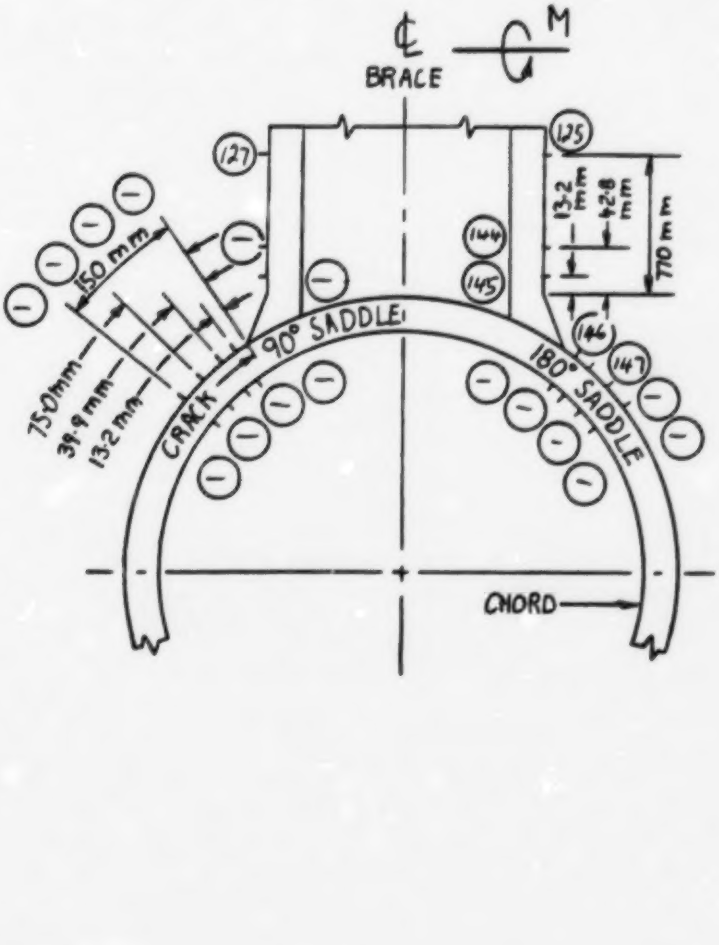
℄
BRACE
M
127
125
144
145
146
147
150 mm
75.0mm
39.9mm
13.2mm
13.2 mm
42.8 mm
770 mm
CRACK
90° SADDLE
180° SADDLE
CHORD

STRAIN GAUGE RESULTS AND EXPERIMENTAL STRESSES (ALL RESULTS AT MAXIMUM LOAD)

SPECIMEN: TB6
STIFFENED T-JOINT
MODE OF LOADING: In-Plane Bending
APPLIED LOAD: 147 KN-m

Gauge No.	Radial Strain ϵ_r $\times 10^{-6}$	Tangential Strain ϵ_θ $\times 10^{-6}$	Shear Strain $\gamma_{r\theta}$ $\times 10^{-6}$	Radial Stress σ_r MPa	Tangential Stress σ_θ MPa	Shear Stress $\sigma_{r\theta}$ MPa	σ_θ/σ_r
44	391	–	–	80.8	–	–	–
45	409	–	–	84.5	–	–	–
46	-107	–	–	-22.1	–	–	–
47	-241	–	–	-49.8	–	–	–
48	-200	–	–	-41.3	–	–	–
82	225	3.4	38	52.2	16.4	3.1	0.31
102	-67.8	-91	-134	-22	-26	-11	1.2
103	29	38	-128	9.3	10.7	-10.4	1.2
104	42.4	41.9	127	12.7	12.6	10.3	1.0
135	472	–	–	97.6	–	–	–
136	441	–	–	91.2	–	–	–

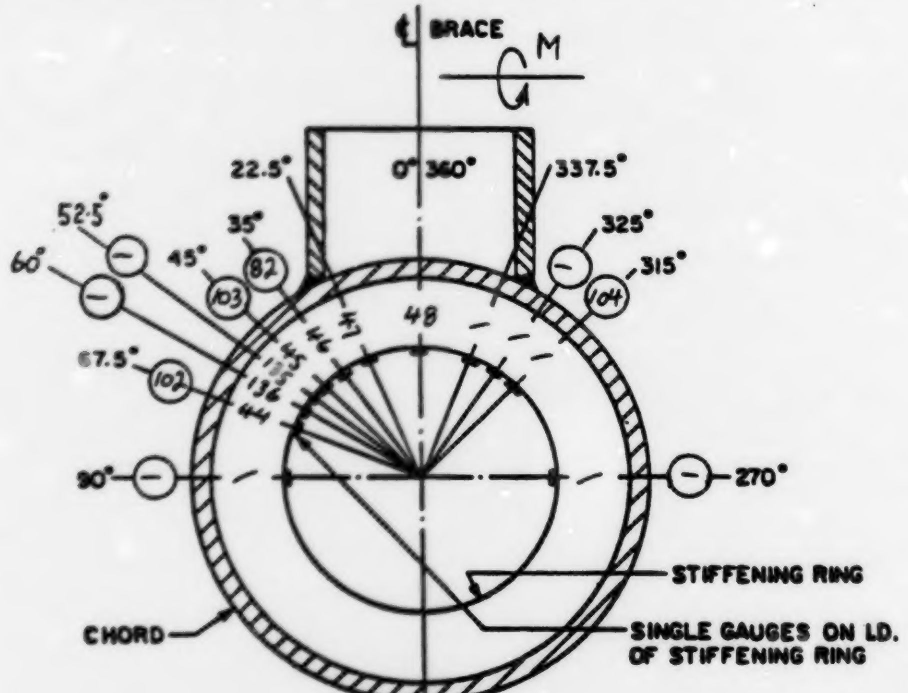
℄ BRACE
M
22.5°
0° 360°
337.5°
52.5°
60°
45°
35°
82
103
325°
104
315°
48
47
46
45
135
136
44
67.5°
102
90°
270°
STIFFENING RING
SINGLE GAUGES ON I.D. OF STIFFENING RING
CHORD
180°

STRAIN GAUGE RESULTS AND EXPERIMENTAL STRESSES (ALL RESULTS AT MAXIMUM LOAD)

SPECIMEN: TB6
STIFFENED T-JOINT
MODE OF LOADING: AXIAL
APPLIED LOAD: 44.5 KN

Gauge No.	Radial Strain ϵ_r $\times 10^{-6}$	Tangential Strain ϵ_θ $\times 10^{-6}$	Shear Strain $\gamma_{r\theta}$ $\times 10^{-6}$	Radial Stress σ_r MPa	Tangential Stress σ_θ MPa	Shear Stress $\sigma_{r\theta}$ MPa	σ_θ / σ_r
125	8.2	-	-	1.7	-	-	-
127	8.2	-	-	1.7	-	-	-
144	4.0	3.9	0.5	1.2	1.2	0	1.0
145	9.9	8.5	0.7	2.9	2.7	0	0.93
146	28.3	14.4	1.2	7.5	5.3	0	0.71
147	13.4	14.2	1.4	4.1	4.2	0.1	1.02

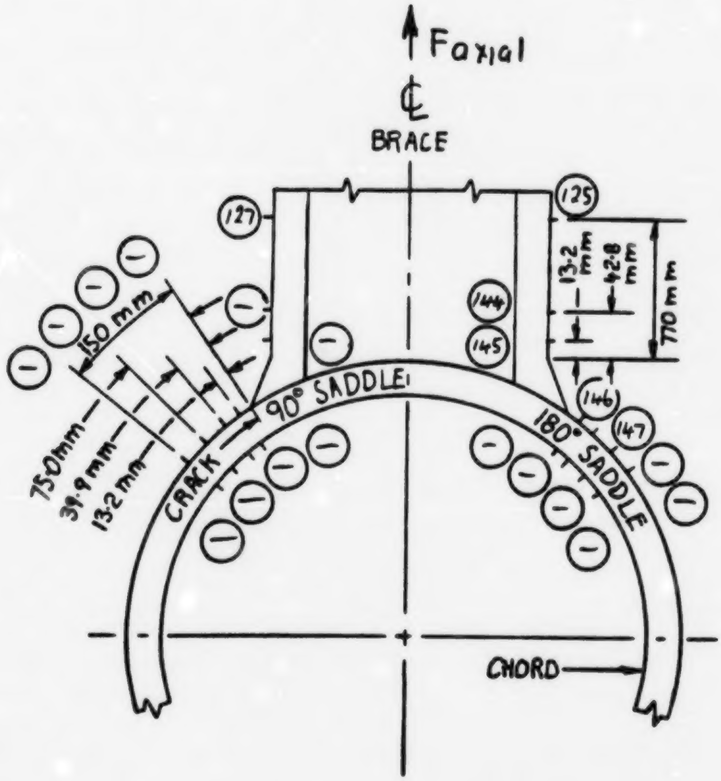

Faxial
℄
BRACE
127
125
13.2 mm
42.8 mm
770 mm
144
145
146
147
150 mm
75.0mm
39.9 mm
13.2 mm
CRACK
90° SADDLE
180° SADDLE
CHORD

STRAIN GAUGE RESULTS AND EXPERIMENTAL STRESSES (ALL RESULTS AT MAXIMUM LOAD)

SPECIMEN: TB6
STIFFENED T-JOINT
MODE OF LOADING: AXIAL
APPLIED LOAD: 44.5 KN

Gauge No.	Radial Strain ϵ_r $\times 10^{-6}$	Tangential Strain ϵ_θ $\times 10^{-6}$	Shear Strain $\gamma_{r\theta}$ $\times 10^{-6}$	Radial Stress σ_r MPa	Tangential Stress σ_θ MPa	Shear Stress $\sigma_{r\theta}$ MPa	σ_θ / σ_r
3	5.7	5.0	1.2	1.7	1.6	0	1.0
4	13.4	-3.0	3.4	2.9	0.25	0.3	0
5	15.7	-5.9	3.4	3.2	-0.3	0.3	0
6	-3.9	9.8	-21.6	0	2.0	-1.7	–
53	23.3	8.0	-3.5	5.9	3.5	-0.3	0.60
54	20.3	5.0	-1.2	5.0	2.6	-0.1	0.52
55	14.7	2.7	-1.9	3.6	1.6	-0.2	0.44
56	14.9	0.4	-1.5	3.5	1.1	-0.1	0.31
126	5.0	–	–	–	–	–	–
128	6.0	–	–	–	–	–	–
137	6.3	8.2	0	2.03	2.3	0	1.13
138	0.1	5.7	-0.5	0.42	1.3	0	3.1
140	5.2	-0.8	2.9	1.15	0.17	0.2	0
141	-27	114	2.8	1.62	24.3	0.2	–
142	27	7.2	-1.9	6.7	3.5	-0.16	0.52
143	20.6	6.8	-0.8	5.2	2.9	-0.1	0.56

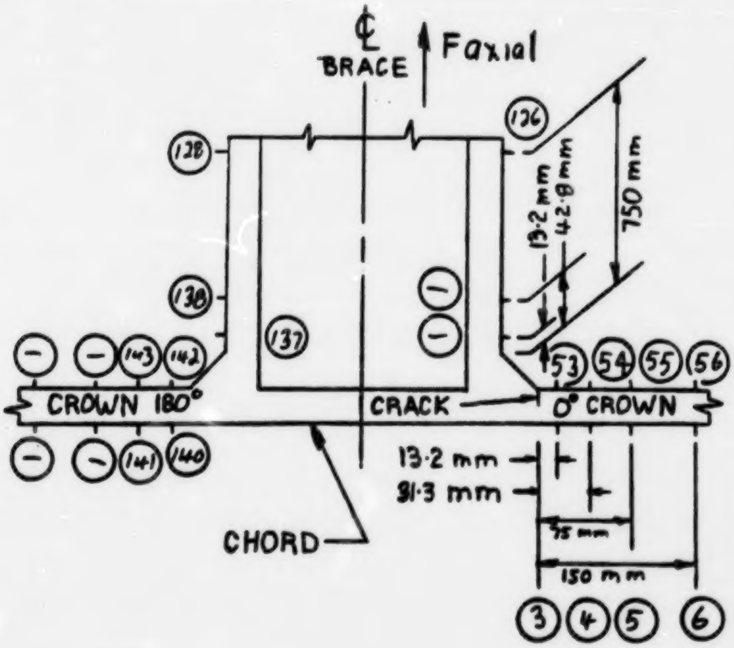
℄ BRACE
Faxial
126
128
13·2 mm
42·8 mm
750 mm
138
137
–
–
–
–
143
142
53
54
55
56
CROWN 180°
CRACK
0° CROWN
–
–
141
140
CHORD
13·2 mm
31·3 mm
75 mm
150 mm
3
4
5
6

STRAIN GAUGE RESULTS AND EXPERIMENTAL STRESSES (ALL RESULTS AT MAXIMUM LOAD)

SPECIMEN: TB6
STIFFENED T-JOINT
MODE OF LOADING: AXIAL
APPLIED LOAD: 44.5 KN

Gauge No.	Radial Strain ϵ_r $\times 10^{-6}$	Tangential Strain ϵ_θ $\times 10^{-6}$	Shear Strain $\gamma_{r\theta}$ $\times 10^{-6}$	Radial Stress σ_r MPa	Tangential Stress σ_θ MPa	Shear Stress $\sigma_{r\theta}$ MPa	σ_θ / σ_r
44	49.7	–	–	10.3	–	–	–
45	Defective	–	–	–	–	–	–
46	-49	–	–	10.1	–	–	–
47	Defective	–	–	–	–	–	–
48	-37	–	–	7.6	–	–	–
82	21	2.2	11	4.9	2.0	0.9	0.41
102	-6.6	3.3	6.7	-1.3	0.3	0.5	0.23
103	4.3	11.5	1.5	1.8	3.0	0.1	1.67
104	0.6	13	0.6	1.0	3.0	0	3.0
135	28.7	–	–	5.93	–	–	–
136	42.1	–	–	8.7	–	–	–
49	16.2	–	–	3.35	–	–	–

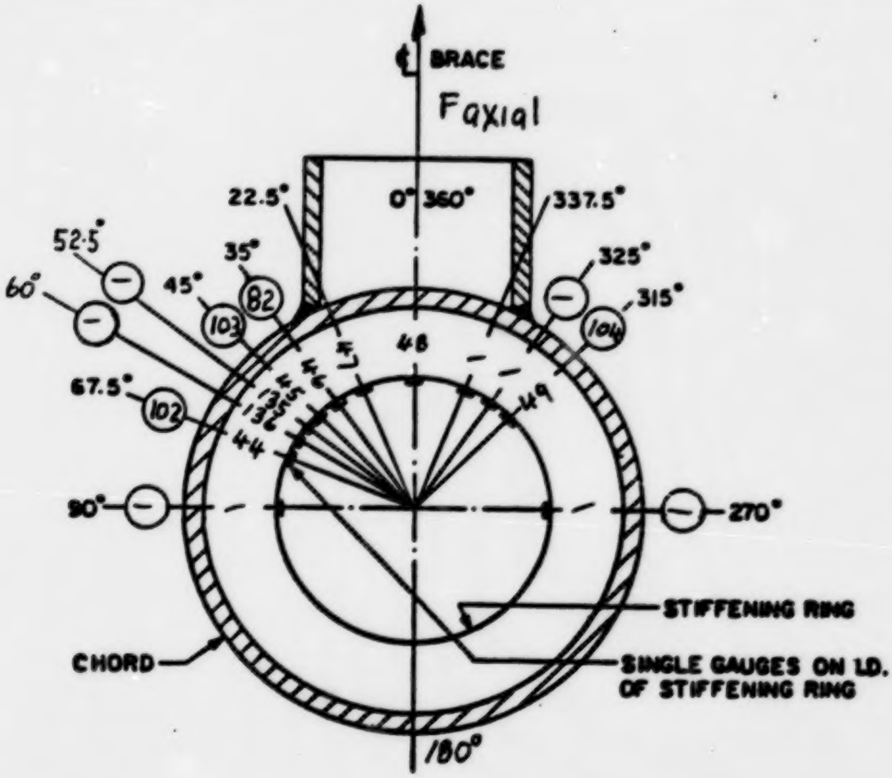
℄ BRACE
Faxial
22.5°
0° 360°
337.5°
52.5°
35°
325°
45°
315°
60°
82
103
104
48
47
46
45
135
136
44
49
67.5°
102
90°
270°
STIFFENING RING
CHORD
SINGLE GAUGES ON I.D. OF STIFFENING RING
180°

APPENDIX 5

MEMORIAL DATA

a vs N and da/dn vs a plots

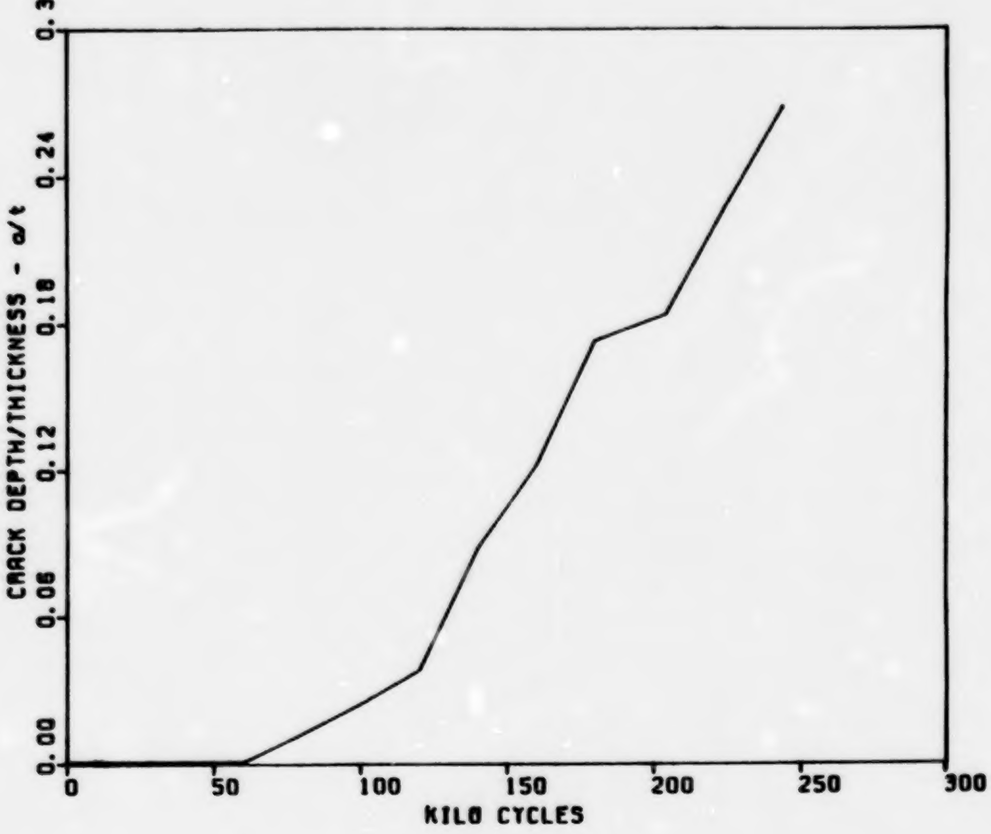

CRACK DEPTH vs CYCLES
INITIATING CRACK POSITION 18mm FROM SADDLE POINT
ANGULAR POSITION FROM SADDLE POINT - 176°
UNSTIFFENED TUBULAR JOINT - TA1 SIDE 2
AXIAL LOAD - HOT SPOT STRESS RANGE 250 MPa

Figure 5-1

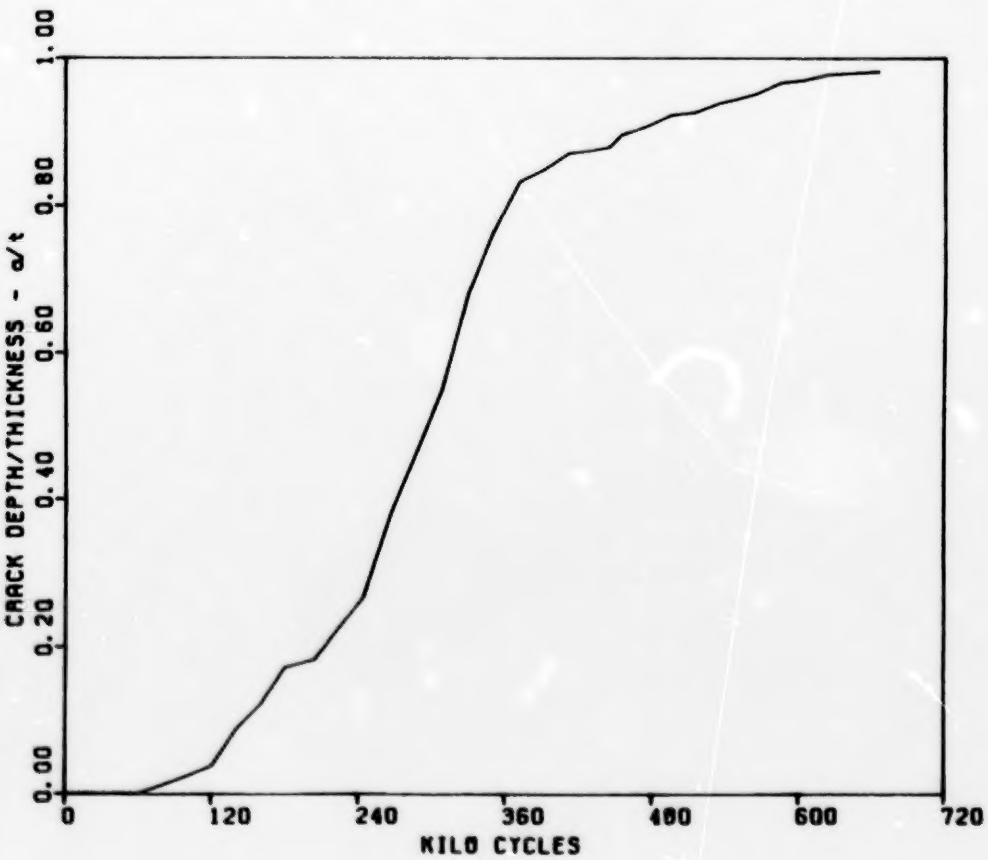

CRACK DEPTH vs CYCLES
INITIATING CRACK POSITION 10mm FROM SADDLE POINT
ANGULAR POSITION FROM SADDLE POINT - 176°
UNSTIFFENED TUBULAR JOINT - TA1 SIDE 2
AXIAL LOAD - HOT SPOT STRESS RANGE 250 MPa

Figure 5-2

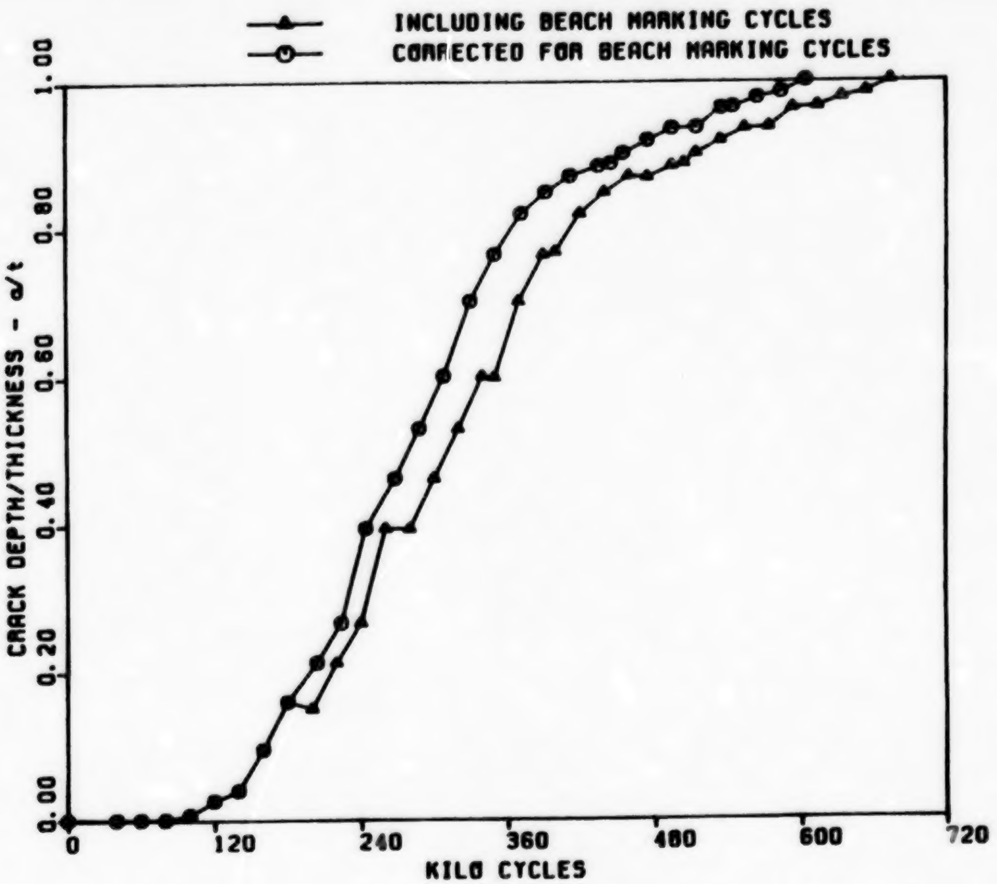

CRACK DEPTH vs CYCLES
FOR DOMINANTLY PROPAGATING CRACK POSITION
AT SADDLE POINT - 180°
UNSTIFFENED TUBULAR JOINT - TA1 SIDE 2
AXIAL LOAD - HOT SPOT STRESS RANGE 250 MPa

Figure 5-3

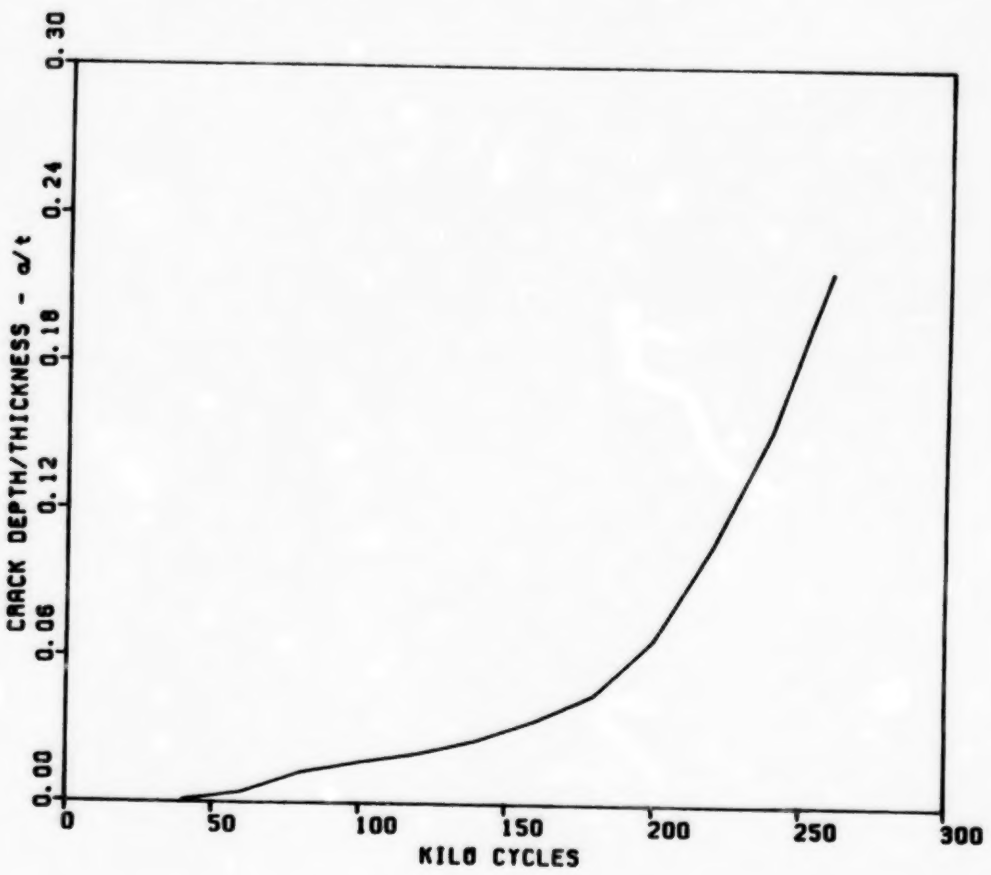

CRACK DEPTH vs CYCLES
INITIATING CRACK POSITION 30mm FROM SADDLE POINT
ANGULAR POSITION FROM SADDLE POINT - 7°
STIFFENED TUBULAR JOINT - TA2 SIDE 1
AXIAL LOAD - HOT SPOT STRESS RANGE 250 MPa

Figure 5-4

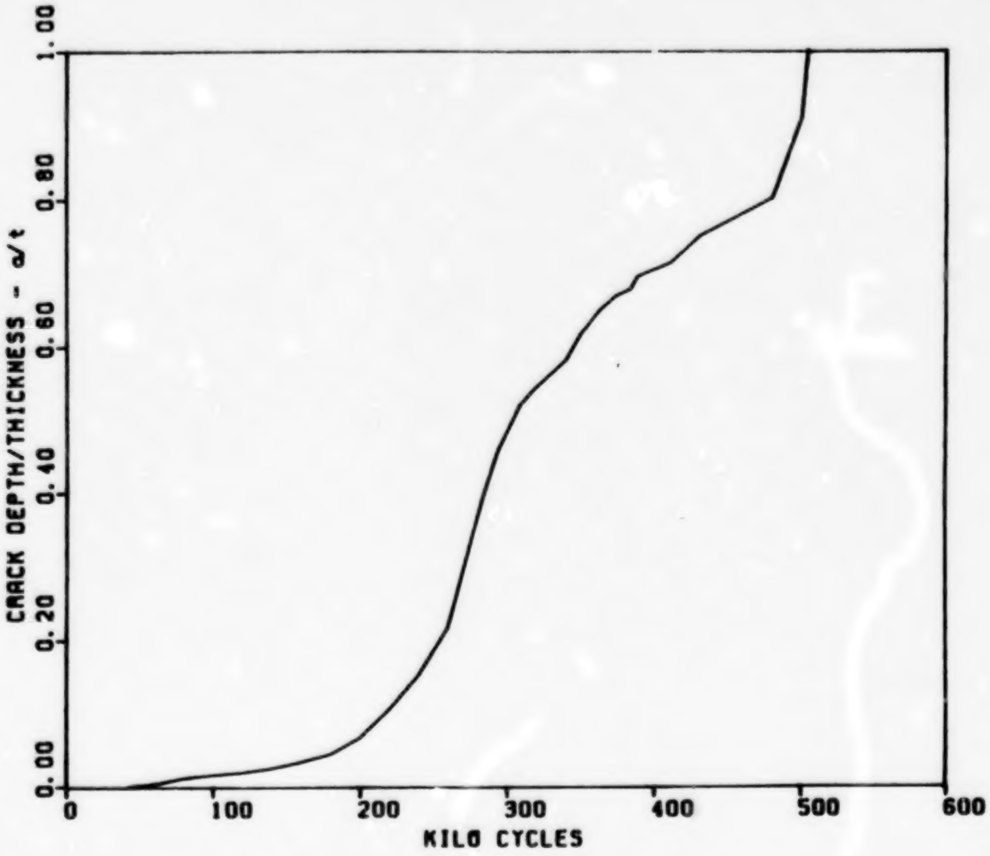

- CRACK DEPTH vs CYCLES
INITIATING CRACK POSITION 30mm FROM SADDLE POINT
ANGULAR POSITION FROM SADDLE POINT - 7°
STIFFENED TUBULAR JOINT - TA2 SIDE 1
AXIAL LOAD - HOT SPOT STRESS RANGE 250 MPa

Figure 5-5

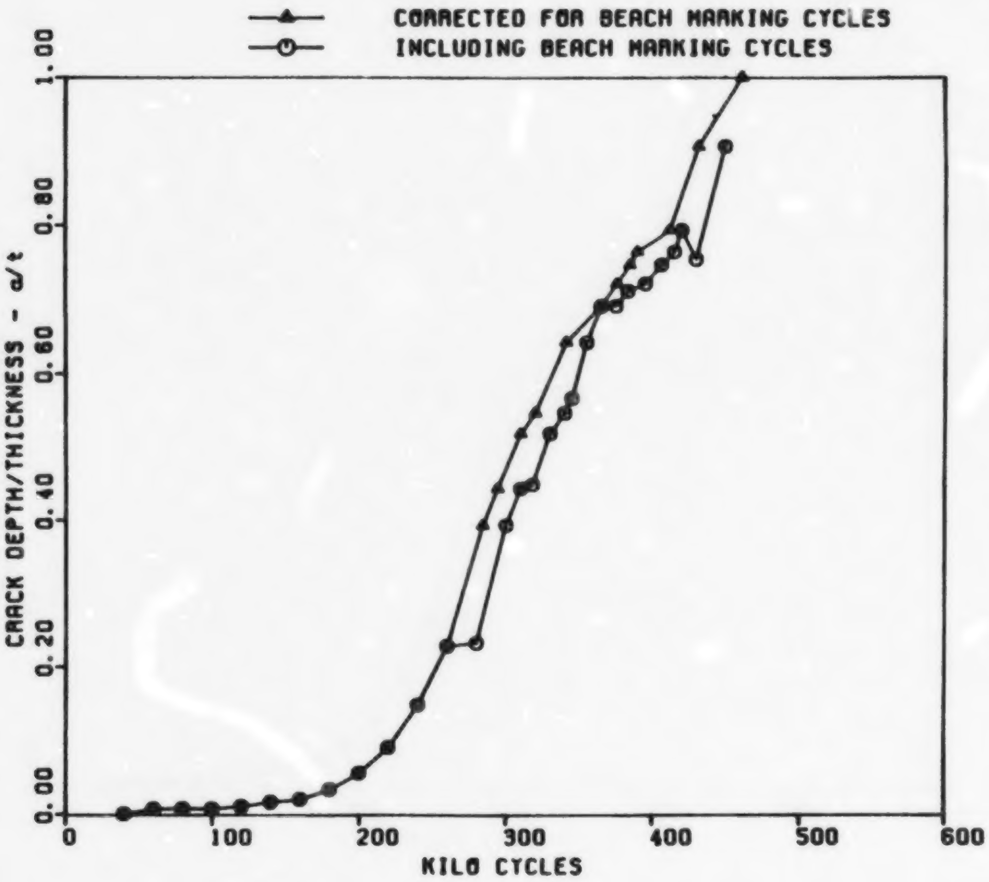

CRACK DEPTH vs CYCLES
FOR DOMINANTLY PROPAGATING CRACK POSITION
AT 60mm FROM SADDLE POINT AND AT 13.7°
STIFFENED TUBULAR JOINT - TA2 SIDE 1
AXIAL LOAD - HOT SPOT STRESS RANGE 250 MPa

Figure 5-6

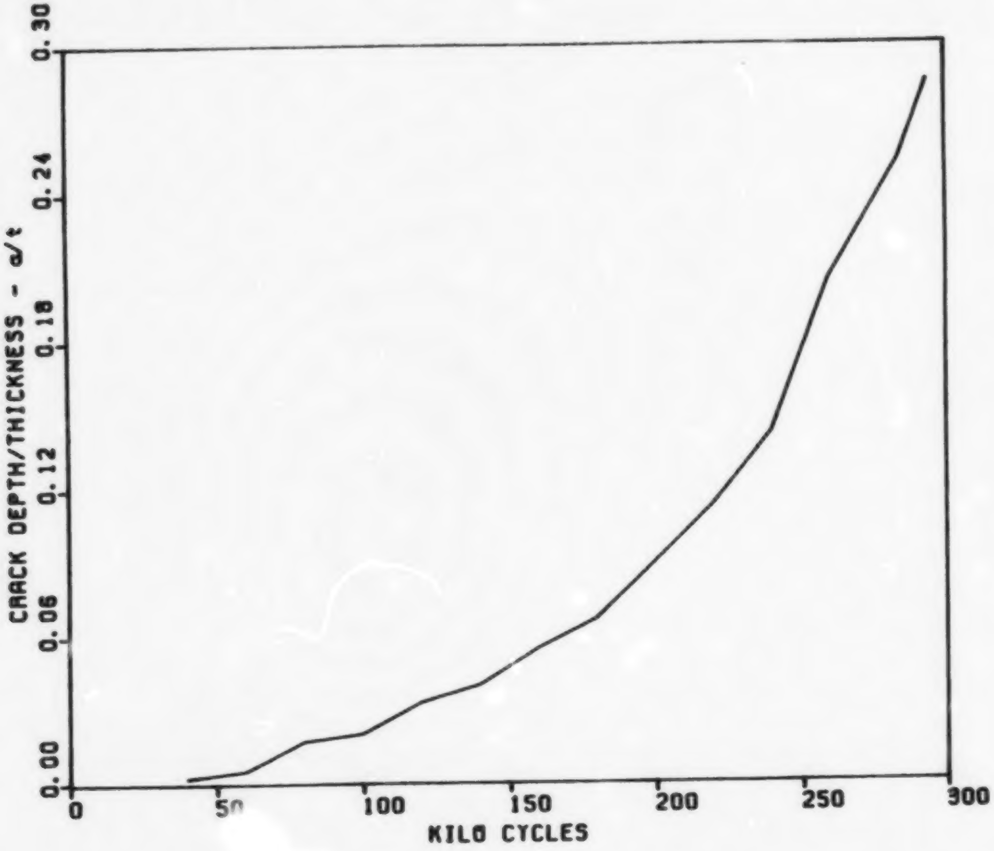

CRACK DEPTH vs CYCLES
INITIATING CRACK POSITION 35mm FROM SADDLE POINT
ANGULAR POSITION FROM SADDLE POINT - 167.5°
STIFFENED TUBULAR JOINT - TA2 SIDE 2
AXIAL LOAD - HOT SPOT STRESS RANGE 250 MPa

Figure 5-7

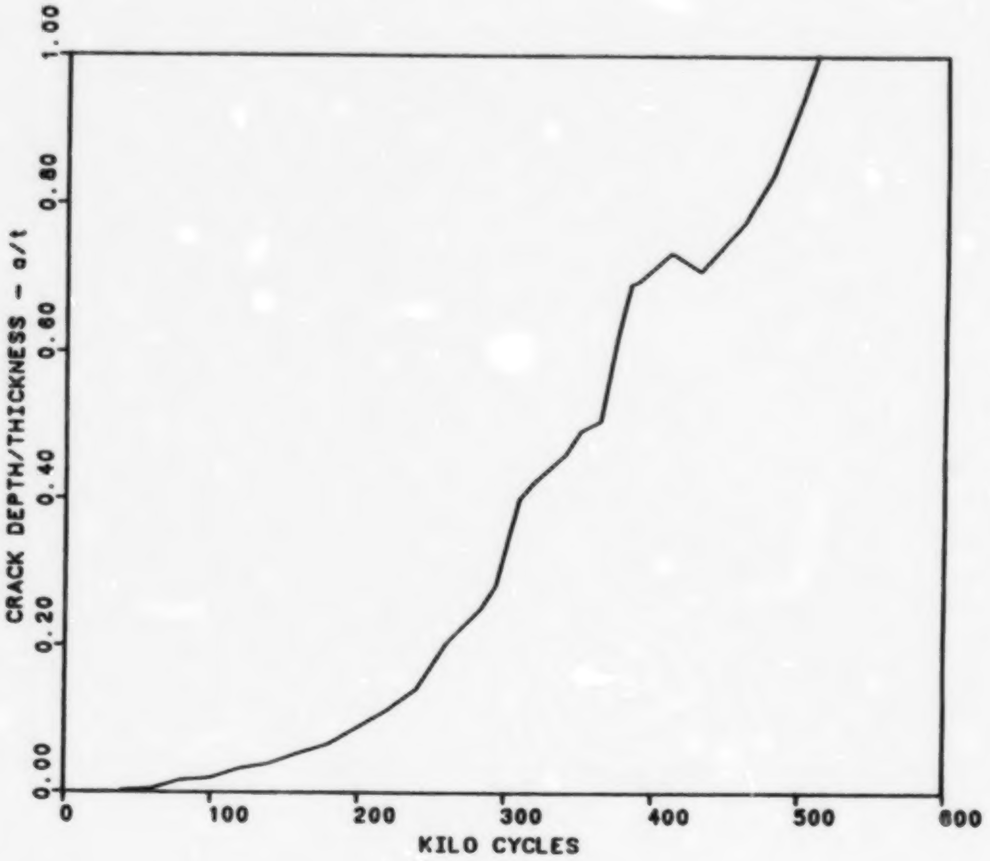

CRACK DEPTH vs CYCLES
INITIATING CRACK POSITION 55mm FROM SADDLE POINT
ANGULAR POSITION FROM SADDLE POINT - 167.5°
STIFFENED TUBULAR JOINT - TA2 SIDE 2
AXIAL LOAD - HOT SPOT STRESS RANGE 250 MPa

Figure 5-8

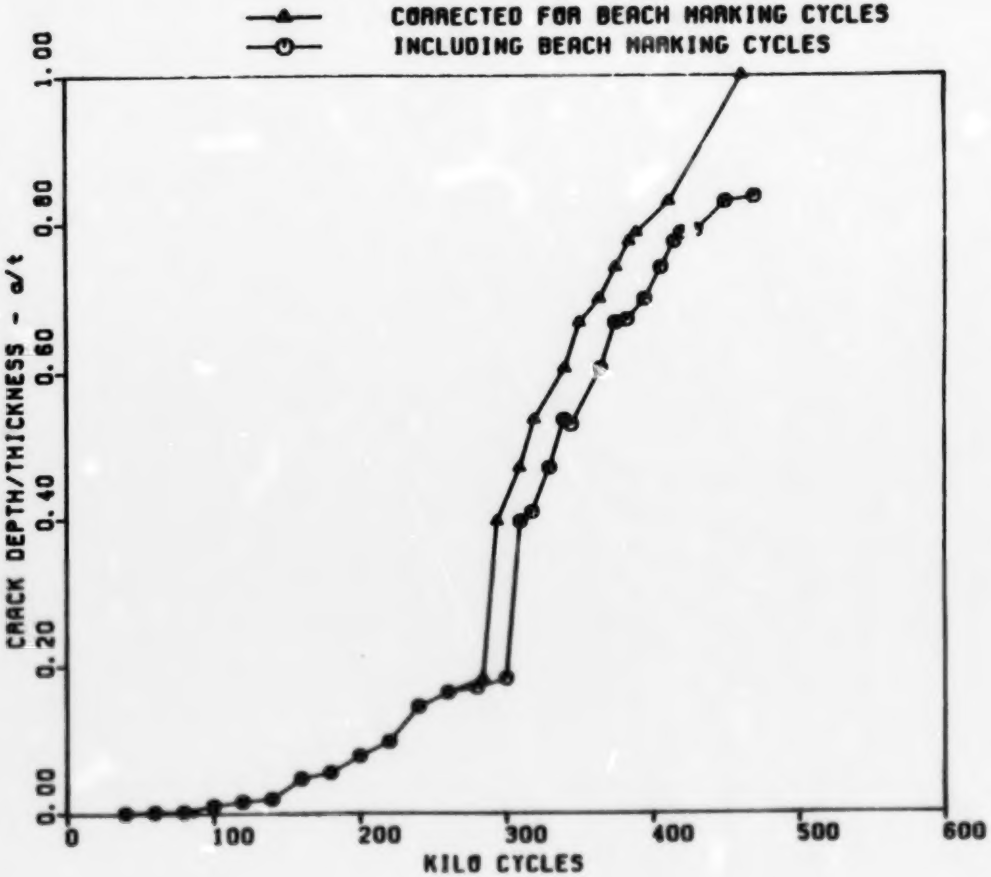

CRACK DEPTH vs CYCLES
FOR DOMINANTLY PROPAGATING CRACK POSITION
AT 84.5mm FROM SADDLE POINT AND AT 161°
STIFFENED TUBULAR JOINT - TA2 SIDE 2
AXIAL LOAD - HOT SPOT STRESS RANGE 250 MPa

Figure 5-9

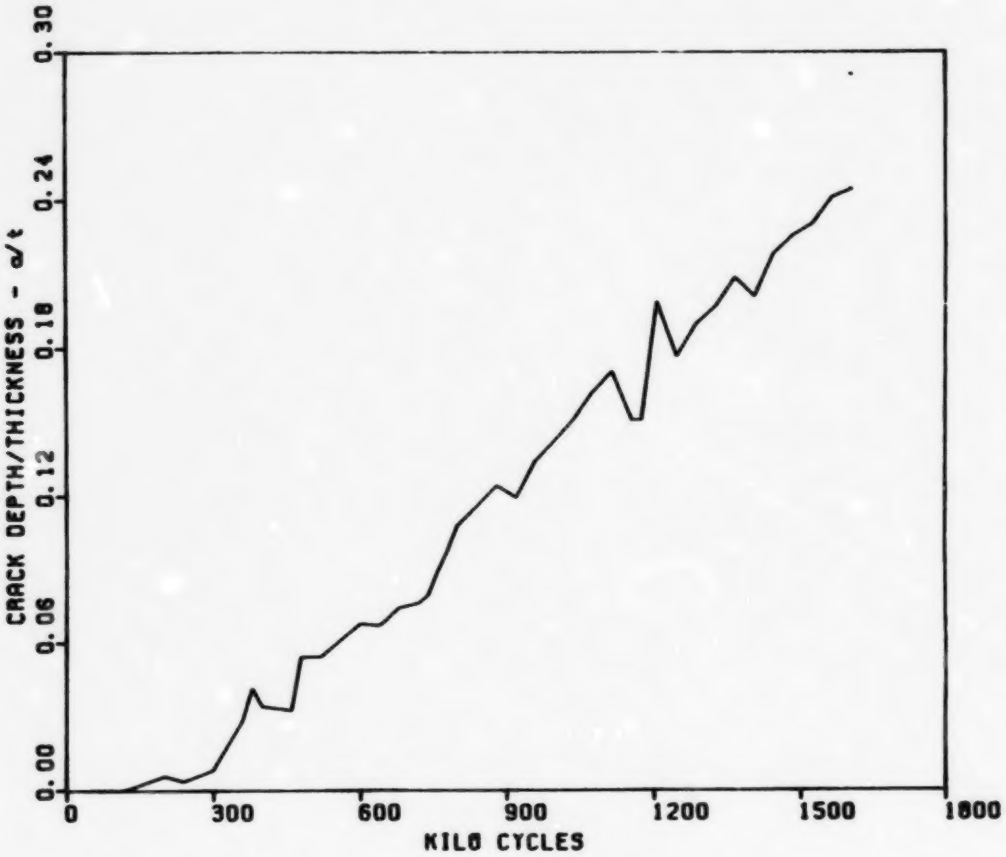

CRACK DEPTH vs CYCLES
INITIATING CRACK POSITION 73 mm FROM SADDLE POINT
ANGULAR POSITION FROM SADDLE POINT - 343.5°
STIFFENED TUBULAR JOINT - TA3 SIDE 1
AXIAL LOAD - HOT SPOT STRESS RANGE 160 MPa

Figure 5-10

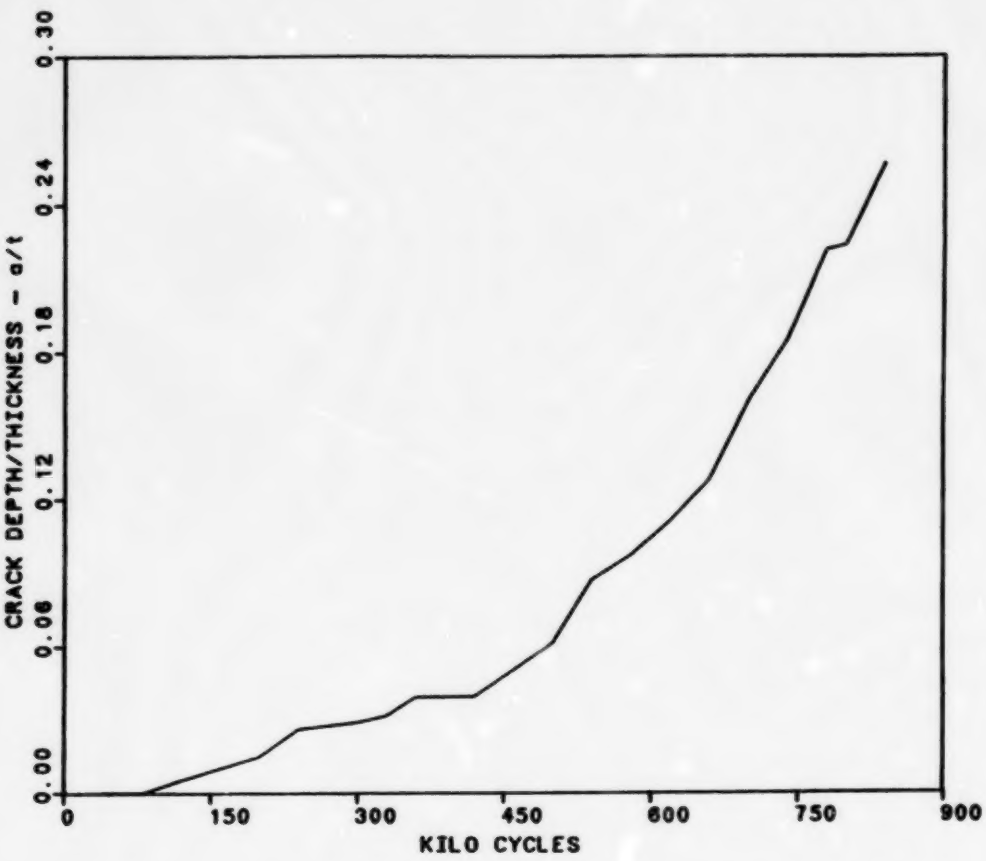

CRACK DEPTH vs CYCLES
INITIATING CRACK POSITION 60.5mm FROM SADDLE POINT
ANGULAR POSITION FROM SADDLE POINT - 166.3°
STIFFENED TUBULAR JOINT - TA3 SIDE 2
AXIAL LOAD - HOT SPOT STRESS RANGE 160 MPa

Figure 5-11

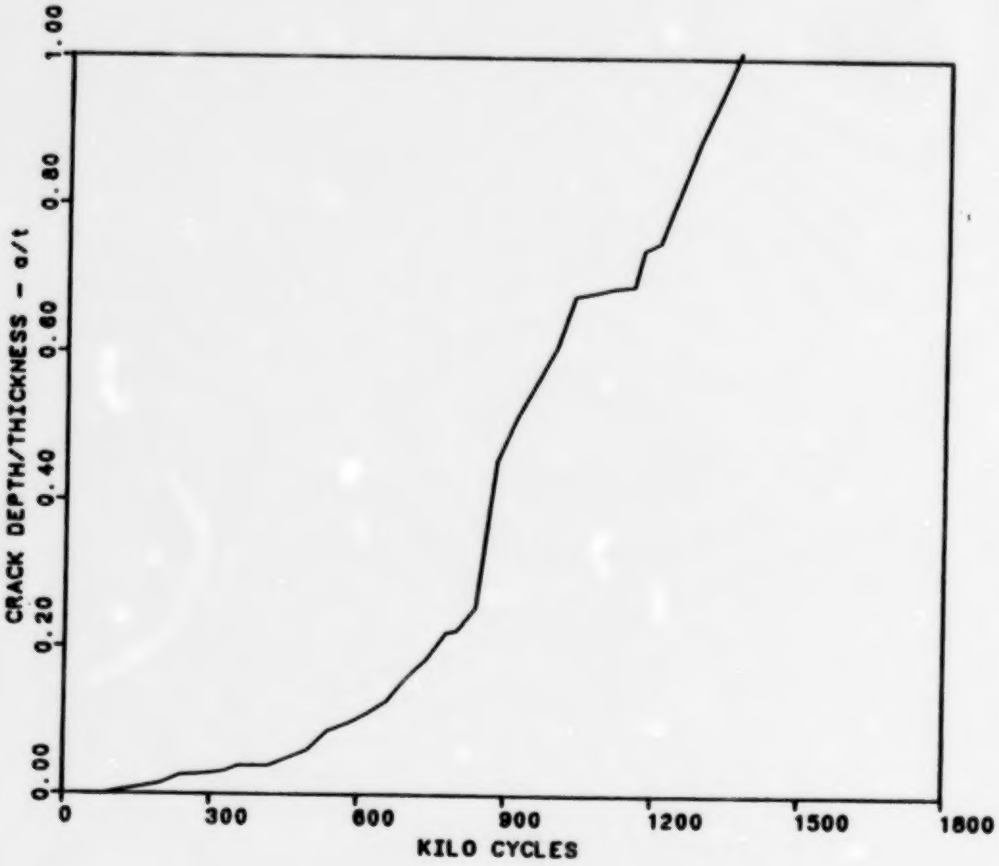

CRACK DEPTH vs CYCLES
INITIATING CRACK POSITION 60.5mm FROM SADDLE POINT
ANGULAR POSITION FROM SADDLE POINT - 166.3°
STIFFENED TUBULAR JOINT - TA3 SIDE 2
AXIAL LOAD - HOT SPOT STRESS RANGE 160 MPa

Figure 5-12

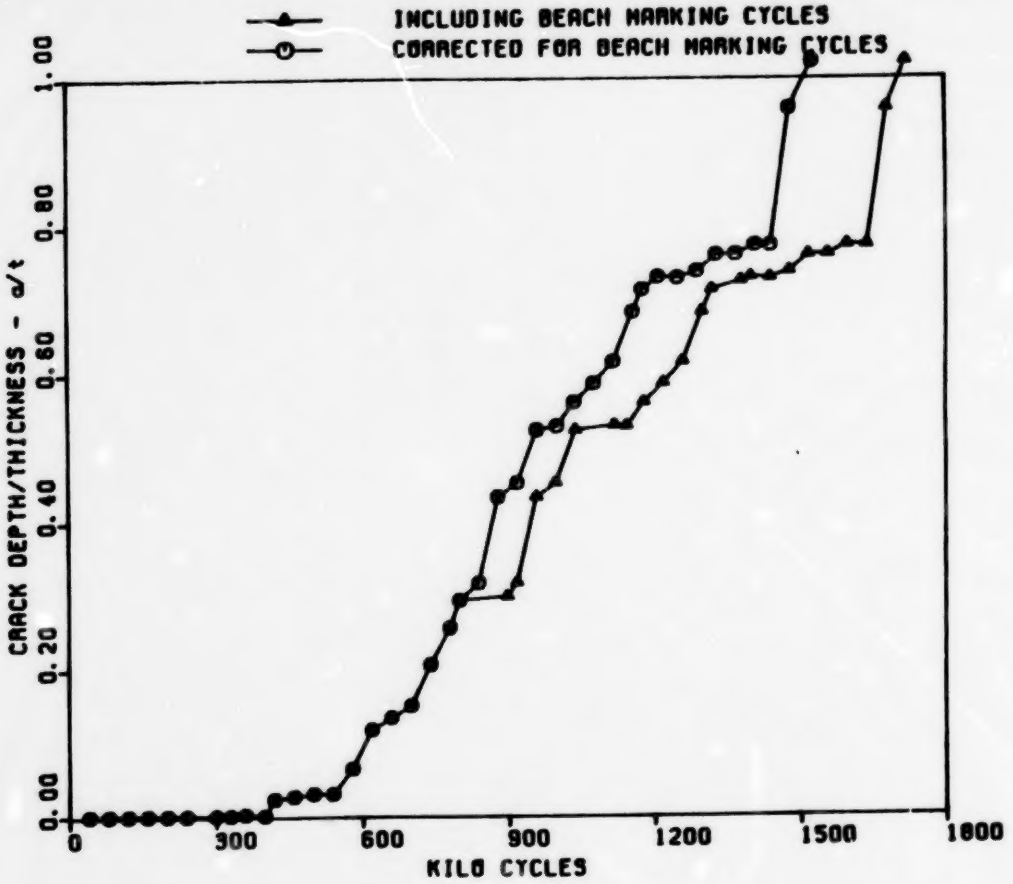

CRACK DEPTH vs CYCLES
FOR DOMINANTLY PROPAGATING CRACK POSITION
AT SADDLE POINT - 180°
STIFFENED TUBULAR JOINT - TA3 SIDE 2
AXIAL LOAD - HOT SPOT STRESS RANGE 160 MPa

Figure 5-13

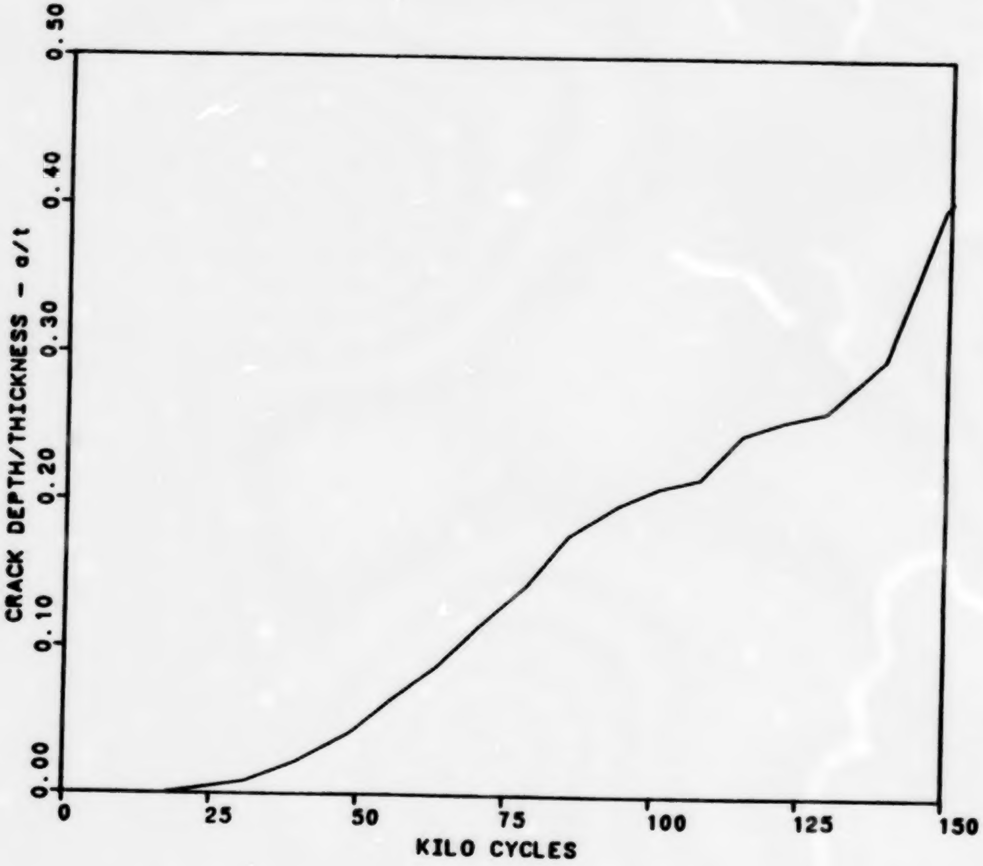

CRACK DEPTH vs CYCLES
INITIATING CRACK POSITION -30.5mm FROM SADDLE POIN
ANGULAR POSITION FROM SADDLE POINT - 7°
STIFFENED TUBULAR JOINT - TA4 SIDE 1
AXIAL LOAD - HOT SPOT STRESS RANGE 250 MPa

Figure 5-14

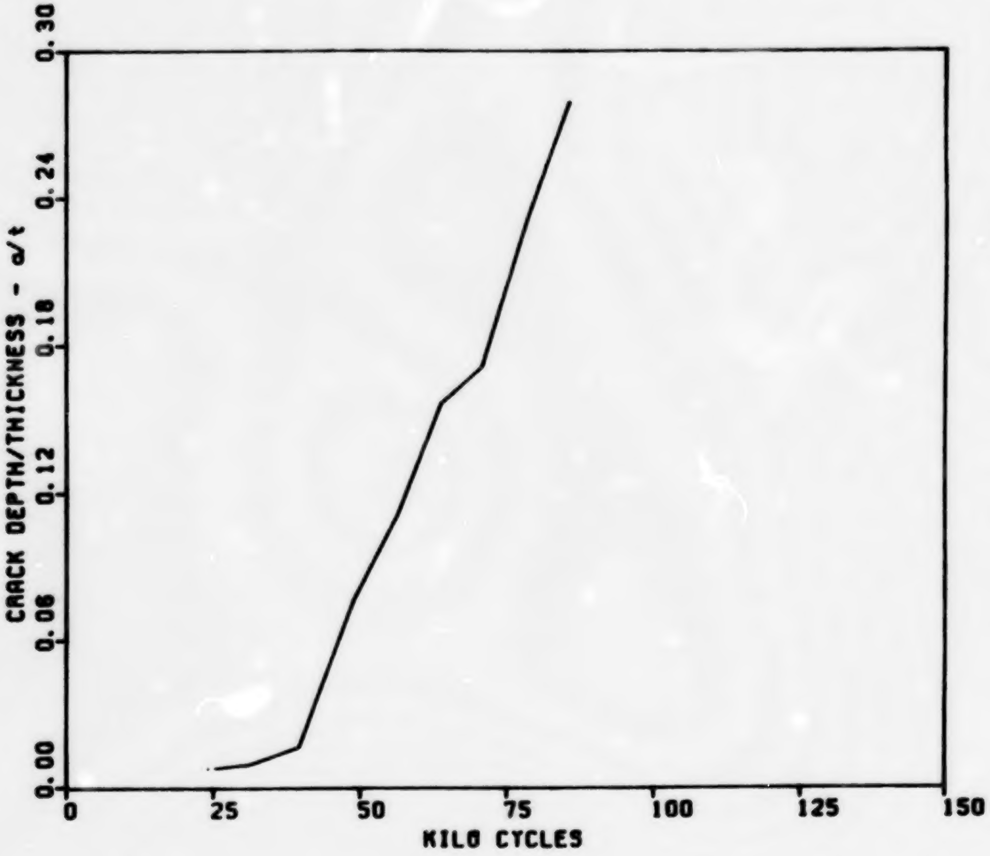

CRACK DEPTH vs CYCLES
INITIATING CRACK POSITION 0 mm FROM SADDLE POINT
ANGULAR POSITION FROM SADDLE POINT - 180°
STIFFENED TUBULAR JOINT - TA4 SIDE 2
AXIAL LOAD - HOT SPOT STRESS RANGE 250 MPa

Figure 5-15

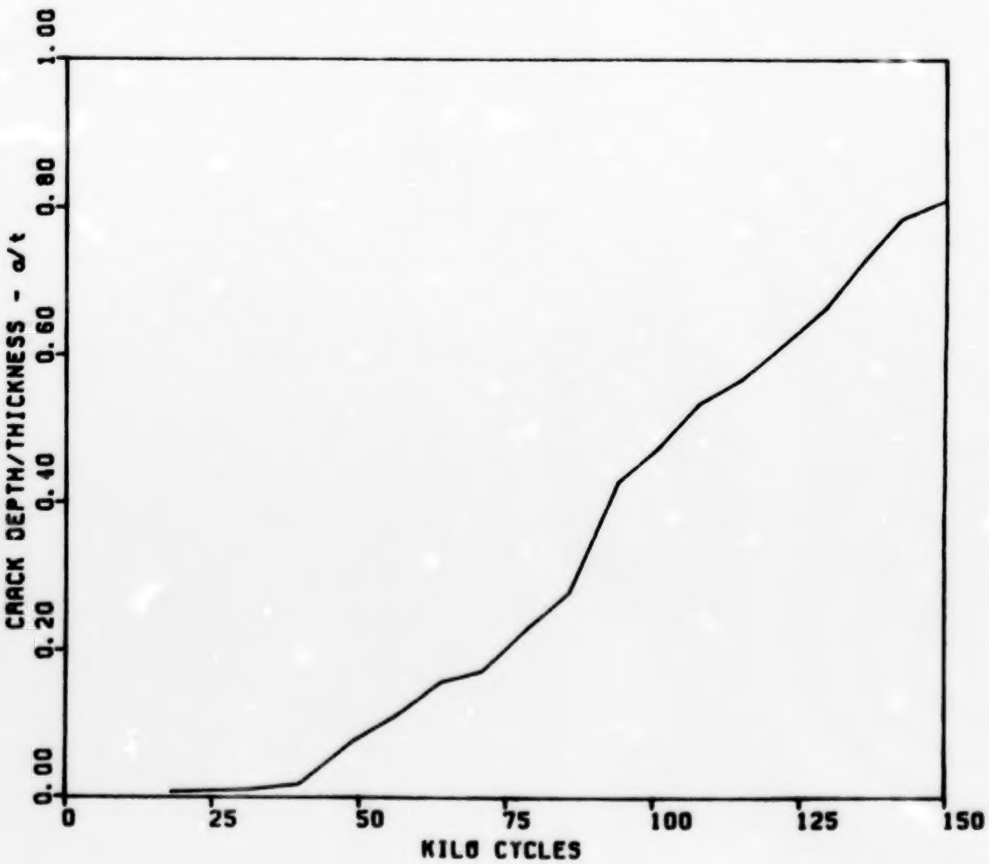

CRACK DEPTH vs CYCLES
INITIATING CRACK POSITION 0 mm FROM SADDLE POINT
ANGULAR POSITION FROM SADDLE POINT - 180°
STIFFENED TUBULAR JOINT - TA4 SIDE 2
AXIAL LOAD - HOT SPOT STRESS RANGE 250 MPa

Figure 5-16

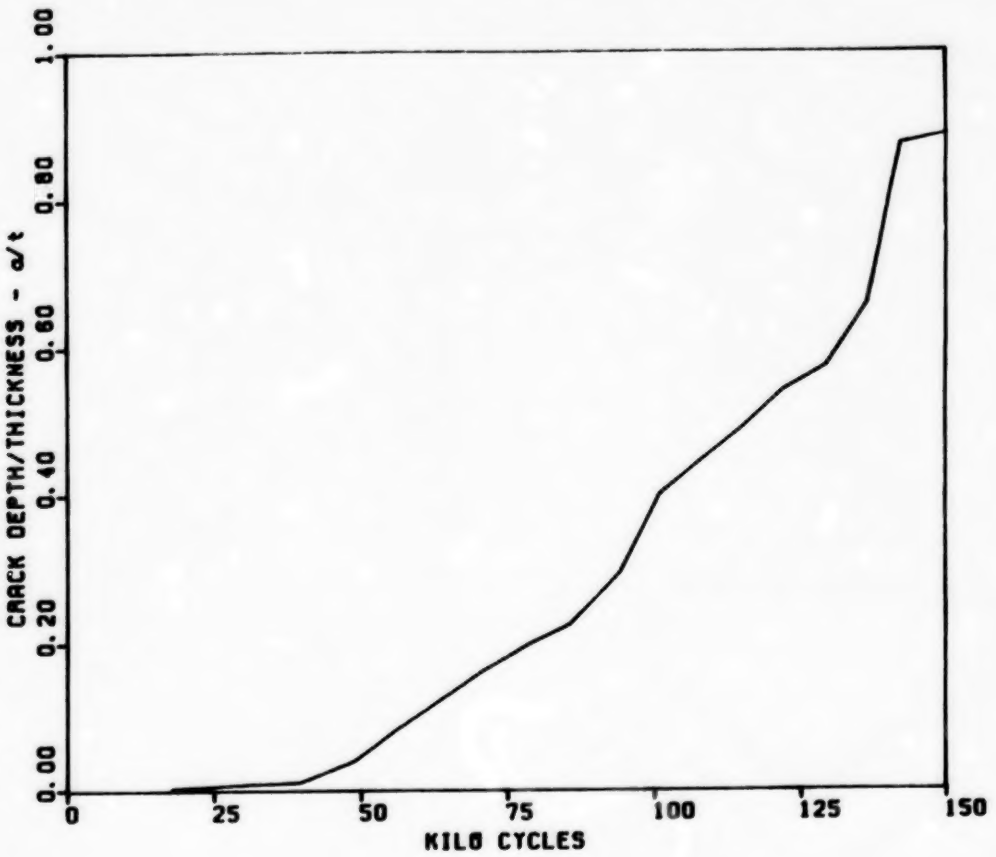

CRACK DEPTH vs CYCLES
DOMINANTLY PROPAGATING CRACK POSITION
60 mm AND 193.7° FROM SADDLE POINT
STIFFENED TUBULAR JOINT - TA4 SIDE 2
AXIAL LOAD - HOT SPOT STRESS RANGE 250 MPa

Figure 5-17

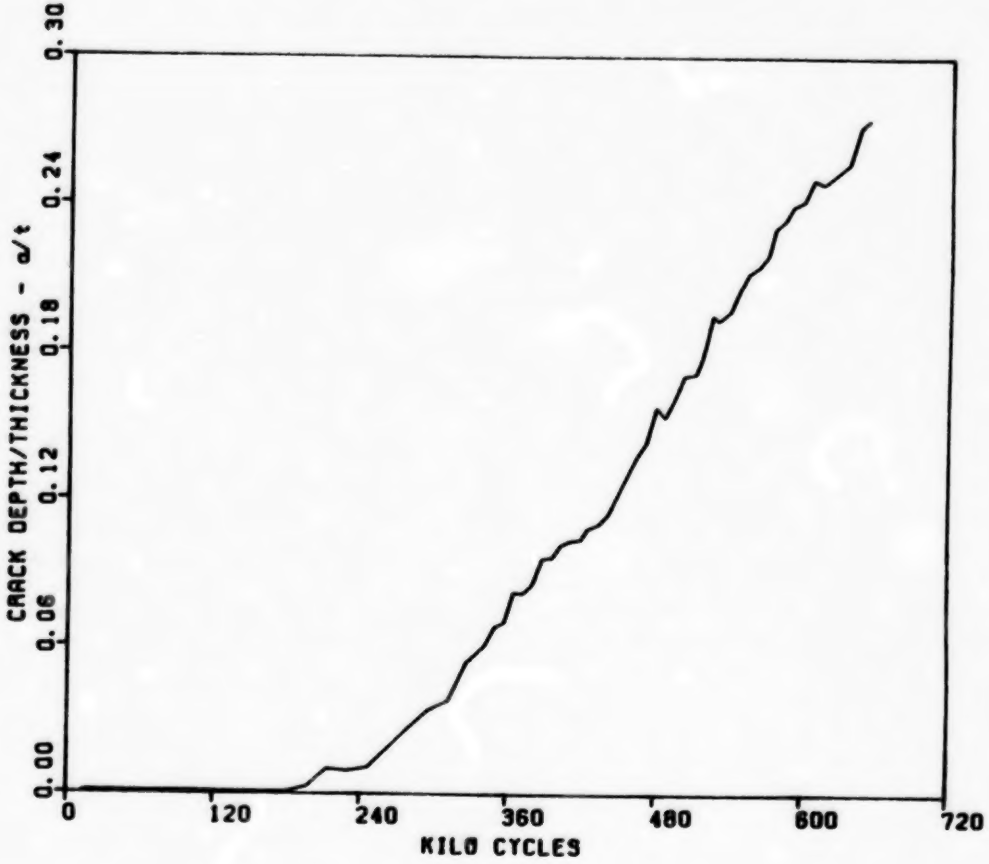

CRACK DEPTH vs CYCLES
INITIATING CRACK POSITION 72.7mm FROM SADDLE POINT
ANGULAR POSITION FROM SADDLE POINT - 343.5°
STIFFENED TUBULAR JOINT - TAS SIDE 1
AXIAL LOAD - HOT SPOT STRESS RANGE 160 MPa

Figure 5-18

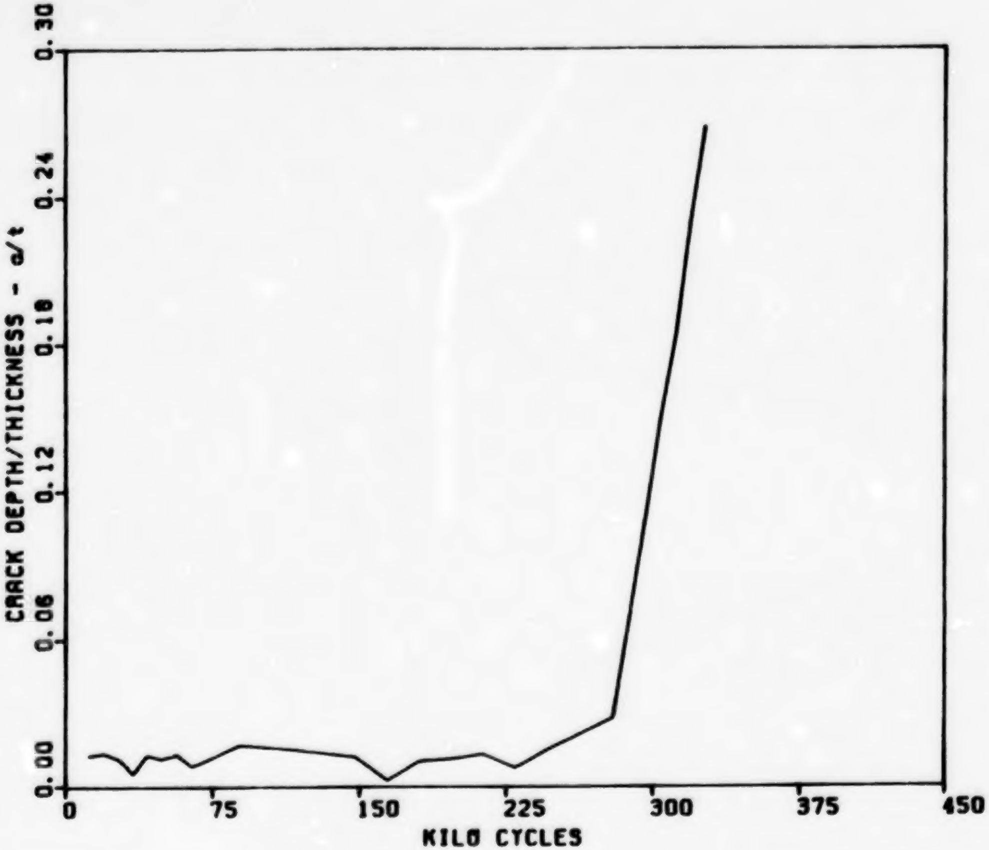

CRACK DEPTH vs CYCLES
INITIATING CRACK POSITION 61mm FROM SADDLE POINT
ANGULAR POSITION FROM SADDLE POINT - 193.9°
STIFFENED TUBULAR JOINT - TAS SIDE 2
AXIAL LOAD - HOT SPOT STRESS RANGE 160 MPa

Figure 5-19

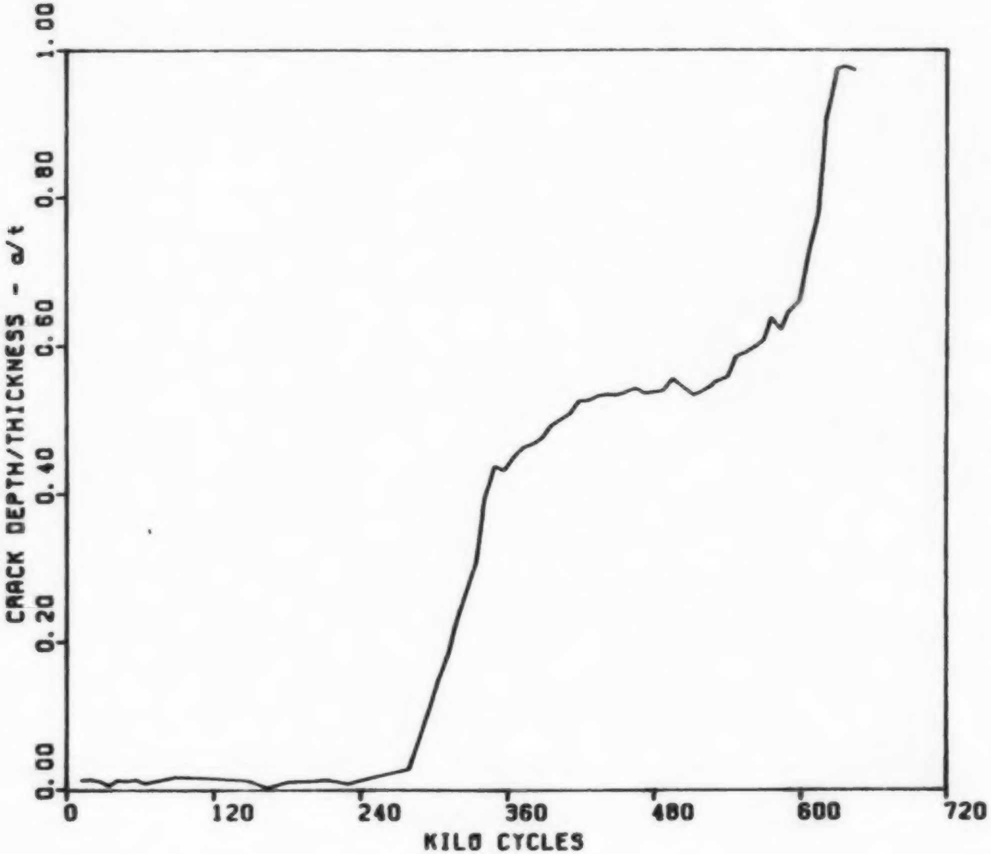

CRACK DEPTH vs CYCLES
INITIATING CRACK POSITION 61mm FROM SADDLE POINT
ANGULAR POSITION FROM SADDLE POINT - 193.9°
STIFFENED TUBULAR JOINT - TAS SIDE 2
AXIAL LOAD - HOT SPOT STRESS RANGE 160 MPa

Figure 5-20

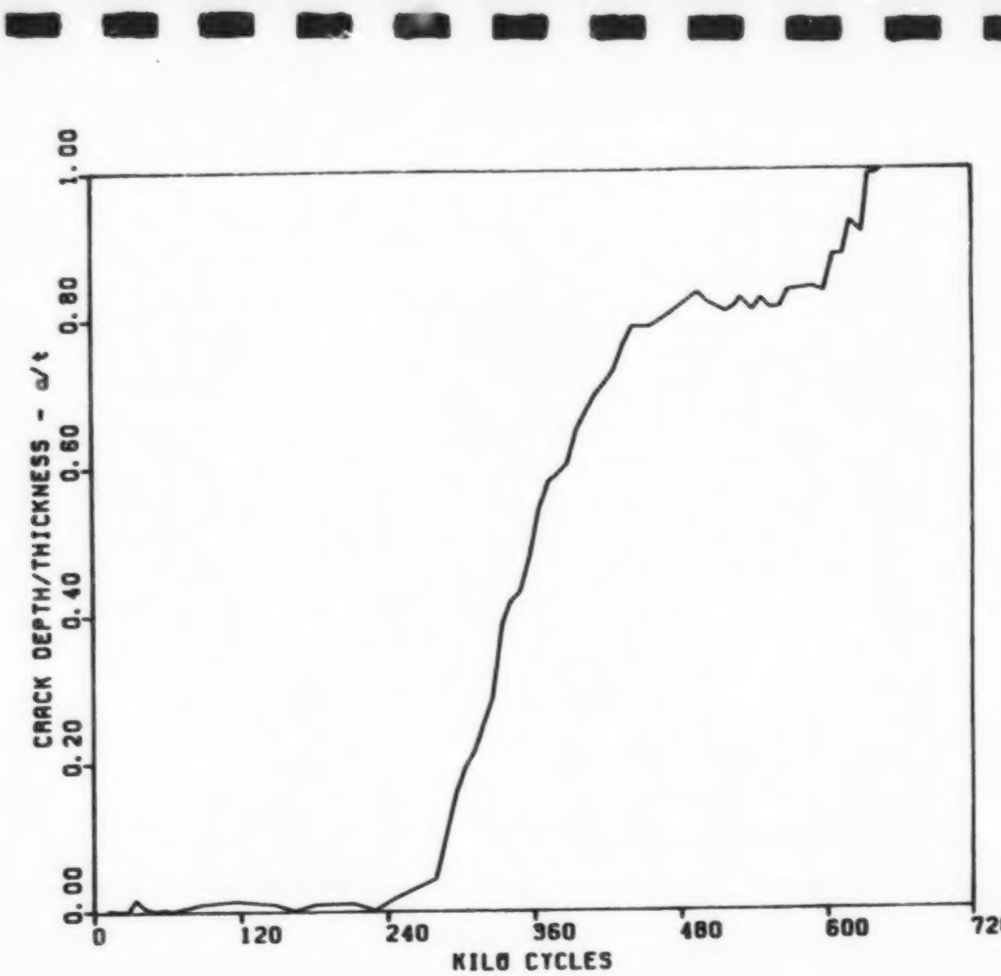

CRACK DEPTH vs CYCLES
DOMINANTLY PROPAGATING CRACK POSITION
AT 30.8mm AND 187°FROM SADDLE POINT
STIFFENED TUBULAR JOINT - TAS SIDE 2
AXIAL LOAD - HOT SPOT STRESS RANGE 160 MPa

Figure 5-21

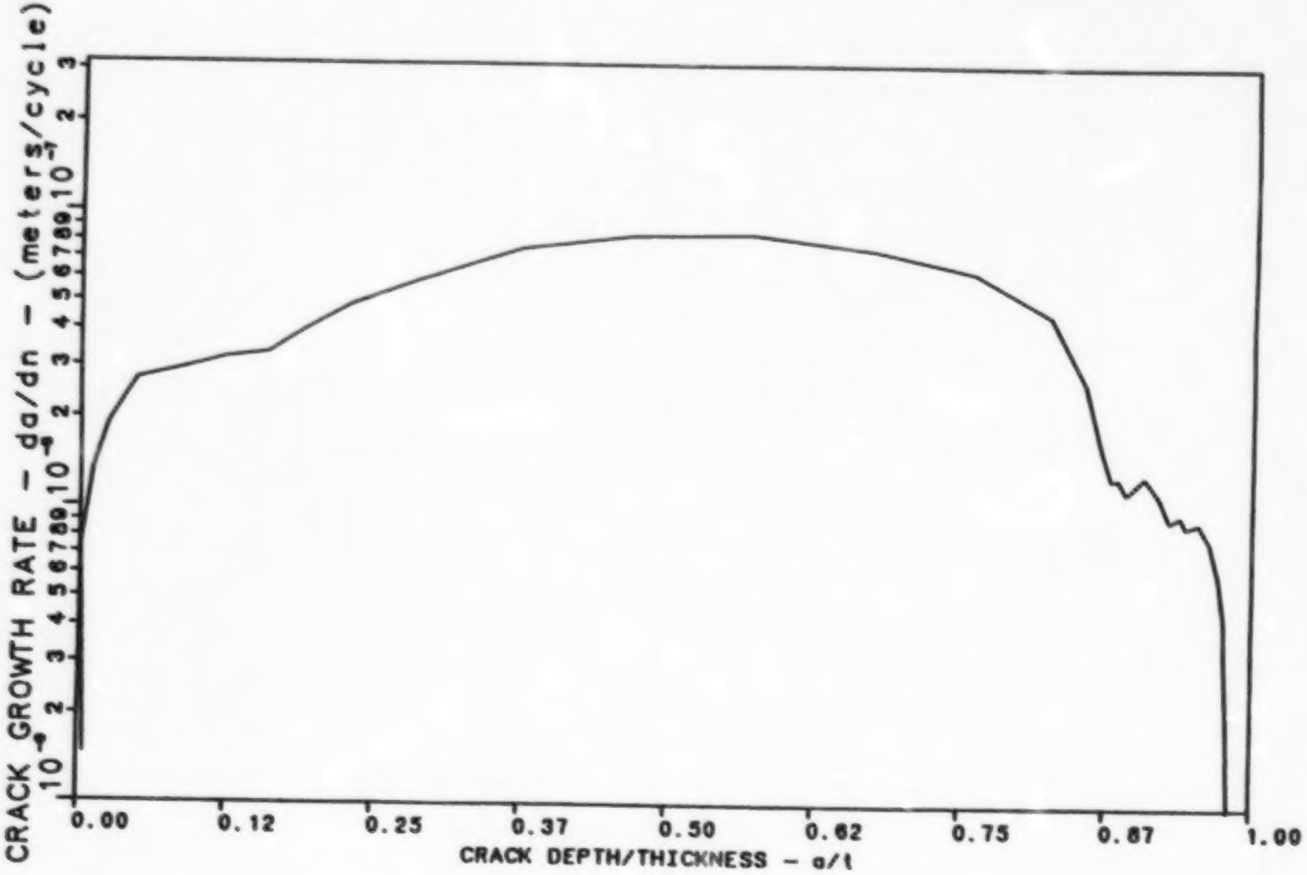

CRACK GROWTH RATE vs. CRACK DEPTH
INTIATING CRACK POSITION 18 mm FROM SADDLE POINT
ANGULAR DISTANCE FROM SADDLE POINT 178°
UNSTIFFENED TUBULAR JOINT - TA1 SIDE 2
AXIAL LOAD - HOT SPOT STRESS RANGE 250 MPa

Figure 5-22

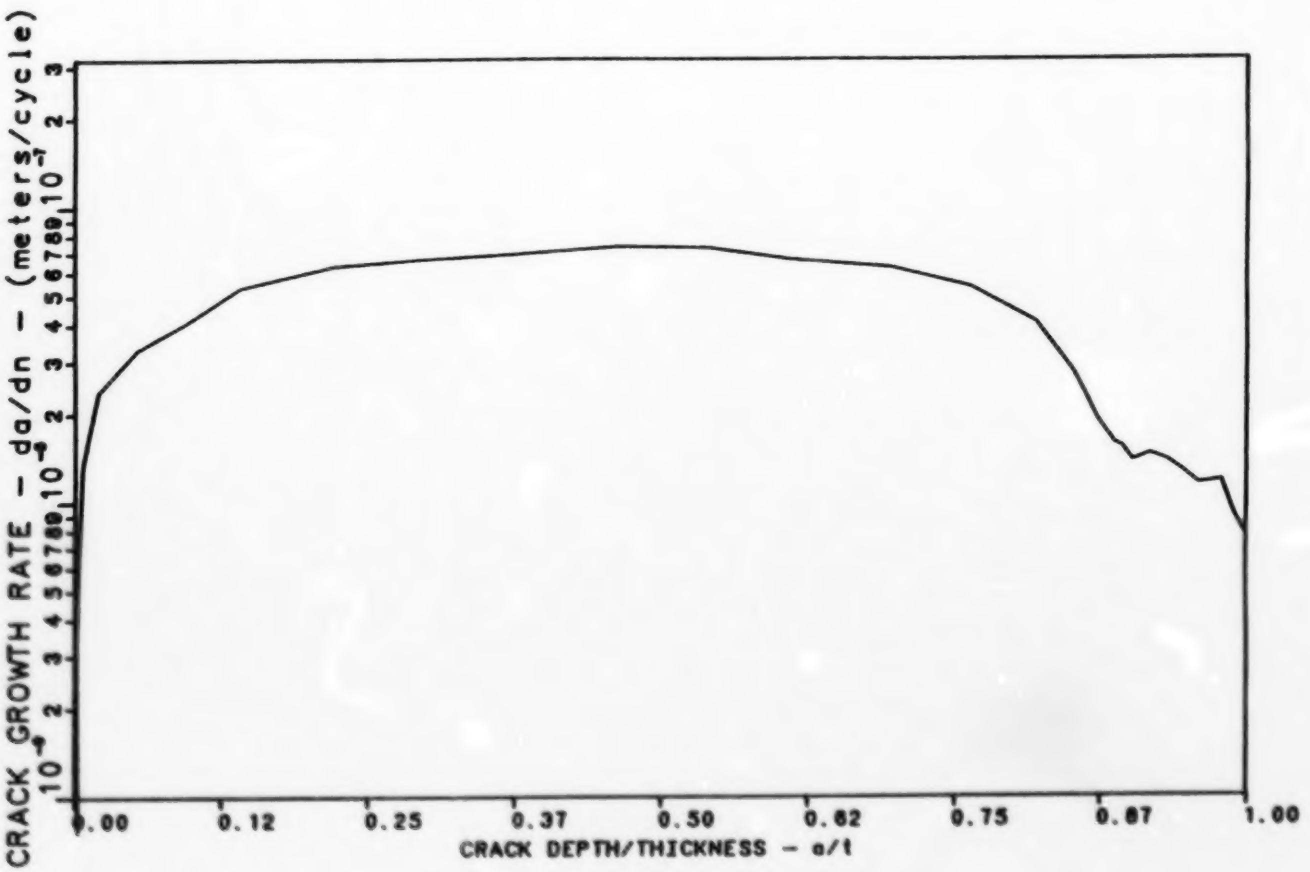

CRACK GROWTH RATE vs. CRACK DEPTH
FOR DOMINANTLY PROPAGATING CRACK POSITION
AT SADDLE POINT 180°
UNSTIFFENED TUBULAR JOINT - TA1 SIDE 2
AXIAL LOAD - HOT SPOT STRESS RANGE 250 MPa

Figure 5-23

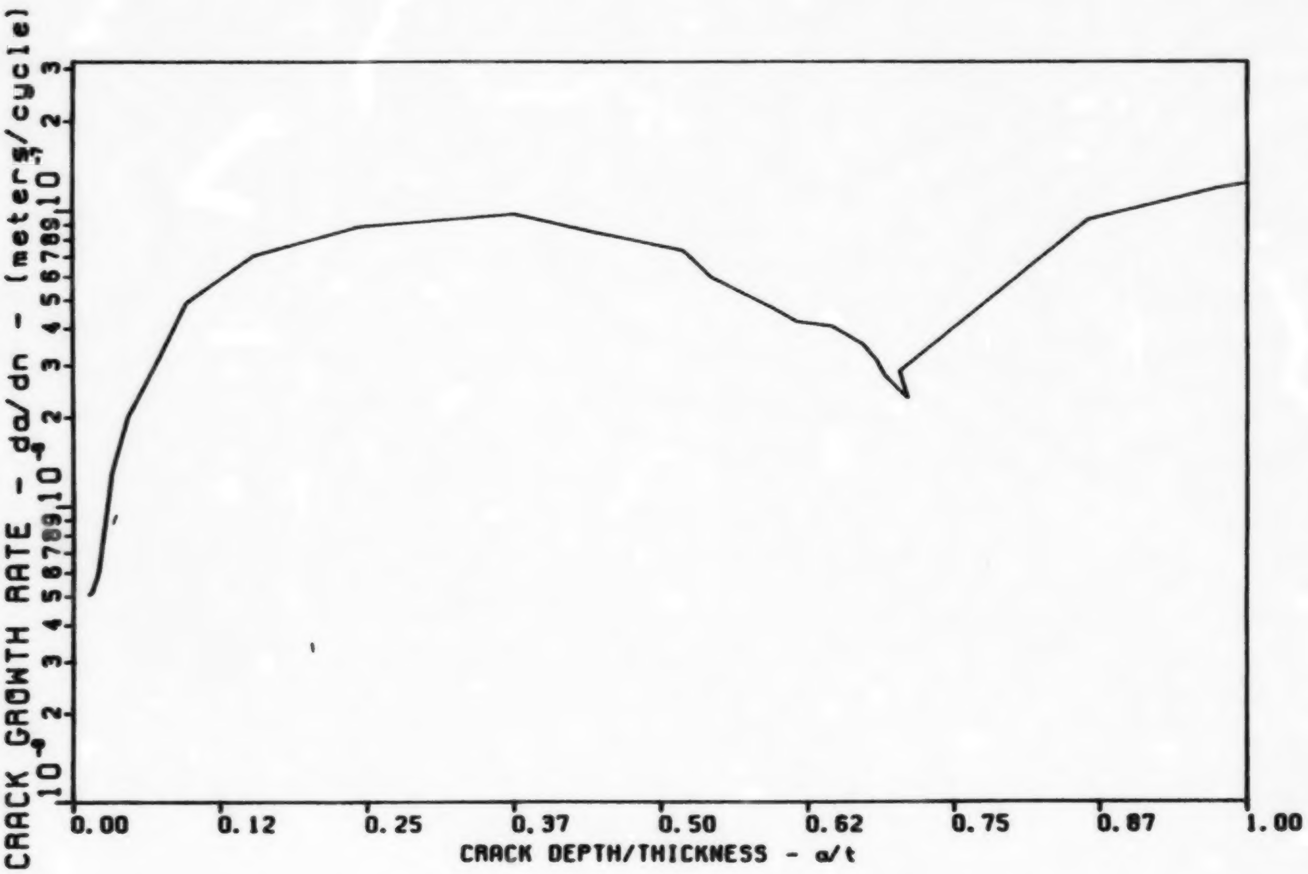

CRACK GROWTH RATE vs. CRACK DEPTH
INTIATING CRACK POSITION 30 mm FROM SADDLE POINT
ANGULAR DISTANCE FROM SADDLE POINT 7°
STIFFENED TUBULAR JOINT - TA2 SIDE 1
AXIAL LOAD - HOT SPOT STRESS RANGE 250 MPa

Figure 5-24

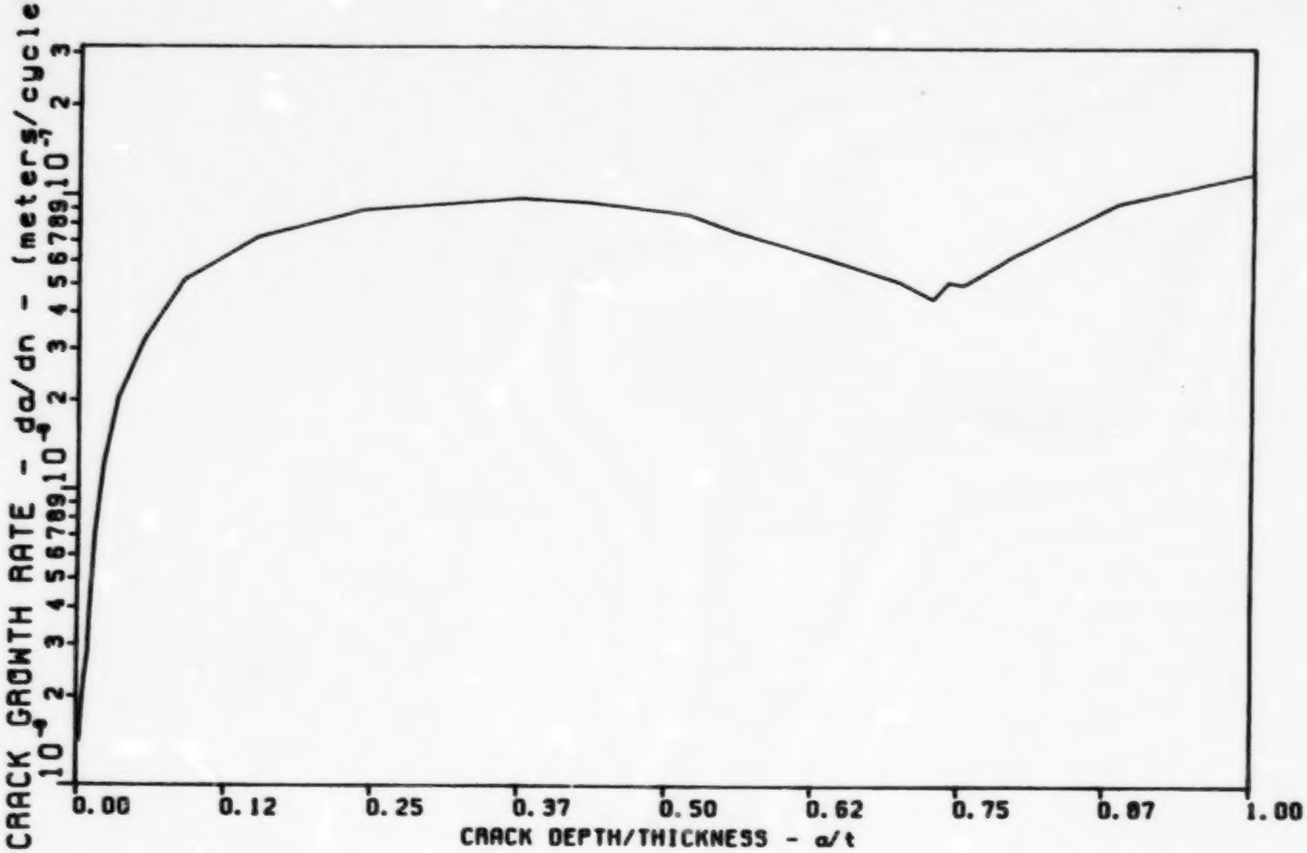

CRACK GROWTH RATE vs. CRACK DEPTH
FOR DOMINANTLY PROPAGATING CRACK POSITION
60mm AND 13.7° FROM SADDLE POINT
STIFFENED TUBULAR JOINT - TA2 SIDE 1
AXIAL LOAD - HOT SPOT STRESS RANGE 250 MPa

Figure 5-25

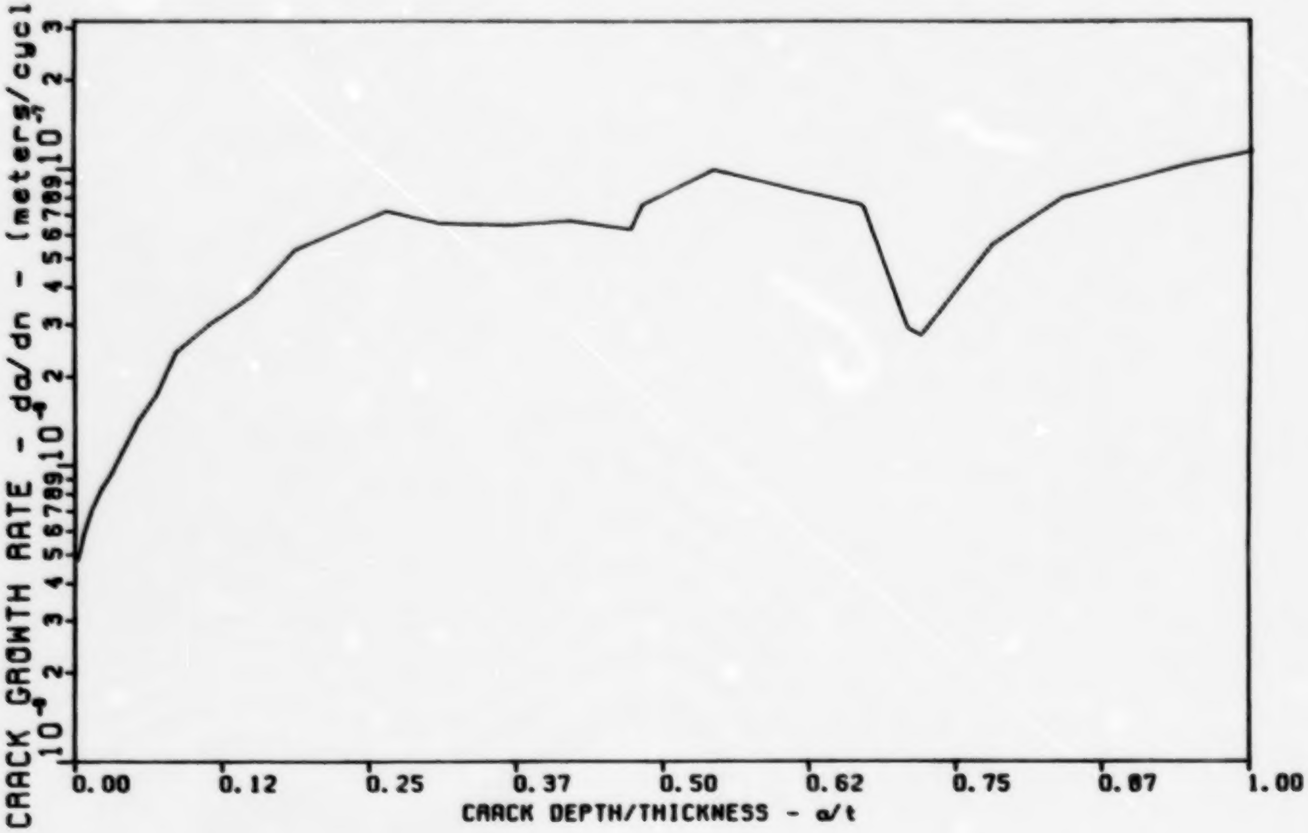

CRACK GROWTH RATE vs. CRACK DEPTH
INTIATING CRACK POSITION 55 mm FROM SADDLE POINT
ANGULAR DISTANCE FROM SADDLE POINT 167.5°
STIFFENED TUBULAR JOINT - TA2 SIDE 2
AXIAL LOAD - HOT SPOT STRESS RANGE 250 MPa

Figure 5-26

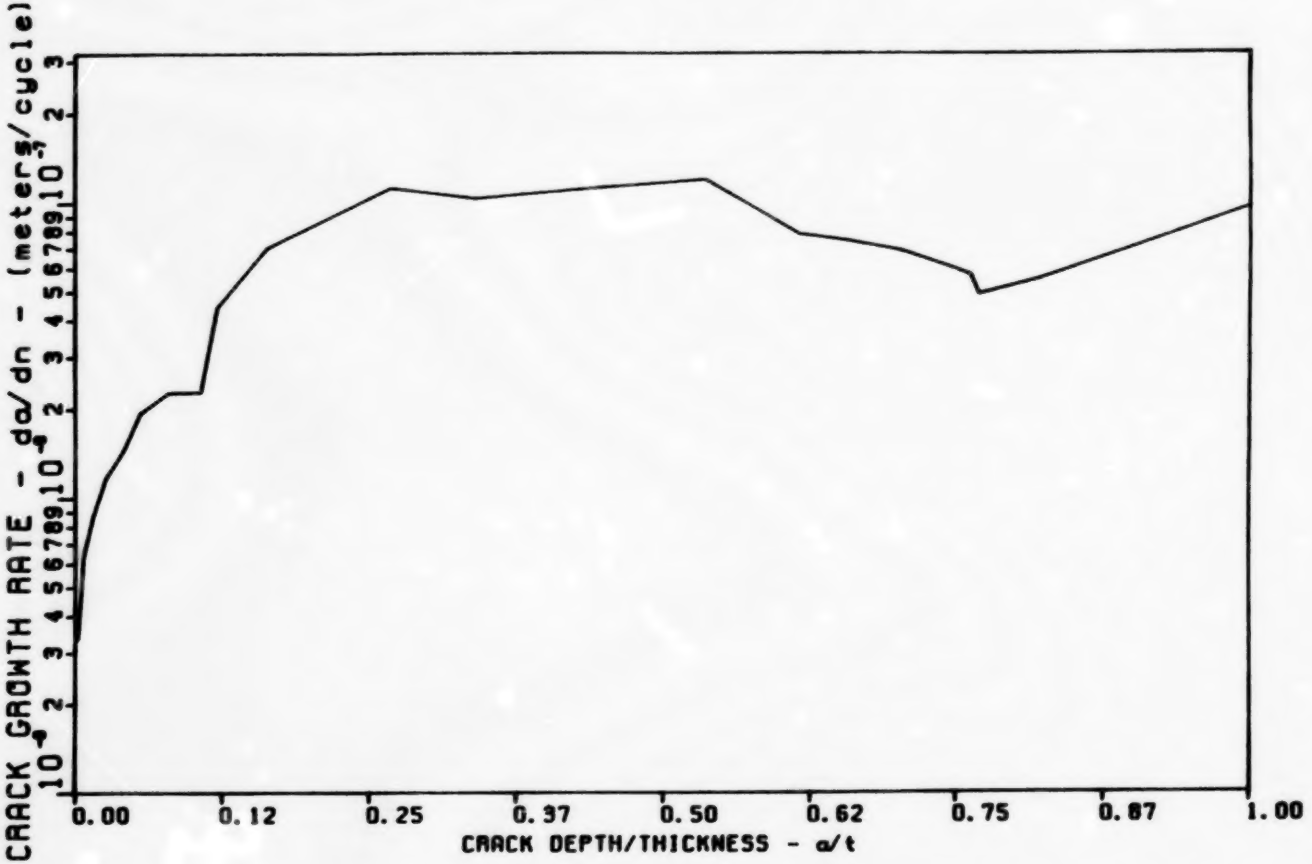

CRACK GROWTH RATE vs. CRACK DEPTH
FOR DOMINANTLY PROPAGATING CRACK POSITION
84.5mm AND 161° FROM SADDLE POINT
STIFFENED TUBULAR JOINT - TA2 SIDE 2
AXIAL LOAD - HOT SPOT STRESS RANGE 250 MPa

Figure 5-27

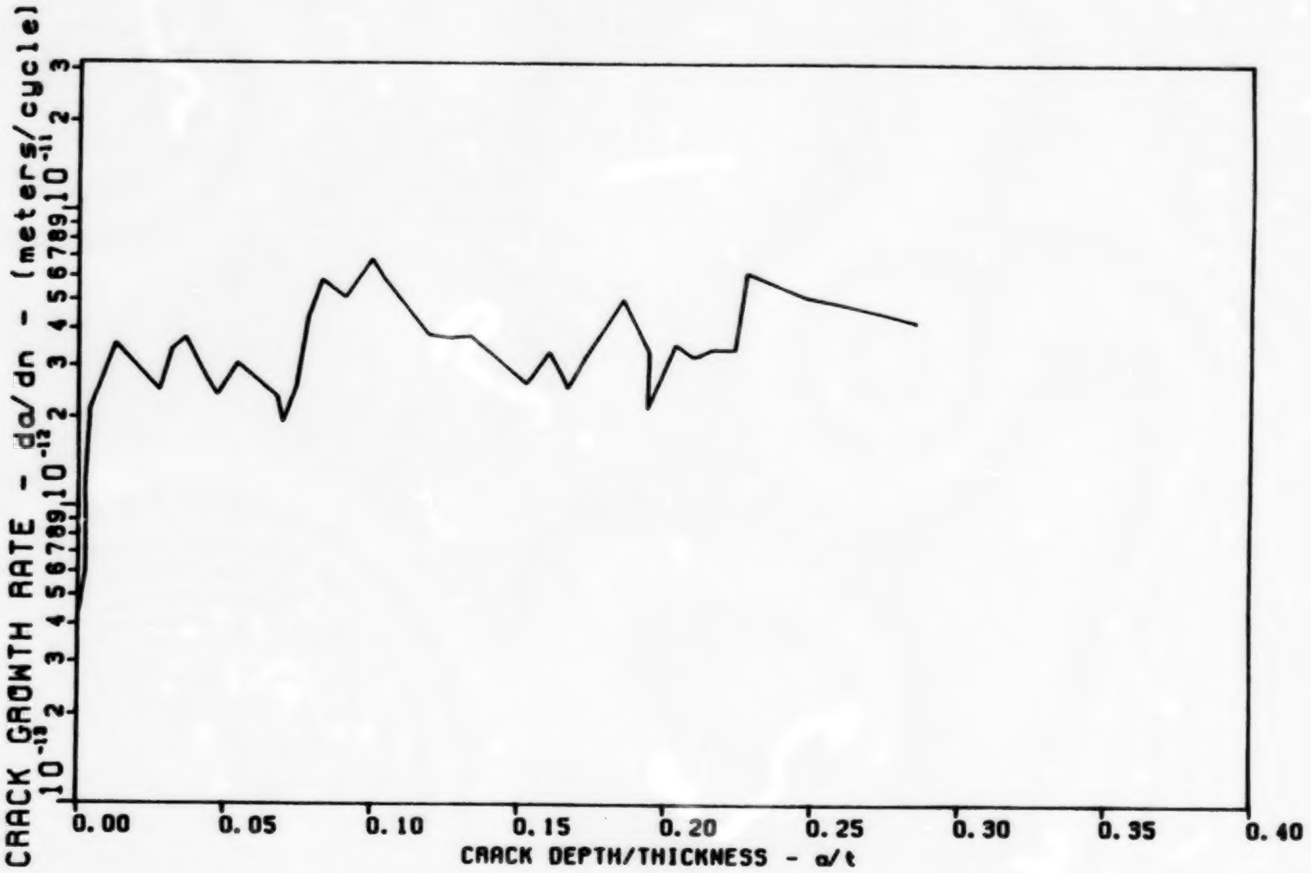

CRACK GROWTH RATE vs. CRACK DEPTH
INTIATING CRACK POSITION 73 mm FROM SADDLE POINT
ANGULAR DISTANCE FROM SADDLE POINT 343.5°
STIFFENED TUBULAR JOINT - TA3 SIDE 1
AXIAL LOAD - HOT SPOT STRESS RANGE 160 MPa

Figure 5-28

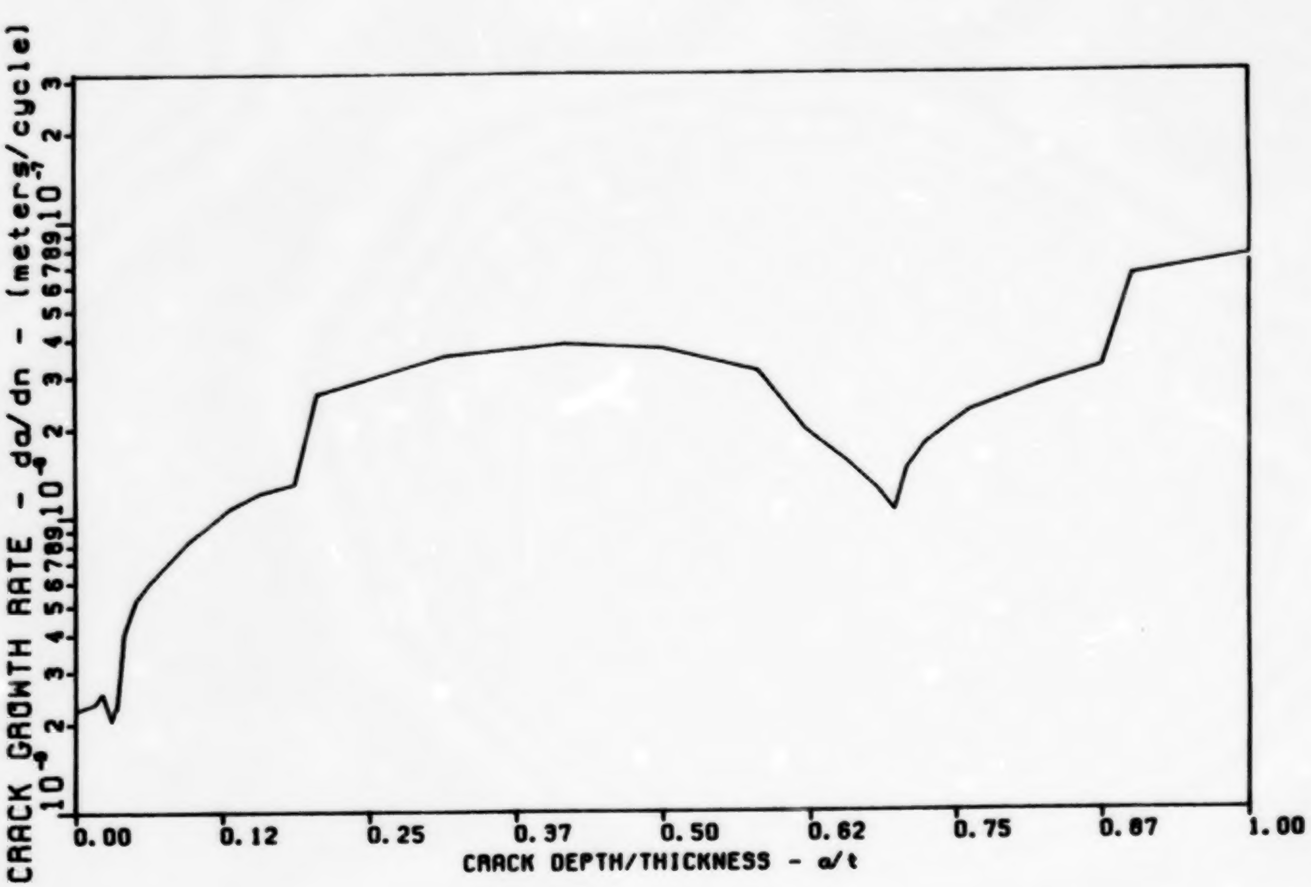

CRACK GROWTH RATE vs. CRACK DEPTH
INTIATING CRACK POSITION 60.5 mm FROM SADDLE POINT
ANGULAR DISTANCE FROM SADDLE POINT 168.3°
STIFFENED TUBULAR JOINT - TA3 SIDE 2
AXIAL LOAD - HOT SPOT STRESS RANGE 160 MPa

Figure 5-29

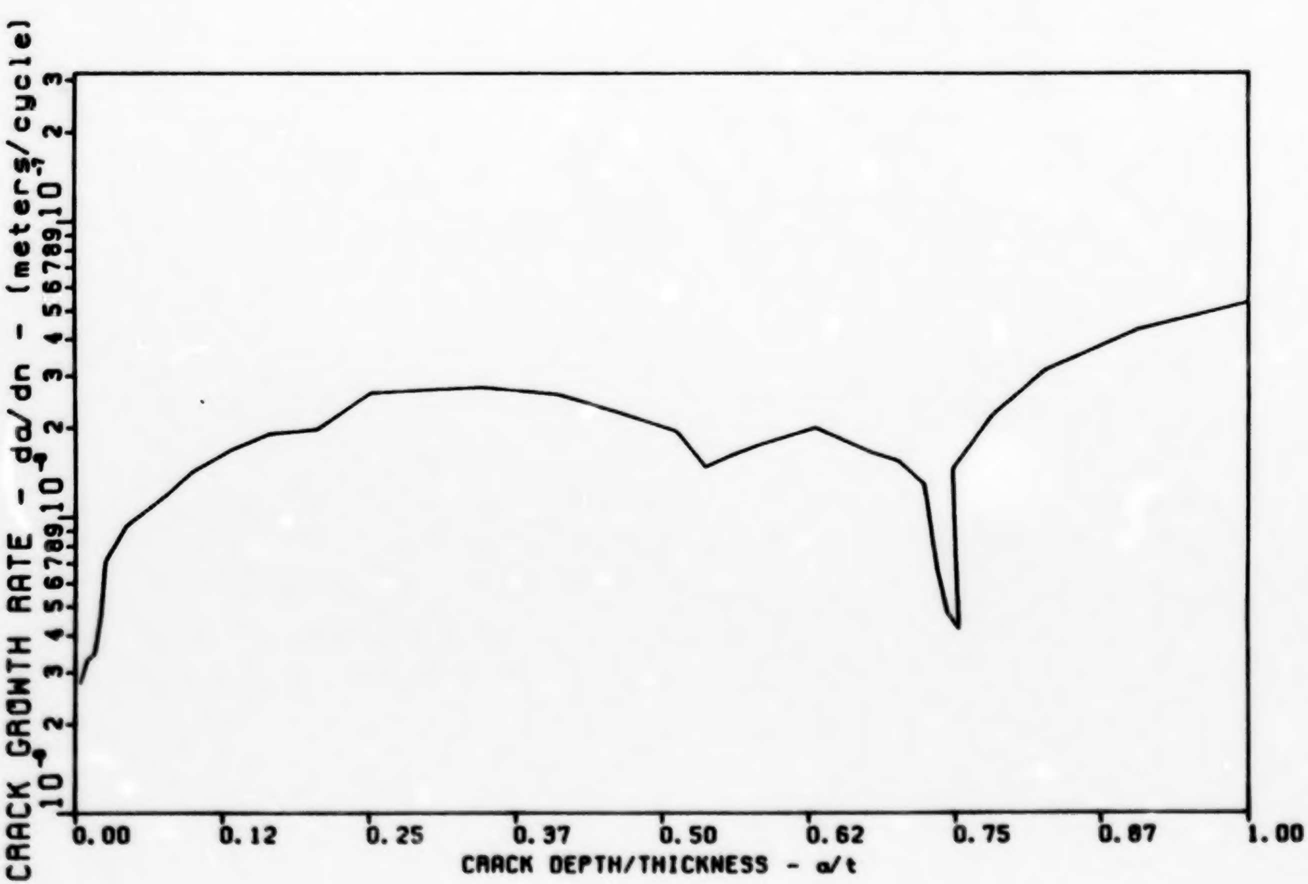

CRACK GROWTH RATE vs. CRACK DEPTH
FOR DOMINANTLY PROPAGATING CRACK POSITION
AT SADDLE POINT 180°
STIFFENED TUBULAR JOINT - TA3 SIDE 2
AXIAL LOAD - HOT SPOT STRESS RANGE 160 MPa

Figure 5-30

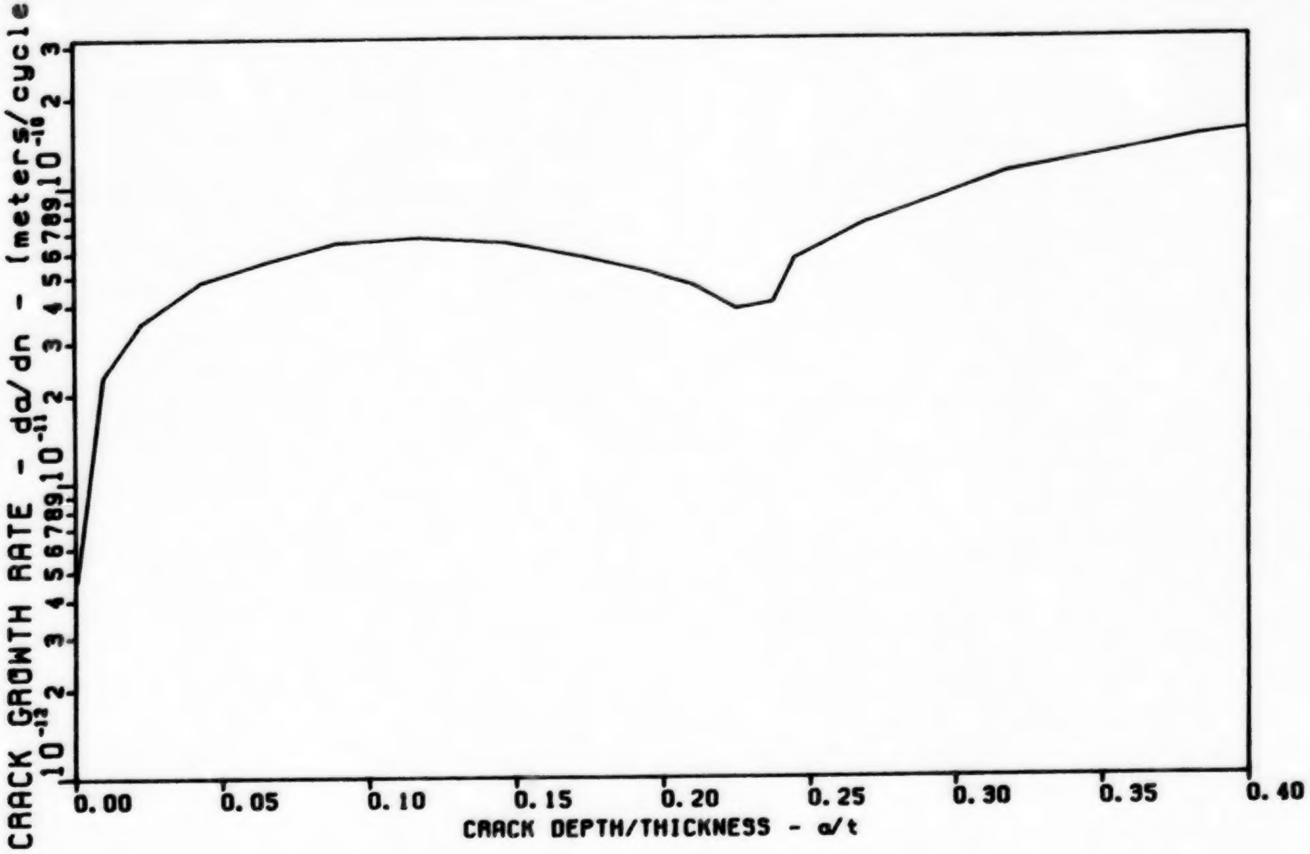

CRACK GROWTH RATE vs. CRACK DEPTH
INTIATING CRACK POSITION -30.5mm FROM SADDLE POINT
ANGULAR DISTANCE FROM SADDLE POINT 7°
STIFFENED TUBULAR JOINT - TA4 SIDE 1
AXIAL LOAD - HOT SPOT STRESS RANGE 160 MPa

Figure 5-31

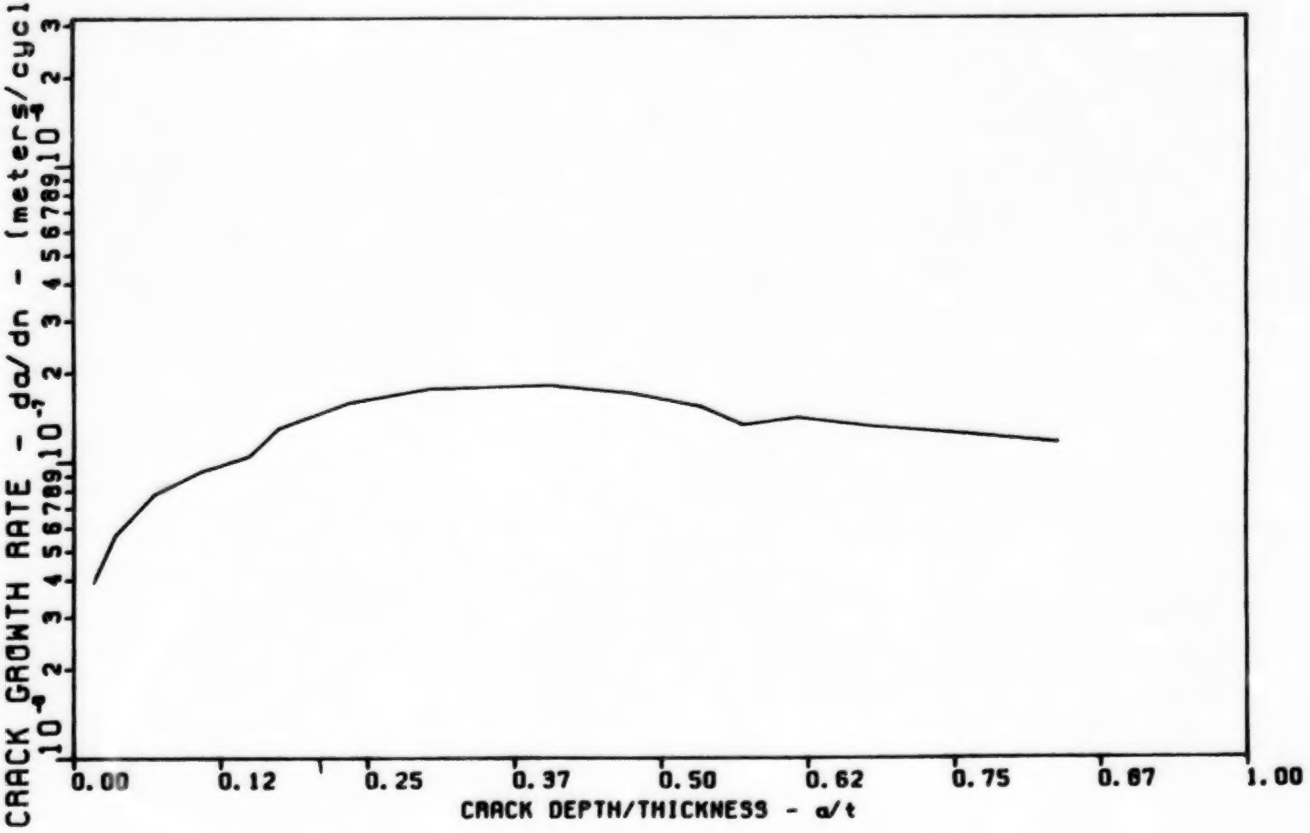

CRACK GROWTH RATE vs. CRACK DEPTH
FOR INTIATING CRACK POSITION 0 mm FROM SADDLE POINT
ANGULAR DISTANCE FROM SADDLE POINT 180°
STIFFENED TUBULAR JOINT - TA4 SIDE 2
AXIAL LOAD - HOT SPOT STRESS RANGE 250 MPa

Figure 5-32

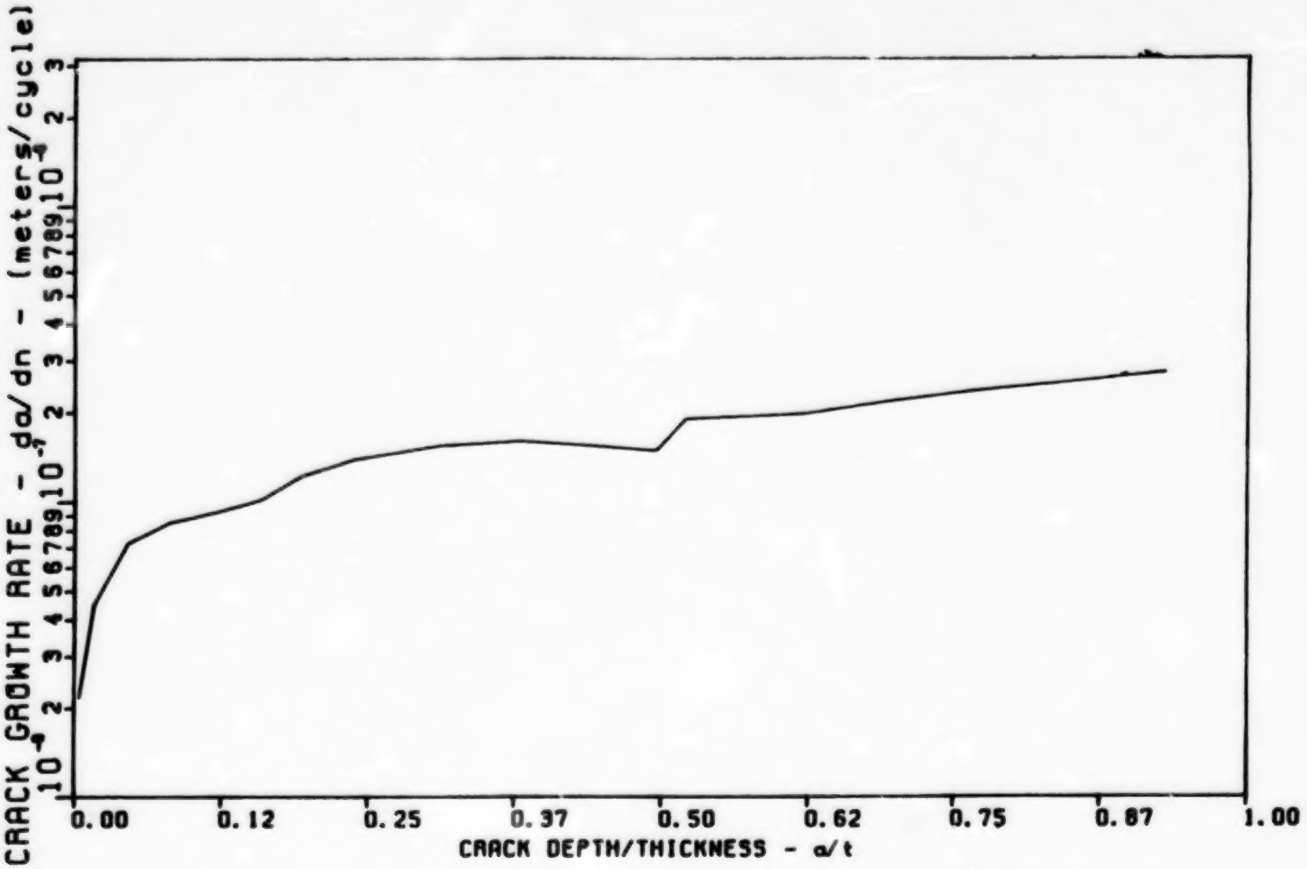

CRACK GROWTH RATE vs. CRACK DEPTH
FOR DOMINANTLY PROPAGATING CRACK POSITION
60 mm AND 193.7° FROM SADDLE POINT
STIFFENED TUBULAR JOINT - TA4 SIDE 2
AXIAL LOAD - HOT SPOT STRESS RANGE 250 MPa

Figure 5-33

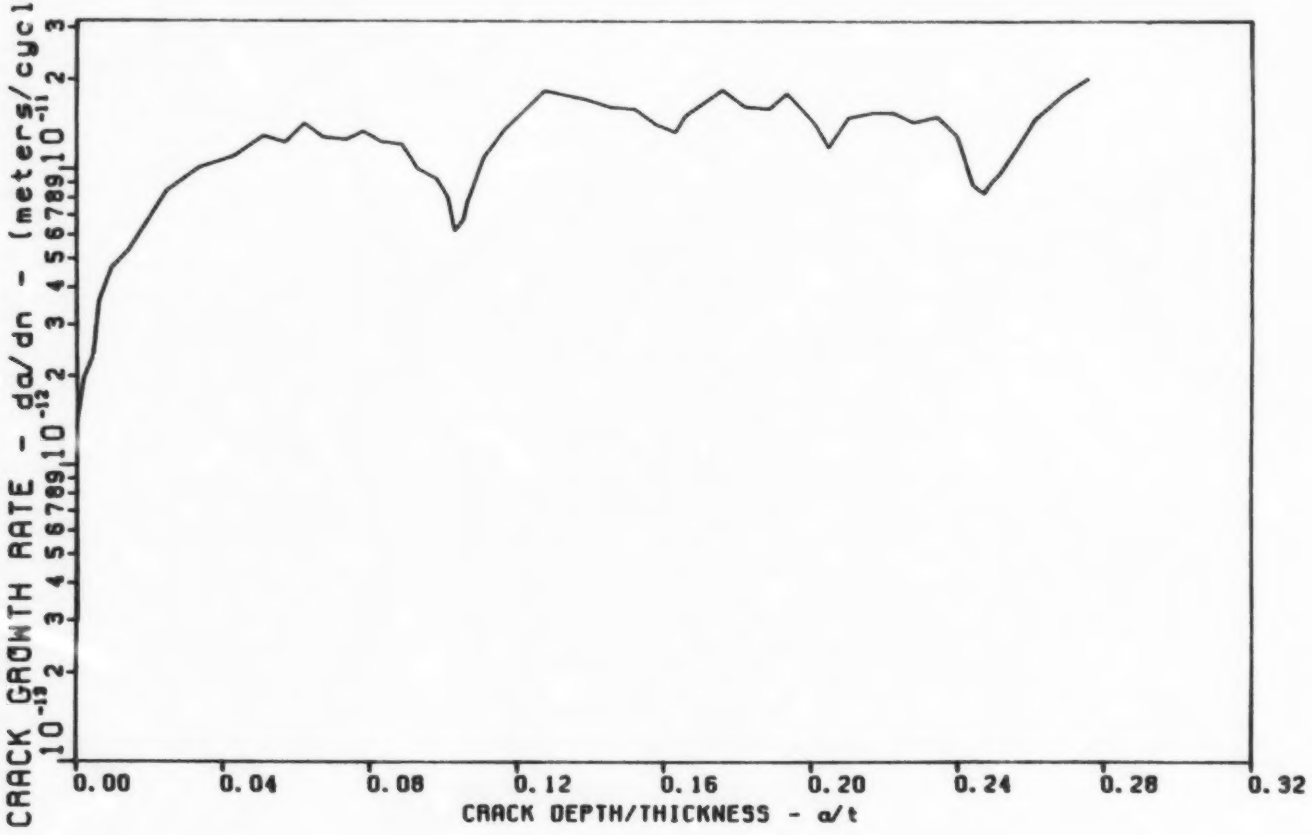

CRACK GROWTH RATE vs. CRACK DEPTH
INTIATING CRACK POSITION 72.7mm FROM SADDLE POINT
ANGULAR DISTANCE FROM SADDLE POINT 343.5°
STIFFENED TUBULAR JOINT - TA5 SIDE 1
AXIAL LOAD - HOT SPOT STRESS RANGE 160 MPa

Figure 5-34

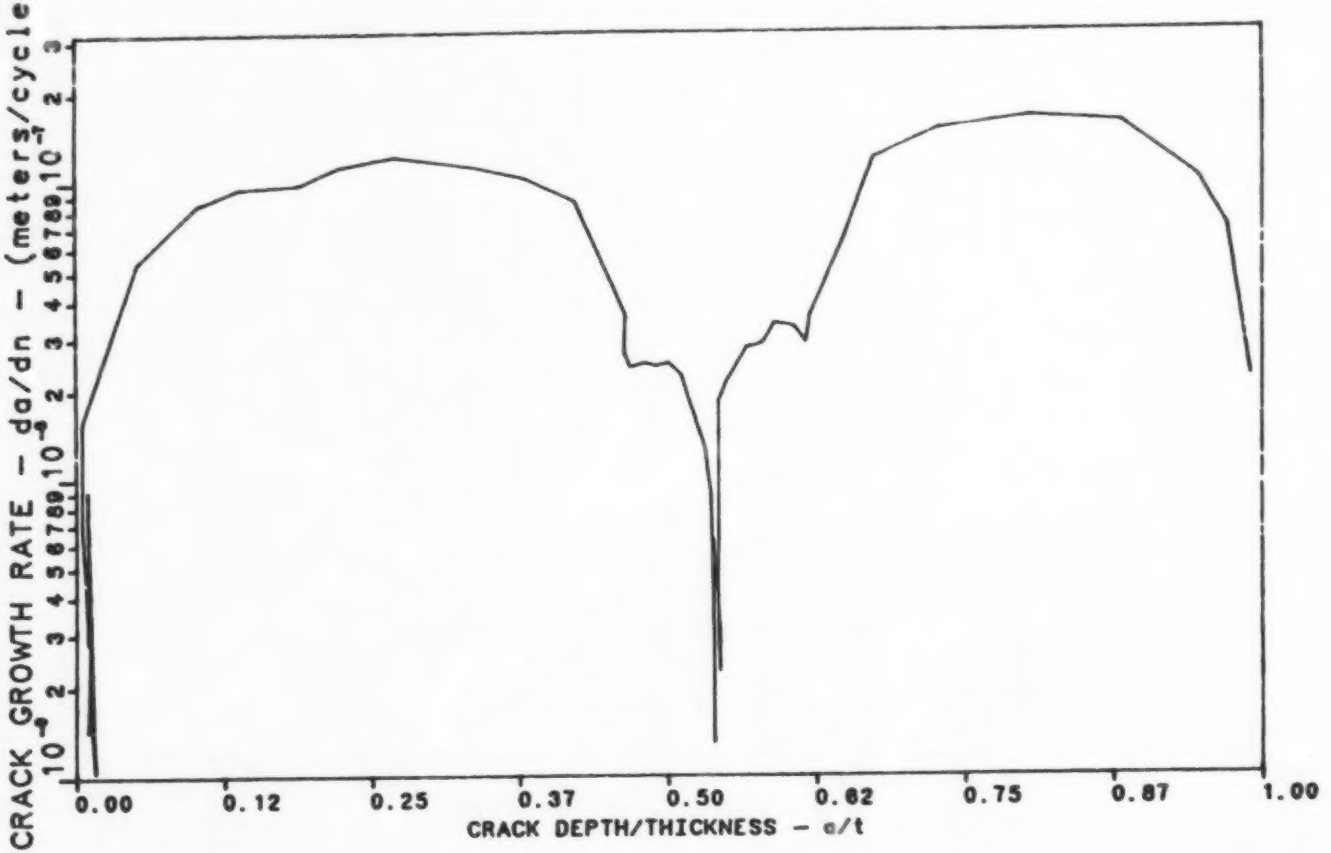

CRACK GROWTH RATE vs. CRACK DEPTH
INTIATING CRACK POSITION
AT 61 mm AND 193.9° FROM SADDLE POINT
STIFFENED TUBULAR JOINT - TA5 SIDE 2
AXIAL LOAD - HOT SPOT STRESS RANGE 160 MPa

Figure 5-35

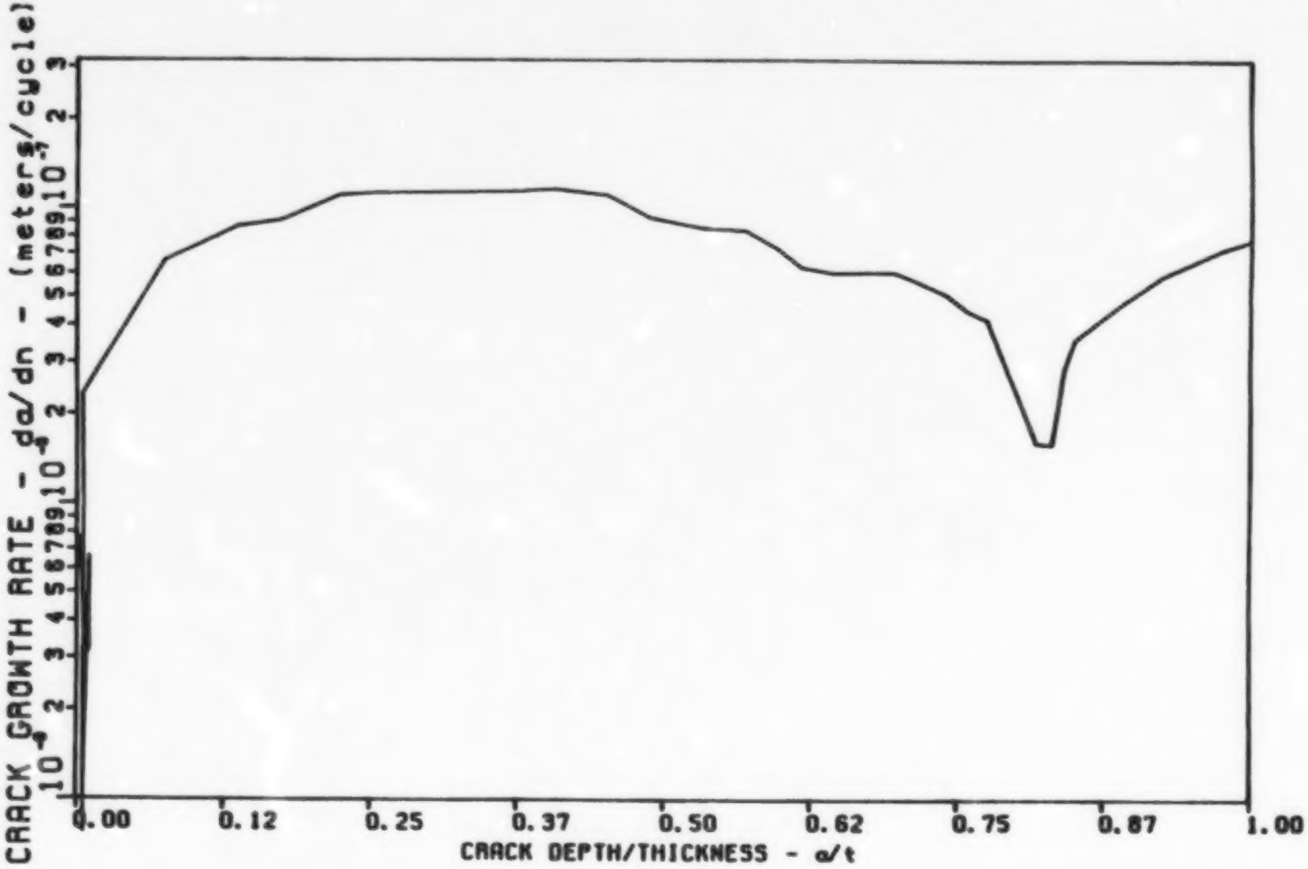

CRACK GROWTH RATE vs. CRACK DEPTH
FOR DOMINANTLY PROPAGATING CRACK POSITION
30.8mm AND 187° FROM SADDLE POINT
STIFFENED TUBULAR JOINT - TAS SIDE 2
AXIAL LOAD - HOT SPOT STRESS RANGE 160 MPa

Figure 5-36